AD NUMBER

AD368356

CLASSIFICATION CHANGES

TO: unclassified

FROM: confidential

LIMITATION CHANGES

TO:

Approved for public release, distribution unlimited

FROM:

Distribution: DoD only: others to Director, Naval Research Lab., Washington, D. C. 20390.

AUTHORITY

1970, Group-4, DoDD 5200.10, 26 Jul 1962.; NRL ltr, 26 Feb 2001.

SUMMARY OF NAVY STUDY PROGRAM

FOR

F4H-1 and F8U-3 WEAPON SYSTEMS

(Appendices to NRL Memo Report 754)

VOLUME IV

Equipment Research Branch
Radar Division
Naval Research Laboratory

SECURITY

This document contains information affecting the national defense of the United States within the meaning of the Espionage Laws, Title 18, U.S.C., Sections 793 and 794. The transmission or the revelation of its contents in any manner to an unauthorized person is prohibited by law.

ANTM #302

NAVY MISSILE STUDY

TECHNICAL REPORT NO. 6

APPENDIX 1

F8U-3 Stability Derivatives (Wind and Body Axes), Dynamic Characteristics, and Basic Performance Data

- 90114 -

Proprietary Information
Chance Vought Aircraft Corp.
Dallas, Texas

by: R. B. Tucker
10/25/57

32 pages

TABLE OF CONTENTS

LIST OF ILLUSTRATIONS

I. SYNOPSIS

This report contains basic aircraft data and some of the basic performance data that are currently available for the F8U-3 aircraft. A brief description of the F8U-3 is also given.

Included as basic aircraft data are the stability derivatives of the F8U-3 in both wind axes and body axes and the airplane characteristics for both the lateral and longitudinal modes. Also given are the performance functions of the lateral and longitudinal variables as influenced by δ_a, δ_r, and δ_e.

The basic performance data contained in this report have been presented in the form of graphs. Some of the data presented were not originally received in the form shown. Where this occurs, the method used to obtain this data will be given.

II. DESCRIPTION OF F8U-3

The F8U-3 is a single seat, high performance all-weather fighter designed to perform the combat air patrol mission or the general purpose fighter mission.

The F8U-3 is a missile carrying aircraft and an armament bay is provided in the fuselage which is capable of housing a variety of armament arrangements. However, as its basic armament, it will carry three Sparrow III missiles - one bottom and two side missiles - which are mounted semi-submerged on the fuselage. The bottom missile when extended (at launch) is orientated 1° 39" down from the aircraft's water line. The side missiles are orientated 19" out from the water line.

This aircraft is powered by one Pratt and Whitney JT4B-22 engine with afterburner. The afterburner on this aircraft is either on or off. When it is on, the turbojet throttle may be adjusted to give any power setting from 16,000 to 24,000 pounds of thrust. This method essentially gives a variable afterburner.

A picture of the F8U-3 as seen from three views is shown in figure 1.

III. BASIC AIRCRAFT DATA

The stability derivatives presented in this report were obtained for the maximum velocity of the F8U-3 at each of three altitudes - 1,000 feet, 30,000 feet, and 50,000 feet. The velocities used in obtaining the stability derivatives will be indicated by cross marks on the F8U-3 maximum velocity profile, which is shown in figure 3.

The wind axes stability derivatives are shown in Table I. The airplane characteristics for both the lateral and longitudinal stick-fixed modes are also included. The body axes stability derivatives are given in Table II. Both tables are contained in Appendix I. There were several stability derivatives for which no data were available and these will be so indicated in the tables.

The pertinent angles of the F8U-3 are shown in figure 2. The angles shown are for the F8U-3 at combat weight-wheels up. The Radar Gimmal Mechanical Axis (RGMA) is located on the water line and the published data by Chance Vought

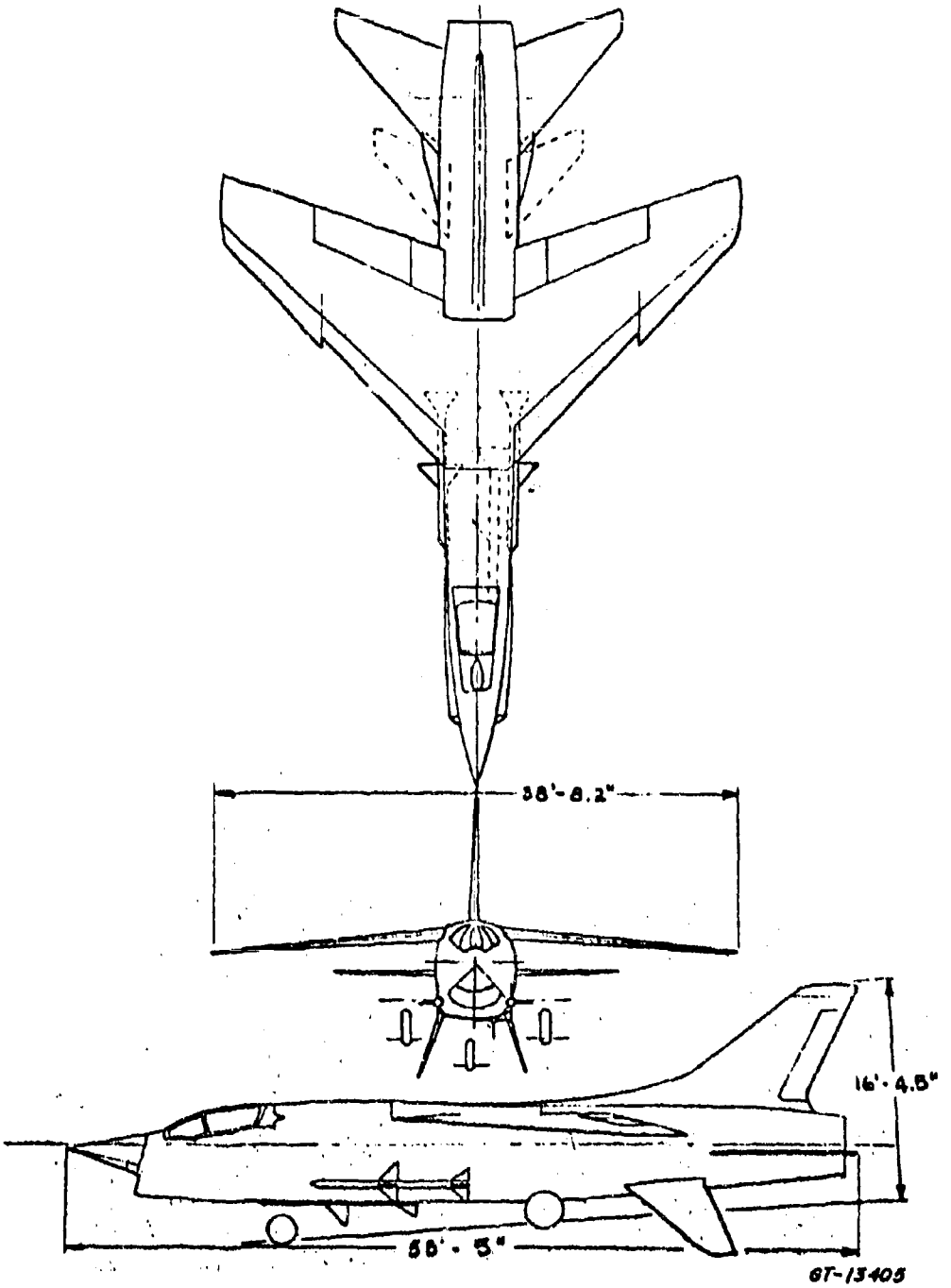

Scale 1/20

Figure 1. F8U-3 General Arrangement

ALTITUDE	1.000'	30,000'	50,000'
MAXIMUM MACH NO.	1.17	2.2	2.2
C_L	0.0348	0.0320	0.0827
$C_{L\alpha}$	0.0530	0.0343	0.0382
α_F	0.6566°	0.9335°	2.163°
$n=\alpha_o$	-1.828°	-1.551°	-0.322°
C_D	0.0358	0.0300	0.0326
q	1951	2122	822
D_o	31,430	28,647	12,059
WEIGHT	30,578	30,578	30,578

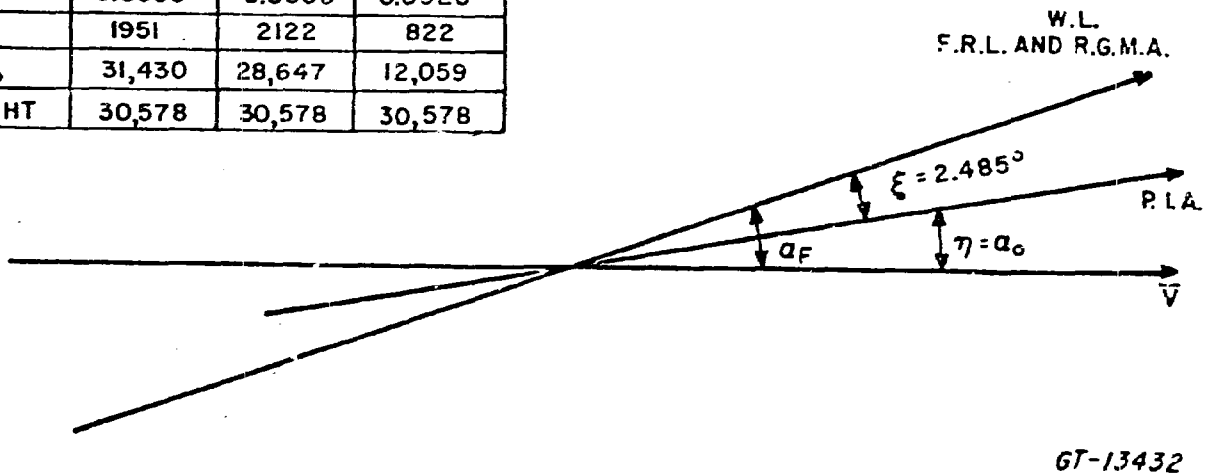

Figure 2. Pertinent Angles of F8U-3

on angle-of-attack is referred to the water line. The borosight tolerance for the missiles is one degree.

Appendix I also contains the equations of motion in both wind and body axes form.

In Appendix II, the performance functions of the lateral and longitudinal variables as influenced by $\delta_a, \delta_r, \delta_e$, are given. The method of obtaining these performance functions is also described.

IV. BASIC PERFORMANCE DATA

The aircraft performance data presented in this report are for the F8U-3 airplane carrying three Sparrow III missiles mounted semi-submerged on the fuselage. All performance data at altitude are at combat gross weight-wheels up, G.W. = 30,578 pounds. Wherever the engine had any effect on the data, they are given for the JT4B-22 engine.

All performance data curves are presented in Appendix III. Since some of the data shown are not in the original form as received from the manufacturer, the method used in obtaining this data will be given.

APPENDIX I

This appendix includes the equations of motion in both the wind axes and body axes forms. Table I gives the stability derivatives in wind axes and Table II contains the body axes stability derivatives. The equations which were used to transform the wind axes stability derivatives into body axes stability derivatives will not be given in this report, but they may be found in Appendix II of reference 5, pages 88 and 89.

Given below are the equations of motion in terms of wind axes

Lateral

Roll:

$$\left(s^2 - \frac{L_p}{I_x}s\right)\phi + \left(-\frac{I_{xz}}{I_x}s^2 - \frac{L_r}{I_x}s\right)\psi - \frac{L_\beta}{I_x}\beta - \frac{L_{\delta_a}\delta_a}{I_x} - \frac{L_{\delta_r}\delta_r}{I_x} = 0$$

or

$$(s^2 - l_p s)\phi + (-i_{xz}s^2 - l_r s)\psi - l_\beta \beta - l_{\delta_a}\delta_a - l_{\delta_r}\delta_r = 0$$

Yaw:

$$\left(-\frac{I_{xz}}{I_z}s^2 - \frac{N_p}{I_z}s\right)\phi + \left(s^2 - \frac{N_r}{I_z}s\right)\psi - \frac{N_\beta}{I_z}\beta - \frac{N_{\delta_a}}{I_z}\delta_a - \frac{N_{\delta_r}}{I_z}\delta_r = 0$$

or

$$(-i_{zx}s^2 - n_p s)\phi + (s^2 - n_r s)\psi - n_\beta \beta - n_{\delta_a}\delta_a - n_{\delta_r}\delta_r = 0$$

Side Force:

$$\left(-\frac{Y_p}{mV}s - \frac{g}{V}\right)\phi + \left(1 - \frac{Y_r}{mV}\right)s\psi + \left(s - \frac{Y_\beta}{mV}\right)\beta - \frac{Y_{\delta_a}}{mV}\delta_a - \frac{Y_{\delta_r}}{mV}\delta_r = 0$$

or

$$\left(-Y_p s - \frac{g}{V}\right)\phi + (1 - Y_r)s\psi + (s - Y_\beta)\beta - Y_{\delta_a}\delta_a - Y_{\delta_r}\delta_r = 0$$

Longitudinal

Pitch:

$$\left(s^2 - \frac{M_q + M_{\dot{\alpha}}}{I_y}s - \frac{M_\alpha}{I_y}\right)\alpha + \left(s^2 - \frac{M_q}{I_y}s\right)\gamma - \frac{M_u}{I_y}u - \frac{M_{\delta_e}}{I_y}\delta_e = 0$$

or

$$\left\{s^2 - (m_q + m_{\dot{\alpha}})s - m_\alpha\right\}\alpha + (s^2 - m_q s)\gamma - m_u u - m_{\delta_e}\delta_e = 0$$

Lift:

$$\left(-\frac{L_q}{mV}S-\frac{L_\alpha}{mV}\right)\alpha+\left(1-\frac{L_{\dot\alpha}}{mV}\right)S\gamma-\frac{L_u}{mV}u-\frac{L_{\delta_e}}{mV}\delta_e=0$$

or

$$(-l_q S-l_\alpha)\alpha+(1-l_{\dot\alpha})S\gamma-l_u u-l_{\delta_e}\delta_e=0$$

Drag:

$$\frac{D_\alpha}{mV}\alpha+\left(\frac{q}{V}\right)\gamma+\left(S+\frac{D_u}{mV}\right)u+\frac{D_{\delta_e}}{mV}\delta_e=0$$

or

$$d_\alpha\alpha+\frac{q}{V}\gamma+(S+d_u)u+d_{\delta_e}\delta_e=0$$

The six equations of motion in body axes (principal inertial axis) form are listed below:

1. $$\dot u+wq-vr=X_0+X_u(u-u_0)+X_w(w-w_0)+X_q q+X_{\delta_e}\delta_e+\frac{T}{m}-g\sin\theta$$

2. $$\dot v+ur-wp=Y_v v+Y_p p+Y_r r+Y_{\delta_r}\delta_r+g\cos\theta\sin\phi$$

3. $$\dot w+vp-uq=Z_0+Z_u(u-u_0)+Z_w(w-w_0)+Z_q q+Z_{\delta_e}\delta_e+g\cos\theta\cos\phi$$

4. $$\dot p+\left(\frac{I_z-I_y}{I_x}\right)qr=l_v v+l_p p+l_r r+l_{\delta_a}\delta_a+l_{\delta_r}\delta_r$$

5. $$\dot q+\left(\frac{I_x-I_z}{I_y}\right)rp=m_u(u-u_0)+m_w(w-w_0)+m_{\dot w}\dot w+m_q q+m_{\delta_e}\delta_e$$

6. $$\dot r+\left(\frac{I_y-I_x}{I_z}\right)pq=n_v v+n_p p+n_r r+n_{\delta_a}\delta_a+n_{\delta_r}\delta_r$$

Listed below are some dimensional data of the model F8U-3 Airplane which may be of interest.

S, wing area	= 450 sq. ft.
AR, aspect ratio	= 3.55
b, wing span	= 479.4 in.
$\bar c$, mean aerodynamic chord	= 153.43 in.
W, combat weight-wheels up	= 30,578 lbs.

TABLE I

F8U-3 - Stability Derivatives - Wind Axes

Altitude-Feet	1,000	30,000	50,000
Mach No.	1.17	2.20	2.20
Velocity-Ft./Sec.	1300	2185	2134
C_L	0.0348	0.0320	0.0826
q - lbs/ft^2	1,951	2,122	822
$\eta = \alpha_o$ - deg.	-1.8284	-1.551	-0.322
I_x - slug ft^2	19,955	19,924	19,849
I_y - slug ft^2	115,800	115,800	115,800
I_z - slug ft^2	126,478	126,508	126,583
I_{xz} - slug ft^2	3,413	2,886	590
ℓ_p	-9.27	-4.00	-1.79
ℓ_r	-0.2785	-0.165	-0.070
ℓ_β	-164.3	-84.5	-31.1
ℓ_{δ_a}	-21.05	-17.2	-9.28
ℓ_{δ_r}	+5.07	+6.0	+3.28
n_p	+0.0225	+0.0193	-0.00035
n_r	-1.119	-0.508	-0.248
n_β	+30.35	+5.45	+7.15
n_{δ_a}	+1.012	-1.102	-0.314
n_{δ_r}	-1.34	-2.40	-1.715
y_p *	- - - - -	- - - -	- - - -
y_r *	- - - -	- - - -	- - - -
y_β	-0.841	-0.446	-0.195
y_{δ_a}*	- - - -	- - - -	- - -

* - No data was available

TABLE I - Continued

Altitude-Feet	1,000	30,000	50,000
Velocity-Ft./Sec.	1300	2185	2134
$y_{\delta r}$	+0.00645	+0.0068	+0.0049
Roll Time Constant	0.10 sec.	0.23 sec.	0.54 sec.
Spiral Time Constant	61 sec.	32 sec.	107 sec.
Dutch Roll ζ	14.2%	11.7%	6.8%
Dutch Roll W_n(rad/sec.)	5.47	2.24	2.67
m_q	-1.038	-0.318	-0.1835
$m_{\dot{\alpha}}$	+1.464	+0.276	+0.076
m_α	-69.8	-48.0	-27.2
m_u	+1.25	-1.42	-1.38
$m_{\delta e}$	-42.4	-23.0	-12.9
l_q*	---	---	---
l_α	+2.16	+0.90	+0.40
l_u	+0.0114	+0.0222	+0.0238
$l_{\delta e}$	+0.190	+0.075	+0.039
d_α	+0.0302	+0.0308	+0.0364
d_u	+0.040	+0.0210	+0.011
$d_{\delta e}$*	---	---	---
Short Period ζ	10.2%	6.8%	4.9%
Short Period ω_n(Rad./Sec.)	8.49	6.95	5.22
Phugoid ζ	58.4%	-	62.7%
Phugoid W_n(Rad./Sec.)	0.0347	-	0.0073
Phugoid T_1 (sec.)		-353.5	
Phugoid T_2 (sec.)		43.6	

* - No data was available

TABLE II

F8U-3 STABILITY DERIVATIVES - BODY AXES

Altitude-Feet	1,000	30,000	50,000
Mach No.	1.17	2.20	2.20
Velocity-Ft/sec.	1300	2185	2134
$\eta = \alpha_o$ - deg	-1.8284	-1.551	-0.322
δ - deg	0	0	0
ϵ - deg	2.485	2.485	2.486
D_o - lbs	31,430	28,608	12,059
I_x - slug ft^2	19,846	19,846	19,846
I_y - slug ft^2	115,800	115,800	115,800
I_z - slug ft^2	126,587	126,587	126,587
x_u	-0.04273	-0.02269	-0.01126
x_w	-0.07400	-0.04018	-0.02349
$x_{\dot{w}}$	- - -	- - -	- - -
x_{δ_e}	-7.9015	-4.4328	-0.46024
m_u	-0.00075	-0.00124	-0.00072
$m_{\dot{w}}$	-0.05370	-0.02194	-0.01274
$m_{\dot{w}}$	+0.00113	+0.00013	+0.00004
m_q	-1.0380	-0.31800	-0.18350
m_{δ_e}	-42.400	-23.000	-12.900
z_w	-2.1827	-0.91211	-0.40569
z_u	-0.07997	-0.04631	-0.02598
z_q*	- - -	- - -	- - -
z_{δ_e}	-246.87	-163.81	-83.224
l_v	-0.12226	-0.03838	-0.01446
l_p	-9.3232	-4.0162	-1.7906
l_r	-0.20990	-0.14459	-0.06885

TABLE II - Continued

Altitude-Feet	1,000	30,000	50,000
Velocity-Ft/sec.	1,300	2,185	2,134
l_{δ_a}	-20.949	-17.451	-9.2923
l_{δ_r}	+4.8222	+5.6074	+3.2199
y_v	-0.84100	-0.44600	-0.19500
y_p*	---	---	---
y_r*	---	---	---
y_{δ_a}*	---	---	---
y_{δ_r}	+8.3850	+14.858	+10.457
n_v	+0.02395	+0.00266	+0.00336
n_p	+0.03348	+0.02259	-0.00017
n_r	-1.1177	-0.50759	-0.24793
n_{δ_a}	+1.1168	-1.0277	-0.30594
n_{δ_r}	-1.3638	-2.4232	-1.7148

* - No data was available

NOTE: (1) All angles are measured in radians

(2) All velocities are measured in ft/sec.

APPENDIX II

This appendix includes the performance functions of the lateral and longitudinal variables as influenced by δ_a, δ_r, and δ_e. These quantities define the dynamic relationship of the aircraft variables, i.e.

Longitudinal:

$$\theta = \left\{ [PF]_{\alpha,\delta_e} + [PF]_{\gamma,\delta_e} \right\} \delta_e$$

$$u = [PF]_{u,\delta_e}\, \delta_e$$

Lateral:

$$\beta = [PF]_{\beta,\delta_r} \delta_r + [PF]_{\beta,\delta_a} \delta_a$$

$$\psi = [PF]_{\psi,\delta_r} \delta_r + [PF]_{\psi,\delta_a} \delta_a$$

$$\phi = [PF]_{\phi,\delta_r} \delta_r + [PF]_{\phi,\delta_a} \delta_a$$

Before tabulating the values of the performance functions of the F8U-3, the method of obtaining [PF] will be explained.

For the longitudinal case, we refer back to the longitudinal wind axes equations of motion given in Appendix I. These three equations may be written as:

α	γ	u	δ_e
$s^2 - (m_q + m_{\dot{\alpha}})s - m_\alpha$	$s^2 - m_q s$	$-m_u$	$-m_{\delta_e} = 0$
$-l_q s - l_\alpha$	$(1 - l_{\dot{\alpha}})s$	$-l_u$	$-l_{\delta_e} = 0$
d_α	g/V	$s + d_u$	$d_{\delta_e} = 0$

For a δ_e input to the system, we may rewrite above as

α	γ	u	
$s^2 - (m_q + m_{\dot{\alpha}})s - m_\alpha$	$s^2 - m_q s$	$-m_u$	$= m_{\delta_e} \delta_e$
$-l_q s - l_\alpha$	$(1 - l_{\dot{\alpha}})s$	$-l_u$	$= l_{\delta_e} \delta_e$
d_α	g/V	$s + d_u$	$= -d_{\delta_e} \delta_e$

Using Cramer's rule, we can solve for an α response to a δ_e input. We would have

$$\alpha = \frac{\begin{vmatrix} m_{\delta_e}\delta_e & s^2 - m_q s & -m_\mu \\ l_{\delta_e}\delta_e & (1-l_q)s & -l_\mu \\ -d_{\delta_e}\delta_e & g/V & s+d_\mu \end{vmatrix}}{\begin{vmatrix} s^2-(m_q+m_{\dot\alpha})s-m_\alpha & s^2-m_q s & -m_\mu \\ -l_q s - l_\alpha & (1-l_q)s & -l_\mu \\ d_\alpha & g/V & s+d_\mu \end{vmatrix}}$$

The denominator of the above is known as the stick fixed characteristic equation and will be abbreviated as Δ.

The above determinant may be rewritten as below:

$$\frac{\alpha}{\delta_e} = \frac{\begin{vmatrix} m_{\delta_e} & s^2 - m_q s & -m_\mu \\ l_{\delta_e} & (1-l_q)s & -l_\mu \\ -d_{\delta_e} & g/V & s+d_\mu \end{vmatrix}}{\Delta}$$

where

$$[PF]_{\alpha,\delta_e} = \frac{\alpha}{\delta_e} = \frac{N_{\alpha,\delta_e}}{\Delta}$$

Similarly, $[PF]_{\gamma,\delta_e}$ and $[PF]_{\mu,\delta_e}$ may be solved for.

The lateral performance functions may be derived in a similar manner, i.e.

$$\beta = \frac{\begin{vmatrix} s^2 - l_p s & -\iota_{xz} s^2 - l_r s & l_{\delta a}\delta_a + l_{\delta r}\delta_r \\ -\iota_{zx} s^2 - \eta_p s & s^2 - \eta_r s & \eta_{\delta a}\delta_a + \eta_{\delta r}\delta_r \\ -Y_p s - g/V & (1 - Y_r)s & Y_{\delta a}\delta_a + Y_{\delta r}\delta_r \end{vmatrix}}{\begin{vmatrix} s^2 - l_p s & -\iota_{xz} s^2 - l_r s & -l_\beta \\ -\iota_{zx} s^2 - \eta_p s & s^2 - \eta_r s & -\eta_\beta \\ -Y_p s - g/V & (1 - Y_r)s & s - Y_\beta \end{vmatrix}}$$

or

$$\beta = \frac{\delta_a \begin{vmatrix} s^2 - l_p s & -\iota_{xz} s^2 - l_r s & l_{\delta a} \\ -\iota_{zx} s^2 - \eta_p s & s^2 - \eta_r s & \eta_{\delta a} \\ -Y_p s - g/V & (1 - Y_r)s & Y_{\delta a} \end{vmatrix}}{\Delta} + \frac{\delta_r \begin{vmatrix} s^2 - l_p s & -\iota_{xz} s^2 - l_r s & l_{\delta r} \\ -\iota_{zx} s^2 - \eta_p s & s^2 - \eta_r s & \eta_{\delta r} \\ -Y_p s - g/V & (1 - Y_r)s & Y_{\delta r} \end{vmatrix}}{\Delta}$$

Hence,

$$\beta = [PF]_{\beta\delta a}\,\delta_a + [PF]_{\beta\delta r}\,\delta_r = \frac{N_{\beta\delta a}\,\delta_a}{\Delta} + \frac{N_{\beta\delta r}\,\delta_r}{\Delta}$$

The remaining lateral performance functions may be obtained in the same manner.

The performance functions for the F8U-3 for the three flight conditions considered will now be listed:

CaseI: V_T = 1300 fps at 1,000 feet

Lateral

$$\triangle = +0.99538\, s\, (s + 0.01645)\, (s + 9.7107)\, (s^2 + 1.5548\, s + 29.959)$$

$$N_{\beta,\delta_a} = -0.44365\, s\, (s + 0.06283)\, (s + 21.181)$$

$$N_{\beta,\delta_r} = +0.00642\, s\, (s + 0.01200)\, (s + 10.369)\, (s + 187.45)$$

$$N_{\psi,\delta_a} = +0.44365\, (s - 0.78027)\, (s + 1.6901)\, (s + 20.009)$$

$$N_{\psi,\delta_r} = -1.2031\, (s + 10.251)\, (s^2 + 0.68108\, s + 0.13313)$$

$$N_{\phi,\delta_a} = -20.877\, s\, (s^2 + 1.9828\, s + 23.598)$$

$$N_{\phi,\delta_r} = +4.8409\, s\, (s - 2.7732)\, (s + 4.6513)$$

Longitudinal

$$\triangle = (s^2 + 0.04049\, s + 0.00120)\, (s^2 + 1.7335\, s + 72.040)$$

$$N_{\alpha,\delta_e} = -0.19000\, (s + 224.20)\, (s^2 + 0.04000\, s + 0.00042)$$

$$N_{\gamma,\delta_e} = +0.19000\, (s + 0.03971)\, (s + 20.092)\, (s - 20.517)$$

$$N_{u,\delta_e} = +0.00103\, (s + 1.5076)\, (s + 1247.3)$$

Case II; V_T = 2185 fps at 30,000 feet

Lateral

$$\triangle = +0.99670\, s\, (s + 0.03080)\, (s + 4.4127)\, (s^2 + 0.52637\, s + 5.0168)$$

$$N_{\beta,\delta_a} = +1.4942\, s\, (s - 0.02787)\, (s + 3.0289)$$

$$N_{\beta,\delta_r} = +0.00678\, s\, (s + 0.00531)\, (s + 4.2244)\, (s + 334.22)$$

$$N_{\psi,\delta_a} = -1.4942\, (s + 3.3650)\, (s^2 + 0.25335\, s + 0.56235)$$

$$N_{\psi,\delta_r} = -2.2632\, (s + 4.2672)\, (s^2 + 0.35915\, s + 0.27610)$$

$$N_{\phi,\delta_a} = -17.360\, s\, (s^2 + 0.93885\, s + 11.269)$$

$$N_{\phi,\delta_r} = +5.6522\, s\, (s - 5.1835)\, (s + 6.1327)$$

Longitudinal

Δ = (s-0.00283) (s +0.02292) (s^2 + 0.94291 s +48.287)

N_{α,δ_a} = -0.07500 (s +306.98) (s^2 +0.02100 s + 0.00026)

N_{γ,δ_e} = +0.07500 (s +0.02026) (s - 15.078) (s +15.121)

N_{u,δ_e} = +0.00120 (s +0.35568) (s +588.34)

Case III; V_F = 2134 fps at 50,000 feet

Lateral

Δ = 0.99986 s (s +0.00933) (s +1.8593) (s^2 + 0.36496 s + 7.1482)

N_{β,δ_a} = +0.35724 s (s -0.07709) (s +1.2489)

N_{β,δ_r} = +0.00490 s (s +0.00452) (s +1.8311) (s +347.13)

N_{γ,δ_a} = -0.35724 (s +2.2558) (s^2 -0.49660 s + 1.4253)

N_{γ,δ_r} = -1.6997 (s +1.8890) (s^2 +0.09261 s +0.14045)

N_{ϕ,δ_a} = -9.2893 s (s^2 +0.44038 s +8.2419)

N_{ϕ,δ_r} = +3.2291 s (s - 2.8242) (s + 3.2614)

Longitudinal

Δ = (s^2 +0.00915 s +0.00005276) (s^2 +0.50935 s + 27.274)

N_{α,δ_e} = -0.03900 (s +330.95) (s^2 +0.01100 s +0.000296)

N_{γ,δ_e} = +0.03900 (s +0.00875) (s -10.198) (s +10.307)

N_{u,δ_e} = +0.000831 (s +0.13171) (s +565.10)

APPENDIX III

This appendix presents basic performance data currently available on the F8U-3 in the forms of graphs. In several cases, it was necessary to perform calculations to obtain the curves shown. In these cases, the method used to obtain these curves will be stated.

The maximum velocity envelope of the F8U-3 for different altitudes is shown in figure 3. A curve showing where the aircraft structural limitations occur is also given. Indicated in cross marks on the speed profile are the aircraft velocities and altitudes at which the stability derivatives were obtained. The maximum velocity envelope shown is for the JT4B-22 engine. The velocity profile has been obtained through use of the five equations listed below. The points at which calculations were performed to obtain this speed profile are shown by a circled-dot.

1) $q = 1/2 \rho V^2$

2) $C_L = \frac{NW}{qs}$ where N = 1 for the speed profile

3) $C_D = C_{D_o} + \frac{C_L^2}{\pi (AR) e}$

4) $D = C_D qs$

5) When $D = T_{available}$, this is the maximum velocity at that altitude.

In figure 4, the net thrust that is available is given for different altitudes over a range of various mach numbers. These net thrust curves are for maximum reheat power only and are given for the JT4B-22 engine.

Figure 5 shows the zero lift drag versus mach number for the F8U-3. This figure contains curves of the zero lift drag coefficient, C_{D_o}, for either missiles on or missiles off.

The drag due to lift is given in figure 6. Here, oswald's efficiency factor, e, is plotted versus mach number for several different values of the lift coefficient, C_L.

Figure 7 contains the drag summary for the F8U-3, where the lift coefficient, C_L, is plotted versus the coefficient of drag, C_D, for various mach numbers. The curves shown in this figure have been obtained through use of equations 1, 2, and 3 previously-listed in this appendix and figures 5 and 6.

In figure 8, the F8U-3 lift curve slope variation, $C_{L_{\alpha}}$, versus mach number is given. This curve has been obtained through use of the trimmed lift coefficient, $C_{L_{TRIM}}$, versus $\alpha_{FUSELAGE}$ for different mach number curves, which were given in reference 4.

Figure 9 gives the maximum tactically usable lift coefficient for various mach numbers for this aircraft.

In figures 10 through 12, the amount of thrust that is required for the aircraft to sustain different steady state load factors for various fighter speeds is shown. Also shown in the figure is the net thrust available from maximum power settings. The data shown in each figure has been obtained for the aircraft flying at a constant altitude and using the JT4B-22 engine. These curves have been calculated by using equations 1 through 4 previously listed in this appendix and figure 4. However, in equation 2, N now assumes values of either 1,2,3 or 4 gees.

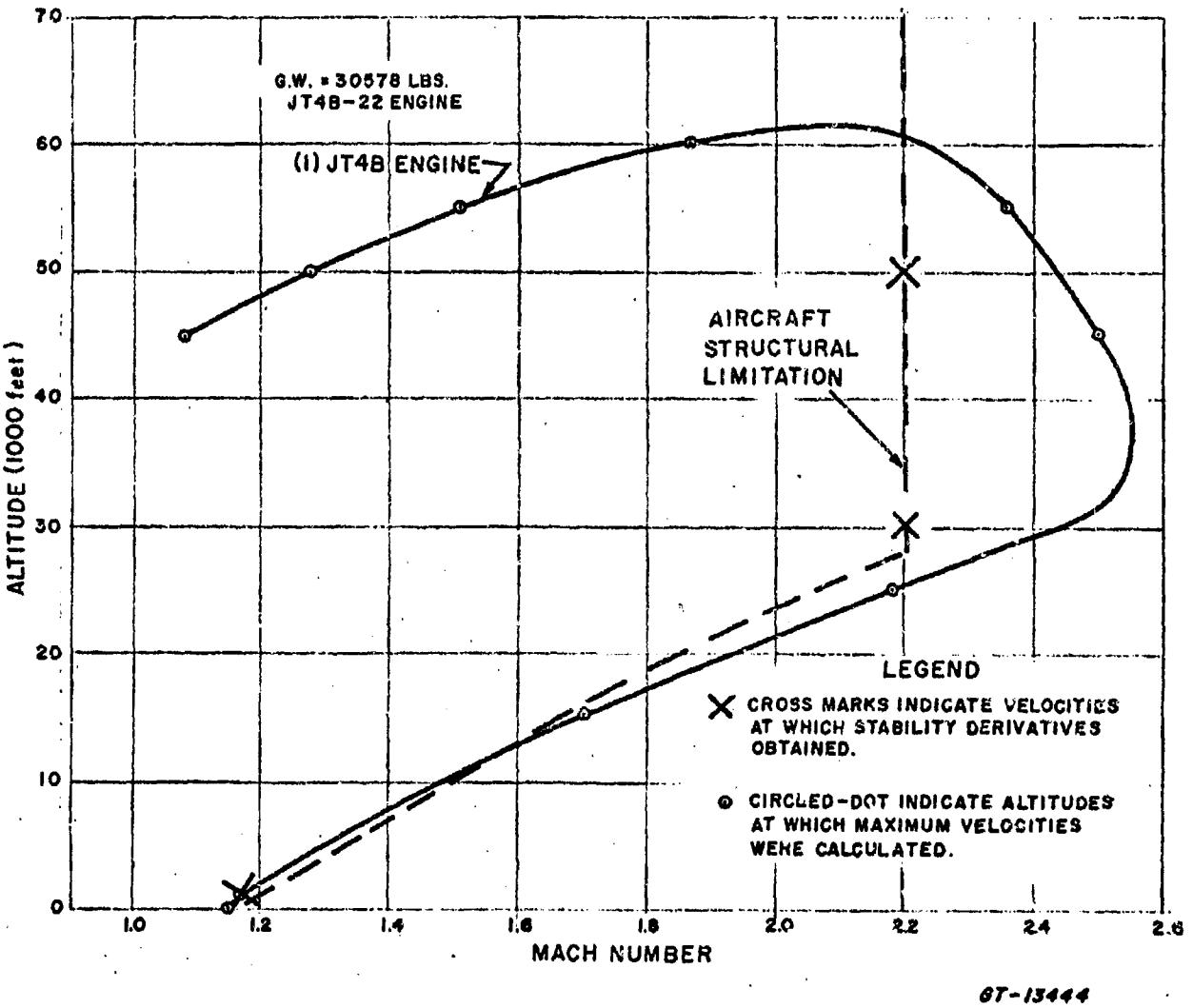

Figure 3. F8U-3 Maximum Velocity Profile

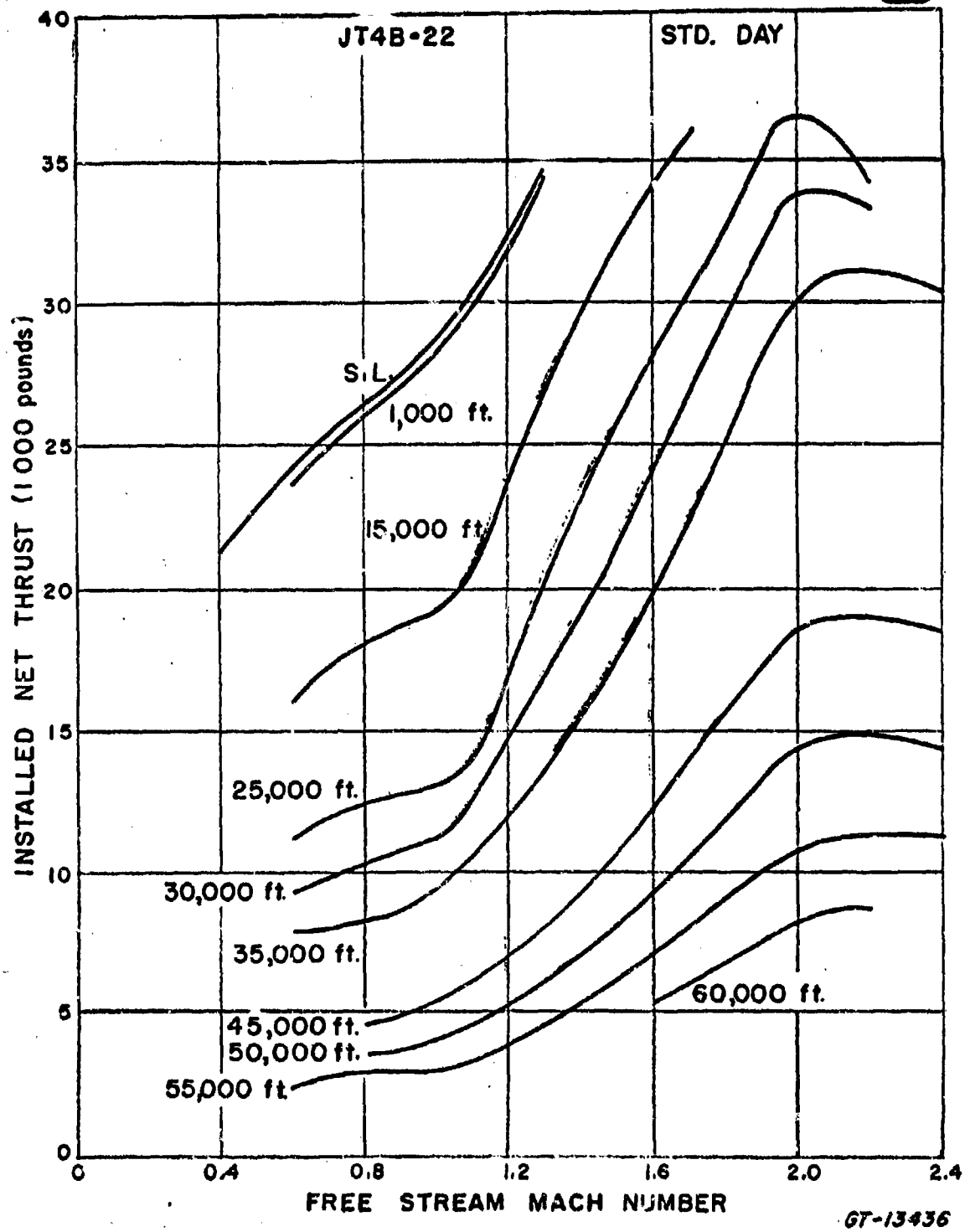

Figure 4. F8U-3 Estimated Installed Net Thrust, Maximum Reheat, for JT4B-22 Engine

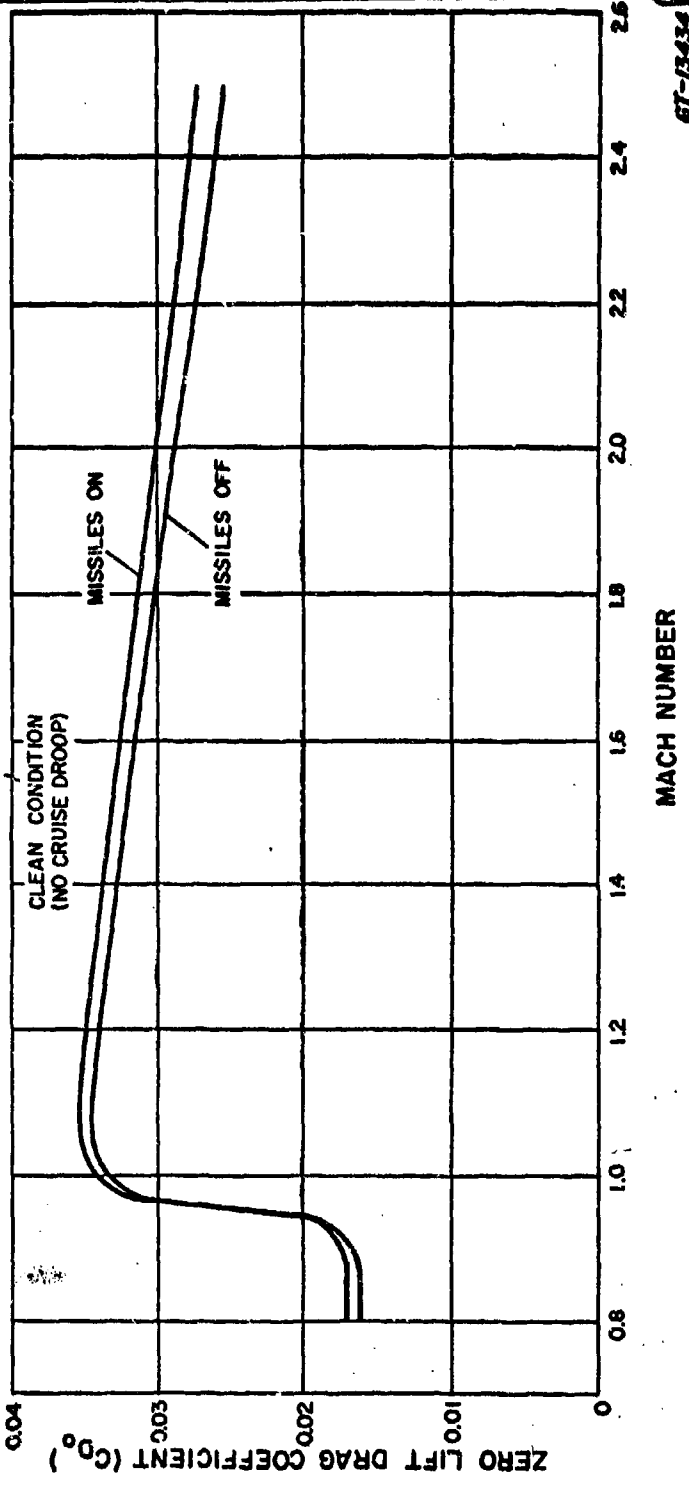

Figure 5. F8U-3 Zero Lift Drag vs. Mach Number

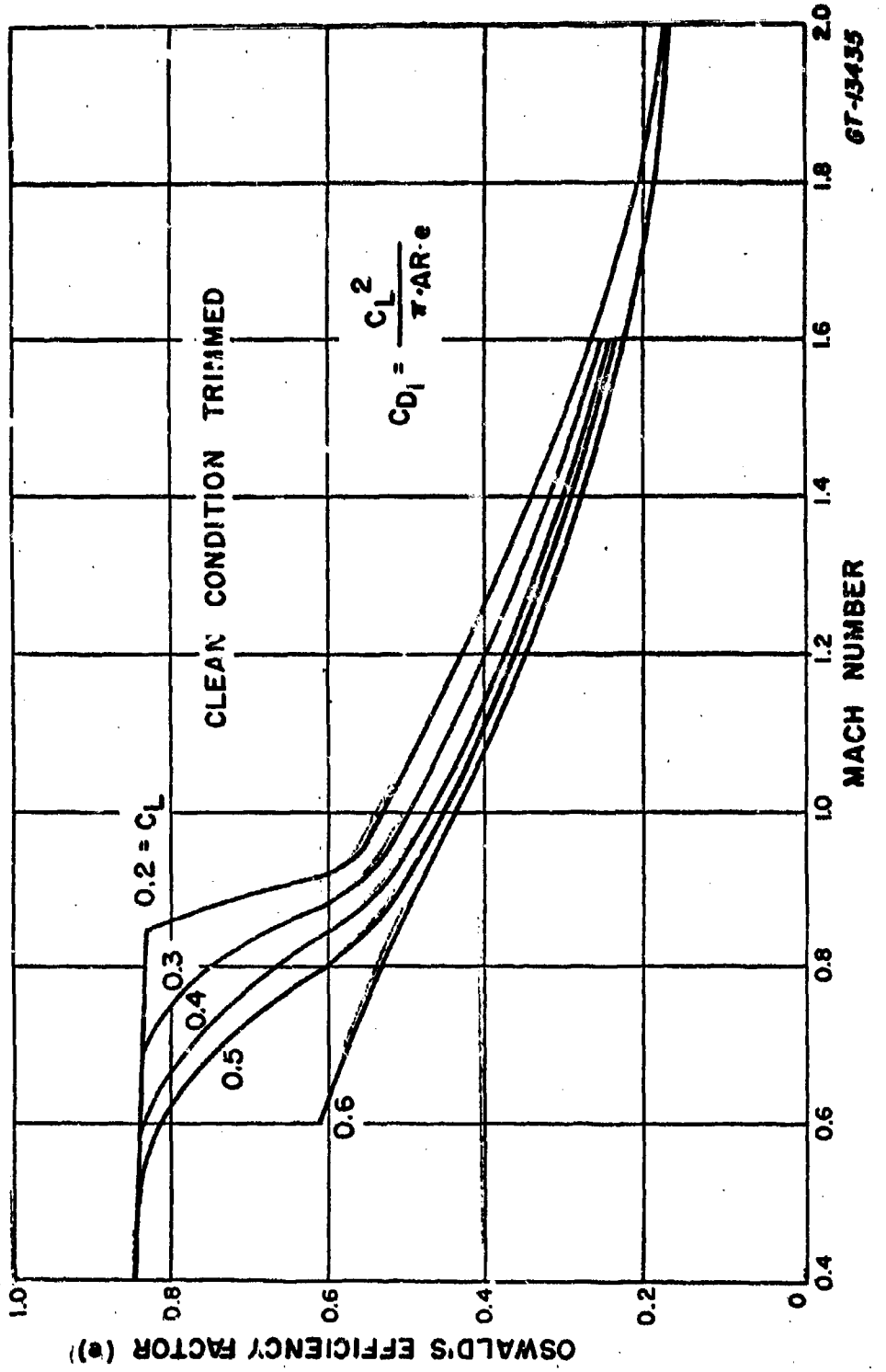

Figure 6. F8U-3 Drag Due to Lift

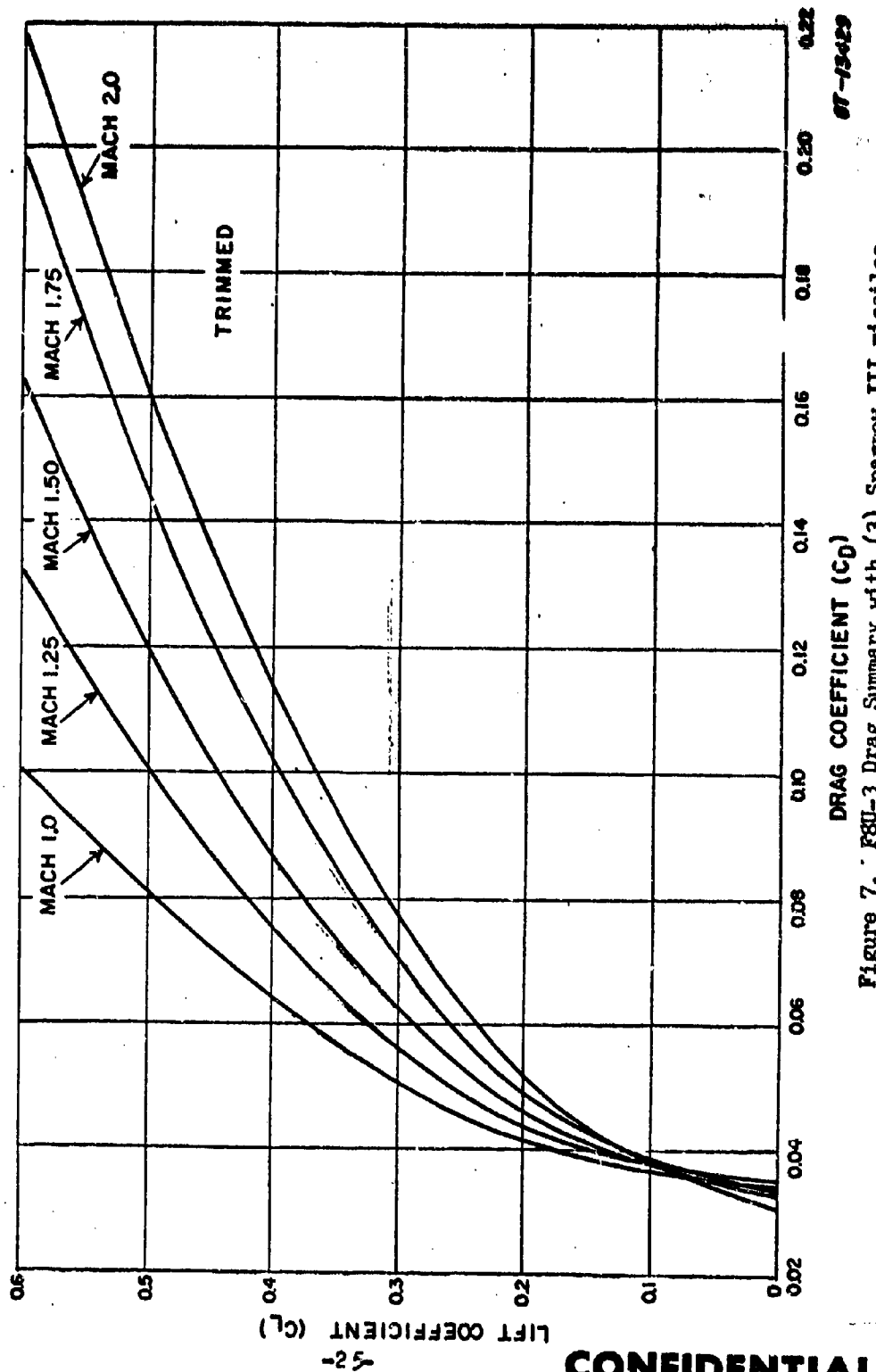

Figure 7. F8U-3 Drag Summary with (3) Sparrow III missiles

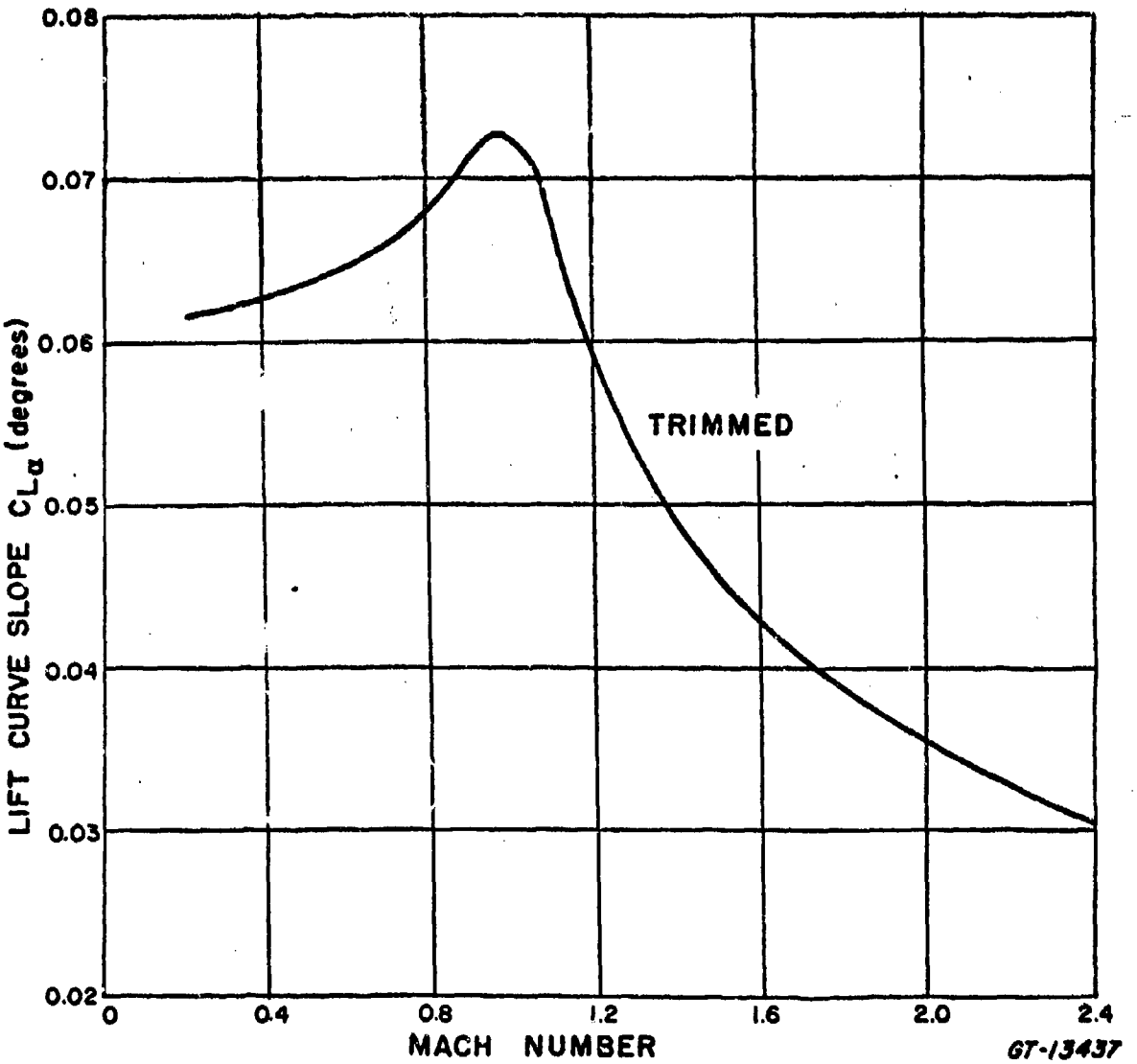

Figure 8. F8U-3 Lift Curve Slope Variation With Mach Number

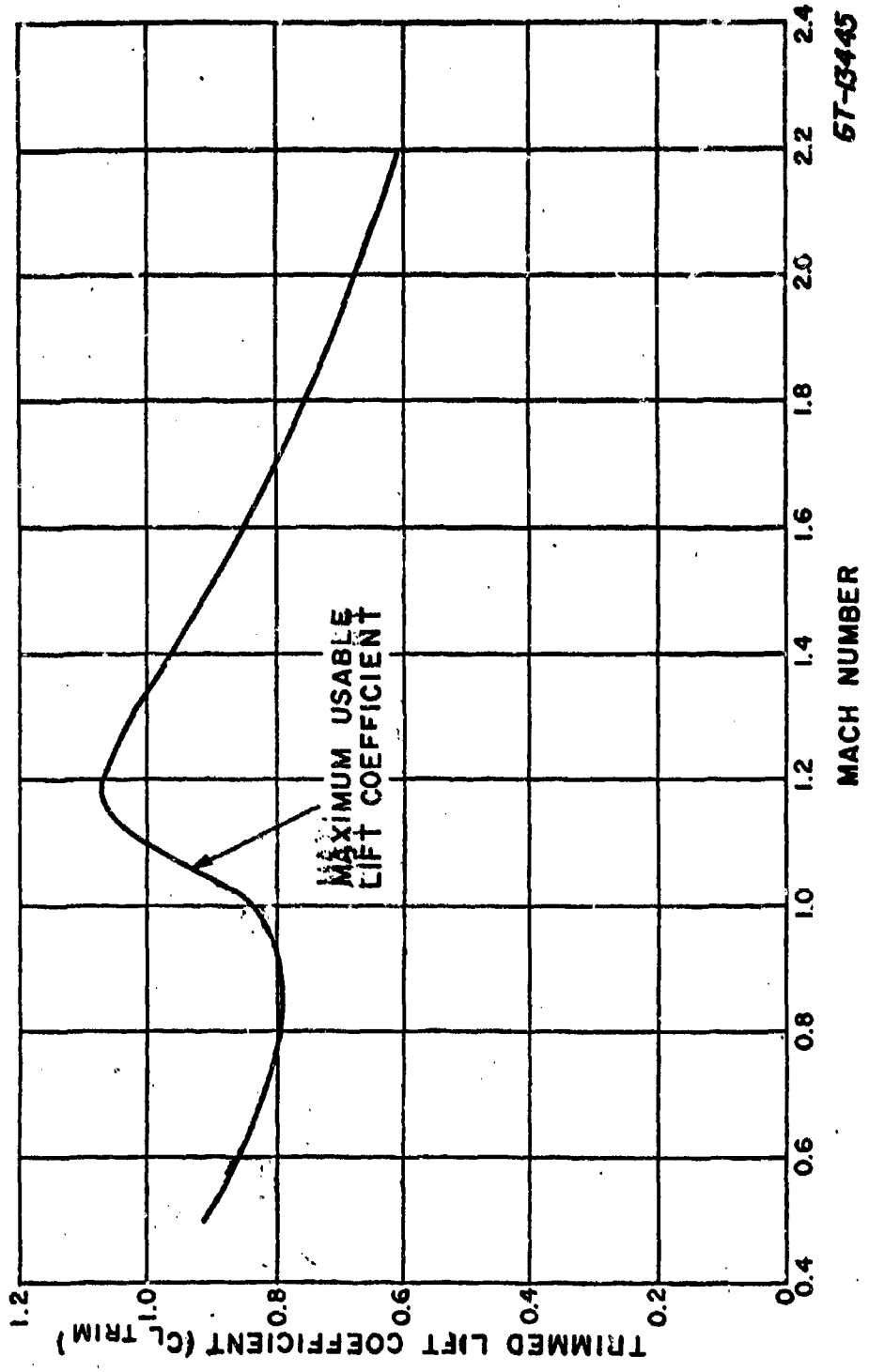

Figure 9. F8U-3 Maximum Usable Lift

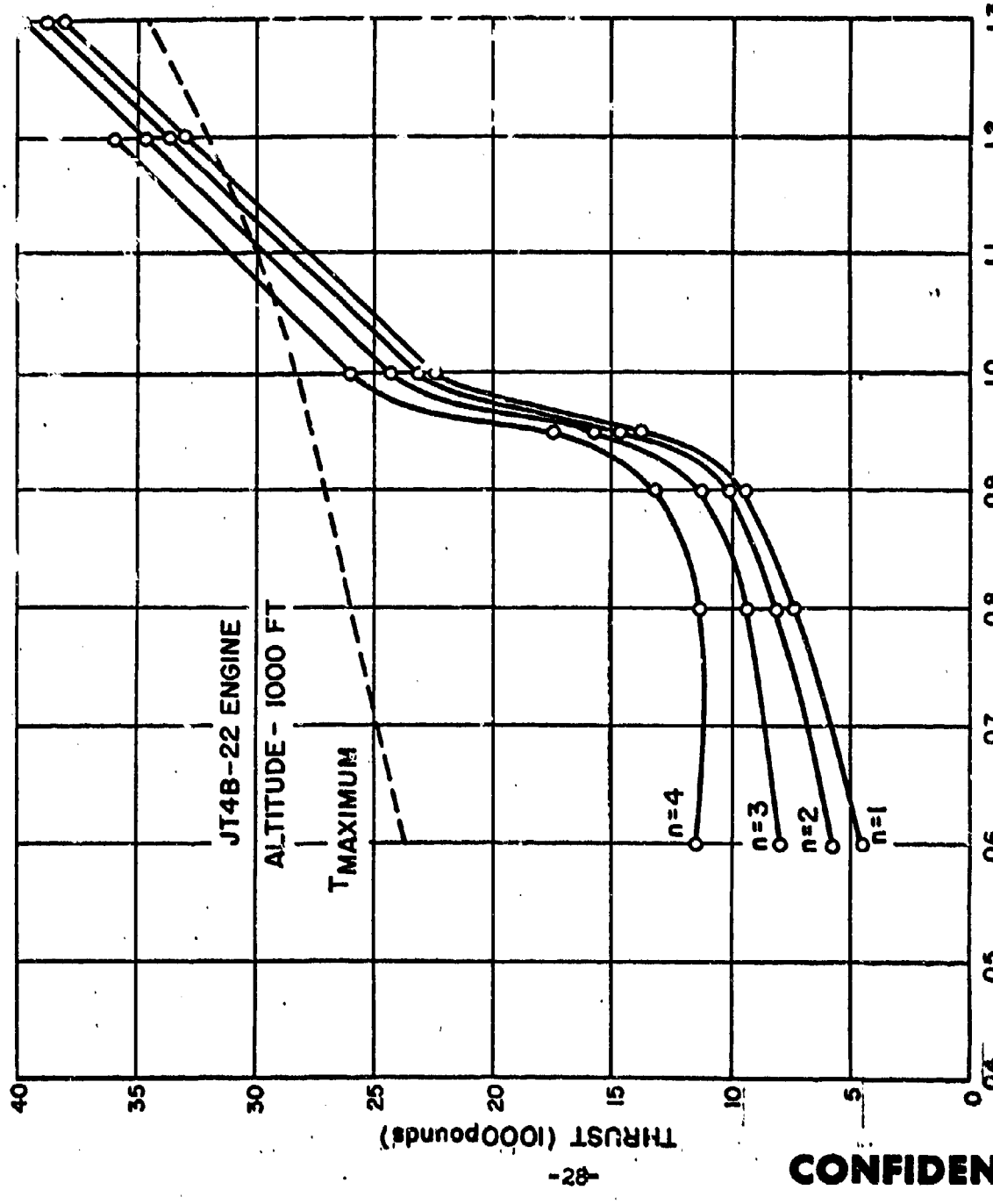

Figure 10. Required and Available Thrust versus Mach Number for Different Steady-State Load Factors

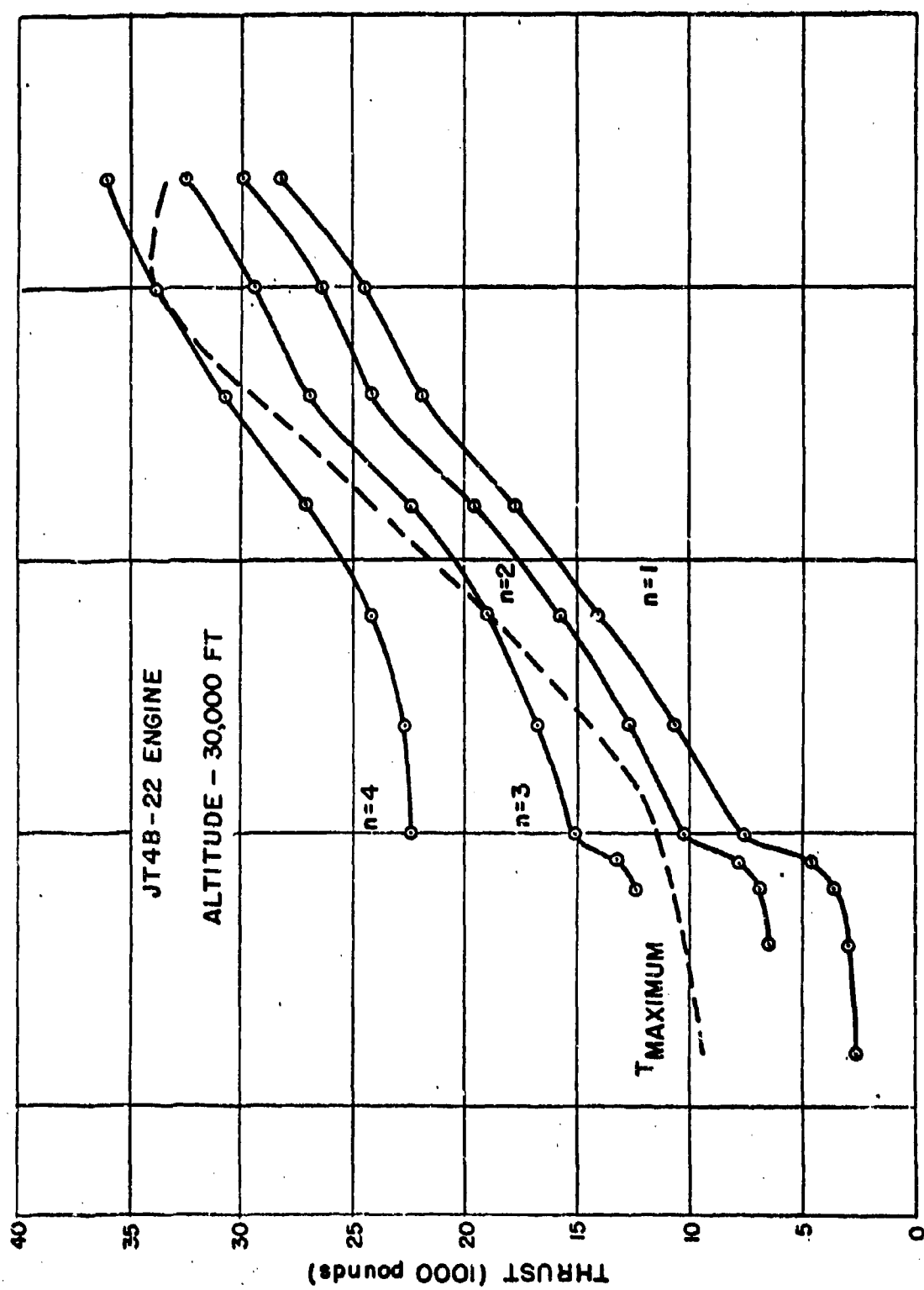

67-13446

Figure 11. Required and Available Thrust versus Mach Number for different Steady State Load Factors

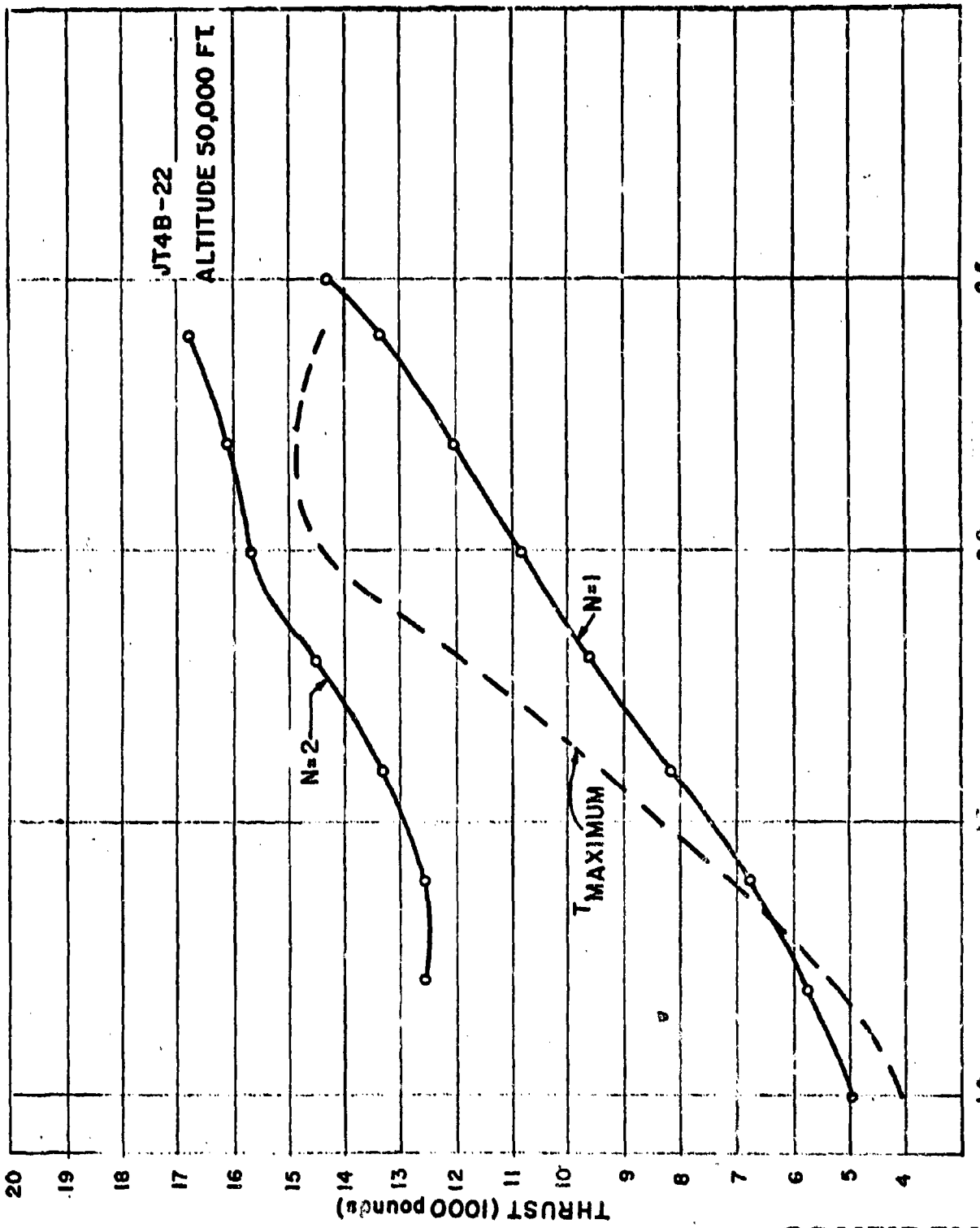

Figure 12. Required and Available Thrust versus Mach Number for Different Steady-State Load Factors

GLOSSARY OF SYMBOLS

α_F	- Angle between the velocity vector and the water line of the aircraft.
γ	- Climb angle of the aircraft.
η, α_o	- Angle between the velocity vector and the principal inertia axis of the aircraft.
ξ	- $\alpha_F - \eta$
ρ	- Density (slugs/ft^3)
AR	- Aspect Ratio
b	- Wing span
$\bar{c}$	- Mean aerodynamic chord
C_D	- Coefficient of drag
C_{D_o}	- Zero lift drag coefficient
C_L	- Coefficient of lift
C_{L_α}	- Partial of lift with respect to α
D	- Drag of aircraft
e	- Oswald's efficiency factor
M	- Mach number
m	- Mass of aircraft
N	- Number of gees
q	- Dynamic pressure
s	- Wing area of aircraft
T	- Thrust of aircraft engine
V_F	- Velocity of aircraft (ft/sec.)
W,C.W.	- Weight of aircraft at combat-wheels up

REFERENCES

1. Navy Missile Study Technical Report #1, "F4H-1 Stability Derivatives (Wind and Body Axes) and Dynamic Characteristics", (Proprietary Information, McDonnell Aircraft Co.), by R. B. Tucker, Westinghouse Electric Corp., Air Arm Plant, dated 9 May 1957, Confidential.

2. Chance-Vought Report No. 11002, "F8U-3 Preliminary Aerodynamic Data for Autopilot Design", dated 13 August 1957, Confidential.

3. Chance-Vought Report No. 9876. "This report presents the performance characteristics of the Chance-Vought Model V-401 airplane". Confidential.

4. Chance-Vought Letter E-7-3378, dated 20 August 1957 to NRL, Washington, D.C., Enclosures 1 through 8. Subject: "Model F8U-3 Airplane - Aerodynamic and Propulsion Data." Confidential.

5. McCourt, A. W., Westinghouse Electric Corp., Air Arm Plant, "Aspects of the Linearized Equations of Aircraft Motion Used in Flight Control System Design", Appendix I, page 84 and Appendix II, pages 88 and 89. Doctoral Dissertation, University of Pittsburgh, Pittsburgh Pennsylvania, dated 1956.

6. Navy Missile Study Trip Report #3, by J. F. Buchan, Westinghouse Electric Corp., Air Arm Plant, dated 3 July 1957. Place - Chance-Vought Aircraft, Dallas, Texas, Confidential.

7. Westinghouse Trip Report No. 2746, by J. F. Buchan, dated 4 March 1957. Place - Chance-Vought Aircraft, Dallas, Texas. Confidential

Analytical Section Technical Memorandum No. 229

APPENDIX II

A METHOD OF EVALUATING RECOVERY CAPABILITY OF AN INTERCEPTOR AFTER A PULLUP ATTACK

By

E. C. Quesinberry

Distribution:

100 - D. J. Povejsil, Mgr.
103 - K. N. Satyendra, Adv. Engr.
103 - R. J. Clanton, Supv. Engr.
103 - F. H. Tyaack, Supv. Engr.
103 - L. Atran
103 - J. F. Buchan
103 - R. R. Dougan
103 - M. Mazina
103 - B. O. Van Hook (5)
103 - R. B. Tucker
103 - E. C. Quesinberry (4)

003 - 103 - 100 - C - 90114
9-16:rr

Synopsis

This report concerns the criteria for detecting the failure of pullup attacks by examining the recovery maneuver which must follow the attack.

The minimum value of load factor N_Z or $\frac{L}{W}$ during the recovery exposes the worst flight limitations of the maneuver. The minimum value of N_Z is calculated by assuming a constant-energy trajectory with variable load factor and constant $C_{L\ max}$.

Recovery From Pull-up Attacks

I. Introduction

In processing digital computer calculations of pull-up trajectories, some unsuccessful attacks can be classified immediately. Other attacks which appear to be satisfactory are actually unsuccessful because the fighter has difficulty in recovering from the flight conditions occuring at the end of the pull-up.

In order to determine which attacks fail from poor recovery conditions, the type of recovery maneuver must be specified, as well as the parameter limits which determine a suitable recovery. After these decisions are made, a method of calculating the quantities which indicate undesirable recoveries without involving additional computer use is desirable. Such a method can be derived from the constant energy pull-up concept discussed in an existing Air Arm report.* This proposed method is discussed in Sections 3.2 and 3.3.

2. Discussion of Recovery Maneuvers

A pull-up attack is assumed to end at the impact of the missile with the target. The recovery maneuver then begins. This maneuver should most rapidly allow the aircraft to (1) avoid the impact vicinity and (2) regain speed and a desirable flight attitude.

Some pull-up attacks break off with the fighter in an inverted position, that is, the flight path angle is between 90 and 180 degrees. From this position, a fast recovery is to utilize the pull of gravity in increasing the rate of rotation of the Velocity Vector. It is assumed that the flight path angle will be equal to or greater than 180° before the aircraft is rolled upright or the loop completed by the pilot.

Other pull-up attacks break of with the flight path angle between 0° and 90°. The pilot can then decrease the angle of attack, roll the plane into an inverted position, regain the angle of attack and again allow gravity to aid in increasing the rate of rotation of the velocity vector so that a rapid recovery may be achieved.

It seems reasonable to assume that the value of normal g's, N_z, at the top of the recovery trajectory will indicate the lowest performance capability of the aircraft during the recovery maneuver, since deceleration has ended at this point and velocity is a minimum. See equation (5) section 3.1. At all points occuring later, velocity has been regained and the performance capability of the aircraft should have improved. A minimum load factor, N_z can be specified for a particular aircraft and all pull-up attacks whose recovery maneuvers involve N_z less than that specified can be rejected as unsuccessful.

* Air Arm Report No. AA-1416
Pull-up Manouvers by R. R. Dougan

3. Equations of Motion

3.1 Basic Assumptions

As discussed in a previous report* the constant energy pull-up results if thrust is assumed equal to drag throughout the maneuver. The simplified equations of motion of an aircraft in the vertical plane then become

$$m\dot{V} = -mg\sin\gamma \qquad (1)$$

$$mV\dot{\gamma} = N_z mg - mg\cos\gamma \qquad (2)$$

where m = mass of aircraft in slugs

V = velocity of aircraft in ft/sec.

g = 32.17 ft/sec^2.

N_z = Load factor $\frac{L}{W}$

where L = lift in pounds
W = weight of aircraft in pounds

The conditions of the recovery maneuver may be approximated by assuming constant energy and constant C_L max with variable load factor.

$$\text{Load factor } N_z = \frac{L}{W} \qquad (3)$$

$$L = C_L \tfrac{1}{2} \rho V^2 S \qquad (4)$$

where C_L = Coefficient of lift

ρ = air density

S = wing area

W is assumed constant

ρ is assumed constant for the altitude change of the recovery maneuver. S is constant.

For the low velocity and high altitude at the end of a pull-up attack V and ρ are small so that the maximum value of lift coefficient C_L is needed for the value of lift, L, required for the maneuver. C_L is assumed equal to $C_{L_{max}}$ and $C_{L_{max}}$ is assumed constant at the altitude and speed of the recovery maneuver.

V is, therefore, the variable affecting N_z, and N_z is proportional to the square of aircraft velocity. For this assumption

$$N_z = N_{z_0} \frac{V^2}{V_0^2} \qquad (5)$$

The subscript zero donates conditions at the start of the recovery maneuver.

3.2 Equation of Recovery Trajectory

Since N_z at the top of the recovery trajectory has been selected for evaluation of satisfactory maneuvers, an equation of this trajectory involving only flight path angle, γ, and load factor N_z is desirable.

To obtain this equation, V can be eliminated from equations (1) and (2) by substituting the relationship from equation (5). If the resulting two equations are then multiplied together and integrated between the limits γ_0, N_{z_0} and γ, N_z, the desired equation is obtained:

$$(6) \quad N_z^3 - 6N_z^2 \cos\gamma + 9\cos^2\gamma N_z = N_{z_0}^3 - 6N_{z_0}^2 \cos\gamma_0 + 9\cos^2\gamma_0 N_{z_0}$$

Since γ is 180° for minimum N_z, (-1) can be substituted for $\cos\gamma$ above. Equation (6) then becomes

$$(7) \quad N_z^3 + 6N_z^2 + 9N_z = N_{z_0}^3 - 6N_{z_0}^2 \cos\gamma_0 + 9\cos^2\gamma_0 N_{z_0}$$

The values of N_{z_0} and γ_0 at the start of the recovery maneuver are the N_z max and γ existing at the end of the pull-up attack if the aircraft is not rolled. If roll effects and roll time are assumed negligible, N_{z_0} remains after roll as the value for $C_L = C_{L\,max}$ at the end of the pull-up attack, and γ immediately before roll becomes 180 - γ after roll.

3.3 Solution of Recovery Trajectory Equation

When values for initial conditions are substituted in equation (6) for a given recovery trajectory, this equation assumes the form

$$N_z^3 + 6N_z^2 + 9N_z - K = 0$$

In solving this equation by Lin's method the significant root is the one obtained by starting with a trial divisor equal to $-\frac{K}{9}$. This root can be quickly determined.

3.4 Comparison of Results

Solutions of equation 6 have been compared with values obtained from calculation of trajectories of a modern military aircraft by a digital computer. The agreement was found to be good.

As an example, a portion of a loop trajectory calculated by a digital computer for a representative aircraft was chosen with limits corresponding to a recovery maneuver starting with $\gamma_o = 123.6°$ and $N_{z_o} = 1.70$, and ending by completing the loop. Since the main point of interest was for minimum N_z at $\gamma = 180°$, equation 7 was used and N_z at $\gamma = 180°$, was found to be 1.13. The nearest point to $\gamma = 180°$ tabulated by the computer was 180.97° for which N_z equaled 1.129. Flight was at $C_{L\ max}$ between the limits studied. The portion of the maneuver examined began at 26,000 feet and ended at 28,000 feet.

4. Conclusions

Equation 6 is recommended for use when evaluating recovery maneuvers of the type discussed in this report.

If maneuvers are performed at low altitudes and involve large altitude changes or if thrust differs greatly from drag the validity of equation 6 should be tested before its use.

For maneuvers involving reasonable altitude increments at moderate to high altitudes, results calculated should agree closely with actual conditions.

Contours of Constant Load Factor
Ng at Top of Recovery Trajectory
Vs. Max. Load Factor and Flight-Path
Angle At Start of Recovery Maneuver

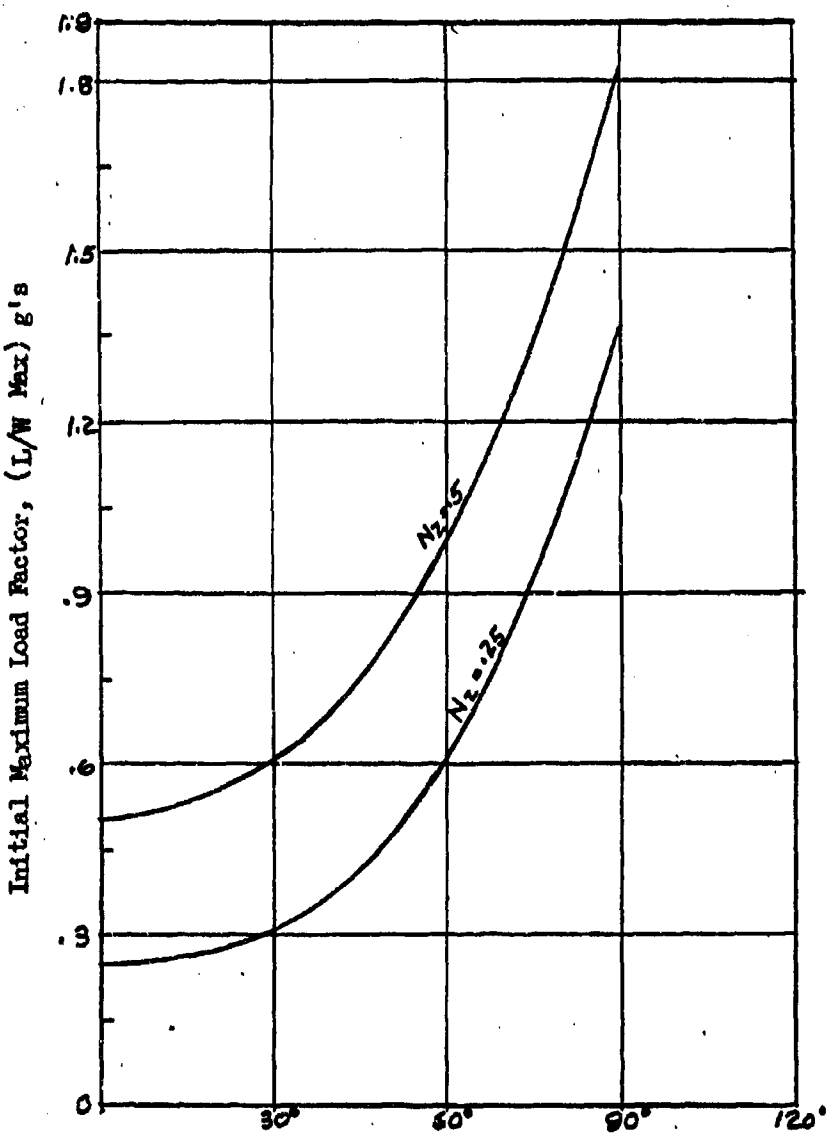

NAVY MISSILE STUDY TECHNICAL REPORT # 7

APPENDIX III

Head-On Pull-Up Capability Of XIA Weapon System With F4H-1

by

B. O. Van Hook

Navigation and Flight Control Group

October 29, 1957

Charge No. 003-10?-100-C-90114
10/30/57

Abstract

This report presents the results of an investigation of the pull-up capability of the XIA interceptor weapon system against targets at higher altitudes flying a head-on course.. F4H-1 aircraft characteristics were used. Missile capability is described by means of maximum and minimum range equations and an expression for the average relative missile speed. In general the attacks involved detection, an acquisition manuver, a lead pursuit course to within firing range, a lead pursuit illumination segment and an analysis of the recovery manuver. The limitations on capability resulting from various system parameters are presented.

TABLE OF CONTENTS

List of Figures

List of Tables

1. Objective - This study was undertaken to determine the capability of the XIA Weapon System for pull-up attacks in the head-on case.

2. Investigation Procedure

2.1 Scope - For this investigation targets at 65,000, 50,000 and 30,000 feet are examined for vulnerability. Target and interceptor speeds of Mach 2.0 or V max. and Mach 0.9 are considered. Figure 1 gives V max. figures for the F4H-1 below 30,000 feet.

2.2 Attack Doctrine - The attack begins at the AI radar detection range. For Mach 0.9 interceptors, maximum thrust acceleration is begun while maintaining level flight. Mach 2.0 interceptors continue level flight. At a specified time after detection, pull-up to a lead-pursuit course is begun. The pull-up is accomplished at a constant value of normal acceleration (L/W) or at maximum lift (C_L max.) if this limitation of L/W is less than the specified value. When the following criteria are met, the missile is launched.

1. Launch error (ϵ) $< 10°$
2. $R_{max} > R > R_{min}$.

A lead-pursuit course is maintained by the interceptor after launch to provide illumination of the target until impact. If the acceleration of the course exceeds the capability of the interceptor a $C_{L\ max.}$ course is flown. The time of flight of the missile is computed by

1. $\dfrac{\text{Sin } \gamma}{(Vo + V_F)\, t_f} = \dfrac{\text{Sin } \psi}{R}$

2. $t_f = \dfrac{\text{Sin } \gamma}{\text{Sin } \psi} \dfrac{R}{(Vo + V_F)}$

See Figure 2

At impact the interceptor performs a breakaway maneuver to complete the attack. For this evaluation the breakaway maneuver consists of completion of a loop with a minimum value for L/W of 0.5 g's at the peak altitude of the maneuver. See Reference 1.

2.3 Attack Computation

2.3.1 AI Detection Range is determined by using the head-on, co-altitude range for a B-47 target. Figure 3 shows the ranges of the current AI radar for cumulative detection probabilities of 50 and 85%. The horizontal separation at detection was assumed to be constant for all incremental altitudes.

2.3.2 Interceptor Horizontal Acceleration data was obtained from a digital computation that used the model developed from lift, drag and power plant data of the F4H-1. See Reference 2 and 3.

MODEL F4H-1
$V_{MAX.}$ VS ALTITUDE
0 TO 30,000 FT
G.W 36,000 LBS.
MAXIMUM VELOCITY OF F4H-1
FIGURE 1

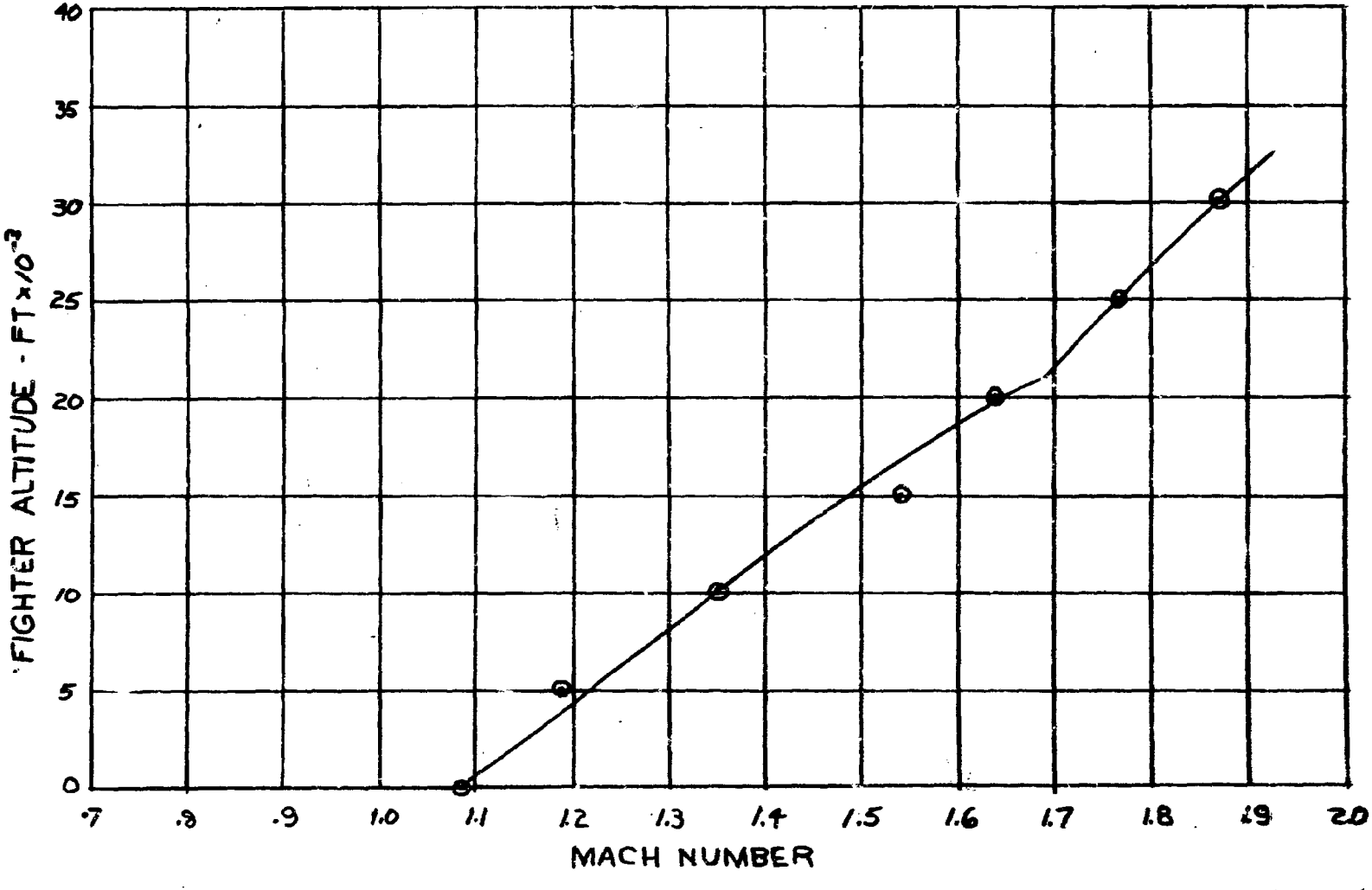

V_o - AVERAGE RELATIVE MISSILE VELOCITY - FT/SEC

V_F - INTERCEPTOR VELOCITY - FT/SEC.

V_T - TARGET VELOCITY - FT/SEC

t_f - MISSILE TIME OF FLIGHT - SEC

R - RANGE - FT.

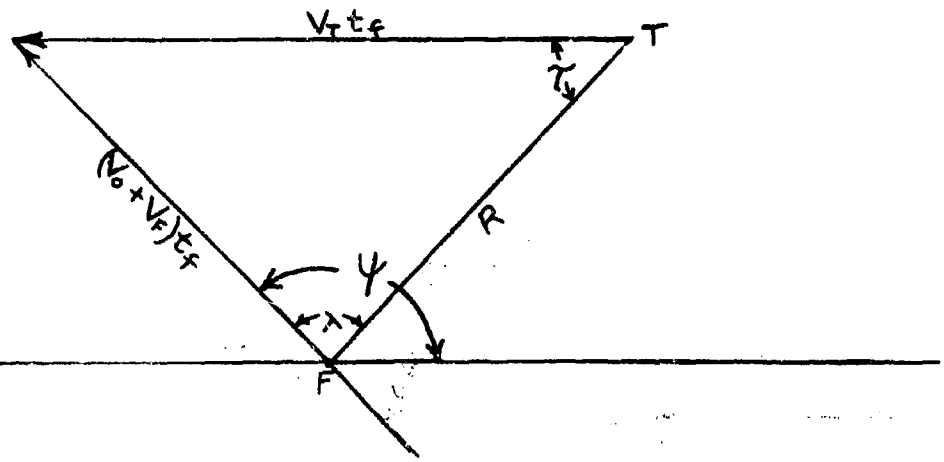

LEAD PURSUIT GEOMETRY

FIGURE 2.

HORIZONTAL DETECTION RANGE VS. RANGE RATE
CUMULATIVE PROBABILITY OF DETECTION - 50% AND 85%
B-47 TARGET, HEAD ON

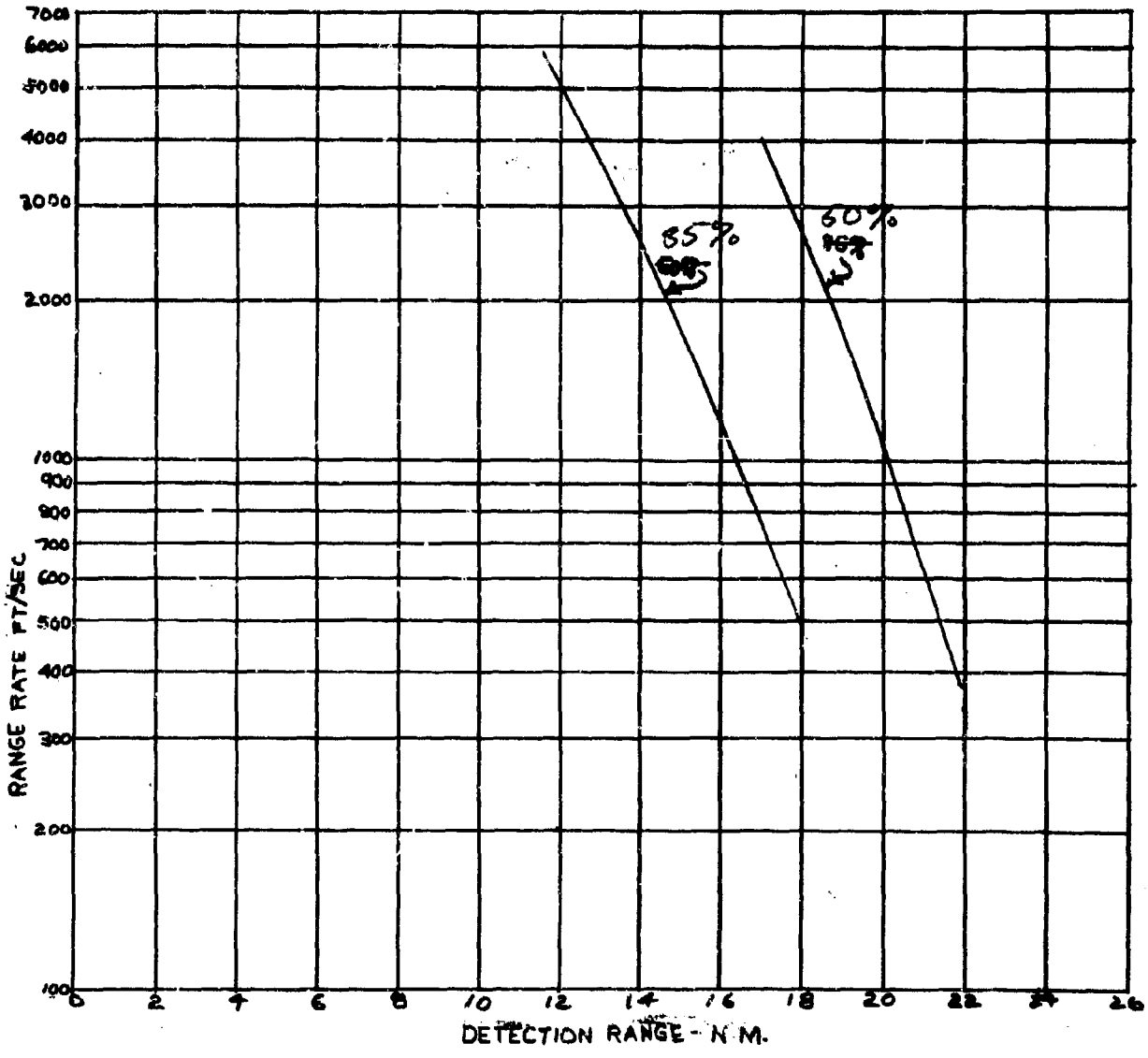

HEAD-ON DETECTION RANGE - AN/APQ-72, -74
FIGURE 3

2.3.3 Pull-Up and Lead-Pursuit Trajectories are computed on the digital computer. F4H-1 aircraft characteristics were taken from the model of Reference 2. The equations used for the trajectories are developed in Reference 4. It is of interest to note that the computer program accounts for the following factors.

1. Lead-Pursuit based on Vo values from the AN/APA-128 computer.
2. Airplane Lift-Drag relationship that varies with Mach No.
3. The displacement of the Radar Gimbal Mechanical Axis (R.G.M.A.) from the (F.R.L.). Fuselage Reference Line.
4. The variation of the trimmed angle of attack with flight condition.
5. Thrust variation with Mach No. and altitude.
6. $C_L$max. as limited by buffet and control authority.

The expressions for $R_{max.}$, $R_{min.}$ and Vo are given in Appendix I.

2.4 Data Developed - Procedures were adopted to develop the following data.

1. Altitude - Time of Pull-Up zones of target vulnerability.
2. The effect on capability of increased AI radar range.
3. The limitations on capability due to gimbal angle limits.
4. The effect of excluding - L/W courses.
5. Recovery limitations of system capability.

The parameters of the present XIA system constitute the basic configuration. Detection Range data are shown in Figure 1. Pitch gimbal angles (λ_e) are +47° (up), -38° (down).

2.4.1 Altitude-Time of Pull-Up Zones of Target Vulnerability are generated by the results of trial attacks at different incremental altitudes. At each altitude the initiation of the attack will be delayed by a trial number of seconds after AI radar detection until a failure is encountered. Attack failure is defined in 2.5.

2.4.2 The Effect of Increased AI Radar Range is demonstrated by a trial increase corresponding to a cumulative detection probability of .50 for the AI radar. See Figure 3. Attacks successful with these trials would apply regardless of the cause of the range increase.

2.4.3 Gimbal Angle Limitations are examined by study of the courses that failed due to gimbal angle limitation.

It is necessary to determine that system capability would be increased by raising the limit. This is done by observing the proximity of other performance limitations.

2.4.4 The Effect of Excluding L/W Courses is determined by examination of the L/W limited courses in a manner similar to 2.4.3.

2.4.5 The Specification of a Recovery $L/W \geq 0.5$ will exclude some areas. As in 2.4.3 and 2.4.4, the excluded courses must be examined to see if an adjustment of the specified limit would yield a significant increase in capability. The requirements of 2.4.4 and 2.4.5 are the presumed limits of flight manuvering in the absence of flight test investigations.

2.5 Attack Failure is established when any of the following conditions are met.

1. A lead-pursuit condition ($\epsilon < 10°$) is not achieved for $R_{max} > R > R_{min}$.
2. Gimbal angle limits ($+47° > \lambda_g > -38°$) are exceeded when R detection $>$ R $>$ R impact.
3. Recovery manuver results in $L/W < 0.5$ g's.
4. Trajectory requires negative values of L/W.

3.0 Results and Conclusions - Pull-up capability as presented in Figures 4 to 14 has been summarized in Tables 1,2 and 3 for targets at 65,000, 50,000 and 30,000 feet. The principal limitations of pull-up capability are given. Outstanding areas of restriction may be noted by study of the limitations remaining at the increased range (50% cumulative probability) pull-ups.

1. Interceptors at a Mach 0.9 flight condition are useless for attacking 65,000 foot targets.
2. AI radar range holds the incremental altitude attack capability of the Mach 2.0 interdeption of a Mach 2.0 target to a very low value (13,000 feet) for 65,000 and 50,000 foot targets.
3. A Mach 0.9 interceptor has more capability than a Mach 2.0 interceptor against Mach 2.0 targets at 50,000 feet and equal capability at 30,000 feet.
4. Negative gimbal angle limits restrict pull-up capability against Mach 2.0 targets at 50,000 and 30,000 feet.
5. Recovery problems limit system capability against Mach 0.9 targets at 50,000 feet.
6. The exclusion of courses with negative values of L/W does not basicly limit system capability.
7. There is a marked improvement in pull-up capability when detection is made at the range of 50% cumulative probability instead of the range of 85% cumulative probability.

PULL-UP ATTACKS - HEAD ON
MACH 2.0 TARGET, 65,000 FT
85% DETECTION PROBABILITY-B47
PULL-UP 3 g OR C_L MAX.
FIGURE 4

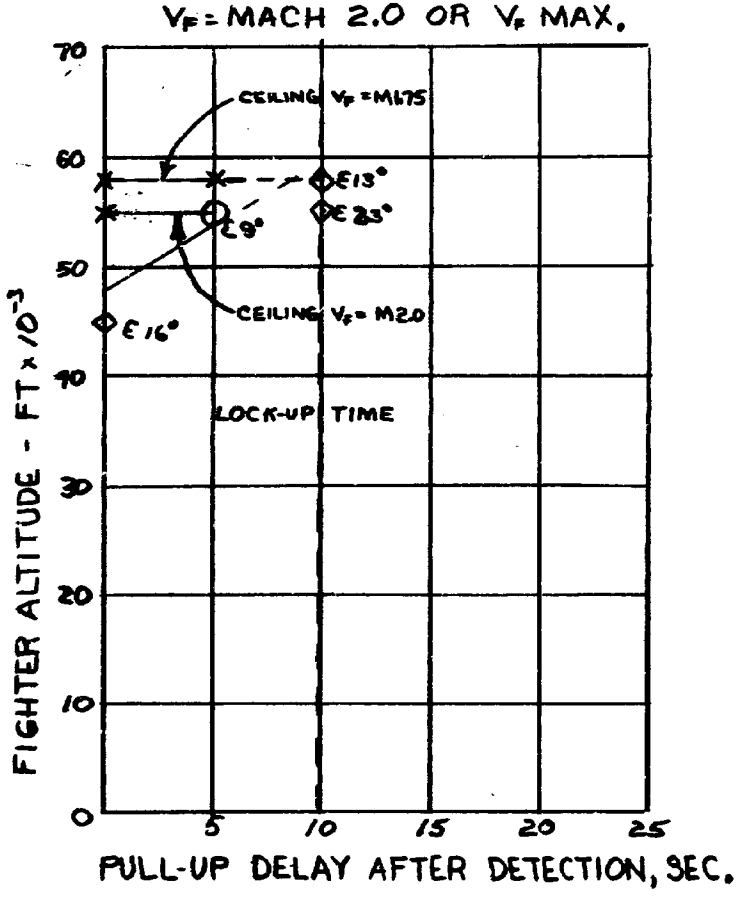

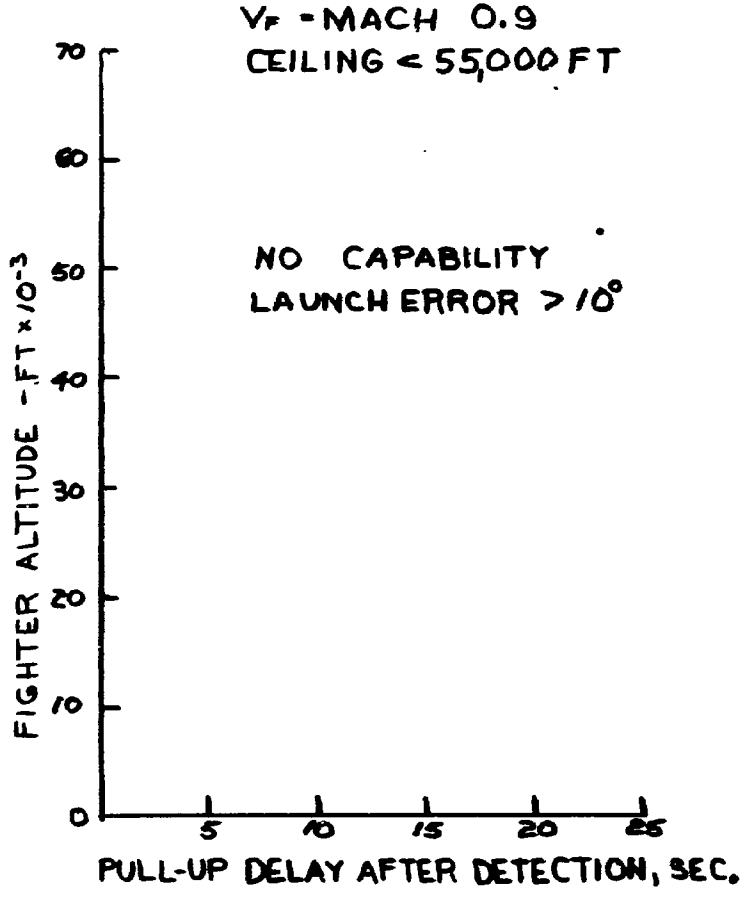

X - LAUNCH ERROR - 0°
⊙ - LAUNCH ERROR < 10°
◇ - UNSUCCESSFUL ATTACKS

CONFIDENTIAL

PULL-UP ATTACKS - HEAD ON
MACH 0.9 TARGET, 65,000 FT.
85% DETECTION PROBABILITY - B47
PULL-UP 3g OR C_L MAX
FIGURE 5

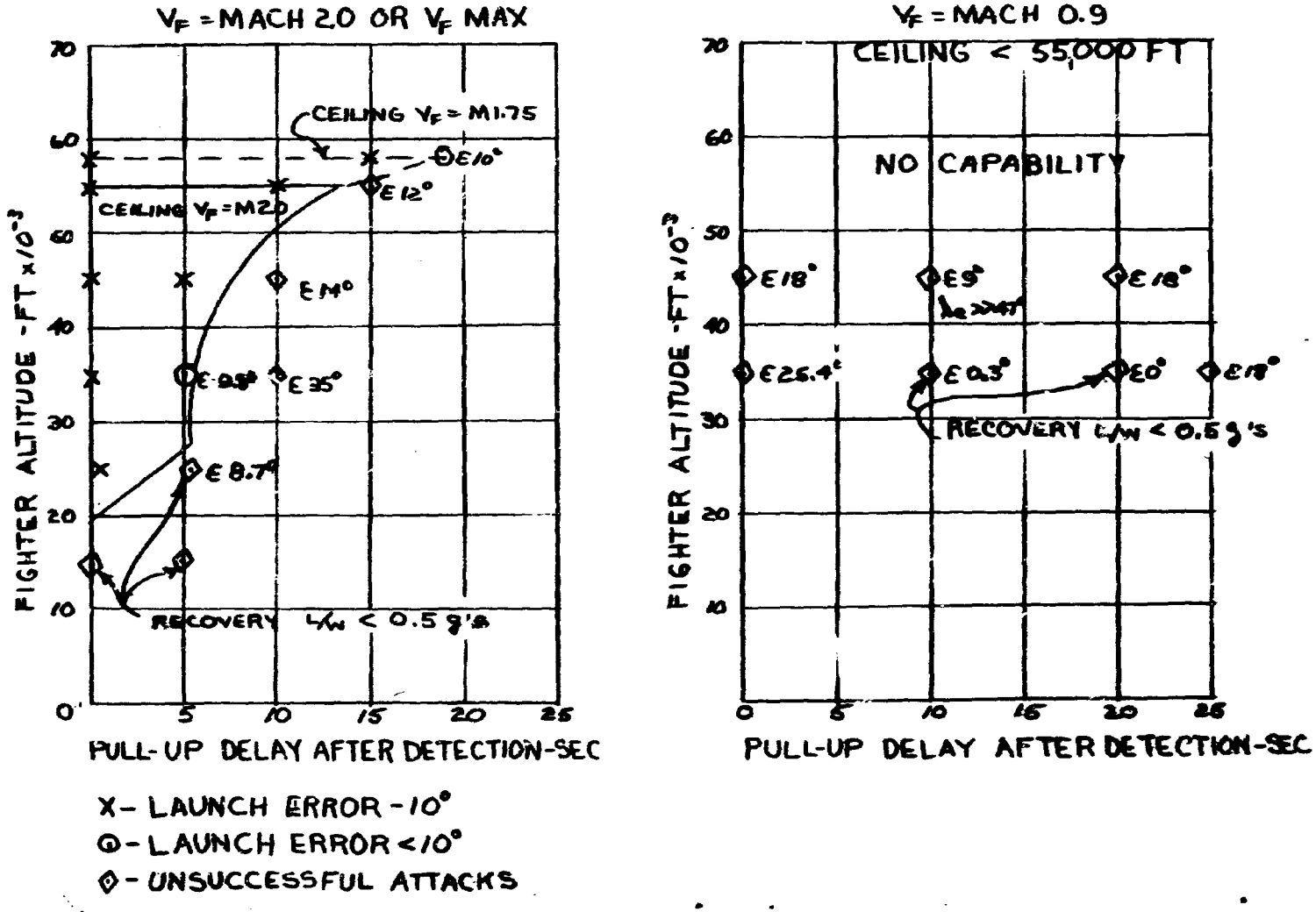

X - LAUNCH ERROR - 10°
⊙ - LAUNCH ERROR < 10°
◇ - UNSUCCESSFUL ATTACKS

CONFIDENTIAL

CONFIDENTIAL

PULL-UP ATTACKS - HEAD ON
MACH 2.0 TARGET, 50,000 FT.
85% DETECTION PROBABILITY - B47
PULL-UP 3g OR C_L MAX.
FIGURE 6

V_F = MACH 2.0 OR V_F MAX.

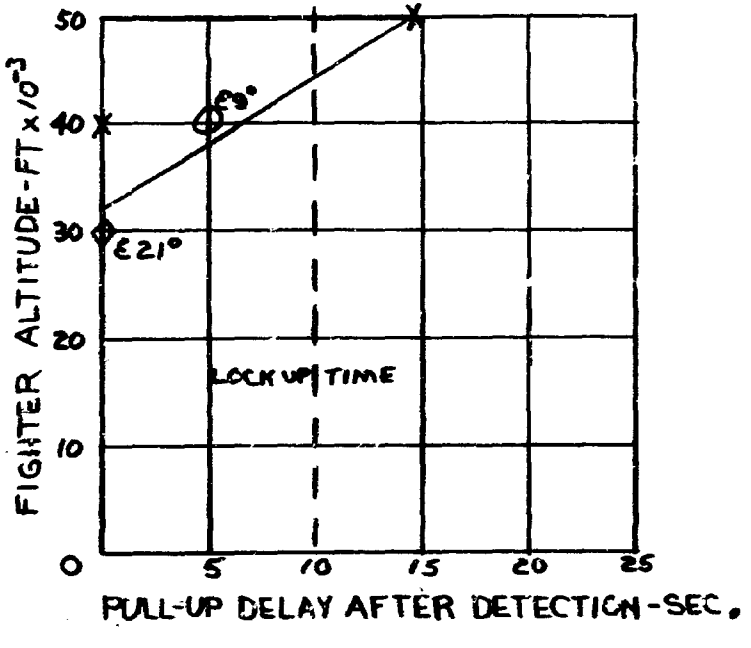

V_F = MACH 0.9

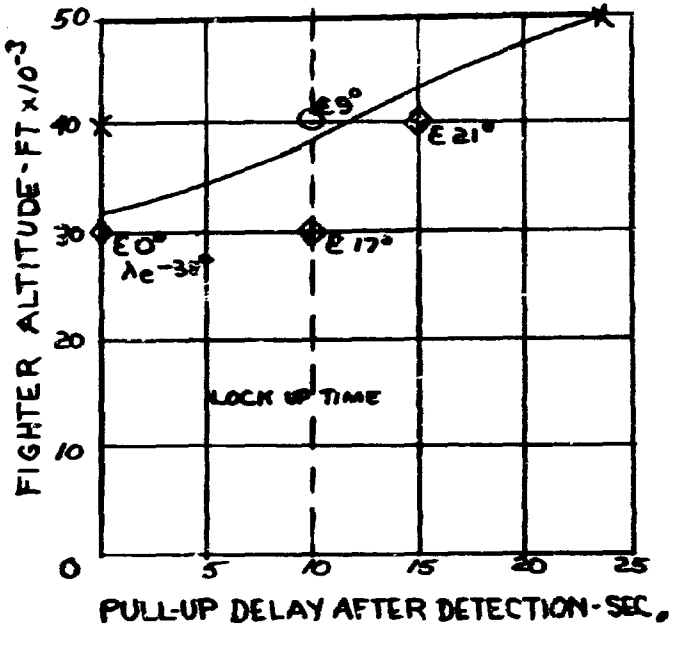

X - LAUNCH ERROR 0°
⊙ - LAUNCH ERROR < 10°
◊ - UNSUCCESSFUL ATTACKS

PULL-UP ATTACKS- HEAD ON
MACH 0.9 TARGET, 50000 FT
85% DETECTION PROBABILITY - B47
PULL-UP 3 g OR C_L MAX.
FIGURE 7

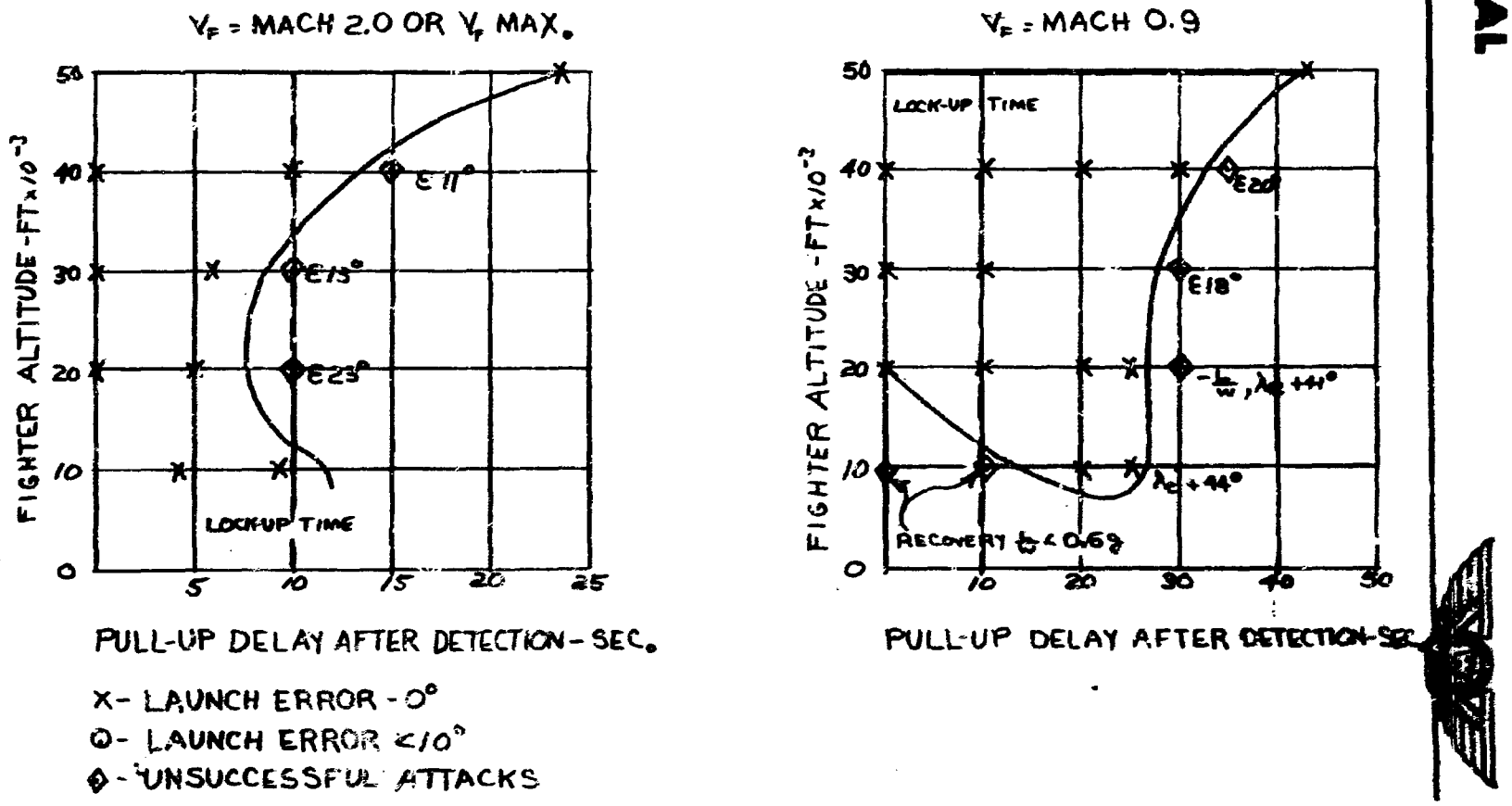

X - LAUNCH ERROR - 0°
O - LAUNCH ERROR <10°
◊ - UNSUCCESSFUL ATTACKS

CONFIDENTIAL

CONFIDENTIAL

10

PULL-UP ATTACKS - HEAD ON
MACH 2.0 TARGET, 30,000 FT
85% DETECTION PROBABILITY-B47
PULL-UP 3g OR C_L MAX.
FIGURE 8

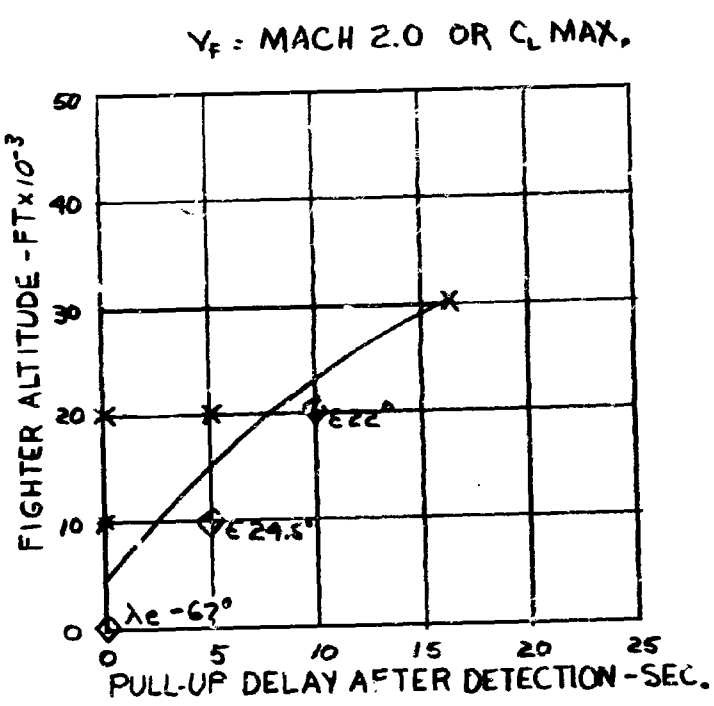

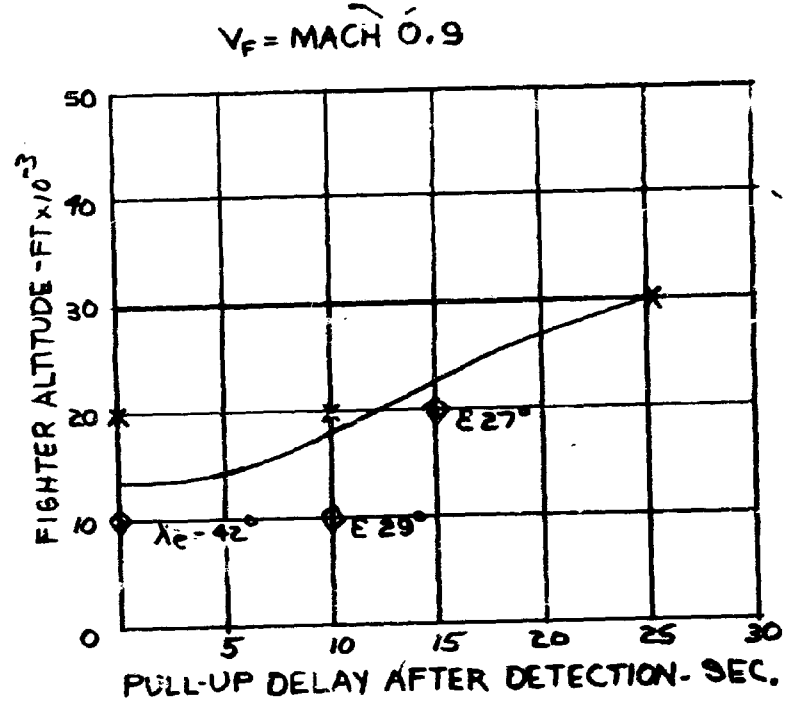

X - LAUNCH ERROR 0°
⊙ - LAUNCH ERROR < 10°
◆ - UNSUCCESSFUL ATTACKS

CONFIDENTIAL

CONFIDENTIAL

PULL-UP ATTACKS - HEAD ON
MACH 0.9 TARGET, 30,000 FT
85% DETECTION PROBABILITY - B47
PULL-UP 3 g OR C_L MAX.

FIGURE 9

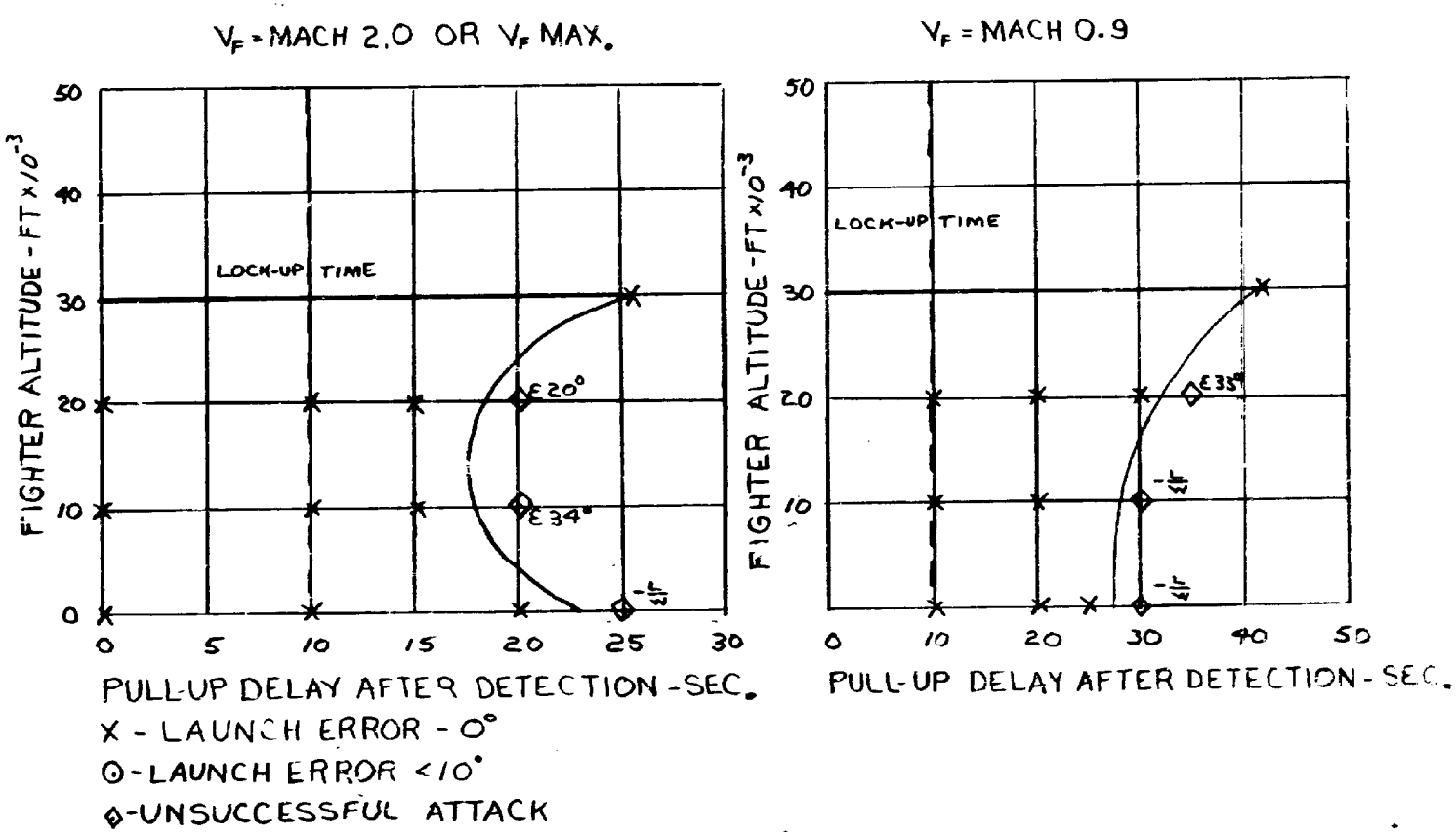

CONFIDENTIAL

PULL-UP ATTACKS - HEAD ON
MACH 2.0 TARGET, 65,000 FT
50% DETECTION PROBABILITY - B47
PULL-UP 3g OR C_L MAX.
FIGURE 10

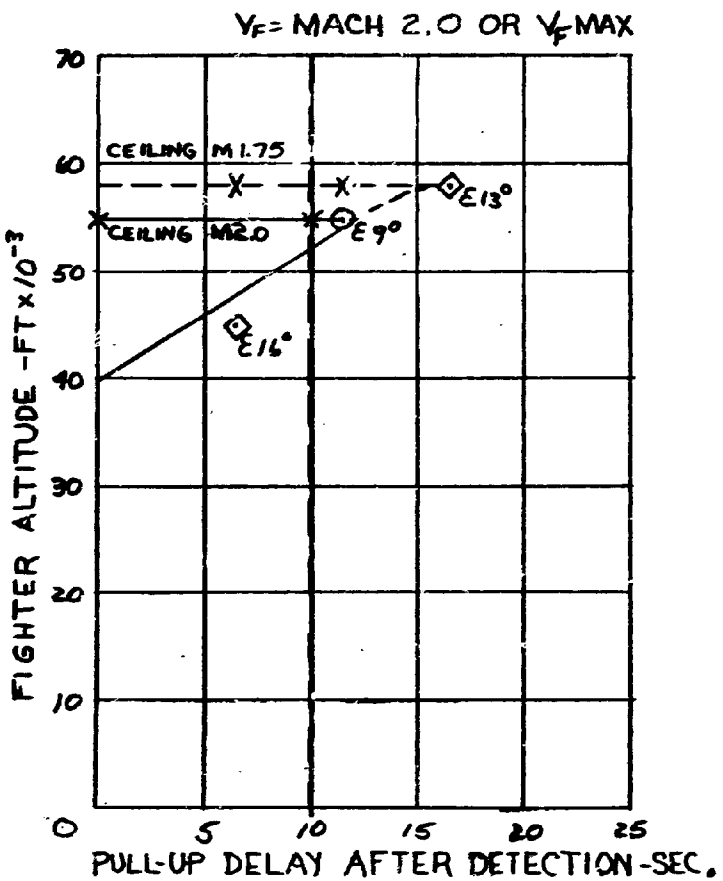

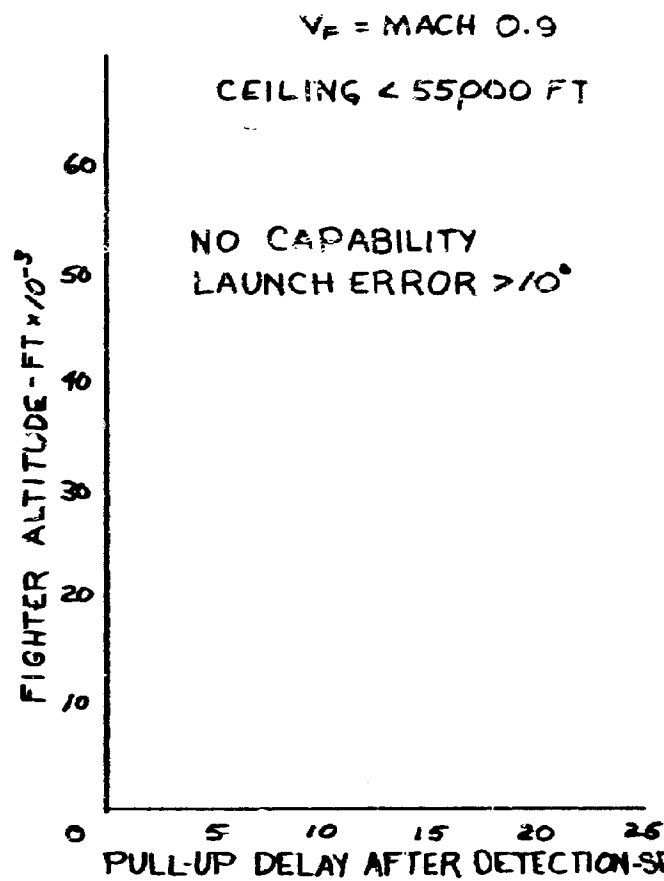

X - LAUNCH ERROR - 0°
⊙ - LAUNCH ERROR < 10°
◈ - UNSUCCESSFUL ATTACK

PULL-UP ATTACKS - HEAD ON
MACH 0.9 TARGET, 65,000 FT
50% DETECTION PROBABILITY - B47
PULL-UP 3g OR C_L MAX.
FIGURE 11

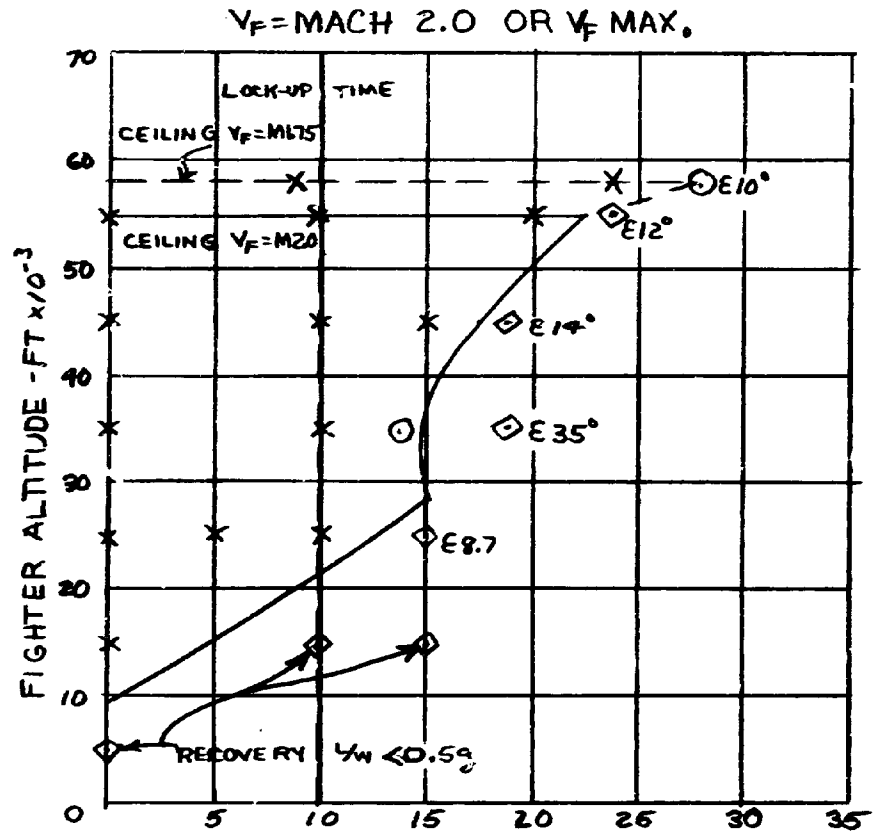

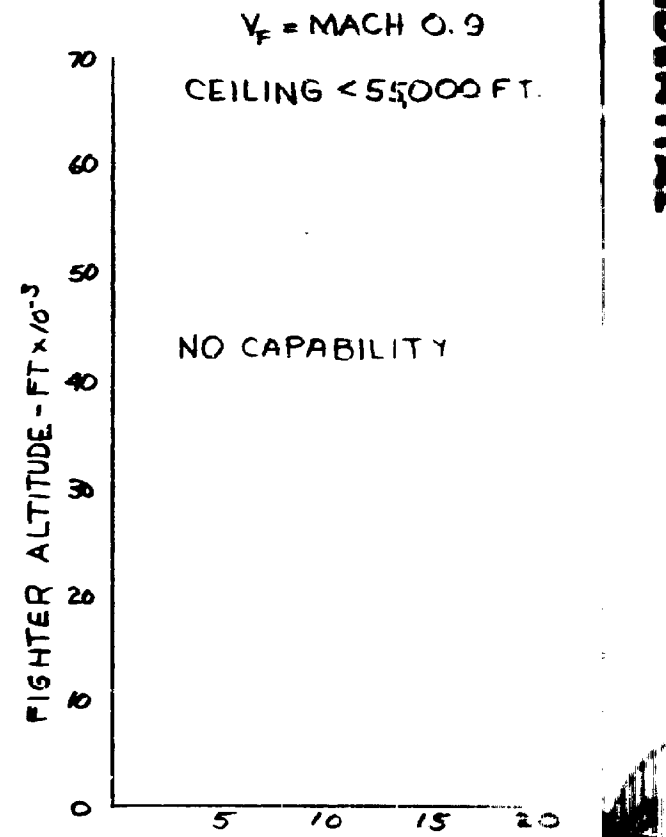

X - LAUNCH ERROR - 0°
⊙ - LAUNCH ERROR < 10°
◇ - UNSUCCESSFUL ATTACK

CONFIDENTIAL

CONFIDENTIAL

PULL-UP ATTACKS - HEAD ON
MACH 2.0 TARGET, 50,000 FT
50% DETECTION PROBABILITY - 84°
PULL-UP 3g OR C_L MAX.
FIGURE 12

V_F = MACH 2.0 OR V_F MAX.

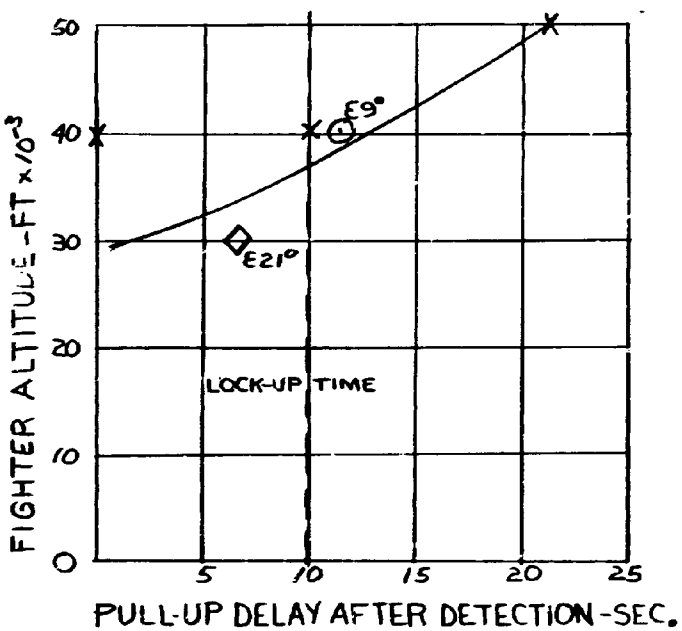

V_F = MACH 0.9

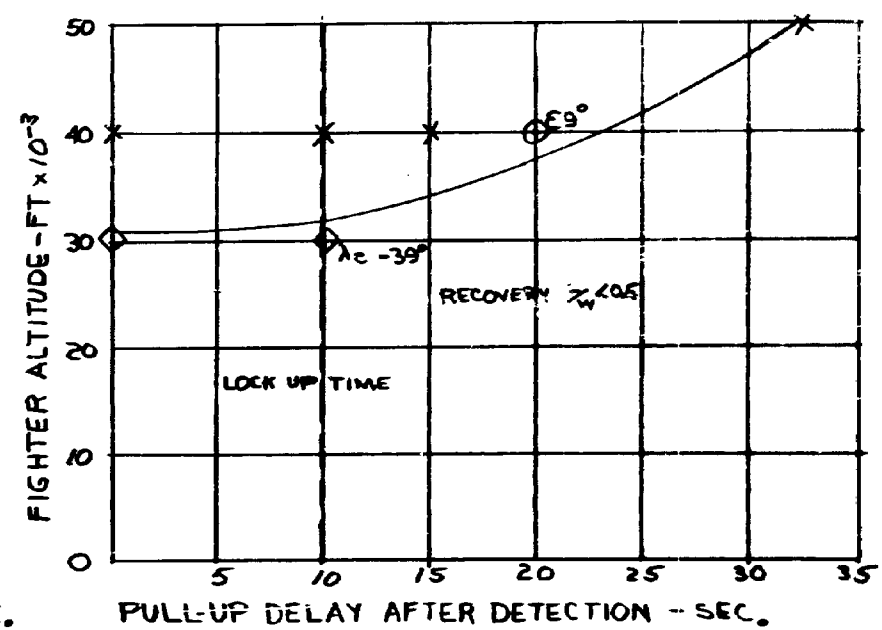

X - LAUNCH ERROR - 0°
⊙ - LAUNCH ERROR < 10°
◇ - UNSUCCESSFUL ATTACK

CONFIDENTIAL

PULL-UP ATTACKS - HEAD ON
MACH 0.9 TARGET, 50,000 FT.
50% DETECTION PROBABILITY - B47
PULL-UP 3g OR C_L MAX.
FIGURE 13

V_F = MACH 2.0 OR V_F MAX.

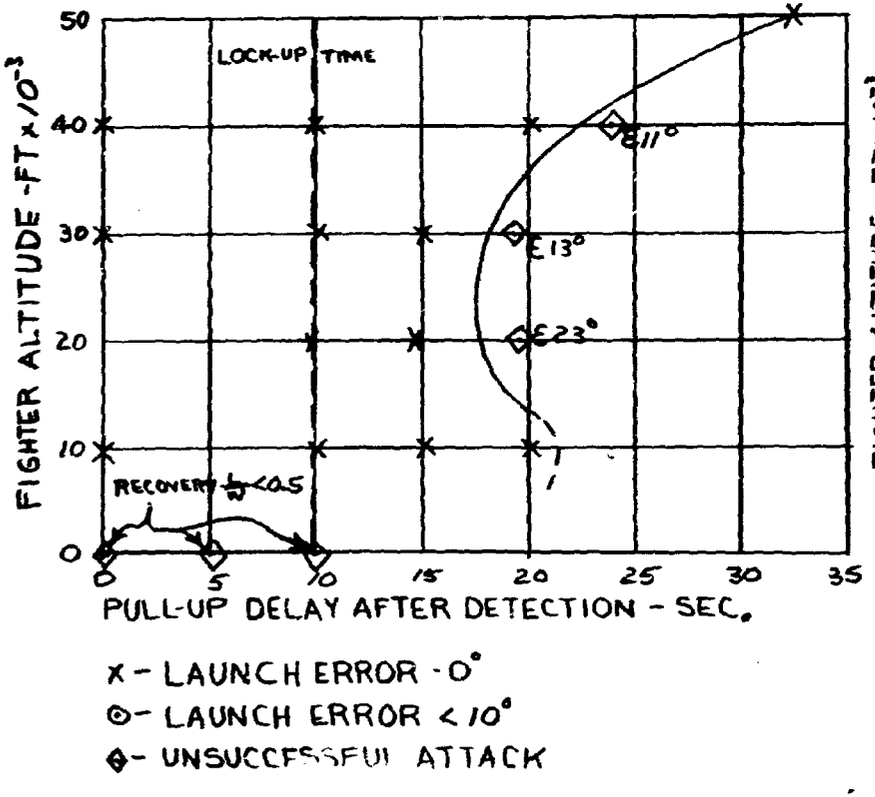

V_F = MACH 0.9

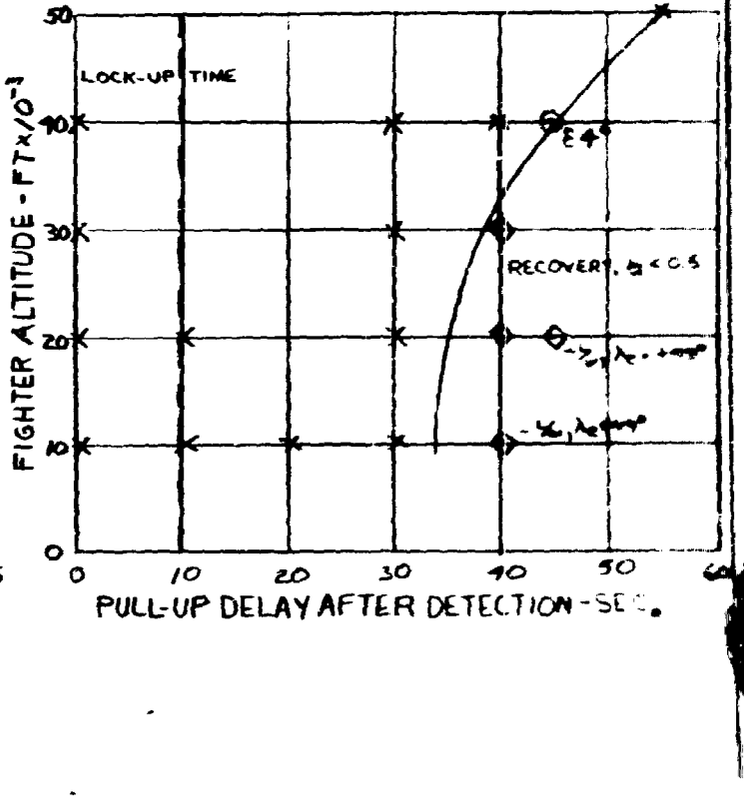

x - LAUNCH ERROR - 0°
⊙ - LAUNCH ERROR < 10°
◈ - UNSUCCESSFUL ATTACK

PULL-UP ATTACKS - HEAD ON
MACH 2.0 TARGET, 30,000 FT
50% DETECTION PROBABILITY - B47
PULL-UP 3g OR C_L MAX.
FIGURE 14

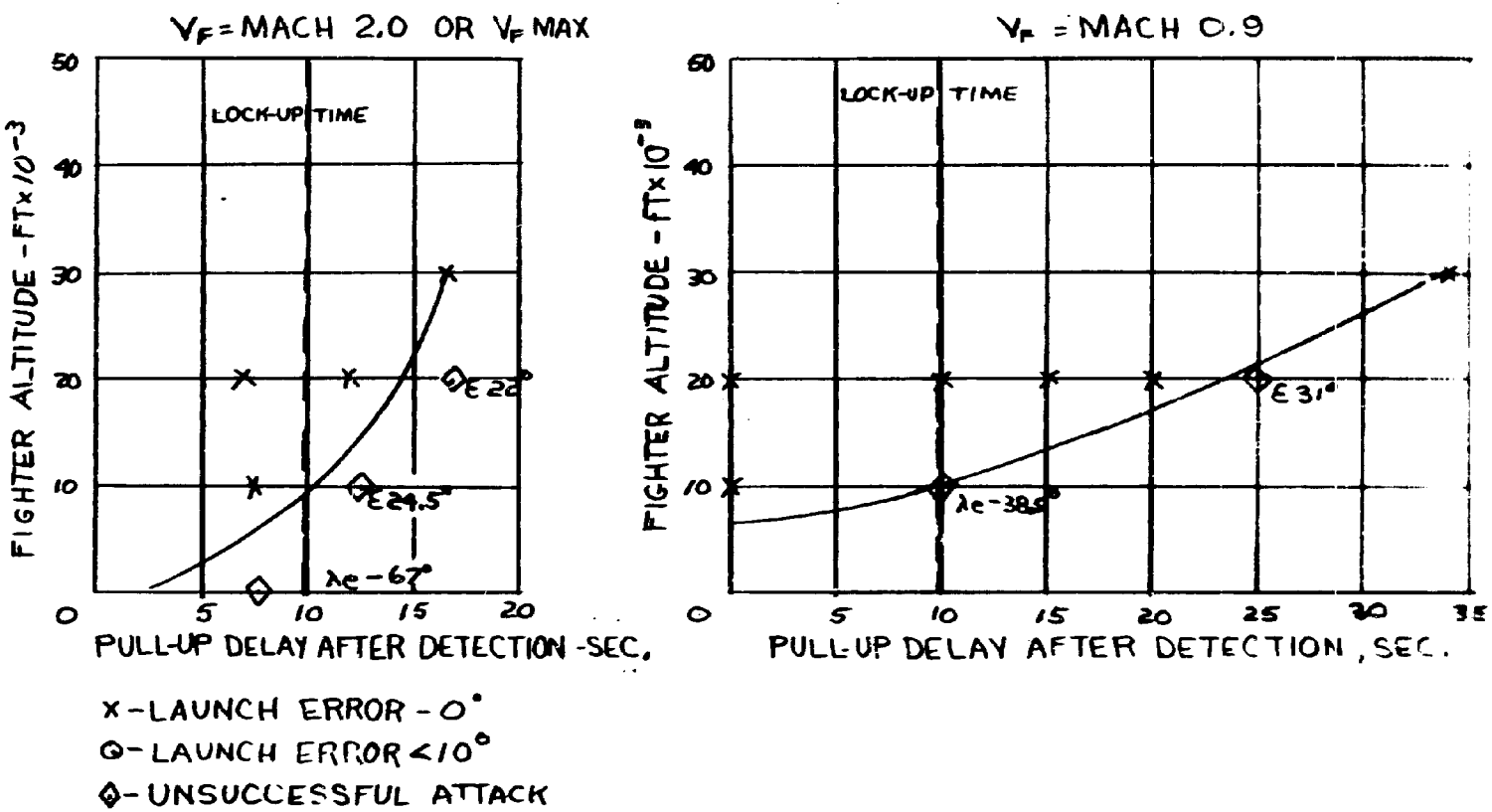

PULL-UP -3g OR C_L max.

V_P MACH	V_F MACH	DETECTION AT RANGE OF 85% CUMULATIVE PROBABILITY: MIN. INTERCEPTOR ALTITUDE-FTX10-3	PRINCIPAL LIMITATION OF CAPABILITY *	DETECTION AT RANGE OF 50% CUMULATIVE PROBABILITY: MIN. INTERCEPTOR ALTITUDE-FTX10-3	PRINCIPAL LIMITATION OF CAPABILITY *
2.0	2.0	No Capability	AI Radar Range (T,A)	52	AI Radar Range (T,A)
2.0	0.9	No Capability	Fighter Manuverability	No Capability	Fighter Manuver-ability
0.9	2.0	50	AI Radar Range (T,A)	22	AI Radar Range (T) Recovery L/N (A
0.9	0.9	No Capability **	Fighter Manuverability	No Capability	Fighter Manuver-ability

* Principal Limitations are in time-T, and altitude-A

TARGET VULNERABILITY AT 65,000 ft.

Table 1

PULL-UP - 3g OR $C_{L_{max}}$

V_T Mach	V_F Mach	DETECTION AT RANGE OF 85% CUMULATIVE PROBABILITY: MIN. INTERCEPTOR ALTITUDE-FTX10^{-3}	PRINCIPAL LIMITATION OF CAPABILITY *	DETECTION AT RANGE OF 50% CUMULATIVE PROBILITY: MIN. INTERCEPTOR ALTITUDE-FTX10^{-3}	PRINCIPAL LIMITATION OF CAPABILITY *
2.0	V max.	44	AI Radar Range (T,A)	37	AI Radar Range (T,A)
2.0	0.9	38	AI Radar Range (T,A)	32	Gimbal Angle (T,A)
0.9	V max.	34	AI Radar Range (T,A)	10	Recovery L/W (A)
0.9	0.9	12	Recovery L/W (A)	10	None

* Principal Limitations are in Time-T, and Altitude-A

TARGET VULNERABILITY AT 50,000 ft.

Table 2

CONFIDENTIAL

TARGET AT 30,000 ft.
PULL-UP - 3g OR C_L Max.

V_T MACH	V_F MACH	DETECTION AT RANGE OF 85% CUMULATIVE PROBABILITY: MIN. INTERCEPTOR ALTITUDE-FTX10^{-3}	DETECTION AT RANGE OF 85% CUMULATIVE PROBABILITY: PRINCIPAL LIMITATION OF CAPABILITY *	DETECTION AT RANGE OF 50% CUMULATIVE PROBABILITY: MIN. INTERCEPTOR ALTITUDE-FTX10^{-3}	DETECTION AT RANGE OF 50% CUMULATIVE PROBABILITY: PRINCIPAL LIMITATION OF CAPABILITY *
2.0	V max.	23	AI Radar Range (T,A)	10	AI Radar Range (T,A)
2.0	0.9	18	AI Radar Range (T,A)	10	Gimbal Angle (T,A)
0.9	V max.	0	None		
0.9	0.9	0	None		

* Principal Limitations are in Time-T and Altitude-A

TARGET VULNERABILITY AT 30,000 ft.

Table 3

Appendix I

The equations for the maximum and minimum launch ranges for the Sparrow III and the expressions for the average relative missile speed may be expressed as follows:

1. $R_{max.} = R_1(h) + T_1(Vc - V_F)$, limited to 6.5 N.M.

where:

$R_{max.}$ = maximum launch range

$R_1(h)$ is defined in Figure 15

$T_1 = 11$ SEC $\quad Vc \geq V_F$
$\quad\quad f_1(h)$ SEC $Vc < V_F$ (See Figure 15)

V_c = Range rate (positive when closing) (ft/sec)
V_F = Interceptor Velocity - (ft/sec)

2. $R_{min.} = R_2(h) + T_2 V_c$

where: $R_{min.}$ = minimum launch range

$T_2 = 3.3$ sec.

$R_2(h)$ is defined in Figure 15

3. $V_o = 935 \left[1 + 0.43 \left(1 - \frac{P}{P_o}\right) \right]$ ft/sec

where: V_o is average relative missile speed.

P/P_o is pressure ratio to a sea level reference.

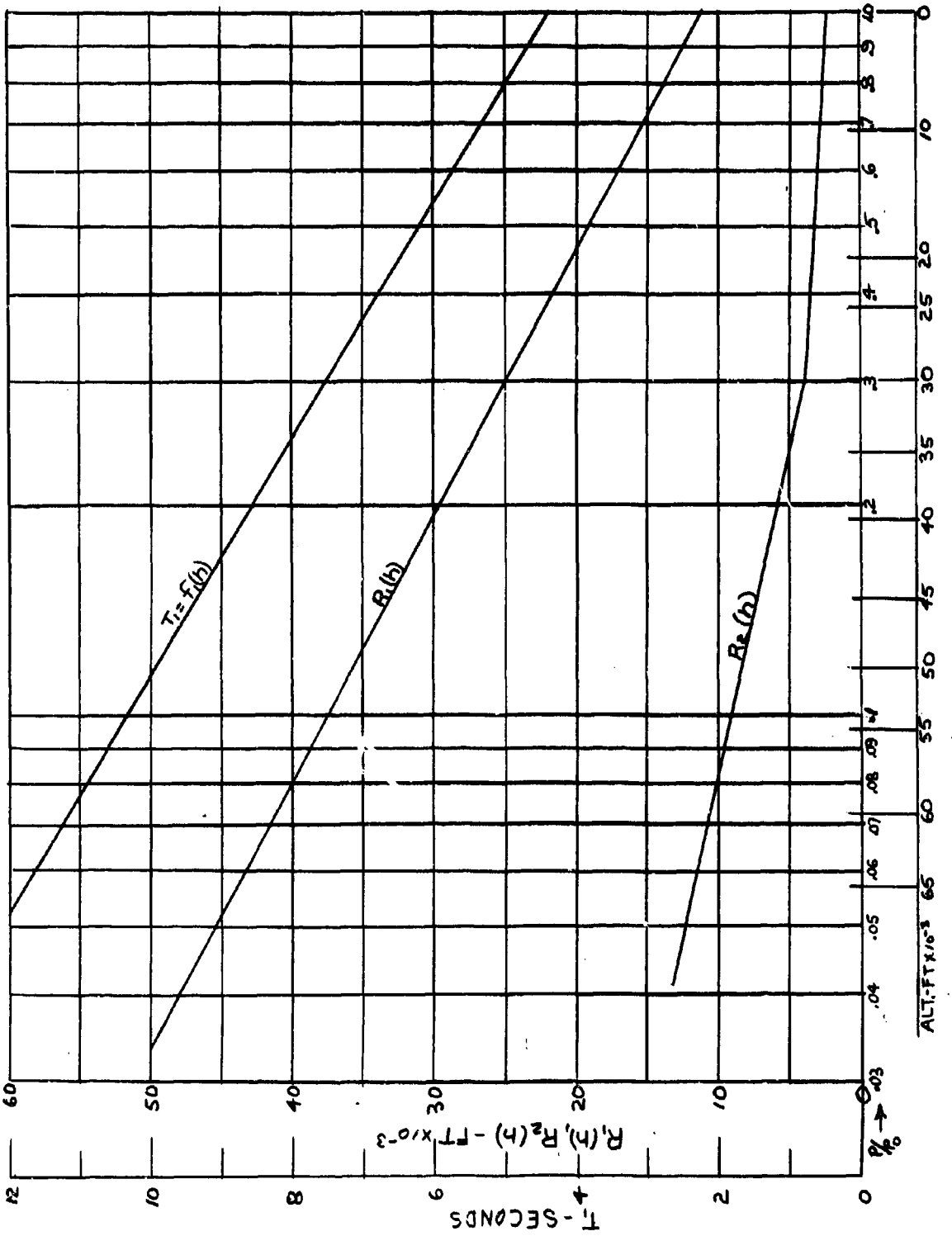

PARAMETERS OF AN/APA 128 COMPUTER
FIGURE I-1

References

1. A METHOD OF EVALUATING RECOVERY CAPABILITY OF AN INTERCEPTOR AFTER A PULL-UP ATTACK, E. C. Quesinberry

ANTM 229, Westinghouse Air Arm Division

9/16/57

2. F4H-1 BASIC PERFORMANCE DATA, R. B. Tucker

NMSTR No. 2, Westinghouse Air Arm Division

5/8/57

3. ADDENDUM TO NAVY MISSILE STUDY TECHNICAL REPORT NO.2. F4H-1 BASIC PERFORMANCE DATA, R. B. Tucker,

Westinghouse Air Arm Division

6/12/57

4. AERODYNAMIC LEAD PURSUIT EQUATION, J. F. Buc' n

ANTM 175, Westinghouse Air Arm Division

March, 1957

Analytical Section Technical Memorandum No. 273

APPENDIX IV

X1A & X1B Settling Time Requirements

R. G. Clanton

Assisted By
D. Nadolski
T. A. Priscilla

1/15/58

Restricted Distribution	Uniterms	Charge No
100, D. J. Povejsil, Mgr. (30) 103, R. G. Clanton, Supvr. Engr.	F-4H1 F-8U3 X1a & X1B Radar Range Rqts.	90114 1/15/58:lm

ABSTRACT

The ability of a pilot to control an interceptor to reduce the lock on errors for a lead pursuit attack course from various starting ranges and target aspect angles with various target speeds are presented. Comparison to ideal performance is made and a recommendation of a method for generating additional data is given.

Table of Contents

Table of Figures

Table of Figures (Con't)

1. Introduction

In an air-to-air intercept problem in which an interceptor aircraft must destroy an incoming bomber a series of sequential events occur. These can be sequentially listed as:

1. Detection of an impending attack
2. Vectoring of the interceptor to meet the attack
3. Detection of the incoming bomber by the interceptor detection system
4. Lock-on to and tracking of the incoming bomber by the interceptor tracking system.
5. Reduction of the steering error of the attack course to a magnitude such that the armament may be launched at the bomber to achieve a kill.
6. Execution of post launch procedures by the interceptor.

This report deals in detail with the fifth item of this list. - reduction of the steering error. This is the second report written on this subject with regards to the F4H-1 and F8U-3 Weapon Systems. The first report utilized only the F4H-1 aircraft characteristics and one target speed. There was also no absolute limit to the magnitude of normal acceleration which the pilot could employ to reduce the steering error. As a consequence, g's in excess of 4 were employed by the pilots in many cases to reduce the steering errors.

This report presents a comparison of F4H-1 and F8U-3 aircraft operating against various target speeds with a limit of 3 g's for the corrective maneuver.

2. Summary of Results

2.1 As a consequence of the initial condition used in this study in conjunction with the high closing speeds and limited starting ranges it was impossible to reduce the steering errors in many of the test cases. See Figure 1 and 2 for test cases studied.

2.2 Due to the limited ranges, the majority of the maneuvers executed to reduce the steering error are constant rate turns. Examination of the simulator recordings indicate extremely slight variation in interceptor turn rate. Consequently a good approximation to the manner in which steering errors are reduced can be achieved by calculations which ignore the effects of pilot and aircraft. The methods of performing this calculation are detailed in reference 1.

2.3 Table 1 summarizes the results of the settling time study. The table lists the test conditions, whether or not the steering error was reduced, and the minimum value to which the steering error was reduced for 85% cumulative probability and 50% cumulative probability. This table also lists the figures which should be consulted for detailed information concerning a particular test case.

TEST CASES STUDIED

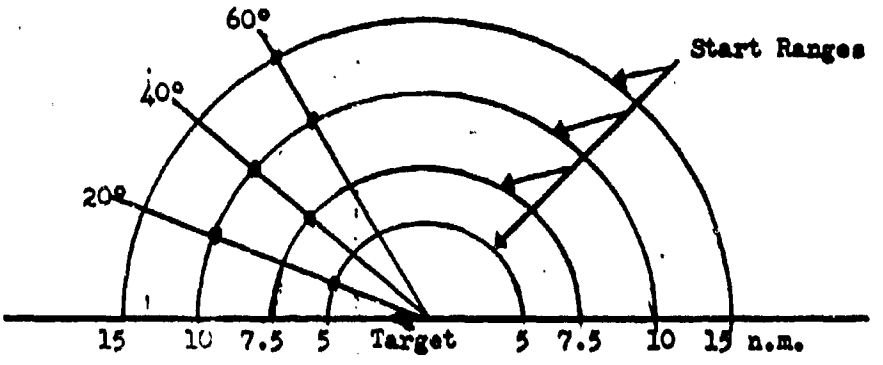

F8U-3 V_F = 2185 ft/sec V_T = 1518 ft/sec

Initial Errors = 20°, 30° (γ = 20°, 40°)

Initial Errors = 20°, 30°, 40° (γ = 60°)

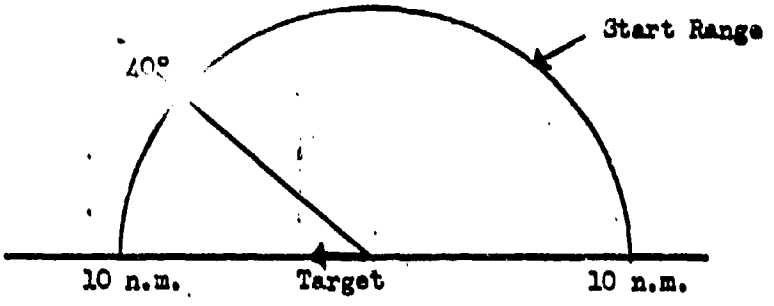

F8U-3 V_F = 2185 ft/sec V_T = 854 ft/sec.

F4H-1 V_F = 1897 ft/sec V_T = 854 ft/sec.

Initial Errors = 20°, 30°

Figure 1

TEST CASES STUDIED

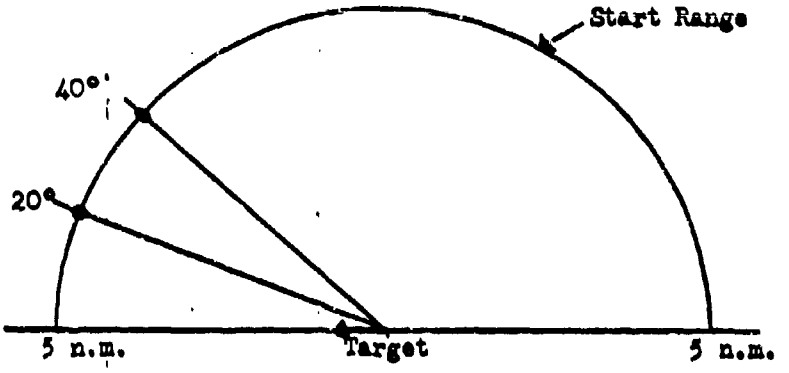

F4H-1 $V_T = V_P \approx 1897$ ft/sec

Initial Errors = 20°, 30°

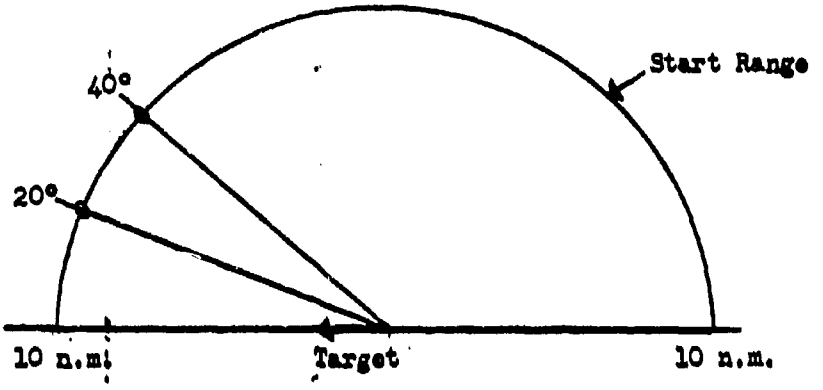

F8U-3 $V_P = 2185$ ft/sec $V_T = 1897$ ft/sec

Initial Errors = 20°, 30°

Figure 2

Test Situations

Table 1

Case	Interceptor	Interceptor Speed (ft/sec)	Target Speed (ft/sec)	Angle Off Target's Nose (deg)	Steering Error (deg)	Initial Range (NM)	Is Steering Error Reduced?	Refer to Figure	Min. Error (deg) 85%	Min. Error (deg) 50%	Statistical Data
1	F-80J	2185	1897	20	20	10	No	8 & 9	1	1	Yes
2	"	"	"	40	30	"	No	8 & 9	1	1	Yes
3	"	"	"	20	20	"	Yes	8 & 10	16	12.5	Yes
4	"	"	"	40	30	"	No	8 & 10	1	1	Yes
5	F-84J	1897	1897	20	20	5	No	11	1	1	Yes
6	"	"	"	40	30	"	No	11	1	1	No
7	"	"	"	20	20	"	No	11	1	1	No
8	"	"	"	40	30	"	No	11	1	1	No
9	F-80J	2185	1518	20	20	5	No	12	1	1	No
10	"	"	"	"	30	"	No	12	1	1	No
11	"	"	"	"	20	10	Yes	13	14	10	Yes
12	"	"	"	"	30	"	No	13	1	1	Yes
13	"	"	"	40	20	7.5	No	14	1	1	Yes
14	"	"	"	"	30	"	No	15	1	1	No
15	"	"	"	"	20	10	Yes	14	7	7	Yes
16	"	"	"	"	30	"	Yes	16	28	26	Yes
17	"	"	"	60	20	10	Yes	16	17	5	Yes
18	"	"	"	"	30	"	Yes	17	28	23	Yes
19	"	"	"	"	20	15	Yes	18	38.8	37	Yes
20	"	"	"	"	30	"	Yes	19	3	3	Yes
21	"	"	"	"	40	"	Yes	20	22	3	Yes
22	"	"	"	"	20	10	Yes	21	5	3.5	Yes
23	"	"	854	"	30	"	Yes	21	26.5	24.5	Yes
24	"	"	"	"	20	"	Yes	22	2.5	3	Yes
25	F4H-1	1897	"	"	30	"	Yes	23	14	7	Yes
26	"	"	"	"	"	"	"	"	"	"	"

2.4 It can be stated for the test cases studied that no reduction in steering error is possible for starting ranges of 7.5 n.m. or 5 n.m. For the cases of maximum target speed extremely limited capability exists to reduce the steering error in all cases studied.

For the case of the target traveling at 1518 ft/sec (M-1.53) with an aspect angle 20° off of the target's nose starting at 10.n.mi. the capability to reduce the steering error is marginal. With greater aspect angles or slower speeds this capability is increased.

2.5 There were no significant differences noted in the ability to control the F-4H1 and the F8U-3 aircraft in the required maneuvers during this study.

3. Simulation

The simulation employed in this study was exactly the same as that used in the earlier settling time study with the exception that a buzzer sounded whenever a maneuver of greater than 3 g's was in process. The pilot restricted the maneuver to just keep the buzzer chattering.

The data describing the F8U-3 aircraft contained in (reference 2) was used in the simulation of the F8U-3 aircraft.

The effects of interceptor slow down were neglected on a basis of the information presented in Figure 3A and 3B.

4. Probability of Lock-On Errors - Collision Vectoring

Figures 4, 5, 6, and 7 present the cumulative probability of lock-on errors for different aspect angles. The method of calculating this data is the same as used in reference 1.

5. Discussion of Results

5.1 Time. The results of this study presented in Figures 8 through 23 illustrates the prime necessity of sufficient time to perform the error settling function. This time is made available by either increasing lock on range or else operating against slow speed targets.

5.2 Data Assessment and Interpretation. The data as presented yields the times required for 85% off the runs and 50% of the runs to reduce the steering error below the values listed as the ordinate of the curves. The points at which the curves terminates are the points at which no longer 85% and 50% of the cases were reducing the errors. The curves were produced with a requirement that the error must remain below the error-time reading point for at least three seconds. It was observed that changing this requirement to six seconds would have negligable effects upon the results

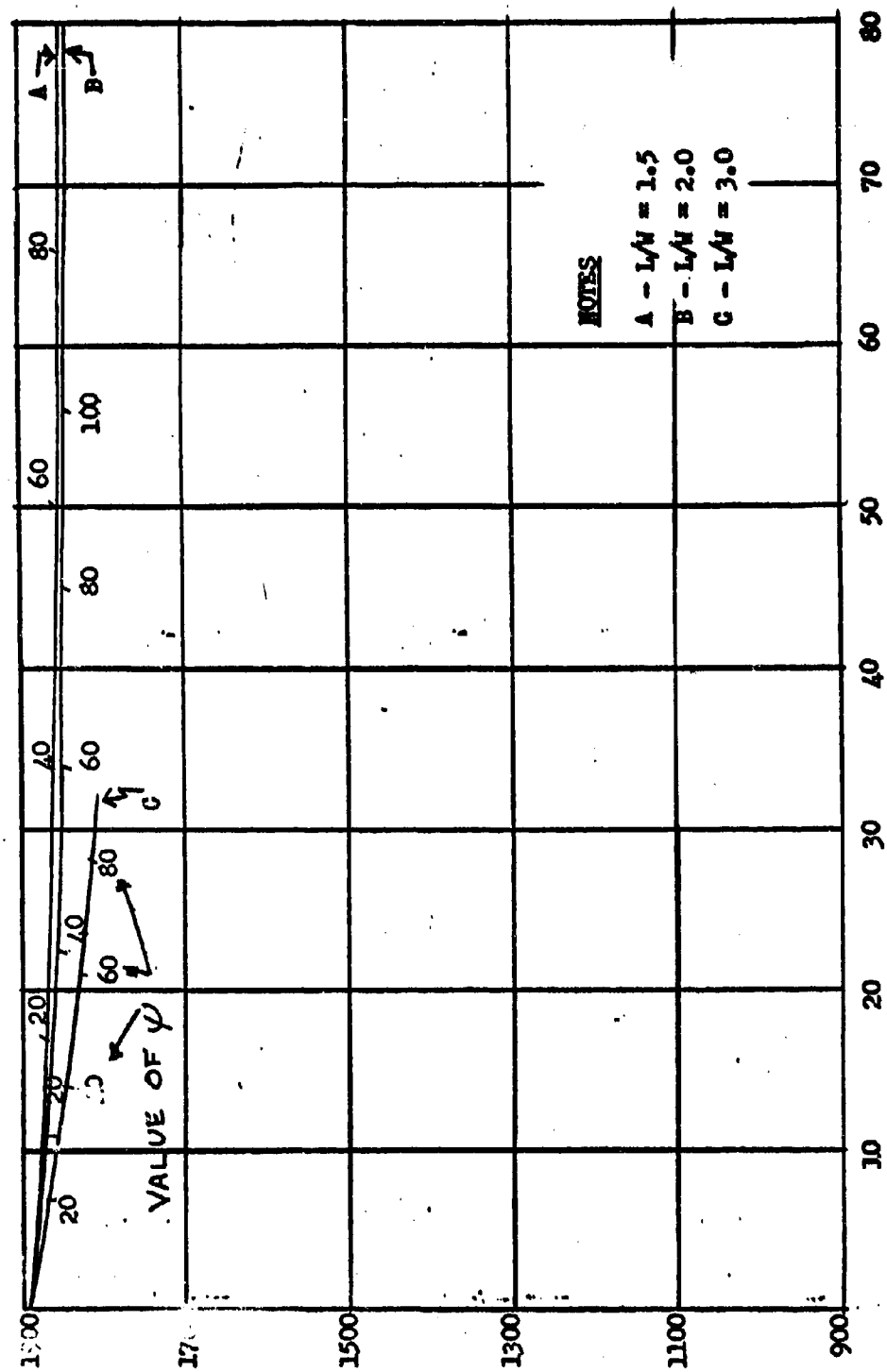
30,000' SLOWDOWN - HORIZONTAL TURNS
F4H-1
NOTES
A - L/W = 1.5
B - L/W = 2.0
C - L/W = 3.0
VALUE OF ψ
A
B
C
Interceptor Velocity Ft/Sec
1700
1500
1300
1100
900
Time - Seconds
10
20
30
40
50
60
70
80

Figure 3(a)

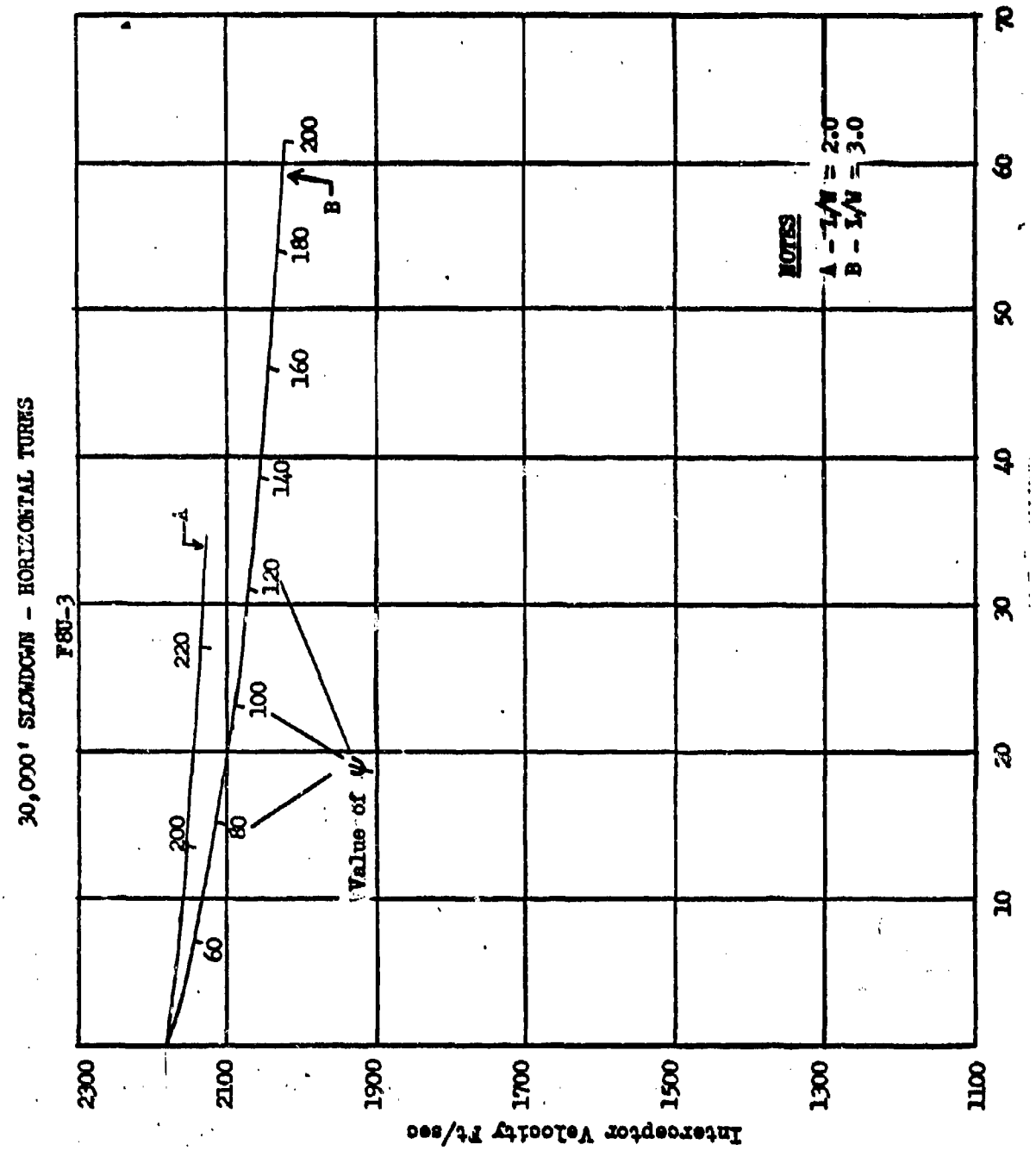
30,000' SLOWDOWN - HORIZONTAL TURNS
F8U-3
Interceptor Velocity Ft/sec
2300
2100
1900
1700
1500
1300
1100
Value of ψ
60
80
100
120
140
160
180
200
220
200
A
B
NOTES
A - L/N = 2.0
B - L/N = 3.0
10
20
30
40
50
60
70
Time - Seconds

Figure 3(b)

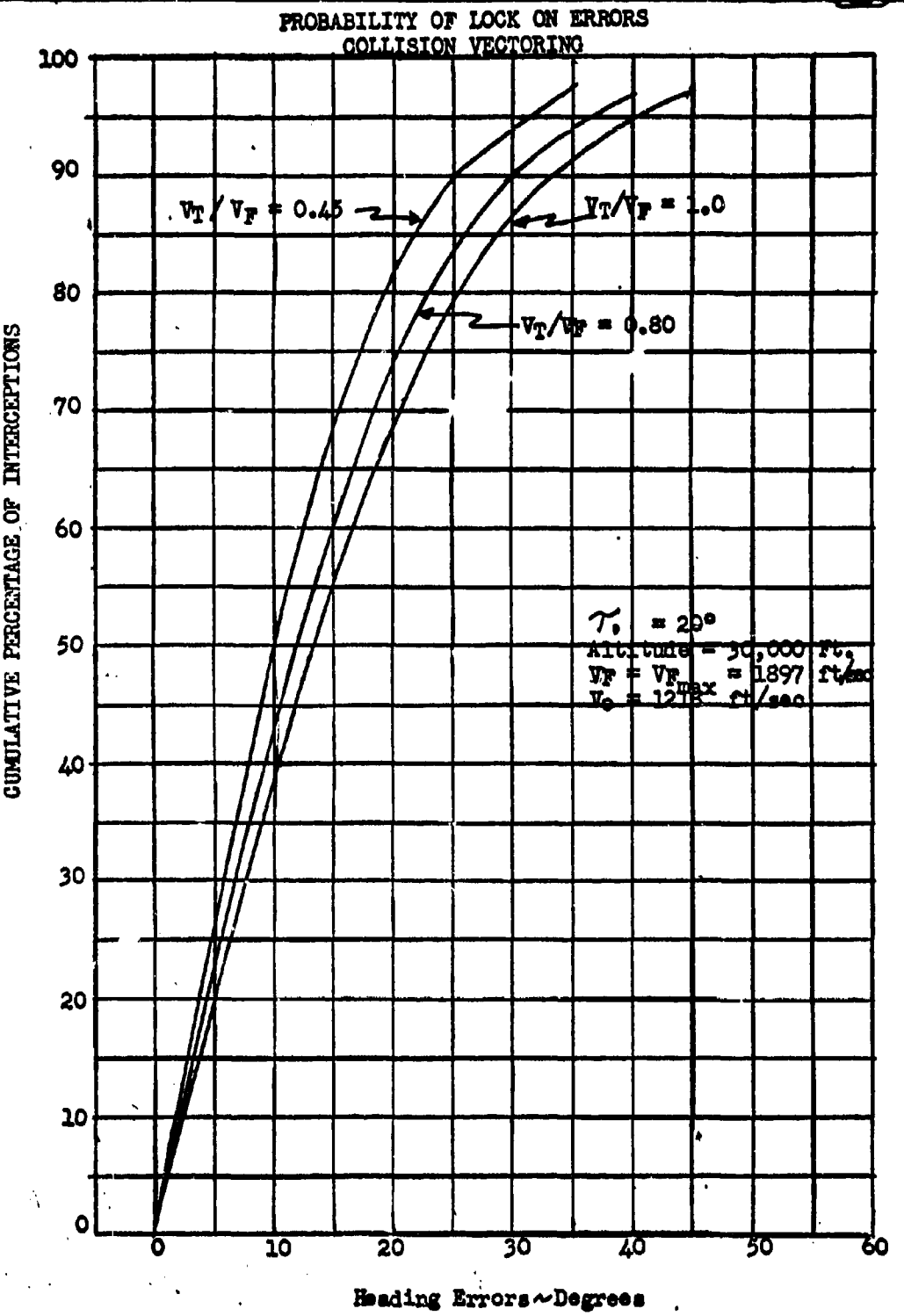
PROBABILITY OF LOCK ON ERRORS
COLLISION VECTORING
CUMULATIVE PERCENTAGE OF INTERCEPTIONS
100
90
80
70
60
50
40
30
20
10
0
0
10
20
30
40
50
60
Heading Errors ~ Degrees
$V_T / V_F = 0.45$
$V_T / V_F = 1.0$
$V_T / V_F = 0.80$
$\tau_o = 20°$
Altitude = 30,000 ft.
$V_F = V_{F_{max}} = 1897$ ft/sec
$V_o = 1218$ ft/sec

Figure 4

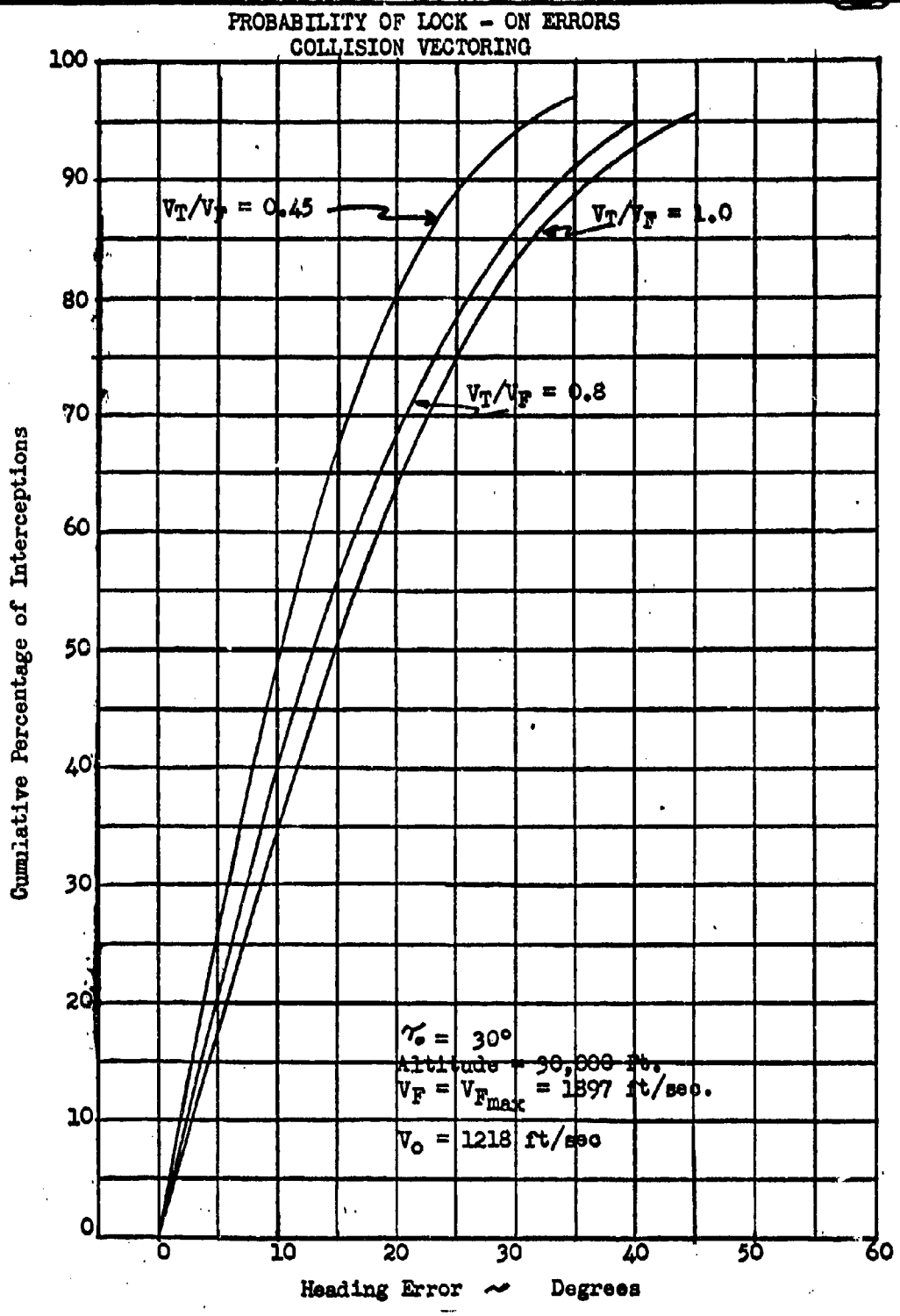
PROBABILITY OF LOCK - ON ERRORS
COLLISION VECTORING
Cumulative Percentage of Interceptions
Heading Error ~ Degrees
V_T/V_F = 0.45
V_T/V_F = 1.0
V_T/V_F = 0.8
τ_o = 30°
Altitude = 30,000 ft.
$V_F = V_{F_{max}}$ = 1397 ft/sec.
V_o = 1218 ft/sec
0
10
20
30
40
50
60
70
80
90
100

Figure 5

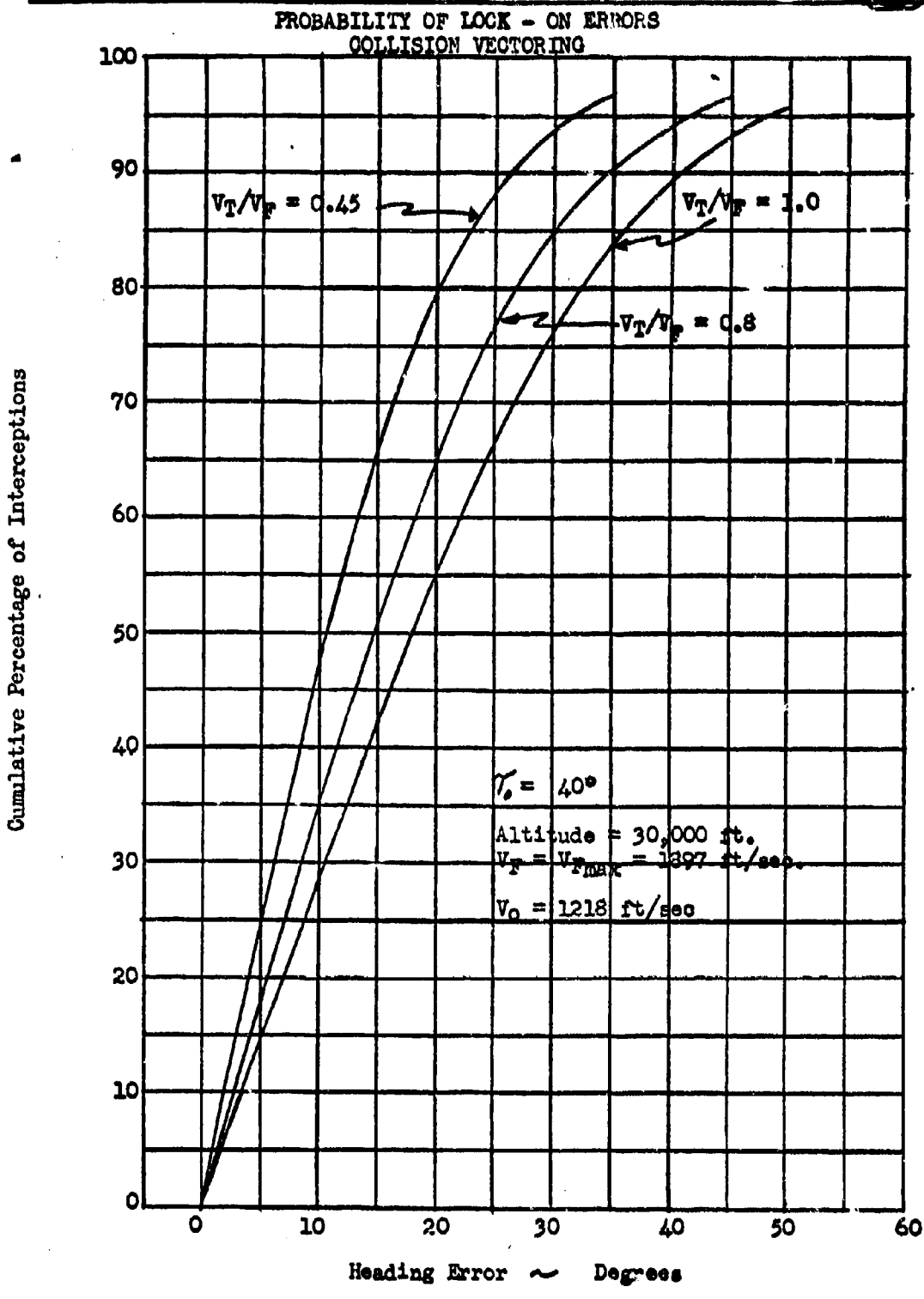
PROBABILITY OF LOCK - ON ERRORS
COLLISION VECTORING
Cumulative Percentage of Interceptions
100
90
80
70
60
50
40
30
20
10
0
V_T/V_F = 0.45
V_T/V_F = 1.0
V_T/V_F = 0.8
γ_o = 40°
Altitude = 30,000 ft.
$V_F = V_{F_{max}}$ = 1397 ft/sec.
V_o = 1218 ft/sec
0
10
20
30
40
50
60
Heading Error ~ Degrees

Figure 6

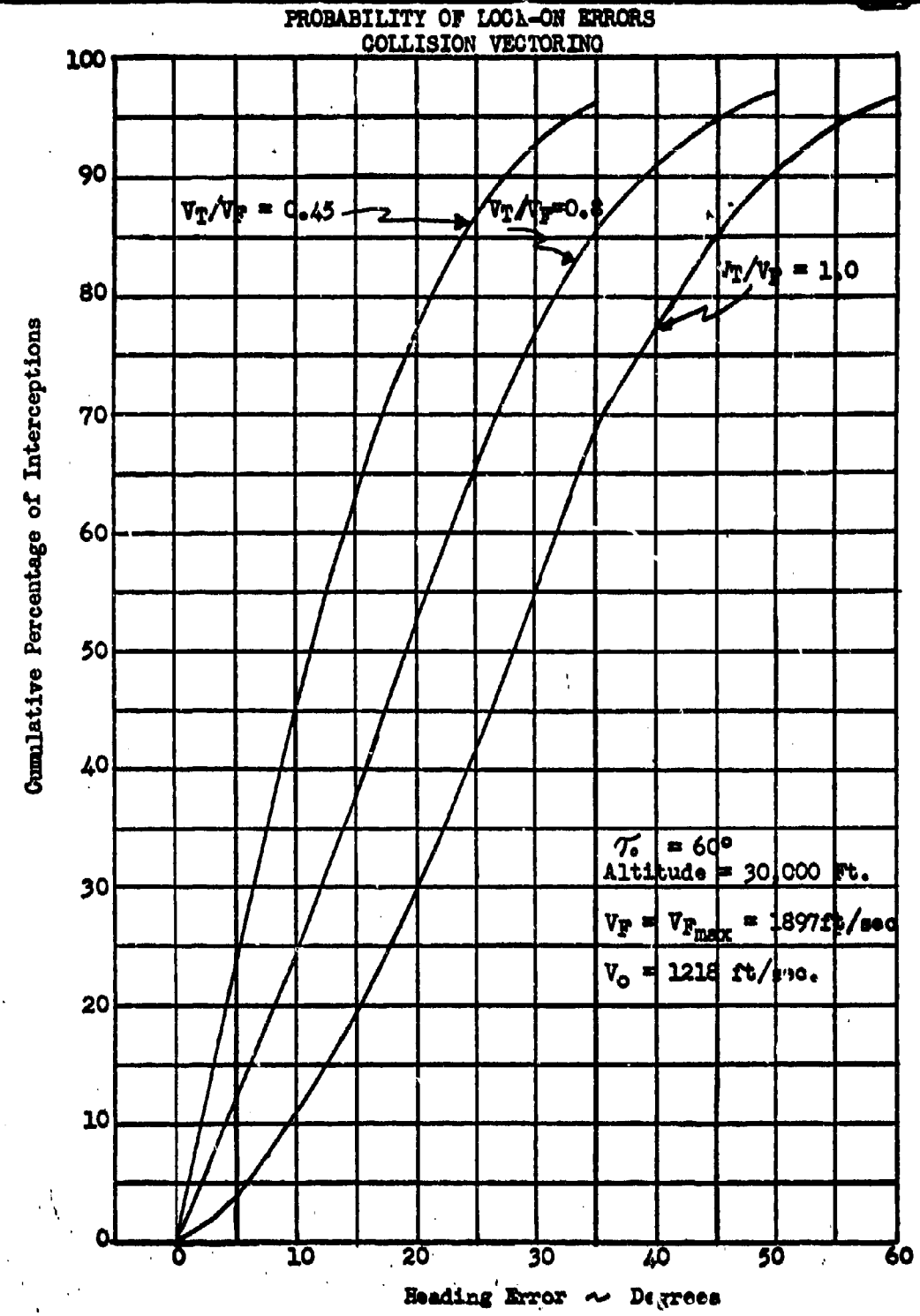
PROBABILITY OF LOCK-ON ERRORS
COLLISION VECTORING
Cumulative Percentage of Interceptions
100
90
80
70
60
50
40
30
20
10
0
V_T/V_F = 0.45
V_T/V_F=0.8
V_T/V_F = 1.0
τ_o = 60°
Altitude = 30,000 Ft.
$V_F = V_{F_{max}}$ = 1897 ft/sec
V_o = 1218 ft/sec.
0
10
20
30
40
50
60
Heading Error ~ Degrees

Figure 7

16

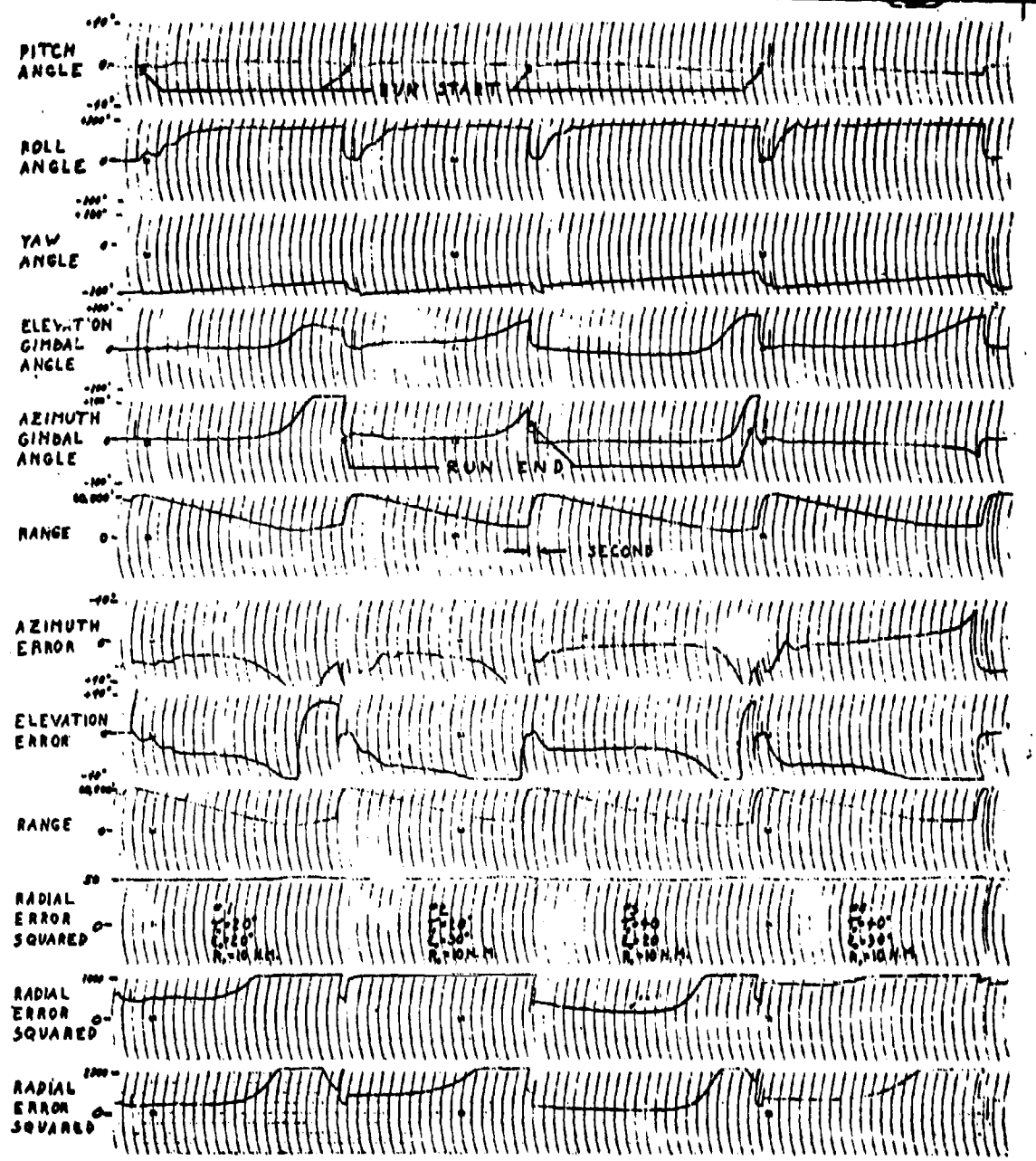

F8U-3 ALTITUDE = 30,000' V_f = 1.91M V_t = 2.20M
LEAD PURSUIT ATTACK

FIGURE 8

FSU-3 STEERING ERROR VS. SETTLING TIME

V_F = 2185 ft/s

V_T = 1897 ft/s

3 g Limit Turn

85% Cumulative Probability

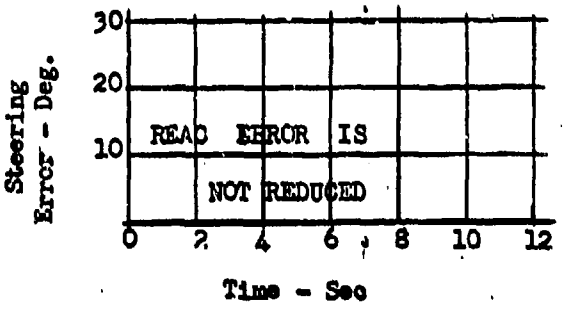

50% Cumulative Probability

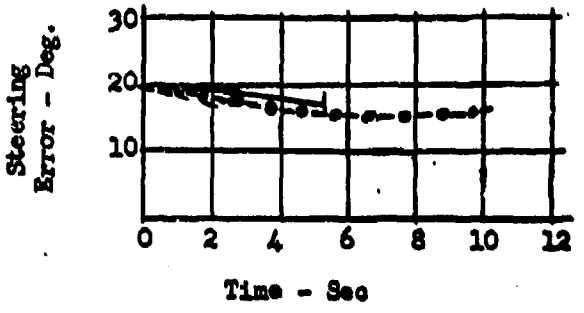

τ_o = 20°

$\mathcal{E}_o$ = 20°

R = 10 N.M.

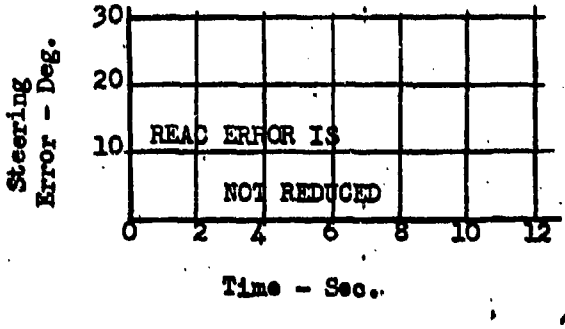

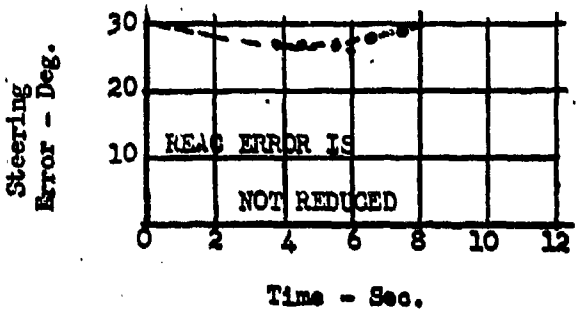

τ_o = 20°

$\mathcal{E}_o$ = 30°

R = 10 N.M.

Notes: ——Reac Generated Data - Pilot Effects

-o-o- FSU-3 IBM Course

Figure 9

F8U-3 STEERING ERROR VS. SETTLING TIME

V_P = 2185 ′/sec
V_T = 1897 ′/sec
3g Limit Turn

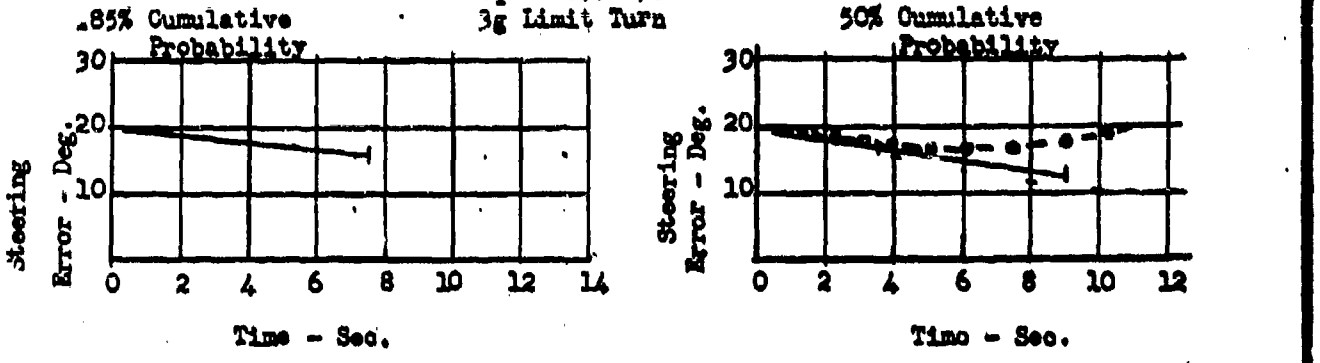

γ_o = 40°
ε_o = 20°
R_o = 10 N.M.

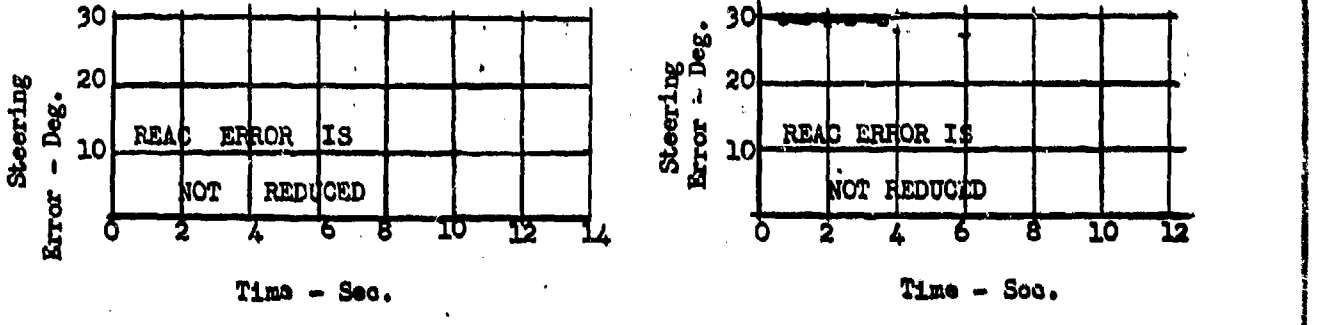

γ_o = 40°
ε_o = 30°
R_o = 10 n.m.

Notes:—Reac Generated Data - Pilot Effects

-o-o- F8U-3 IBM Course

Figure 10

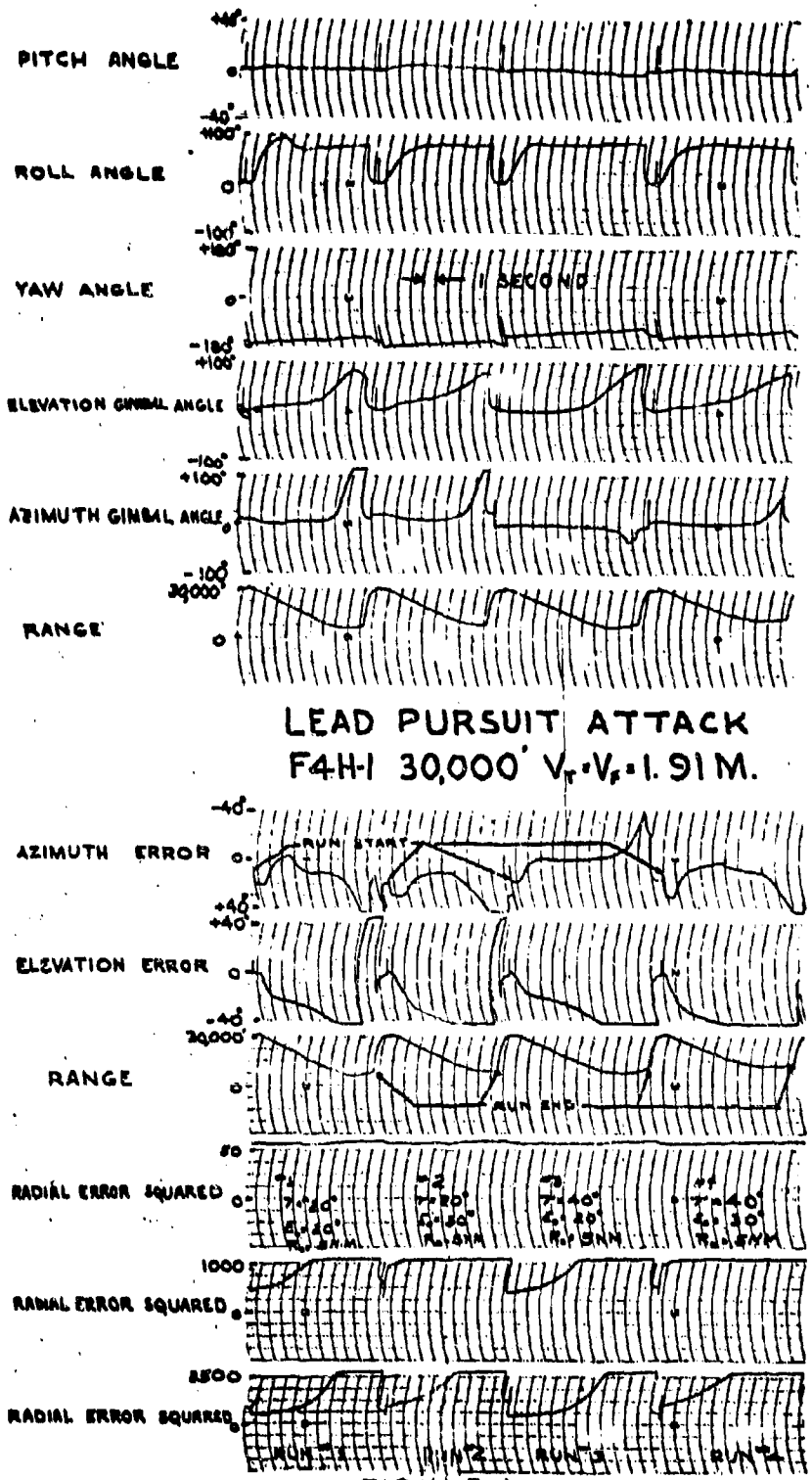
PITCH ANGLE
+45°
0
-45°
ROLL ANGLE
+180°
0
-180°
YAW ANGLE
1 SECOND
ELEVATION GIMBAL ANGLE
+100°
-100°
AZIMUTH GIMBAL ANGLE
+100°
-100°
RANGE
30000'
0
LEAD PURSUIT ATTACK
F4H-1 30,000' $V_T = V_F = 1.91$ M.
AZIMUTH ERROR
-40°
RUN START
0
+40°
ELEVATION ERROR
+40°
0
-40°
RANGE
30,000'
0
RUN END
RADIAL ERROR SQUARED
80
0
RADIAL ERROR SQUARED
1000
0
RADIAL ERROR SQUARED
2500
0
RUN 1
RUN 2
RUN 3
RUN 4

FIGURE 11

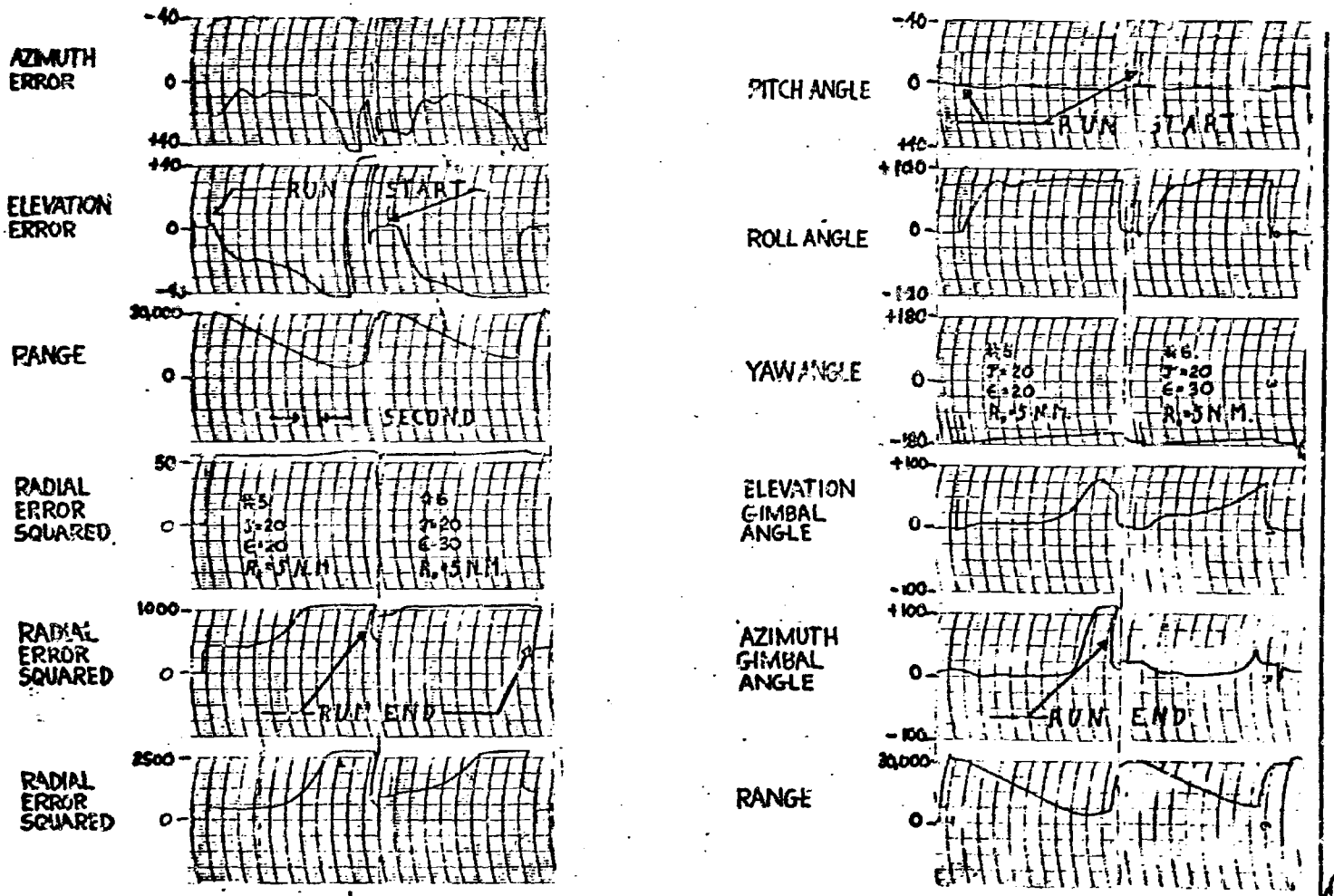

FIGURE 12

F8U-3 ALT.=30,000' V_t=1.52M V_t=2.20 M

LEAD PURSUIT ATTACK

F8U-3 STEERING ERROR VS. SETTLING TIME

V_F = 2185 ft/s

V_T = 1518 ft/s

3g Limit Turn

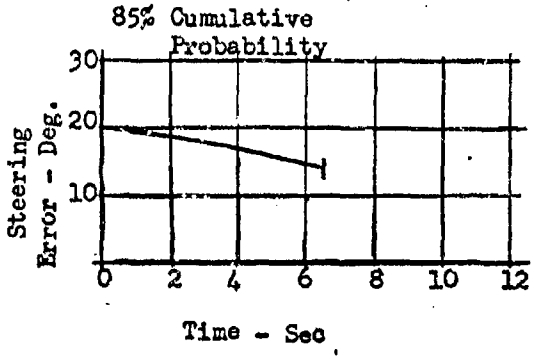

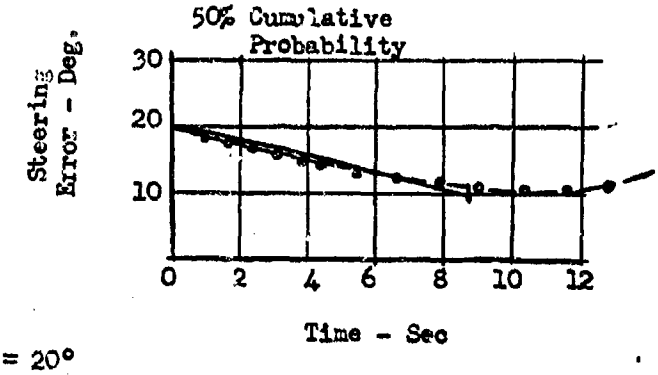

τ_o = 20°

ε_o = 20°

R = 10 N.M.

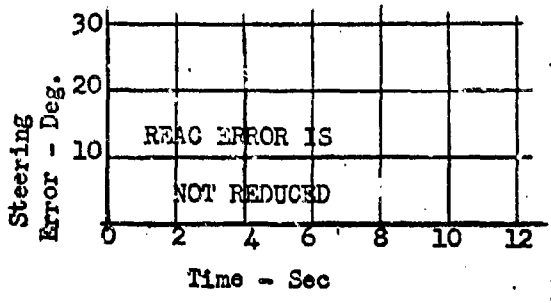

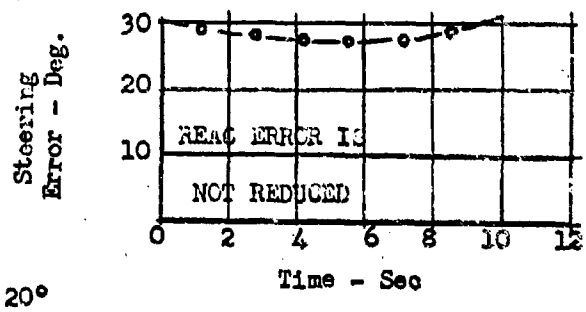

τ_o = 20°

ε_o = 30°

R = 10 N.M.

Notes: ——— REAC Generated Data - Pilot Effects

-o-o- F8U-3 IBM Course

Figure 13

F J-3 STEERING ERROR VS. SETTLING TIME

V_F = 2185 f/s

V_T = 1518 f/s

3g Limit Turn

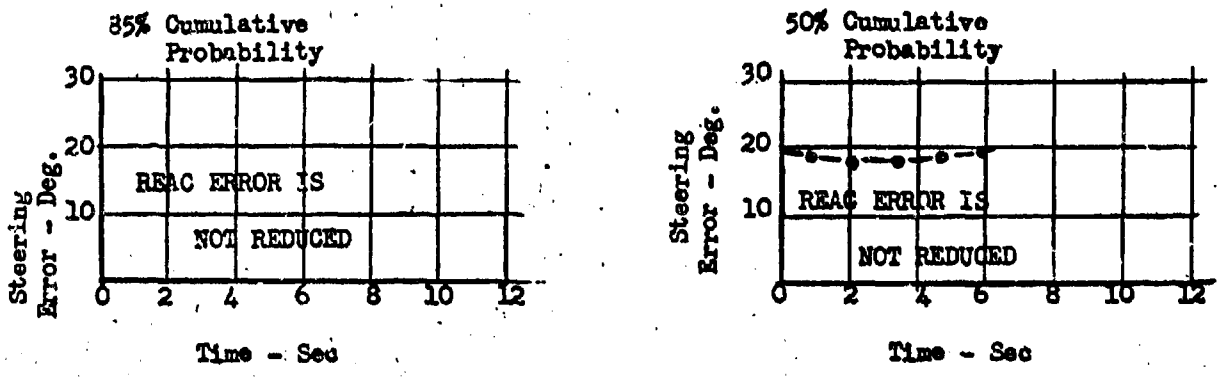

τ_o = 40°

ϵ_o = 20°

R = 7.5 N.M.

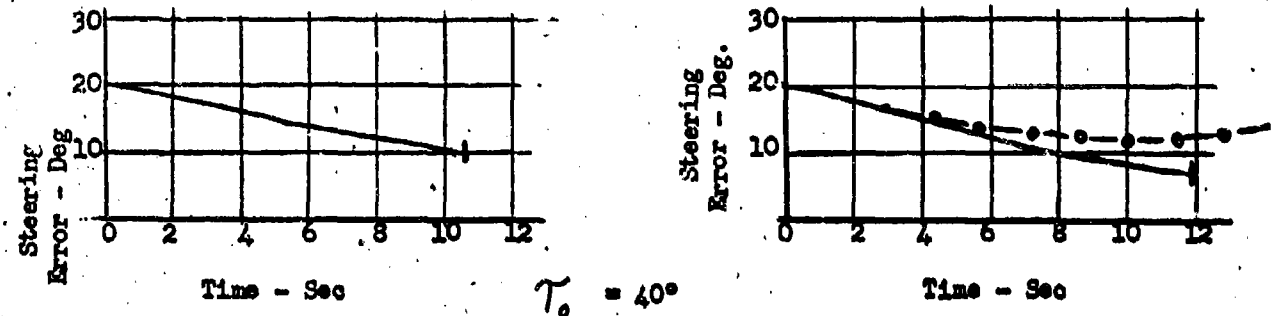

τ_o = 40°

ϵ_o = 20°

R = 10 N.M.

Notes: —— REAC Generated Data - Pilot Effects

-o-o- FSU-3 IBM Course

Figure 14

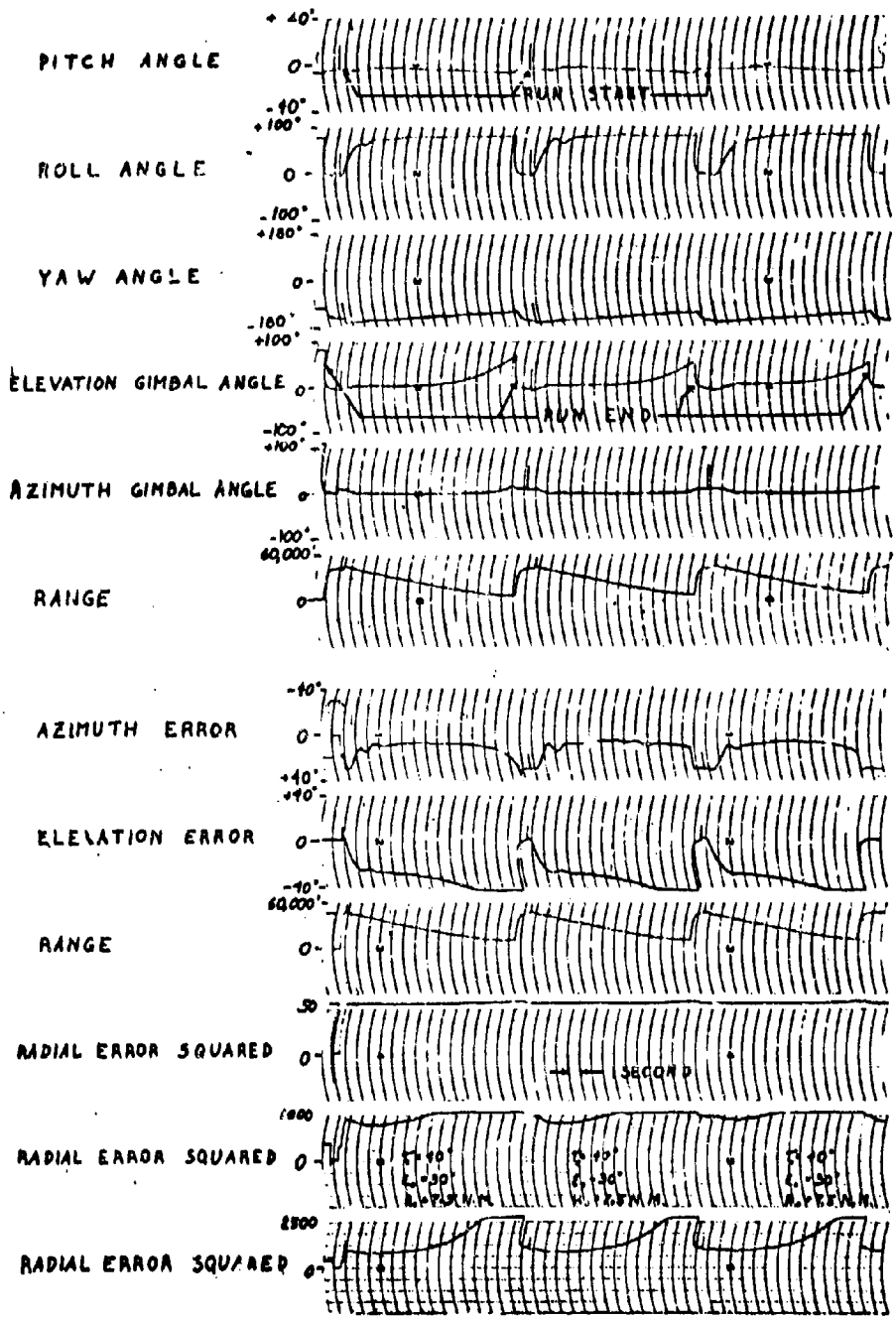

LEAD PURSUIT ATTACK

F8U-3 30,000' V_T=1.53M V_P=2.20M

FIGURE 15

F8U-3 STEERING ERROR VS. SETTLING TIME

V_F = 2185 f/s

V_T = 1518 f/s

3g Limit Turn

85% Cumulative Probability

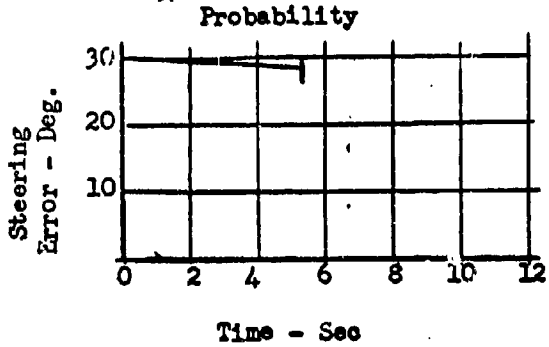

50% Cumulative Probability

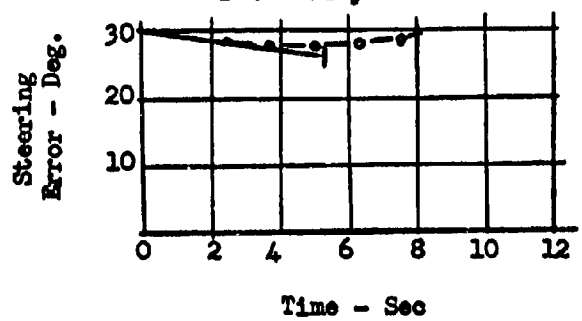

τ_o = 40°

ε_o = 30°

R = 10 N.M.

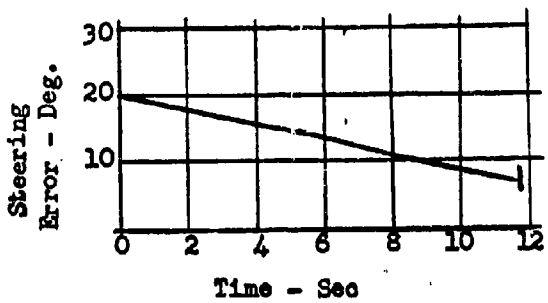

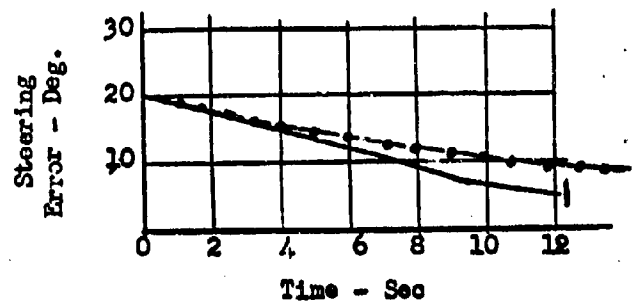

τ_o = 60°

ε_o = 20°

R = 10 N.M.

Notes: ——REAC Generated Data - Pilot Effects

-o-o- F8U-3 IBM Course

Figure 16

F8U-3 STEERING ERROR VS. SETTLING TIME

V_F = 2185 f/s

V_T = 1518 f/s

3g Limit Turn

85% Cumulative Probability

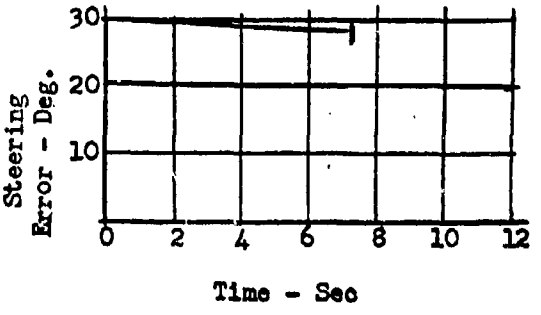

50% Cumulative Probability

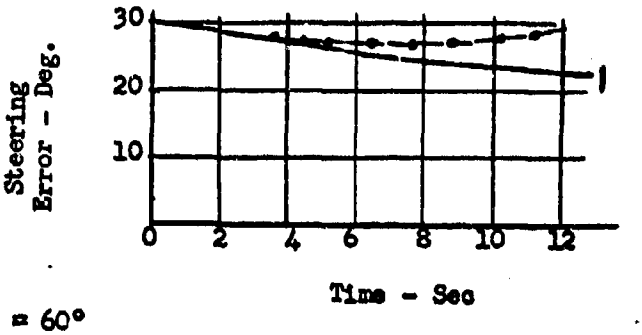

τ_o = 60°

ε_o = 30°

R = 10 N.M.

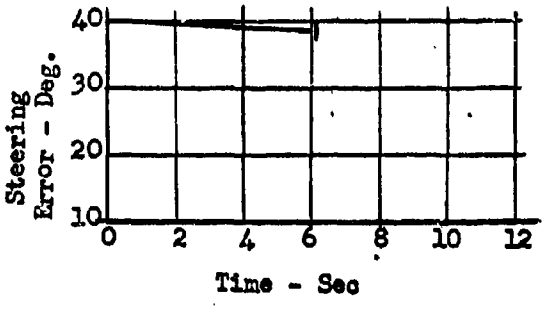

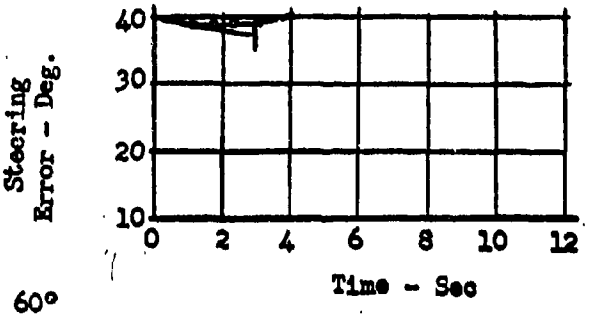

τ_o = 60°

ε_o = 40°

R = 10 N.M.

Notes: ——— REAC Generated Data - Pilot Effects

-o-o- F8U-3 IBM Course

Figure 17

FBU-3 STEERING ERROR VS. SETTLING TIME

V_P = 2185 ′/s

V_T = 1518 ′/s

3g Limit Turn

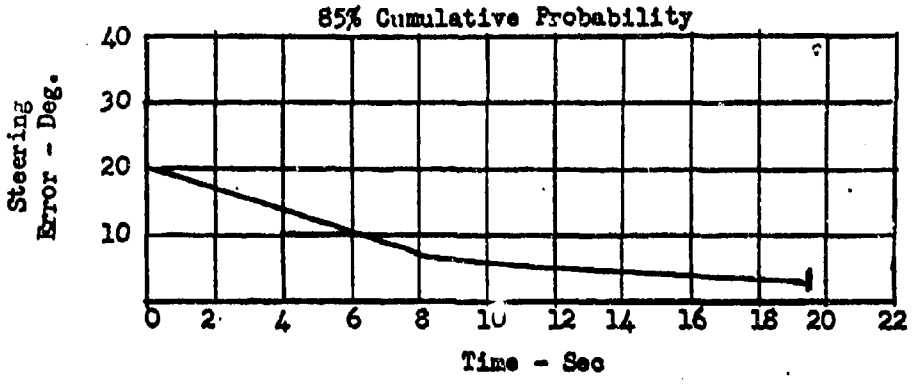

τ_o = 60°

ε_o = 20°

R = 15 N.M.

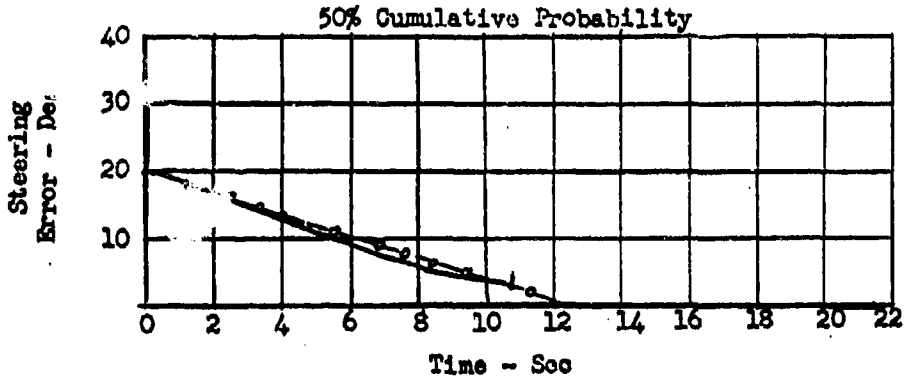

NOTES: ——— Roac Generated Data - Pilot Effects

-o-o- FBU-3 IBM Course

Figure 18

F8U-3 STEERING ERROR VS. SETTING TIME

V_F = 2135 ft/s

V_T = 1518 ft/s

3g Limit Turn

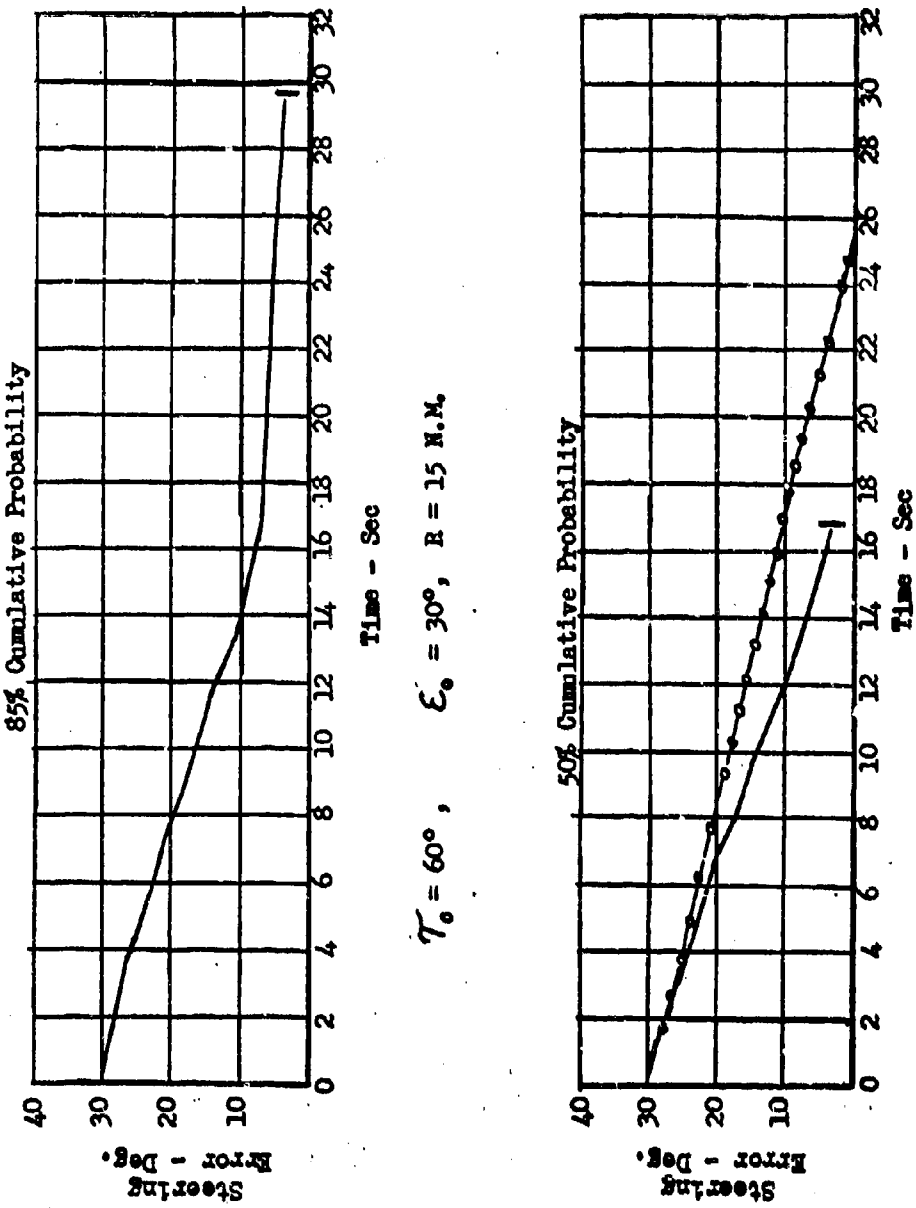

$\tau_o = 60°$, $\mathcal{E}_o = 30°$, R = 15 N.M.

NOTES: ——Reac Generated Data - Pilot Effects

-o-o- F8U-3 IBM Course

Figure 19

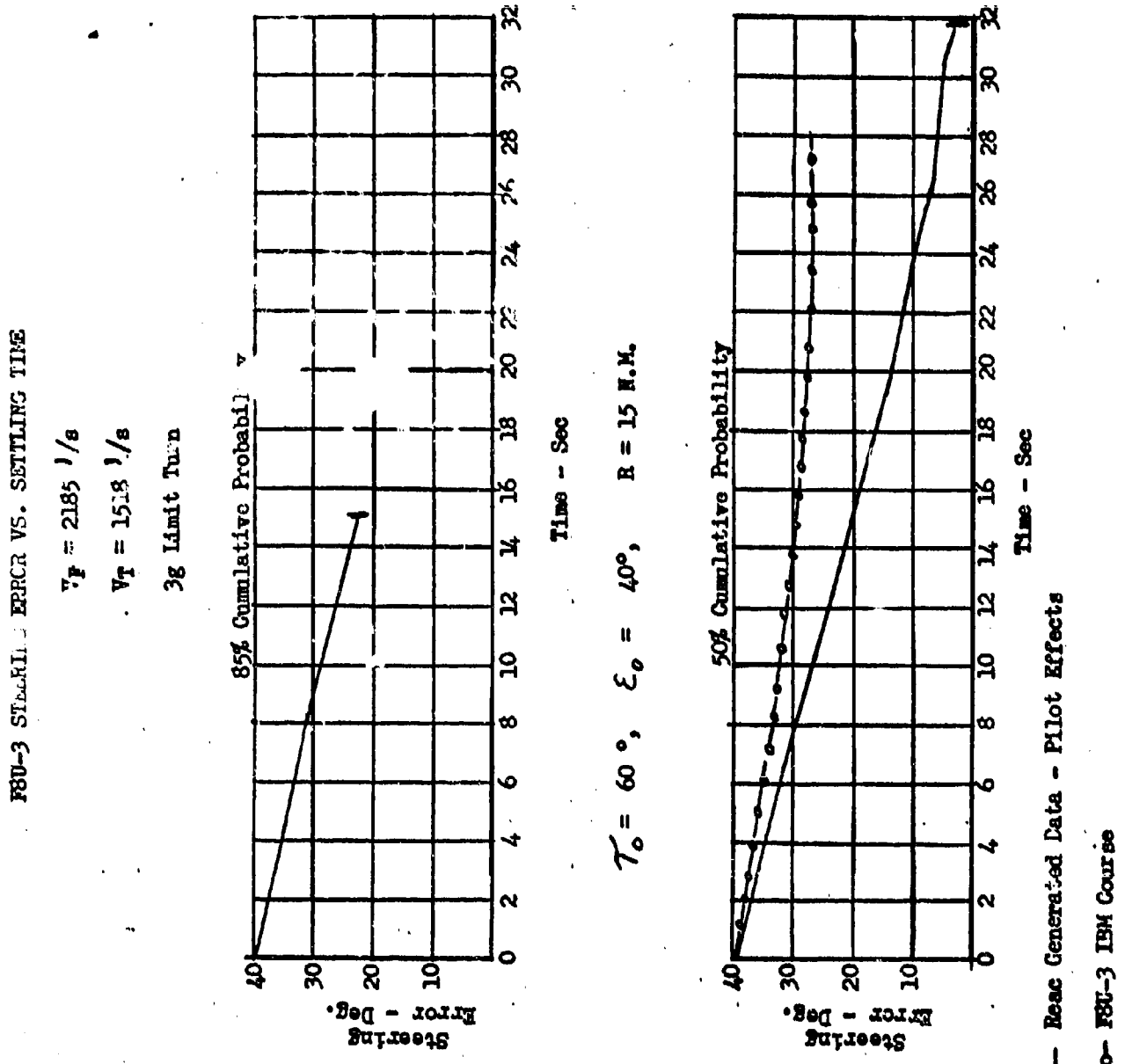
F8U-3 STEERING ERROR VS. SETTING TIME
V_F = 2185 f/s
V_T = 1518 f/s
3g Limit Turn
85% Cumulative Probability
50% Cumulative Probability
Steering Error - Deg.
Time - Sec
T_o = 60°, $\mathcal{E}_o$ = 40°, R = 15 N.M.
NOTES:
—— Reac Generated Data - Pilot Effects
-o-o- F8U-3 IBM Course

Figure 20

F8U-3 STEERING ERROR VS. SETTLING TIME

V_F = 2185 ft/s

V_T = 854 ft/s

3g Limit Turn

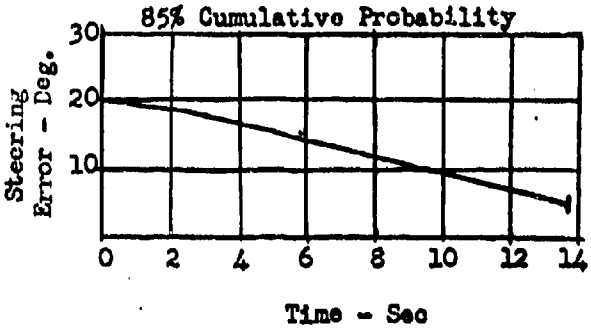

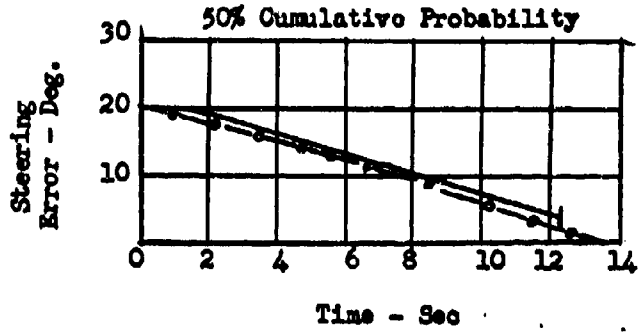

τ_o = 40°

ε_o = 20°

R = 10 N.M.

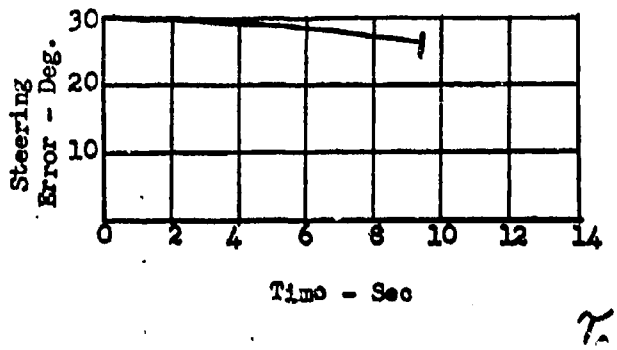

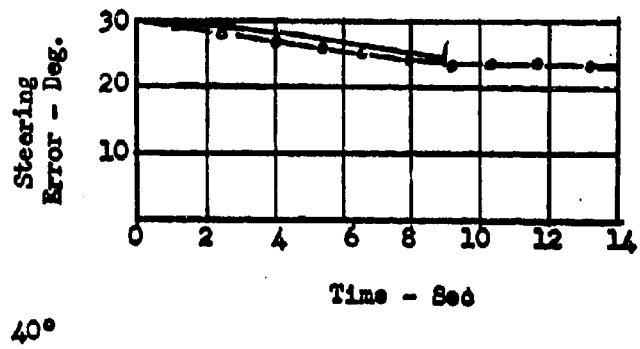

τ_o = 40°

ε_o = 30°

R = 10 N.M.

NOTES: —— Reac Generated Data - Pilot Effects

-o-o- F8U-3 IBM Course

Figure 21

F4H-1 STEERING ERROR VS. SETTLING TIME

V_F = 1697 ft/s

V_T = 854 ft/s

3g Limit Turn

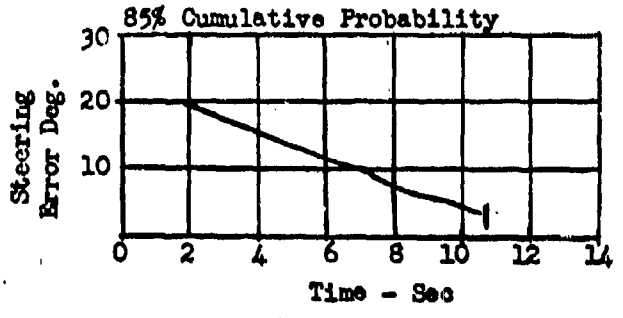

τ_e = 40°

ε_o = 20°

R = 10 N.M.

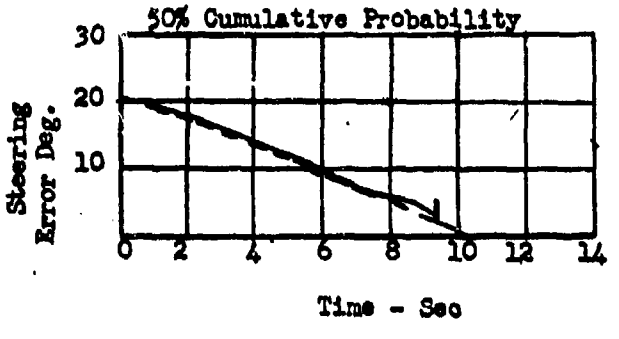

NOTES: ——— Reac Generated Data - Pilot Effects
- - - F4H-1 IBM Course

Figure 22

31

F4H-1 STEERING ERROR VS. SETTLING TIME

V_P = 1897 ft/s

V_T = 854 ft/s

3g Limit Turn

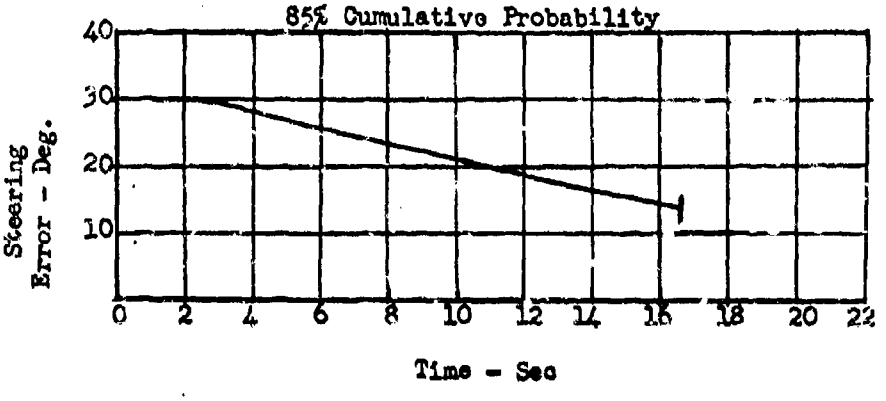

τ_o = 40°

ε_o = 30°

A = 10 N.M.

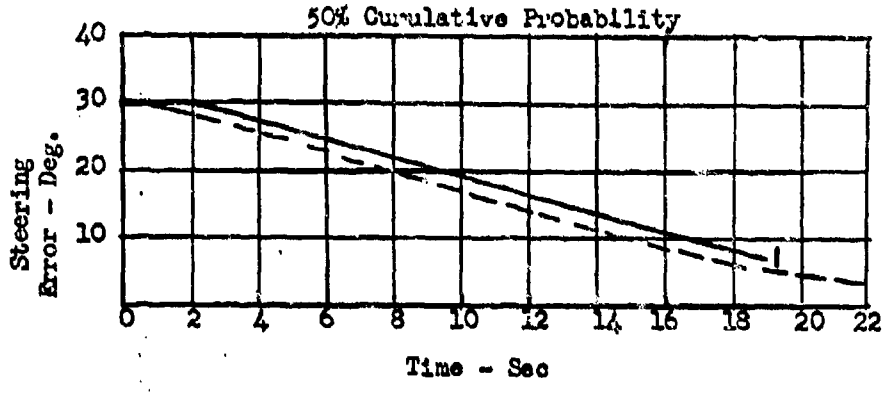

NOTES: ——— Rouc Generated Data - Pilot Effects
- - - F4H-1 IBM Course

Figure 23

and consequently the data was not assessed with respect to this criteria.

5.3 Reac Results and IBM Results. From a study of the Reac simulation recordings it appeared that the majority of the maneuvers could be approximated by constant rate turns. Figures 9,10,11,13,14, 16-23 compare settling time curves generated by a single course on the IBM to the statiscally generated results from the Reac study. The dashed lines represent the IBM generated data. In most cases the agreement is excellant. In a few cases it appears that the Reac runs were performing a maneuver just slightly in excess of 3 "g"s load factor. A slight excess integrated for a period of time would produce such a disagreement. It indicates that the buzzer sounds between on and off were weighted slightly towards the on situation for these few cases.

6. References

1. NMSTR #5, Time Required For Pilot To Settle System Errors in XIA Type System, 7-15-57, R. F. Wancowicz, Confidential

2. NMSTR #6, F8U3 Stability Derivatives, Dynamic Characteristics, and Basic Performance Data, R. D. Tucker, Confidential.

Analytical Section Technical Memorandum No. 279

AN-FNC

APPENDIX V

Probability of Successful Launch of Sparrow III From F4H-1 Pull-up Attacks

by

E. C. Quesinberry

Navigation and Flight Control Group

February 6, 1958

Distribution:

Restricted, Proprietary

D. J. Povejsil, Mgr. ~~100~~
R. G. Clanton, - 103
(50) E. C. Quesinberry - 103

Uniterms:

Air-to-air
Attacks
Capabilities
Pursuit
Detection
Probability
Distributions
Interceptor
Gimbal
Lock-on
F4H
Sparrow III
APQ-72

Charge No.:

003-103-100-C-90114

2:6:58/lm

ABSTRACT

This report presents the results of an investigation of the pullup capability of the XlA interceptor weapon system against targets flying a head-on course at a higher altitude. The probability of successfully launching the missile is computed after a statistical evaluation of the model.

F4H-1 aerodynamic characteristics are used. Missile capability is described by maximum and minimum launch range equations and an expression for average relative missile speed.

In general an attack consists of the following: Vectoring, detection, lock-on, a conversion maneuver, a lead-pursuit course to within firing range, launch, a post launch lead-pursuit illumination segment and a recovery maneuver.

Data is developed to show the probability of successful missile launch for Mach 2.0 interceptors attacking mach 2.0 and mach 0.9 targets at 50,000 ft. and at 65,000 ft. Results are also given for a realizable radar improvement which greatly increases the capability of the system. It is of interest to note that each computation of the probability of successful launch requires the statistical evaluation of 24 individual attacks.

Table of Contents

List of Figures

1. Objective

This study was undertaken to develop data suitable for use in computing the overall kill probability of the XlA weapon system for head-on pullup attacks.

For various combinations of target velocity, fighter velocity, and incremental altitude, the probability of successfully launching the missile was determined after evaluating the effects of the following:

1. Probability distribution of vectoring errors in a collision vectoring system.
2. Probability distribution of detection.
3. A fixed 10-second lock-on time.
4. A fixed AI gimbal coverage.
5. Probability of converting steering error at lock-on to within $\pm 10^{\circ}$ before minimum launching range, R_{min}.
6. A minimum recovery L/W of 0.5 g's.

2. Conclusions

1. Interceptors using the unimproved radar show little capability against Mach 2.0 targets at 50,000 ft. and 65,000 ft., as shown by Figures 6 and 7.
2. Increasing the AI radar range of 85% cumulative detection probability (from 12.75 N.M. for Mach 4.0 closing rates to 19 N.M.) greatly increases system capability against both Mach 0.9 and Mach 2.0 targets. See Figures 4, 5, 6, and 7.
3. Inability to reduce initial errors to within ± 10 degrees between R_{max} and R_{min} is the greatest restriction on system capability. For a given radar model the principal restriction on success against 50,000 ft. targets is the pilot's limitation to a 3g course. For 65,000 ft. targets aircraft CL_{max} limitations often hold course segments to less than 3g and thus become significant restrictions. Increased AI radar range alleviates the restrictions due to the pilot, and to a lesser degree those due to aircraft performance.
4. Antenna gimbal angle limits restrict pullup capability by only a few percent in the areas indicated in Figures 4-7 except as noted in section 4.2.3.
5. The Criterion of minimum L/W = 0.5g during recovery restricts success for pullups from low altitudes against 65,000 ft. targets.
6. In general, vectoring errors reduce the probability of successful launch. An exception occurs at low fighter initial altitudes when recovery L/W is

the principal limitation. Large vectoring errors then cause the attacks to be made in a slant plane which begins to approach the horizontal ($\beta = 0^{o}$). The interceptor thus suffers less slowdown during the attack and higher values of L/W exist during the recovery maneuver.

3. Investigation Procedure

3.1 Scope - For this investigation, targets at 65,000 ft. and 50,000 ft. altitude are examined for vulnerability. Interceptor speeds of Mach 2.0 or $V_{F_{max}}$ and target speeds of Mach 2.0 and Mach 0.9 are considered. For F4H-1 $V_{F_{max}}$ values below 30,000 ft. see Figure 1.

3.2 Attack Doctrine

3.2.1 Vectoring

This study evaluates pull-up attacks made after the interceptor has been vectored into a head-on course with respect to the target. The attacks are dispersed horizontally as a result of vectoring errors. In order to show the effects of a vectoring error on a pull-up attack, the pullup trajectory must be expressed in three dimensions in the general case. For head-on pull-up attacks, in which the interceptor course and the target course are initially parallel, the pullup trajectory will occur in a slant plane which contains the lead-pursuit triangle as shown in Figure 2. The tangent of the angle, β , between the slant plane and a horizontal reference plane is equal to the initial altitude difference of the interceptor and the target divided by the horizontal component of the separation of their initial courses.

3.2.2 Pull-up Maneuver

After the vectoring phase is completed by detection of the target, a 10-second interval is assumed for lock-on time. The pull-up maneuver is then made at a constant normal acceleration of 3g's or at maximum lift coefficient if this acceleration exceeds the capability of the interceptor.

3.2.3 Launch Criteria

When the following criteria are met the missile is launched.

1. Launch error (ϵ) $<$ 10^{o}

2. $R_{max} > R > R_{min}$

A lead-pursuit course with minimum error is maintained by the interceptor after launch to provide illumination of the target until impact.

MODEL F4H-1
$V_{max.}$ VS ALTITUDE
0 TO 30,000 FT
G.W 35,000 LBS.
MAXIMUM VELOCITY OF 4H-1
FIGURE 1

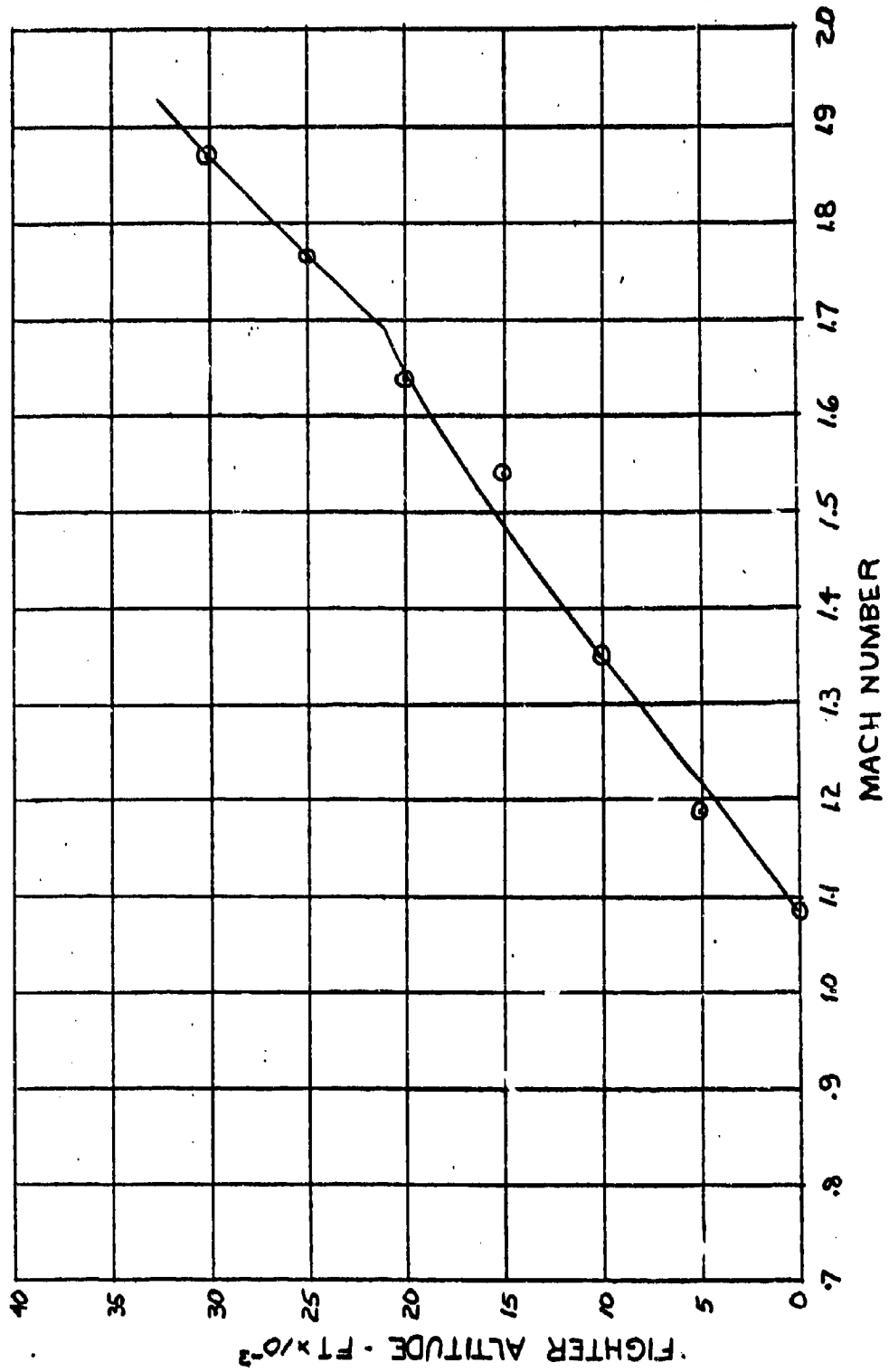

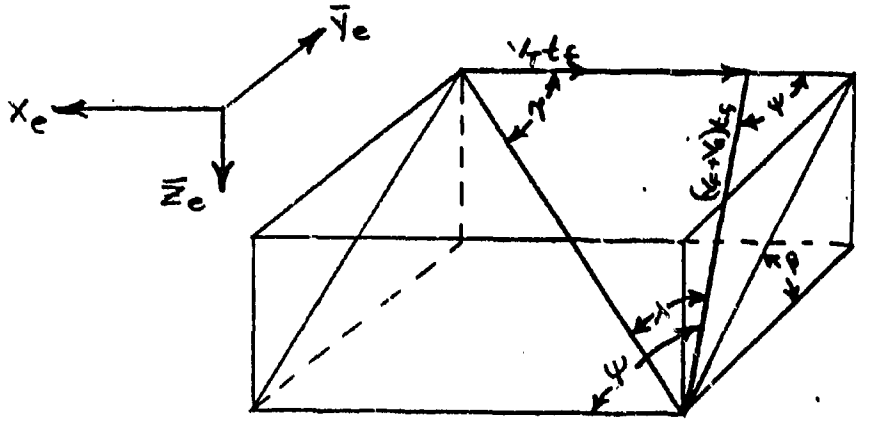

FIGURE 2. LEAD PURSUIT TRIANGLE IN SLANT PLANE

The time of flight of the missile is computed by equation I-16.

$$\text{I-16} \quad t_f = \frac{R \sin \tau}{\sin \psi \ (V_o + V_T)}$$

These equations are confined to the slant plane shown in Figure 2. At impact the interceptor performs a break-away maneuver to complete the attack. For this evaluation the break-away maneuver consists of completion of a loop with a minimum L/W of 0.5 g's at the peak altitude of the maneuver. See reference 2 for details.

3.3 Attack Computation

3.3.1 Radar Model

The probability distribution of detection is assumed normal. The standard deviation of this distribution is taken as 3.5 nautical miles based upon a review of APQ-50 Naval Air Test Center test data. See References 6 and 7.

The head-on coaltitude range of 85% cumulative detection probability (B47 target and APQ-72 radar) at a closing rate of Mach 4.0 is taken as 12.75 N.M. for unimproved radar, and as 19 N.M. for the improved radar. The horizontal separation at detection was assumed to be constant for all incremental altitudes.

Antenna gimbal angle limits are:

1. Unimproved radar
   1. Elevation; $\lambda e = +47^\circ$ (up) and -38° (down).
   2. azimuth; $\lambda a = \pm 41^\circ$
2. Improved radar
   1. $\pm 57^\circ$ in both azimuth (λa) and elevation, λe.

3.3.2 Vectoring Probability Distribution

Vectoring errors were assumed to result in a normal probability distribution of attacks with a standard deviation of 3 N.M., as specified by the Naval Research Laboratory in a memorandum, C-5309-387/57, dated May 14, 1957.

3.3.3 Method of Computation, See Figure 3.

The horizontal plane from which pullups are initiated is divided into two-mile-square boxes. To each box is assigned a probability of success, P_S. The probability of success for a particular box is

$$P_{S(B)} = P_{V(B)} \times P_{LO(B)} \times P_{Q(B)} \times P_{C(B)} \times P_{R(3)}$$

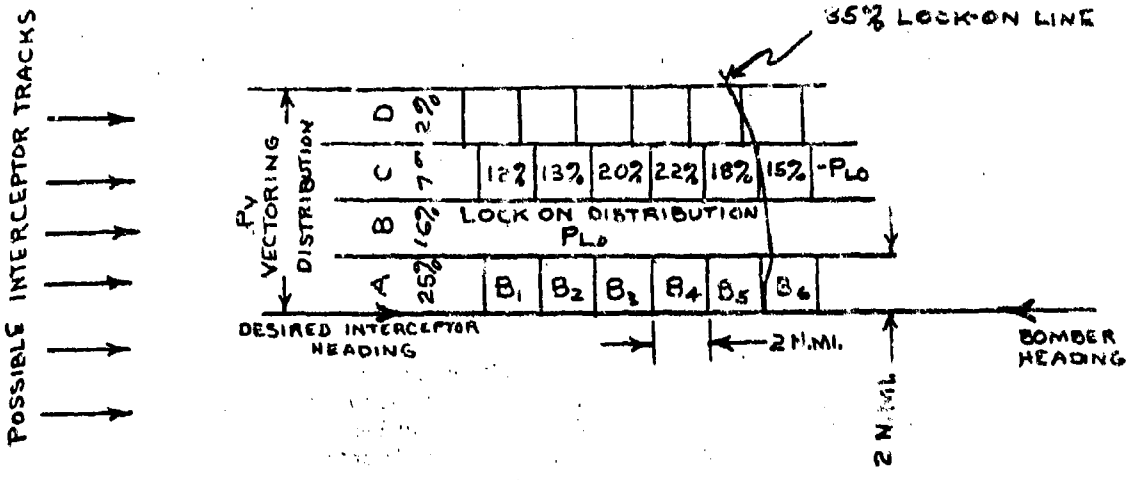

$$P_{S(B)} = P_{V(B)} \times P_{LO(B)} \times P_{G(B)} \times P_{C_B} \times P_R$$

$$P_{S_T} = \sum_{\substack{\text{ALL} \\ \text{BOXES}}} P_{S_B}$$

FIGURE 3. EXAMPLE OF PROBABILITY OF MISSILE-LAUNCH CALCULATION

Where P_V = Vectoring probability

P_{LO} = Lock-on probability

P_G = Gimbal coverage probability

P_C = Conversion probability (probability of converting initial steering error to within $\pm 10^o$ before R_{min}.)

P_R = Probability of recovery L/W of 0.5 g or greater.

Subscript B designates value for a single box.

Then the entire probability of successful missile launch P_S for the attack is

$$P_S = \prod_{\text{All Boxes}} P_S(B)$$

Pumps were assumed to start 10 seconds after detection because of the lock-on time required. For further details see Reference 2.

3.4 Attack Failure

Attack failure is established when any of the following conditions are met:

1. A lead-pursuit launch condition ($\epsilon < 10^o$) is not achieved for $R_{max} > R > R_{min}$.
2. Gimbal angle limits are exceeded when $R_{detection} > R > R_{impact}$.
3. Recovery maneuver results in L/W < 0.5 g's.
4. Trajectory requires negative values of L/W.

4. Results

4.1 General

Figures 4 through 7 present the results of the analysis discussed in section 3.3. Each point used in plotting a given curve is the composite evaulation of 24 separate attacks by the method of section 3.3.3. For variation of probability of successful launch with interceptor altitude Figures 4 through 7 best express the results. A discussion of the characteristics of these curves is given below.

4.2 Characteristics of Probability of Success vs. Interceptor Altitude Curves

4.2.1 Mach 0.9 Target at 50,000 Ft. - Figure 4.

Attack success decreases for the unimproved radar as the interceptor's initial altitude is lowered to 35,000 feet. This trend is caused principally by the larger error between the initial interceptor course and a lead-pursuit course as the incremental altitude is increased. This relation holds because the interceptor maximum velocity between 35,000 ft. and 50,000 ft. is constant at Mach 2 and the pitch-up rate is limited by the L/W = 3g requirement. Below 35,000 feet the decrease in interceptor maximum velocity allows a greater pitch-up rate for a 3g course. The capability to reduce error increases faster than the error itself as the interceptor initial altitude is lowered. This accounts for the break in the curve for unimproved radar.

For improved radar the additional detection range allows the initial error to be converted to within $\pm 10^{\circ}$ before R_{min} even for large incremental altitudes.

The gimbal-angle-limit restrictions on success indicated in Figure 4 are slight. (probability decrease $< 10\%$)

4.2.2 Mach 0.9 Target at 65,000 ft. - Figure 5.

The curves of Figure 5 reverse slope at 35,000 ft for the reasons noted in section 4.2.1. The reduction in probability of success below 15,000 feet is due principally to the minimum L/W criterion of 0.5 g during the recovery maneuver.

4.2.3 Mach 2.0 Targets at 50,000 ft. and 65,000 ft.

The curves of Figures 6 and 7 for Mach 2.0 targets show great reduction in success as attacks are started from lower altitudes. The rate of error reduction is slower for the higher speed targets and the increase in maneuverability gained by the interceptor because of decreased maximum velocity at low altitudes does not compensate for the greater initial error to be overcome. An exception is the V_{Fmax} interceptor with improved radar pulling up from 10,000 ft. to attack a Mach 2 Target at 40,000 ft. A high percentage of lead-pursuit courses is attained but gimbal angle limits are exceeded. In other cases the gimbal angle restrictions indicated in Figures 6 and 7 are slight. (Probability decrease $< 10\%$)

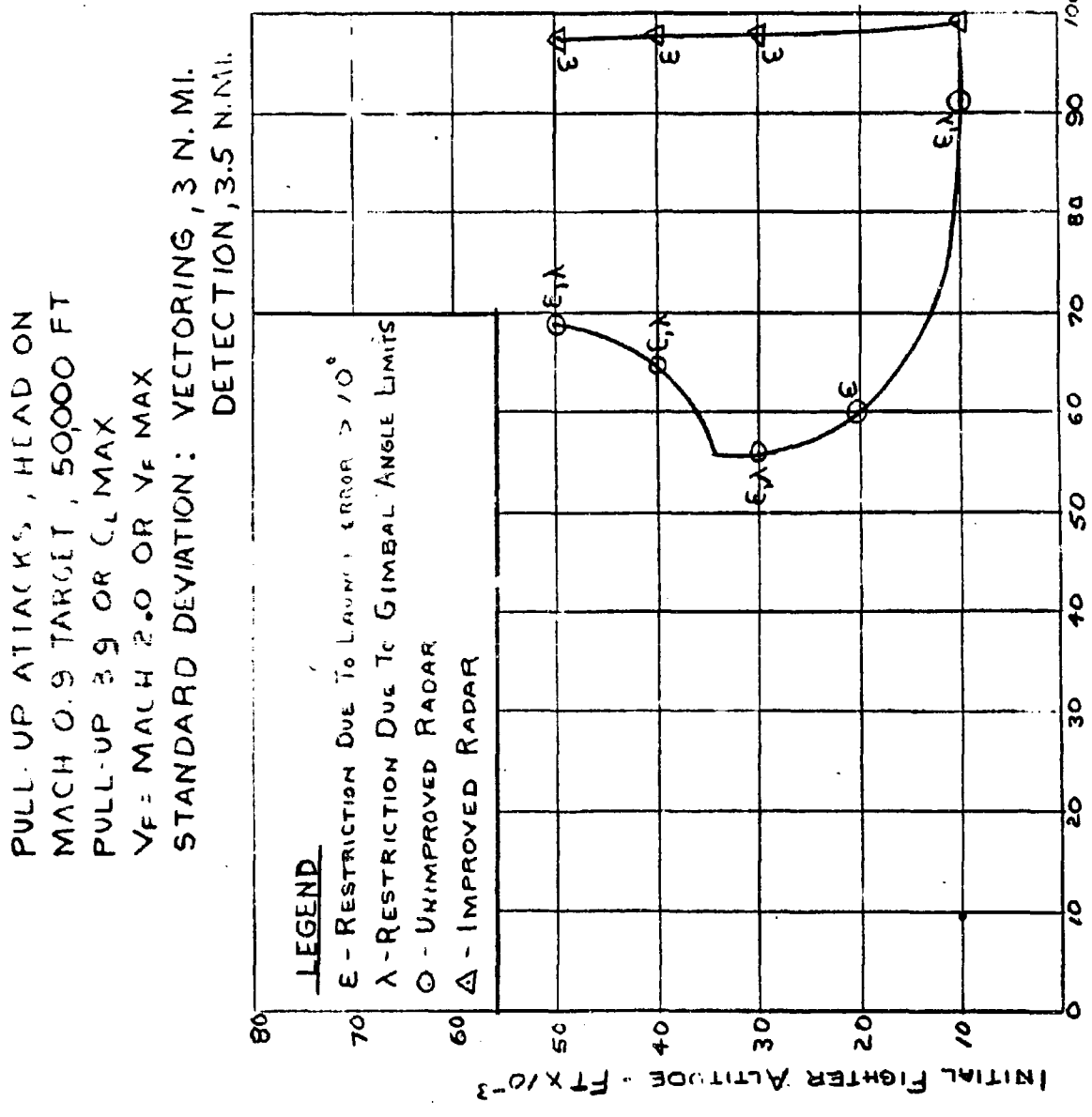
PULL UP ATTACKS, HEAD ON
MACH 0.9 TARGET, 50,000 FT
PULL-UP 3 g OR C_L MAX
V_F = MACH 2.0 OR V_F MAX
STANDARD DEVIATION: VECTORING, 3 N. MI.
DETECTION, 3.5 N.MI.
LEGEND
E - RESTRICTION DUE TO LAUNCH ERROR > 10°
λ - RESTRICTION DUE TO GIMBAL ANGLE LIMITS
O - UNIMPROVED RADAR
Δ - IMPROVED RADAR
INITIAL FIGHTER ALTITUDE - FT X 10^{-3}
PROBABILITY OF SUCCESSFUL LAUNCH, PER CENT
0
10
20
30
40
50
60
70
80
90
100
10
20
30
40
50
60
70
80

FIGURE 4

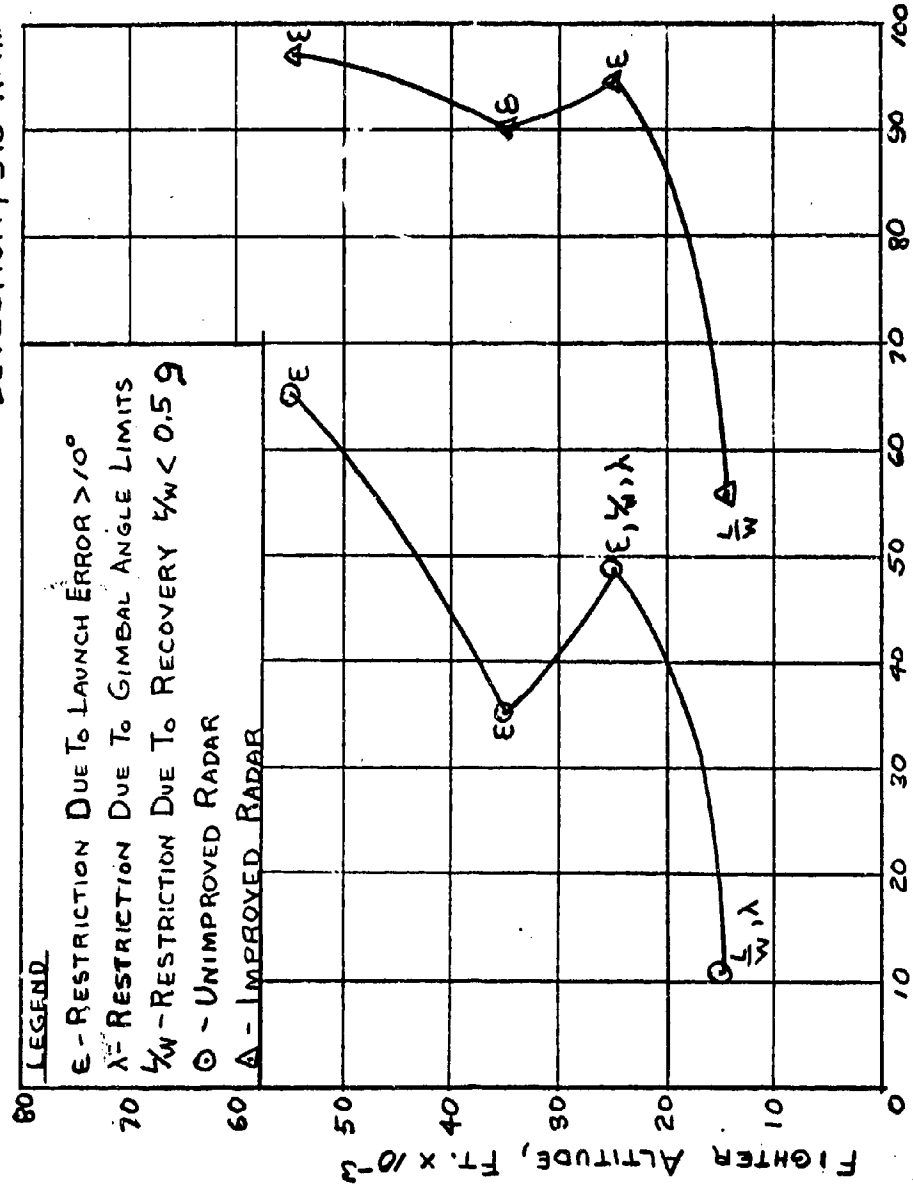
PULL-UP ATTACKS, HEAD ON
MACH 0.9 TARGET, 65,000 FT.
PULL-UP 3g OR C_L MAX
V_F = MACH 2.0 OR V_F MAX
STANDARD DEVIATION: VECTORING, 3 N.M.
DETECTION, 3.5 N.M.
LEGEND
E - RESTRICTION DUE TO LAUNCH ERROR >10°
λ - RESTRICTION DUE TO GIMBAL ANGLE LIMITS
L/W - RESTRICTION DUE TO RECOVERY $L/W < 0.5$ g
O - UNIMPROVED RADAR
A - IMPROVED RADAR
FIGHTER ALTITUDE, FT. x 10^{-3}
PROBABILITY OF SUCCESSFUL LAUNCH, PER CENT
0
10
20
30
40
50
60
70
80
90
100

FIGURE 5.

PULL-UP ATTACKS, HEAD ON
MACH 2.0 TARGET, 50,000 FT.
PULL-UP 3 g OR C_L MAX
N_F = MACH 2.0 OR V_F MAX
STANDARD DEVIATION: VECTORING 3 N.MI.
DETECTION 3.5 N.MI.

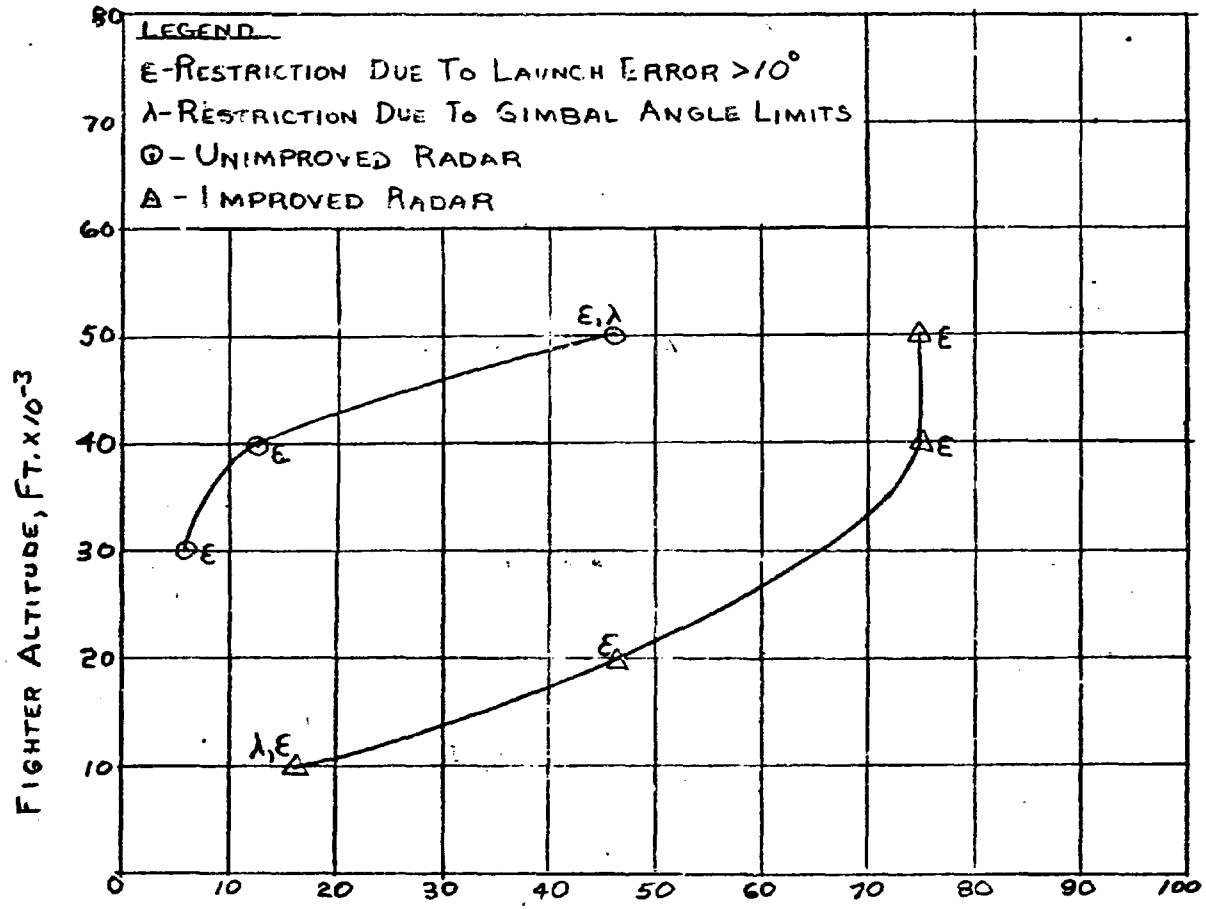

FIGURE 6

CONFIDENTIAL

PULL-UP ATTACKS ; HEAD-ON
MACH 2.0 TARGET 65,000 FT.
PULL-UP 3 g OR C_L MAX
V_F = MACH 2.0 OR V_F MAX
STANDARD DEVIATION: VECTORING 3 N.MI.
DETECTION 3.5 N.MI.

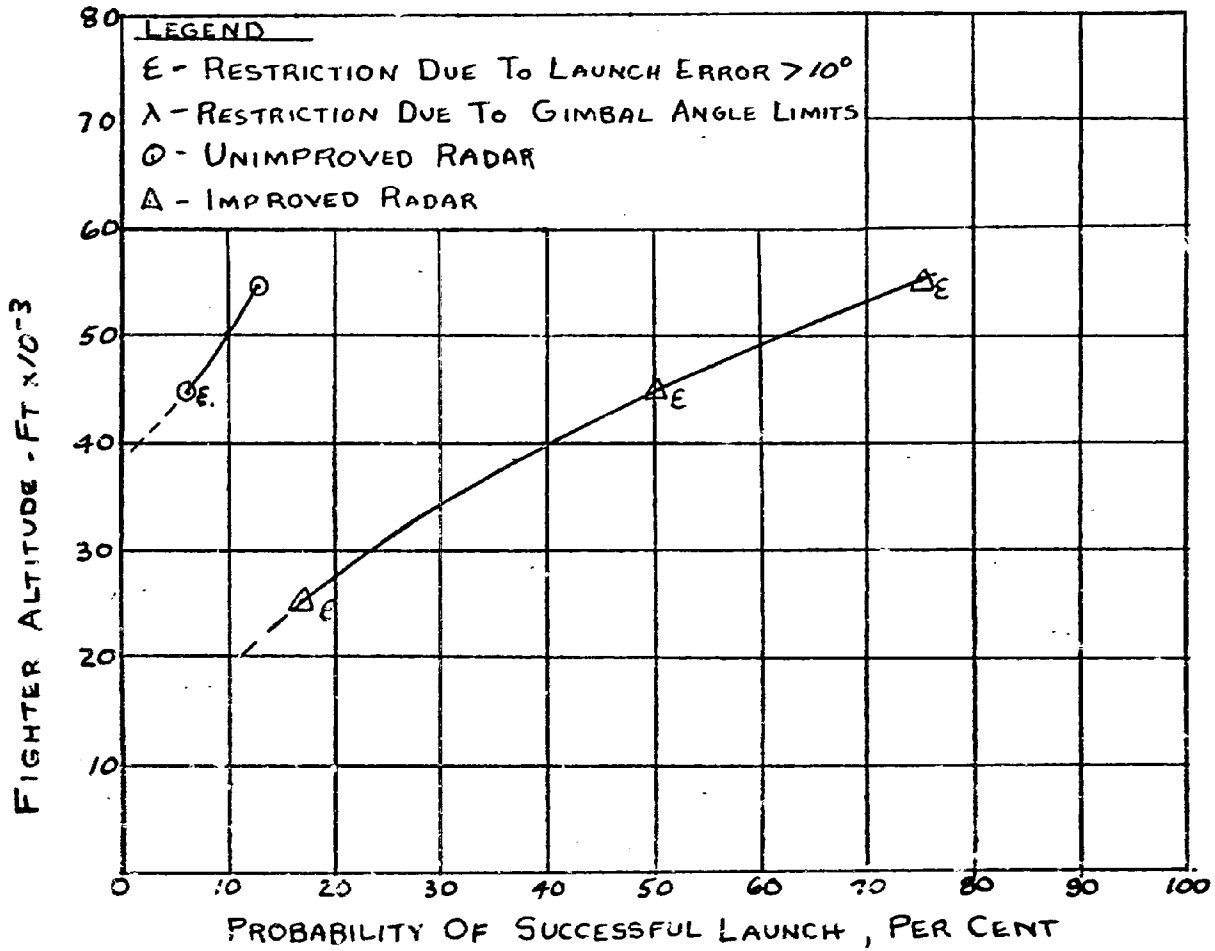

FIGURE 7

APPENDIX I

Aerodynamic Lead-Pursuit Equations In the Slant Plane *

$$m\dot{V}_F = T\cos(\alpha+\varepsilon) - D - mg\sin\beta\sin\psi \tag{1-1}$$

$$mV_F\dot{\psi} = T\sin\phi\sin(\alpha+\varepsilon) + L\sin\phi - mg\sin\beta\cos\psi \tag{1-2}$$

$$mg\cos\beta = T\cos\phi\sin(\alpha+\varepsilon) + L\cos\phi \tag{1-3}$$

$$\dot{R} = -[V_T\cos\tau + V_F\cos\lambda] \tag{1-4}$$

$$R(\dot{\tau} + p_T) = V_T\sin\tau - V_F\sin\lambda \tag{1-5}$$

$$\dot{\psi} = \dot{\lambda} + \dot{\tau} + p_t \tag{1-6}$$

$$\dot{\lambda} = \frac{\dot{\tau}V_T\cos\tau - \dot{V}_F\sin\lambda}{(V_0+V_F)\cos\lambda} \tag{1-7}$$

$$\sin\lambda = \frac{V_T\sin\tau}{V_0+V_F} \tag{1-8}$$

$$\sin\lambda a = \frac{=\sin\lambda\cos\phi}{\cos\lambda e} \tag{1-9}$$

$$\sin\lambda e = -[\cos\lambda\sin(\alpha-\Gamma) + \sin\lambda\sin\phi\cos(\alpha-\Gamma)] \tag{1-10}$$

$$\omega_j = (\dot{\tau}+\dot{p}_T)[\cos\phi\sin(\alpha-\Gamma)\sin\lambda a + \sin\phi\cos\lambda a] \tag{1-11}$$

* From original work by J. F. Buchan.

$$\omega_K = (\dot{\tau}+\rho_T)[\sin\phi\sin\lambda_e\sin\lambda_a+\cos\phi(\cos(\alpha-\Gamma)\cos\lambda_e - \sin(\alpha-\Gamma)\sin\lambda_e\cos\lambda_a)] \quad (1\text{-}12)$$

Eulerian Angles:

$$\text{Yaw,}\quad \psi = \tan^{-1}\left[\frac{\cos\beta\sin\psi}{\cos\psi}\right] \quad (1\text{-}13)$$

$$\text{Pitch,}\quad \gamma = \tan^{-1}\left[\frac{\sin\psi'\sin\beta}{\cos\beta}\right] \quad (1\text{-}14)$$

$$\text{Roll,}\quad \phi' = \tan^{-1}\left[\frac{-\sin\beta\cos\psi\cos\phi+\cos\beta\sin\phi}{\sin\beta\cos\psi\sin\phi+\cos\beta\cos\phi}\right] \quad (1\text{-}15)$$

$$t_f = \frac{R\sin\tau}{\sin\psi(V_o+V_f)} \quad (1\text{-}16)$$

$$R_{max} = R_1(h) + T_1(V_c - V_F), \text{ limited to 6.5 N.M.} \quad (1\text{-}17)$$

where:
- R_{max} = maximum launch range
- $R_1(h)$ = is defined in Figure 1-1
- T_1 = 11 sec for $V_c > V_F$
  $f_1(h)$ sec for $V_c < V_F$
- V_c = Range rate (positive when closing)
- V_F = Interceptor velocity - (ft./sec)

$$R_{min} = R_2(h) + T_2 V_c \quad (1\text{-}18)$$

where:
- R_{min} = minimum launch range
- T_2 = 3.3 sec.
- $R_2(h)$ = is defined in Figure 1-1

$$V_o = 935 \left[1+0.43\left(1-\frac{p}{p_o}\right)\right] \text{ ft/sec} \quad (1\text{-}19)$$

where:
- V_o = Average relative missile speed
- p/p_o = is pressure ratio to a sea-level reference.

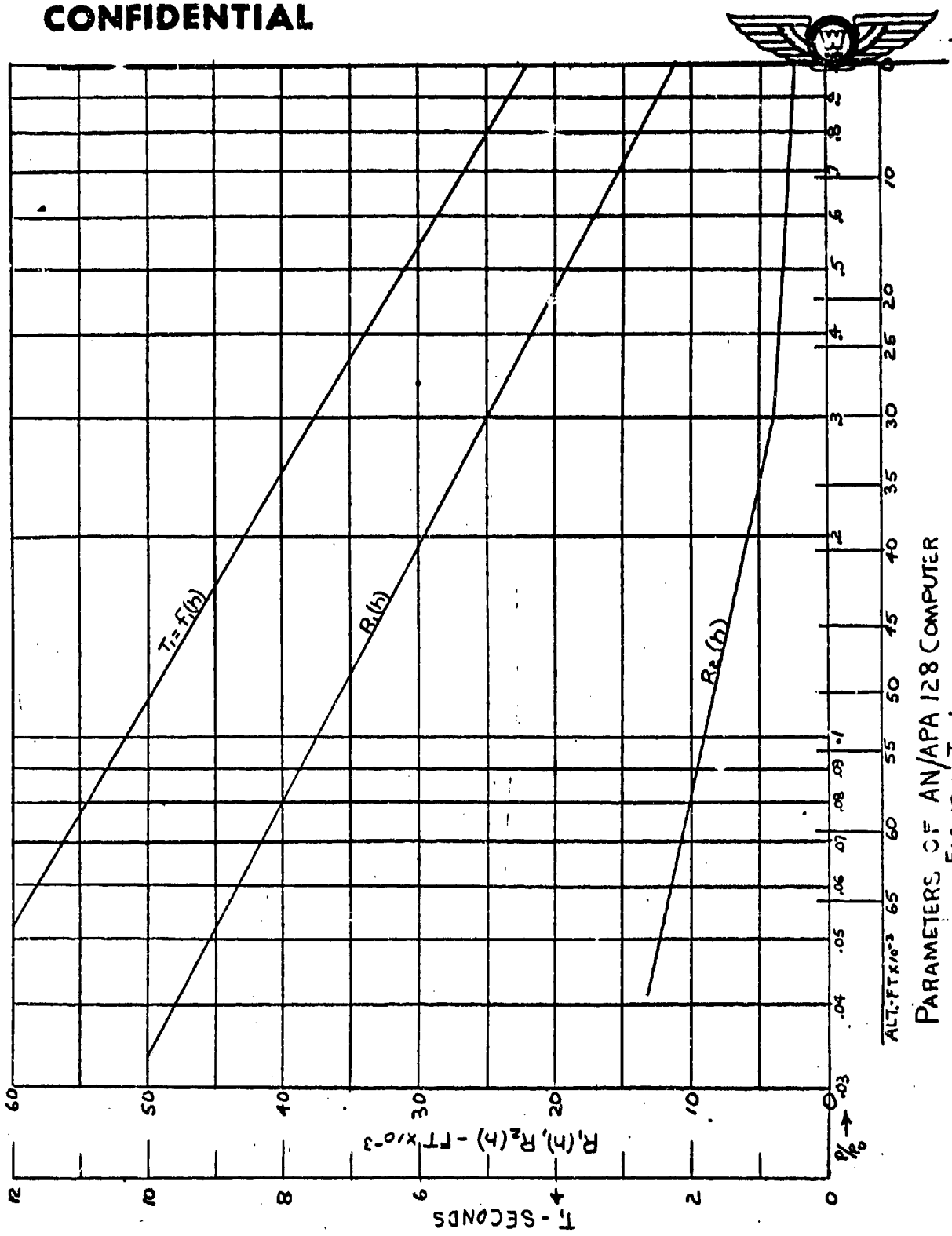

PARAMETERS OF AN/APA 128 COMPUTER
FIGURE I-1

APPENDIX II

Definition of Symbols

$\bar{X}_e, \bar{Y}_e, \bar{Z}_e$ = inertial space orthogonal units vectors.

$\bar{U}, \bar{V}, \bar{W}$ = wind axis orthogonal unit vectors.

γ, ψ, ϕ = angles referring space to wind coordinates.

ε = angle between thrust vector and fuselage reference line.

$\bar{L}$ = lift vector, perpendicular to velocity vector and wings.

$L = |\bar{L}|$ = lift (pounds)

$\bar{D}$ = drag vector, parallel to velocity vector

$D = |\bar{D}|$ = drag (pounds)

$\bar{T}$ = thrust vector

$T = |\bar{T}|$ = thrust, (pounds)

$\bar{W}$ = gravitational force vector on interceptor

$\bar{V}_F$ = interceptor velocity vector

$V_F = |\bar{V}_F|$ = interceptor speed (ft/sec)

$\bar{W}$ = gravitational force vector on interceptor

$W = |\bar{W}| = mg$ = interceptor's weight (pounds)

m = mass of interceptor (slugs)

g = gravitational acceleration, constant (ft/sec^2)

φ_T = turning rate of target with respect to space (rad/sec)

$\bar{R}$ = range vector

$R = |\bar{R}|$ = range (ft.)

λ = total lead angle

τ = angle-off-target's nose

$\dot{\tau}$	= $d\tau/dt$ (rad./sec)
$(\dot{\tau} + \rho_T)$	= total angular rate of the line-of-sight (rad/sec)
$\bar{V}_o$	= average missile velocity vector
$V_o = \lvert\bar{V}_o\rvert$	= average relative missile speed (ft/sec)
Γ	= depression angle of armament control axes to aircraft axes, a constant
$\lambda a, \lambda e$	= antenna train angles in aximuth and elevation, respectively
$\omega j, \omega K$	= angular rates of the line-of-sight in pitch and yaw, respectively (antenna coordinates) (rad/sec)
α	= angle of attack
$\bar{V}_T$	= target velocity vector
$V_T = \lvert\bar{V}_T\rvert$	= target speed (ft/sec)
h	= altitude (feet)
M	= Mach number
T_f	= time-of-flight of missile

References

1. Head-on Pull-up Capability of X1A Weapon System With F4H-1, B. O. VanHook. Navy Missile Study Technical Report #7, Westinghouse Air Arm Division 10/29/57.

2. The Navy Air-to-Air Missile Study, Quarterly Engineering Report, No. 2., July 24, 1957 through October 1957, Contract No. AS 57-663d.

3. F4H-1 Basic Performance Data, R. B. Tucker, NMSTR No. 2, Westinghouse Air Arm Division, 5/8/57.

4. Addendum to Navy Missile Study Technical Report No. 2. F4H-1 Basic Performance Data, Westinghouse Air Arm Division, 6/12/57.

5. Aerodynamic Lead-Pursuit Equation. J. F. Buchan, ANTM 175, Westinghouse Air Arm Division, March 1957.

6. Survey of APQ-50 Detection Test Results Performed by NATC Electronics Tests Division R. G. Clanton, ANTM 192, Westinghouse Air Arm Division, May 31, 1957.

7. Project TED No. PTR EL 43045, Flight Test AN/APQ-50 Radar Set Phase 1, Report No. 1., Electronics Test Division NATC, 9 February 1956.

Analytical Section Technical Memorandum No. 290

APPENDIX VI

Probability of Successful Missile Launch Versus Maneuvering Target

by

R. B. Tucker

2/7/58

Distribution

Restricted - Proprietory

100, D. J. Povejsil, Mgr.
103, R. G. Clanton, Supv.
(2) 103, J. F. Buchan
(50) 103, R. B. Tucker

Uniterms

Probability
Missile
Maneuvering
Target

Charge Number

-90114-

2/12/58:lm

Summary

The results of this analysis showed that a target performing an evasive maneuver against an attacking interceptor did not seriously degrade the probability of success from that obtained against a non-maneuvering target. Other factors, such as insufficient detection range, insufficient gimmal angle coverage, and the limiting attack course (for $V_T/V_F = 1.0$) resulted in limiting the successfulness of missile launch to a greater degree.

The results obtained from use of the radar parameters for condition A yielded low probabilities of success for missile launch while condition B yielded more reasonable results. These two sets of radar parameters, A and B, are defined below. They will be discussed in more detail in Section IV of this report.

Condition A	Condition B
$R_{85\%} \approx 13.00$ n.m.	$R_{85\%} = 19.00$ n.m.
$\lambda_a = +41^\circ$	$\lambda_a = \pm 57^\circ$
$\lambda_e = \begin{cases} +47^\circ \\ -38^\circ \end{cases}$ (minus is down)	$\lambda_e = \pm 57^\circ$

Table of Contents

List of Illustrations

I. Introduction

An analysis of the probability of an interceptor being able to successfully launch a missile at a target, when the interceptor has been vectored to the point of detection on a pure collision course, has been performed. This analysis has been made against both a maneuvering target and a non-maneuvering target in a co-altitude attack.

The primary purpose of this report is to present the results of this analysis for the maneuvering target case and to see how much effect an evasive target maneuver would have on the probability of success. Thus, a comparison shall be made of the probability of success against a maneuvering target with that for a non-maneuvering target.

The probability of successfully launching the missile is obtained as a function of the following quantities:

1. Target maneuver or non-maneuvering target. (The method of maneuvering target will be discussed in Section III).
2. Probability distribution of vectoring errors in a collision vectoring system.
3. Probability distribution of detection.
4. A fixed AI gimmal coverage.
5. Probability distribution of lock-on errors.
6. Probability of reducing this error to within ±10 degrees prior to the interceptor crossing the minimum launch range.

II. Summary

The results of this analysis showed that a target performing an evasive maneuver against an attacking interceptor did not seriously degrade the probability of success from that obtained against a non-maneuvering target. Other factors, such as insufficient detection range, insufficient gimmal angle coverage, and the limiting attack course (for $V_T/V_F = 1.0$) resulted in limiting the successfulness of missile launch to a greater degree.

The results obtained from use of the radar parameters for condition A yielded low probabilities of success for missile launch while condition B yielded more reasonable results. These two sets of radar parameters, A and B, are defined below. They will be discussed in more detail in Section IV of this report.

Condition A	Condition B
$R_{85\%} \approx$ 13,00 n.m.	$R_{85\%} =$ 19.00 n.m.
$\lambda_a =$ [illegible]°	$\lambda_a = \pm 57^\circ$
$\lambda_e = \begin{cases} +47^\circ \\ -38^\circ \end{cases}$ (minus is down)	$\lambda_e = \pm 57^\circ$

III. Maneuvering Target Assumptions

The first assumption will be that the bomber's target will be the fleet center. Thus, the target will be approaching the fleet. Therefore, it will be assumed that any target maneuver will not appreciably change the target's heading from its original path of flight. In this study the maximum change in target's heading from its original flight path was assumed to be ±30 degrees.

For the purpose of this study it was also assumed that the target did not begin to maneuver until interceptor lock-on occurred. The target continued to maneuver from this time until the completion of the attack by the interceptor.

At the altitude - 30,000 feet - at which this analysis was made, the "gee" capability of the target was assumed to be 1 "gee" laterally. This corresponds to a coordinated turn bank-angle of 45°.

The target was allowed to initially maneuver to the right or to the left of its original flight path. The target maintained either of these two maneuvers for a period of time until its heading had changed by 30 degrees from its original flight path. When this change in heading was obtained, the target then maneuvered in the opposite direction until again obtaining a heading change of 30 degrees from the original flight path. This type of maneuvering tactics was continued by the target until the end of the attack being made upon it.

IV. Method of Analysis

The interceptor was vectored to the point of detection on a pure collision course. The vectoring distribution was assumed normal and to have a standard deviation of 3 nautical miles parallel to the collision course line of sight. In all cases, the heading associated with the interceptor was assumed to be that heading which would place it on a collision course at the center of this normal distribution.

The probability distribution of detection was assumed to be normal and to yield the 85 percent cumulative probability of detection ranges as given in reference 1. The standard deviation of this distribution was taken as 3.6 nautical miles and was based upon a review of APQ-50 Naval Air Test Center test data.

Lock-on was assumed to have occurred at a fixed time of 10 seconds after detection. During this time period, the interceptor continued on a pure collision course and to maintain the heading that would place it on a collision course at the center of the normal vectoring distribution.

At lock-on, the interceptor was assumed to execute a 3 "gee" lateral turn in an effort to reduce the error to ±10 degrees prior to reaching the minimum launch range as mechanized in the AN/APA-128 computer. At the same time, the target began to make an evasive maneuver either to the right, or the left of its original flight path, as was discussed in the previous section. If the interceptor was successful in reducing the error to

zero degrees prior to reaching the minimum launch range, it would then fly a lead pursuit course so long as it was able to keep the error at zero degrees.

Two sets of radar parameters were used in this analysis. They are listed below in Table I and will be referred to as Condition A and Condition B for the remainder of this report.

Table I

Condition A	Condition B
$R_{85\%} \approx$ 13.00 n.m.	$R_{85\%} =$ 19 n.m.
$\lambda_a = \pm 41^\circ$	$\lambda_a = \pm 57^\circ$
$\lambda_e = \begin{cases} +47^\circ \\ -38^\circ \text{ (minus is down)} \end{cases}$	$\lambda_e = \pm 57^\circ$

The parameters of condition A were taken to be representative of the first lot AN/APQ-72 and -74 radars, with the 85% cumulative probability detection range occurring at approximately 13.00 nautical miles on the nose.

For condition B, the antenna coverage was decided upon after a discussion with antenna design personnel. An increase of the 85% cumulative probability detection range to 19 nautical miles on the nose was also decided upon.

An illustrative example of the procedures involved in arriving at the probability of successfully launching the missile is shown in figure 1. This example indicates a desired attack objective that would bring the interceptor in on a relative bearing course of 30 degrees off the target's nose. Associated with each box of space shown, there are several probabilities each of which are evaluated in turn. These are:

1. Probability of being vectored into that particular box - $P_{V(Bi)}$
2. Probability of having detected and locked-on in this box - $P_{L(Bi)}$
3. Probability of target being within antenna coverage - $P_{G(Bi)}$ (either 1 or 0)
4. Probability of reducing heading error at lock-on associated with this box to ± 10 degrees prior to reaching the minimum launch range - $P_{C(Bi)}$ (either 1 or 0).

For this particular box, the probability of success is given by:

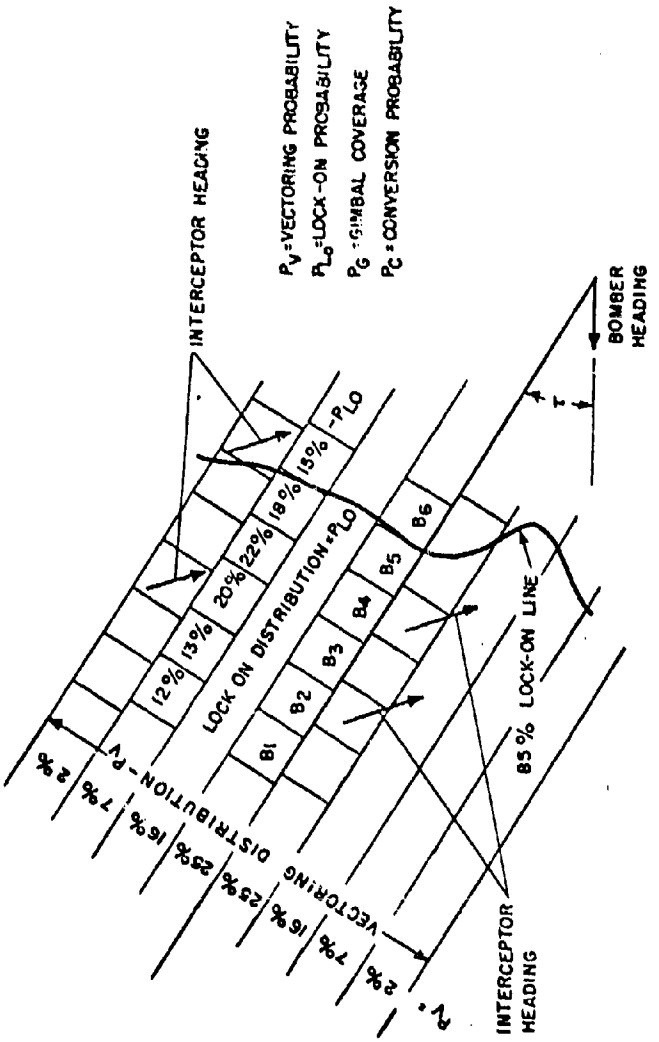

Figure 1 - Example of Probability-of-missile-launch Calculations

$$P_{S(Box_1)} = P_{V(Bi)} \times P_{LO_{(Bi)}} \times P_{G(Bi)} \times P_{C(Bi)}$$

The total probability of success for missile launch at this particular angle off is given by the sum of all the boxes, or

$$P_S = \sum_{i=1}^{n} P_{S(Bi)}$$

where i = 1,2,3,.....,n and n is the total number of boxes evaluated (n = 48 for this analysis).

The analysis was performed for an interceptor being vectored on a pure collision course at either of three relative bearing angles, $T_V = 0^\circ$, 30°, or 60° where τ is the angle off the target's nose. For each bearing angle, three target to interceptor speed ratios, $V_T/V_F = 1.0$, 0.8, and 0.45, were considered. The evaluation was carried only to a relative approach angle of 60 degrees off the target's nose.

V. Results

The results will be presented in the form of graphs, where the probability of successfully launching the missile is given for the relative bearing angles considered. In each figure, with the exception of 2 and 3, the probability will be shown for both sets of radar parameters and for both the case of a maneuvering target and a non-maneuvering target.

The maneuvering target data will be presented from four different aspects. First, a comparison shall be made of the two types of target maneuver, either an initial maneuver to the right or an initial maneuver to the left of its original flight path for the relative bearing angle of $\tau_V = 0^\circ$, 30°, and 60°. For the case of $\tau_V = 30^\circ$ and 60°, an initial target maneuver to the right of its original flight path will be defined as a maneuver towards the attacking interceptor. Similarly, the opposite type of maneuver will be defined as a maneuver away from the attacking interceptor. Figures 2 and 3 illustrate this situation. Figure 2 presents the probability of success for the radar parameters of Condition A while figure 3 contains data for the radar parameters of condition B.

For the nose on condition, $\tau_V = 0^\circ$, the probability of success is the same for an initial target maneuver to either side of its original flight path. However, if only an initial target maneuver always towards or always away from the interceptor is considered, the initial maneuver always towards the interceptor will be higher than the other type. Although the initial maneuver towards the interceptor will decrease the available time for the attack slightly, the target maneuver has the effect of aiding the interceptor in reducing the error.

As the angle off the nose increases, a target maneuver away from the interceptor produces a higher probability of success than that for a target maneuver towards the interceptor. The reason is that the error may be reduced to ± 10 degrees quicker than for the latter maneuver.

Thus, for the three relative bearing angles considered, the following types of target maneuver produced the greatest amount of degradation in the probability of success from that of the non-maneuvering case.

$\gamma_v = 0°$ - Target maneuver initially away from interceptor

$\gamma_v = 30°$ or $60°$ - Target maneuver initially towards the interceptor

Secondly, the data will be presented for the above conditions, or that combination of target maneuvers which will account for the largest decrease in the probability of success. This condition is illustrated in figures 4, 5, and 6.

Figures 7, 8, and 9 will compare the case of an initial target maneuver to the right of its original flight path against that of a non-maneuvering target. Fourth, the case of an initial target maneuver to the left of its original flight path will be presented in figures 10, 11, and 12.

Figures 4, 5, and 6 presents the results of this analysis for a target to interceptor speed ratio of 1.0, 0.8, and 0.45 respectively. For the radar parameters of condition A, the primary reason for the resulting low probabilities of success for relative bearing angles of ± 20 degrees off the target's nose may be attributed to insufficient time to reduce the error to ± 10 degrees, which is the result of insufficient radar lock-on range. As the relative bearing angle off the target's nose increases towards 60 degrees, the available time for an attack increases, but for the cases of $V_T/V_F = 1.0$ and 0.8, difficulties now arise from the limited gimmal angle coverage. For $V_T/V_F = 1.0$, additional difficulties arise due to the existance of a limiting course which will carry the interceptor within the allowable launch zone for the Sparrow III missile.

For the radar parameters of condition B, figures 4, 5, and 6 indicate the probability of success is now more reasonable. However, for the case of $V_T/V_F = 1.0$, a major shortcoming still exists. For low relative bearing angles off the nose, this shortcoming is still traceable to insufficient detection range. For the angle of 60 degrees off the nose, gimmal angle coverage plus the existance of the limiting course previously mentioned account for the low probability of success.

A comparison of the probability of success curves for the maneuvering target versus that for the non-maneuvering target case indicates that an evasive maneuver by the target resulted in only a small decrease of the probability of success, approximately 15% for the worst case.

Figures 7, 8, and 9 compares the probability of successful missile launch for a target which initially maneuvers to the right of its original flight path with that of a non-maneuvering target for speed ratios of $V_T/V_F = 1.0$, 0.8, and 0.45 respectively. This type of target maneuver produces a lower probability of success than that of the non-maneuvering target case. This difference in probabilities is generally rather small, with the largest difference being on the order of 15%.

The comparison of the probability of success for the case of a target which initially maneuvers to the left of its original flight path with that

of a non-maneuvering target is shown in figures 10, 11, and 12 for speed ratios, V_T/V_F = 1.0, 0.8, 0.45, respectively. For this type of initial target maneuver, the probability of success for the maneuvering target is approximately the same as that of the non-maneuvering target.

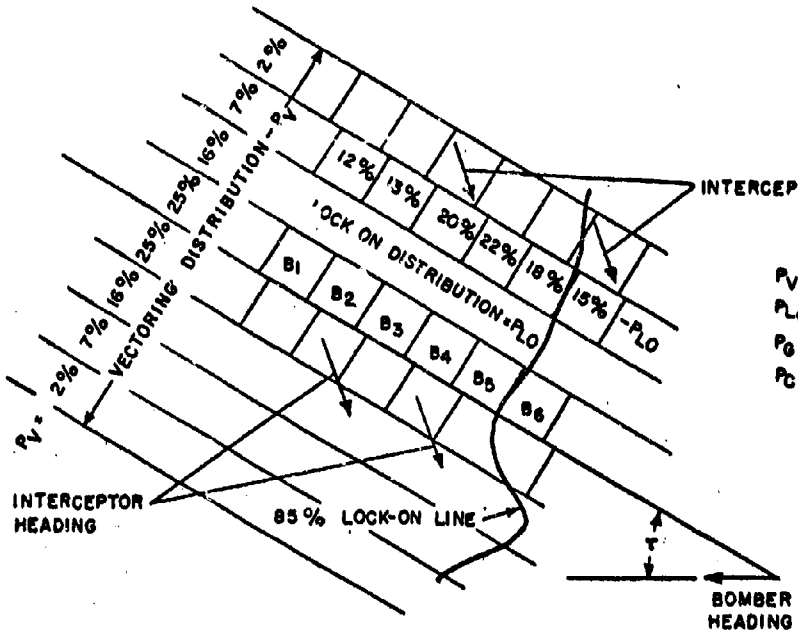

P_V = VECTORING PROBABILITY
P_{LO} = LOCK-ON PROBABILITY
P_G = GIMBAL COVERAGE
P_C = CONVERSION PROBABILITY

$$P_{S(B)} = P_{V(B)} \times P_{LO(B)} \times P_{G(B)} \times P_{C_B}$$

$$P_{S_T} = \sum_{\text{ALL BOXES}} P_{S_{B(\ )}}$$

GT-13450

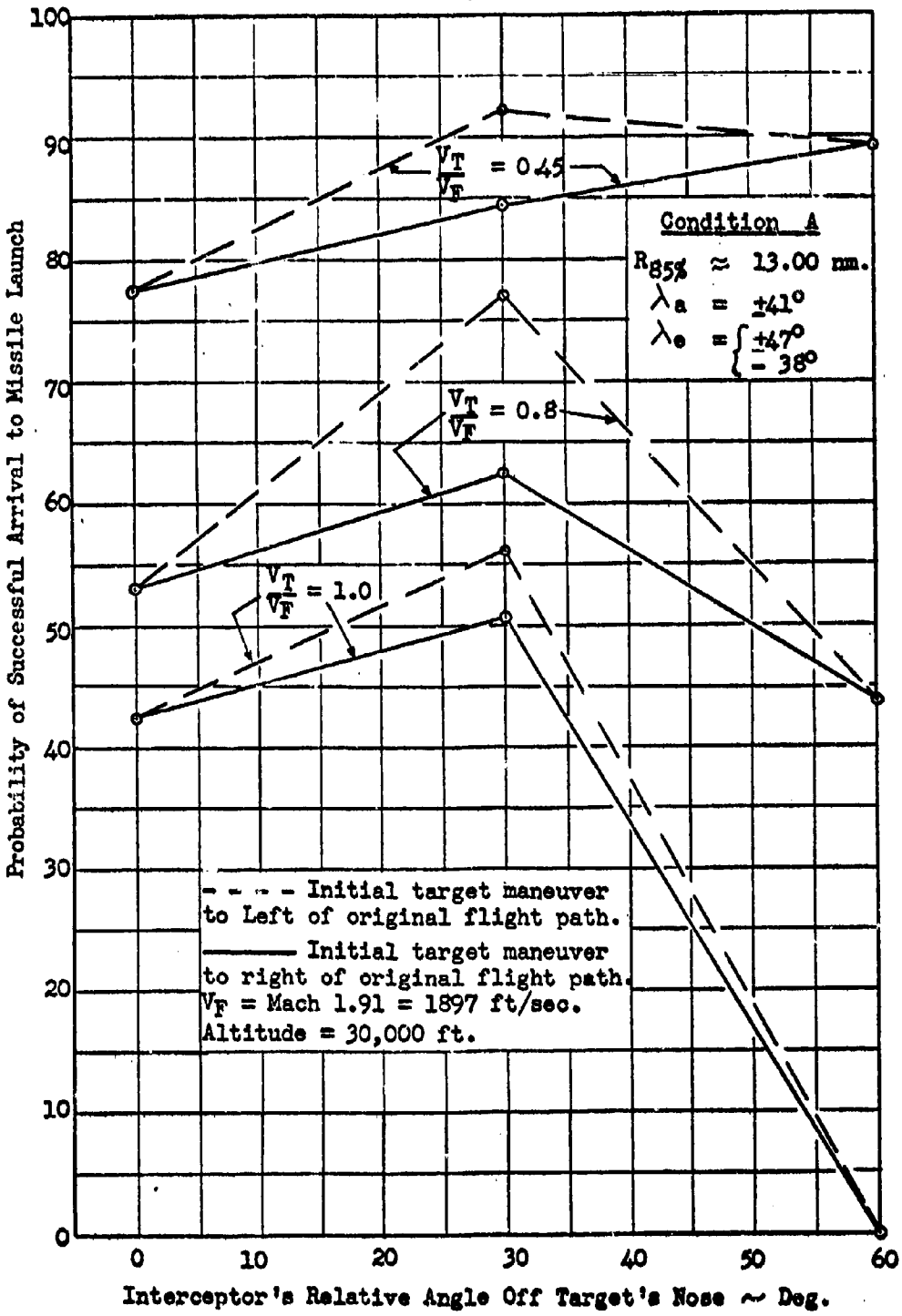

Figure 2 - Probability of Successful Missile Launch Versus Vectoring Angle, Maneuvering Target.

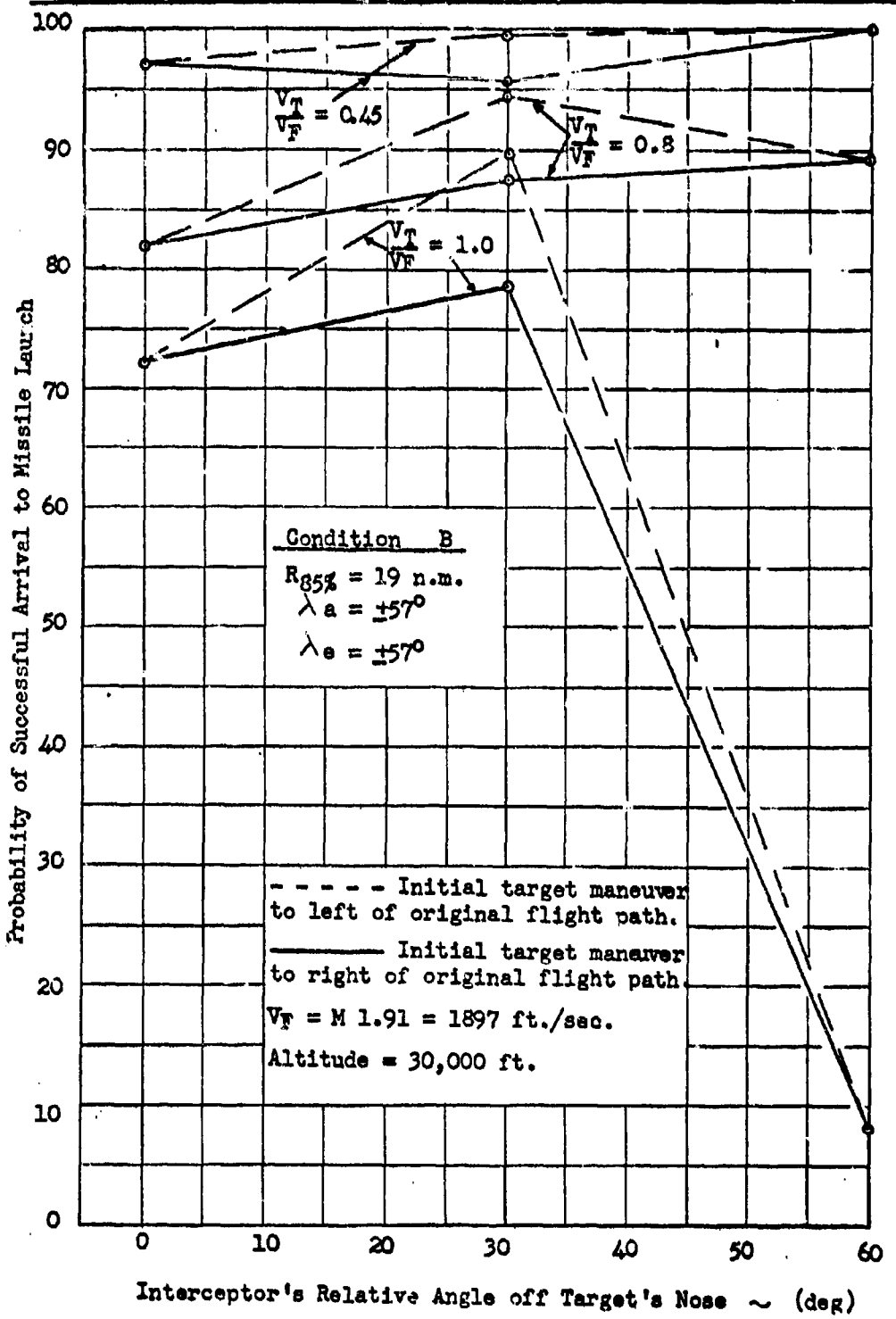

Figure 3 – Probability of Successful Missile Launch Versus Vectoring Angle, Maneuvering Target.

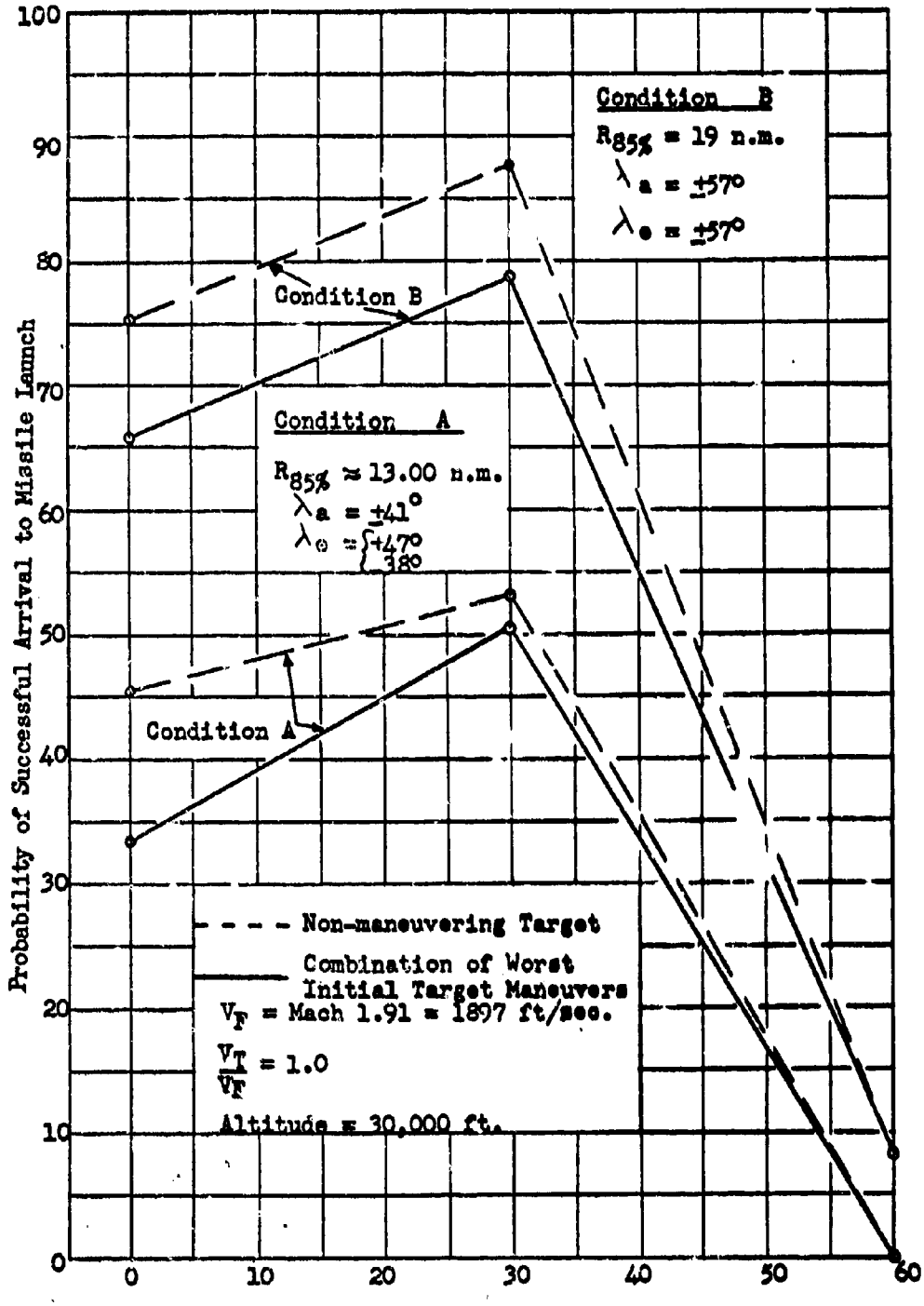

Figure 4 – Probability of Successful Missile Launch Versus Vectoring Angle, $V_T/V_F = 1.0$

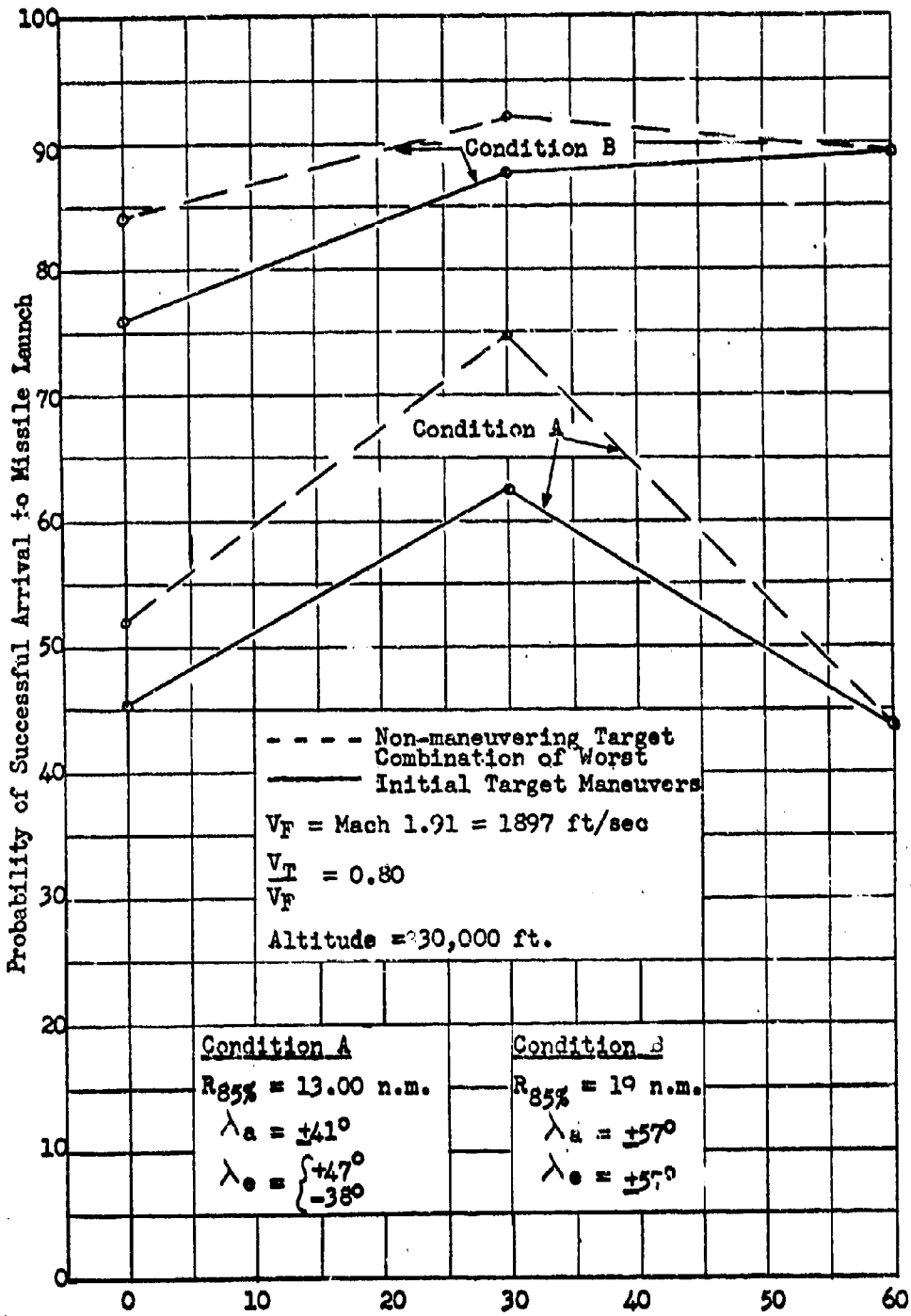

Fig. 5 - Probability of Successful Missile Launch Versus Vectoring Angle
V_T/V_F = 0.80

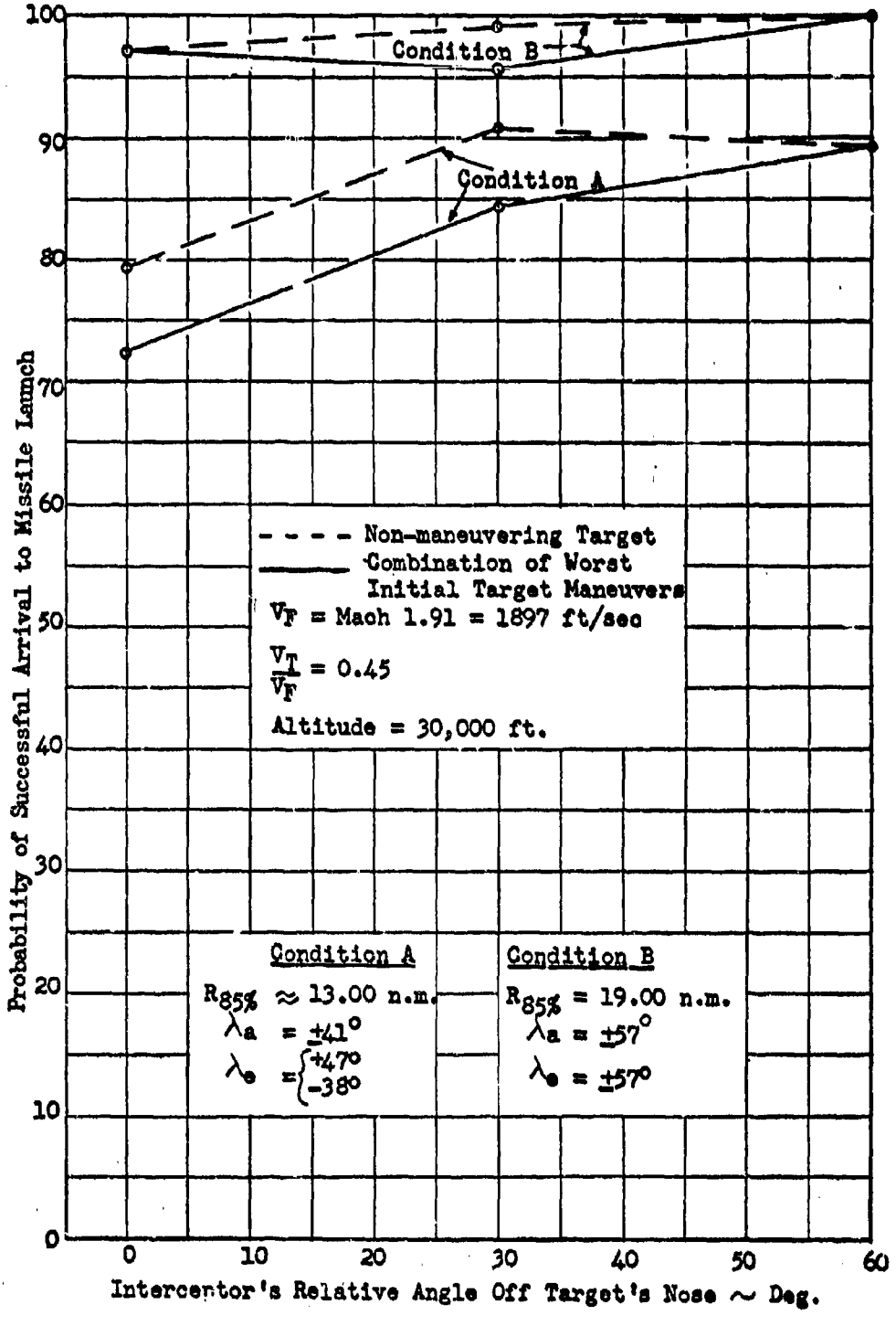

Figure 6 - Probability of Successful Missile Launch Versus Vectoring Angle, $V_T/V_F = 0.45$.

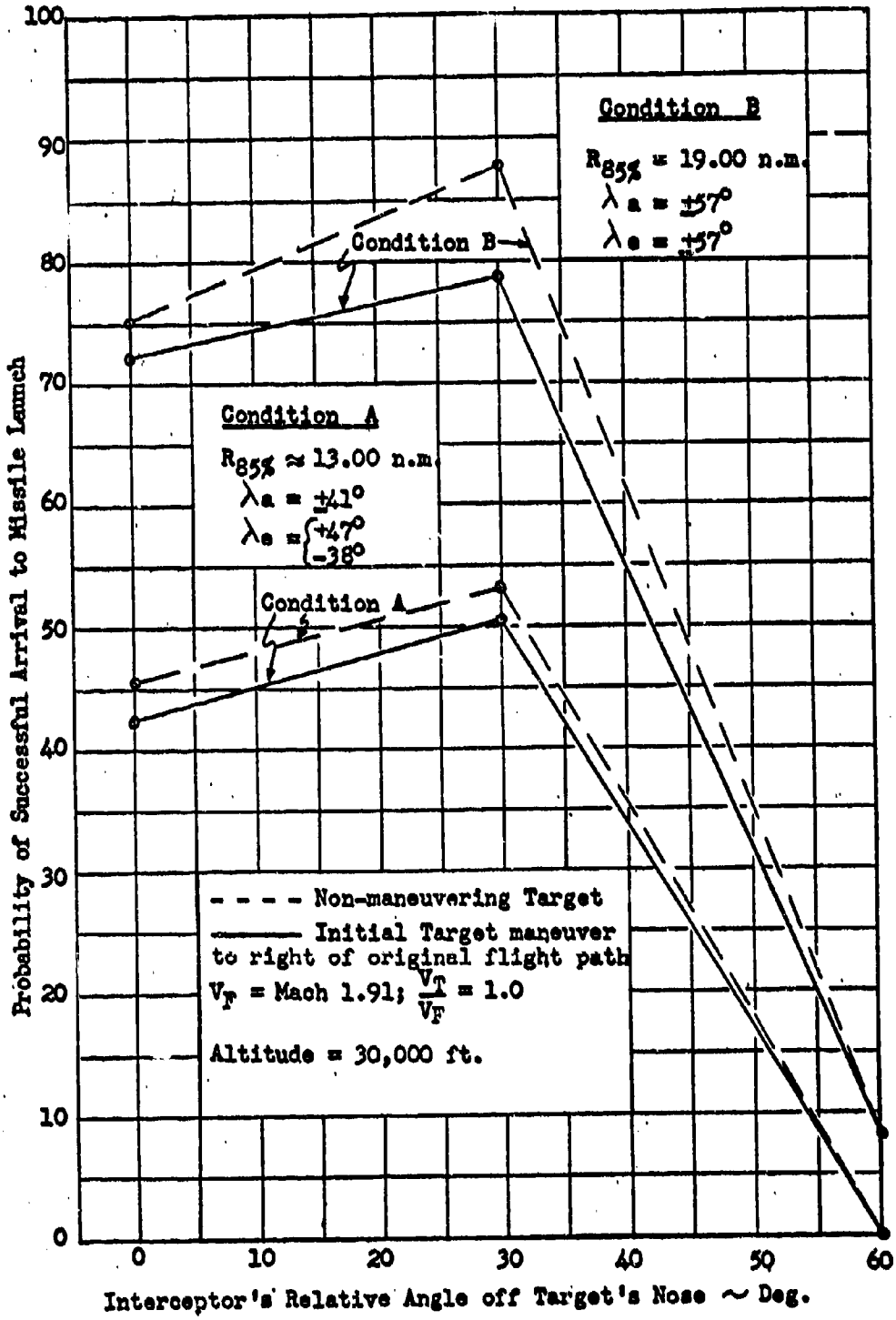

Figure 7 - Probability of Successful Missile Launch Versus Vectoring Angle, $V_T/V_F = 1.0$.

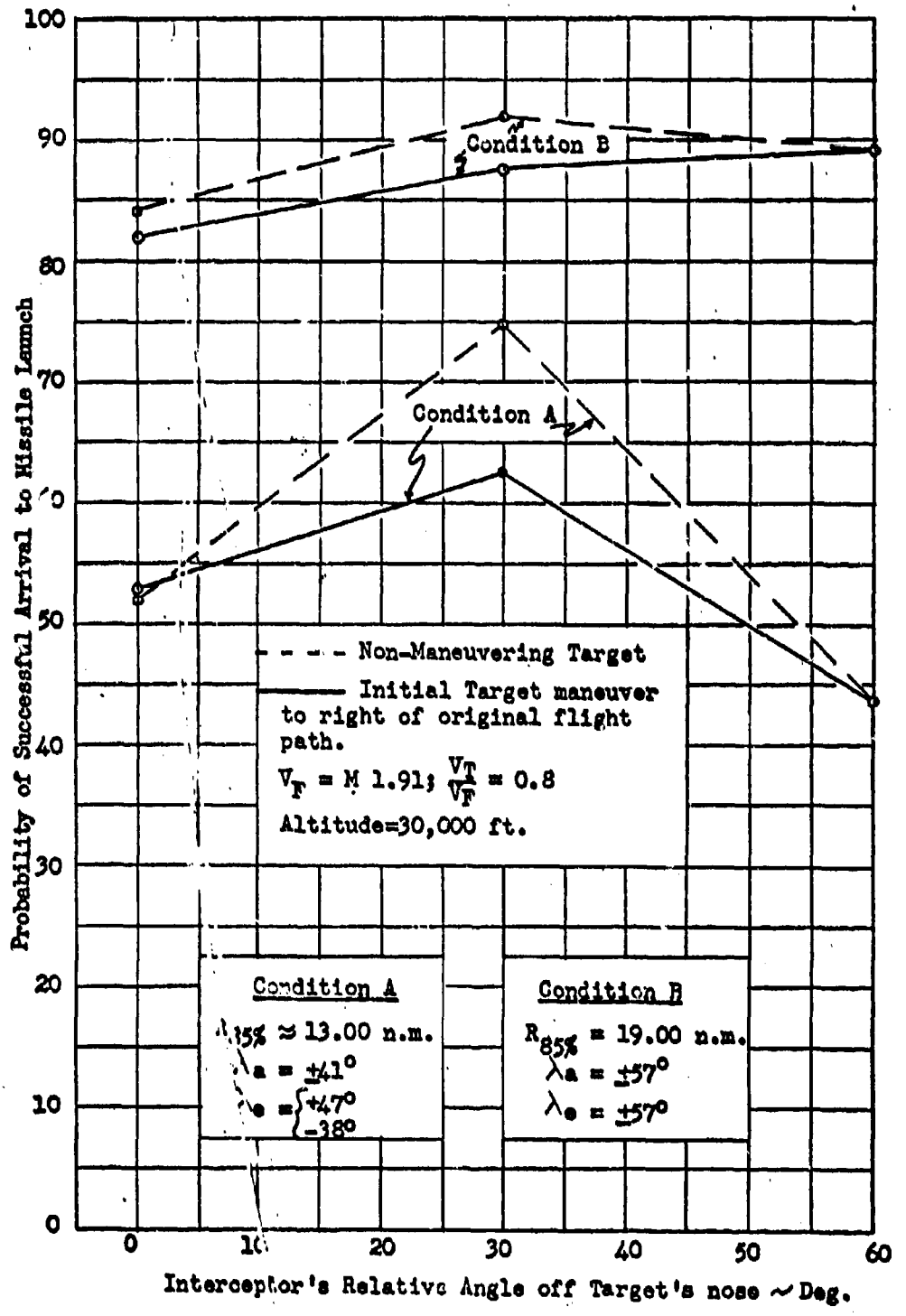

Figure 8 - Probability of Successful Missile Launch Versus Vectoring Angle
V_T/V_F = 0.8

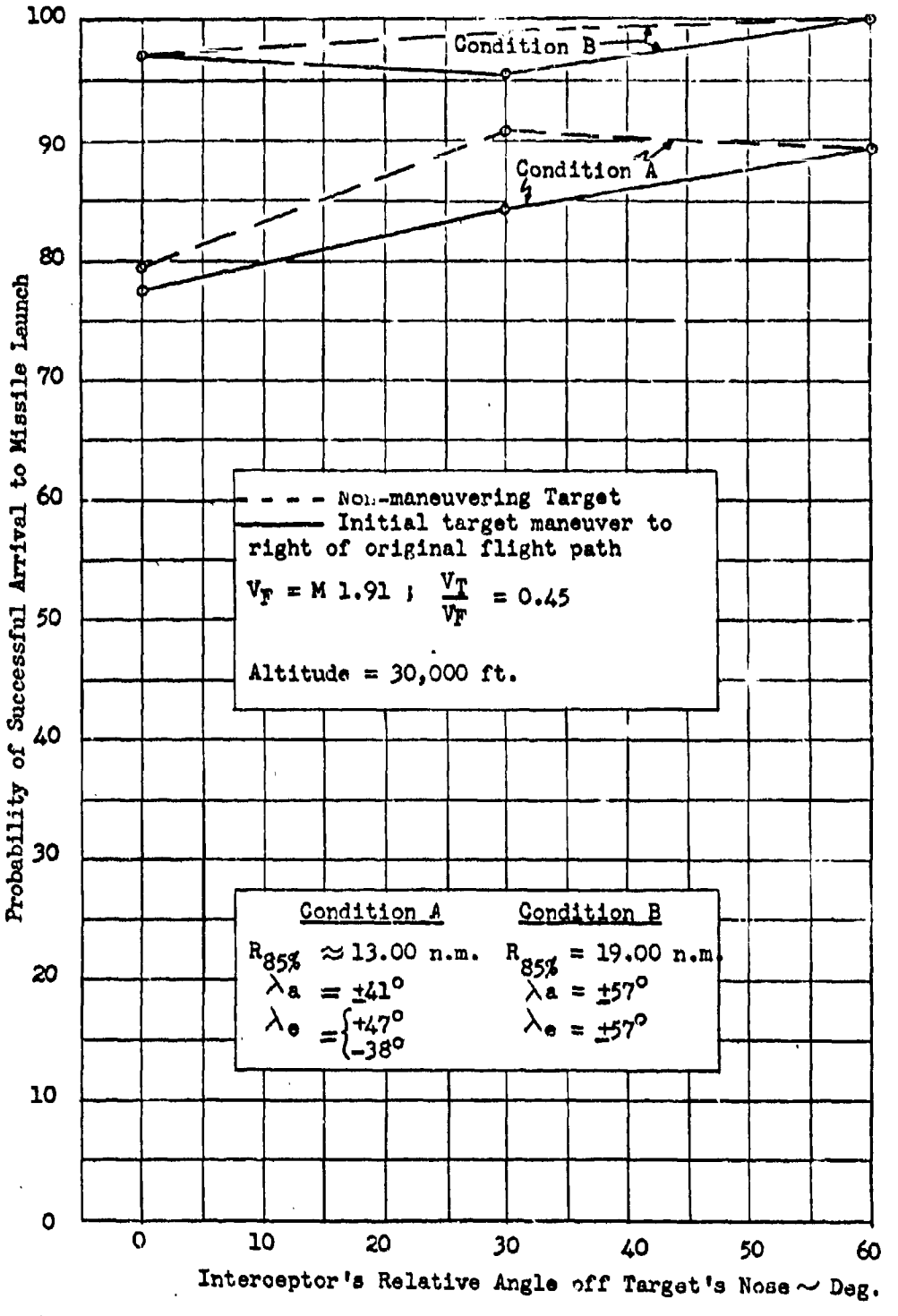

Figure 9 - Probability of Successful Missile Launch Versus Vectoring Angle, V_T/V_F = 0.45.

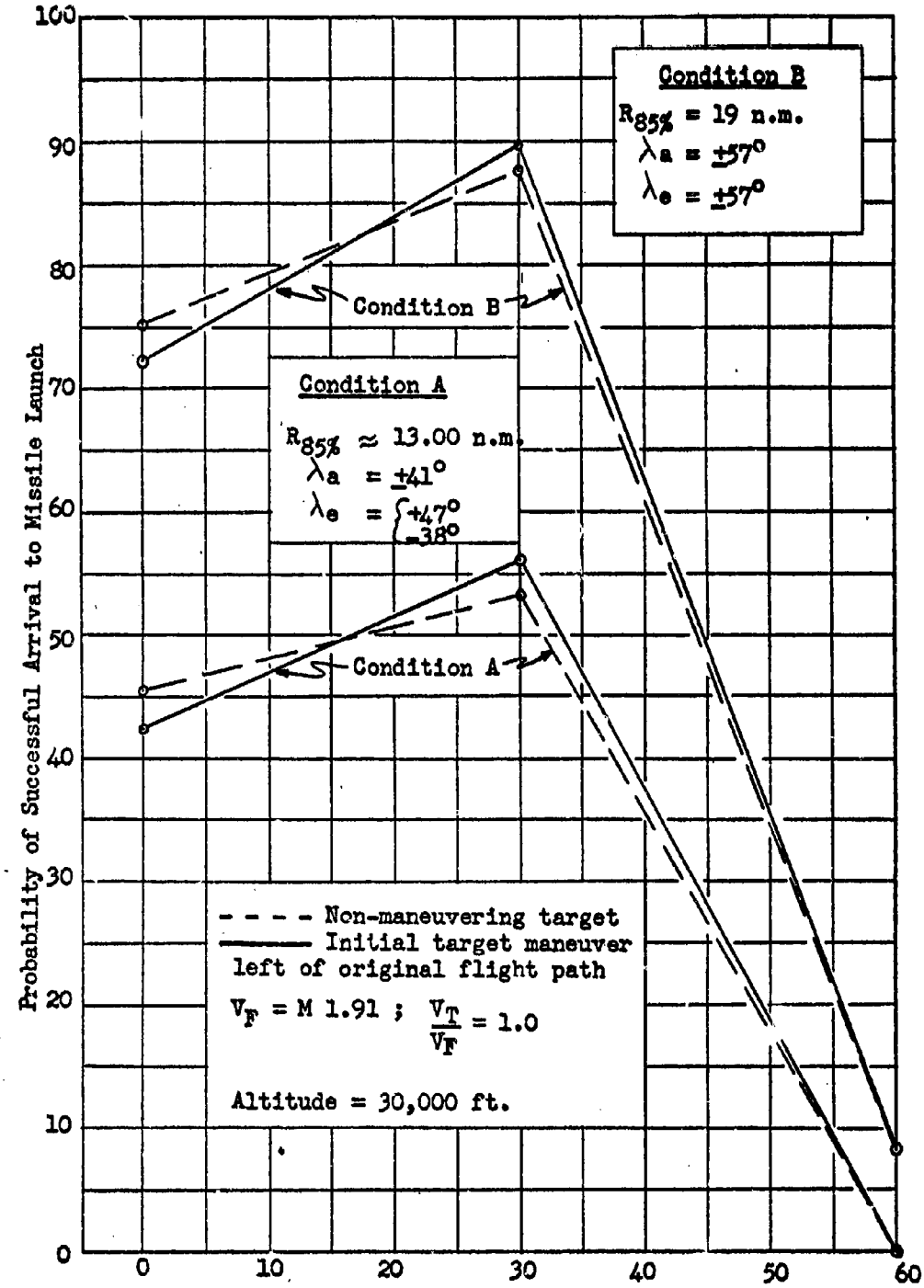

Figure 10 - Probability of Successful Missile Launch Versus Vectoring Angle, $V_T/V_F = 1.0$

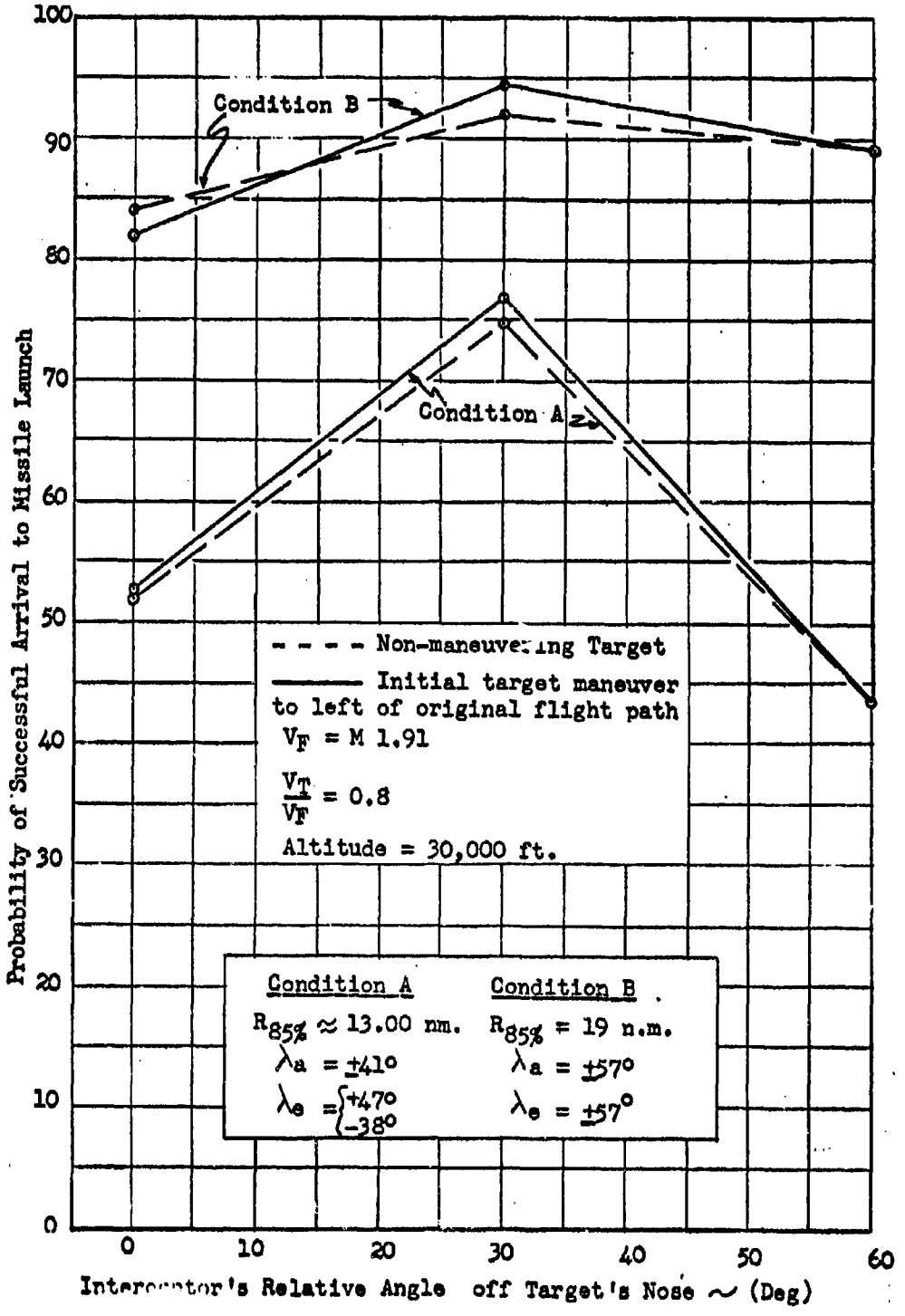

Figure 11 - Probability of Successful Missile Launch Versus Vectoring Angle
V_T/V_F = 0.8

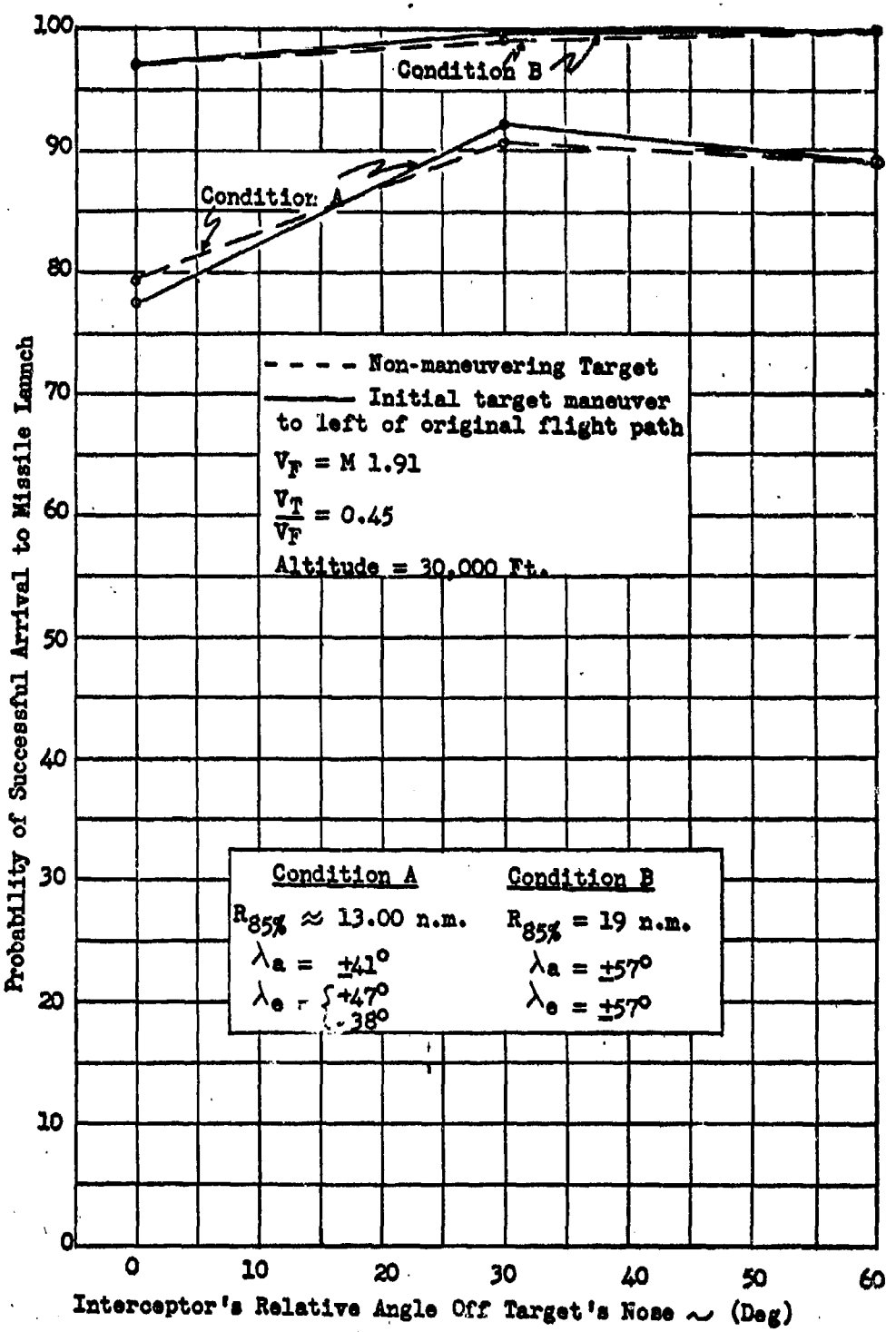

Figure 12 – Probability of Successful Missile Launch Versus Vectoring Angle, $V_T/V_F = 0.45$

References

1. Quarterly Engineering Report No. 1, The Navy Air-to-Air Missile Study, 24 April 1957 through 23 July 1957, by Westinghouse Electric Corporation Air Arm Division, Baltimore, Maryland. Confidential

2. NRL Letter No. C-5309-307/57, Subject: Classification of Vectoring Errors in Airborne Intercept. Confidential

HNTM # 304

Keep from dispersible

APPENDIX VII

NAVY MISSILE STUDY TECHNICAL REPORT NO. 8

EARLY WARNING REQUIREMENTS

- 90114 -

J. F. Buchan

2/11/58:rh

1. Synopsis

The memo presents a study on the early warning detection range requirements. The first section presents the range requirement for a mass raid in which a number of interceptors are launched from the deck. The second section presents a study on the allowable combat time for an interceptor on CAP against 30,000 and 50,000 ft. altitude targets. Also presented in this section is the information on a deck launch interceptor to 30,000 ft. altitude.

2. Range Requirement

The required target detection range will be developed in this section for a target formation at 30,000 ft. altitude. The assumption is made that the picket ship or AEW is located 100 nautical miles from fleet center. The following equation gives the required detection range, see Figure 1, to insure that k interceptors intercept target formation before an allowable target range of R_m.

$$R_D = R_m + V_T (nk + t_o + T) - 100 \qquad (1)$$

where
- n = interceptor launch period (minutes/interceptor)
- T = total system dead time (minutes). This is the time from initial target detection until the first interceptor is launched. Two values will be used, 3 and 6 minutes.
- k = the number of interceptors required to intercept target formation before a minimum range of R_m nautical miles from fleet center.
- R_m = the minimum allowable target range from fleet center. Two values are used, 25 and 100 nautical miles.
- t_o = time required for the interceptor (F4H-1) to reach an altitude of 30,000 feet and traverse 25 nautical miles (2.8 minutes) or 100 nautical miles (6.94 minutes) from fleet center.
- R_D = required detection range to insure that the k^{th} launched interceptor intercepts the target formation R_m nautical miles from fleet center.

Figure 2 shows target speed in nautical miles per minute versus Mach number for an altitude of 30,000 feet. Equation 1 is shown in Figures 3 and 4 for an R_m of 25 and 100 nautical miles respectively.

As an example, let the task force have a capability of launching one interceptor per minute and let the required number of interceptors be 30 (nk = 30). For a 6 minute delay time and a target speed of approximately Mach one (V_T = 10 n.m./min) the required detection range is 319 and 430 nautical miles for a minimum required target range of 25 and 100 nautical miles respectively.

These curves are optimistic since factors such as required combat time, human factors, etc., are neglected.

3. Allowable Combat Time

This section develops the time allotted for target penetration for the F4H-1 interceptor. The development is based upon the following assumed conditions.*

*See Fleet Air Defense Study - 1 August 55, Office of Naval Research - Secret

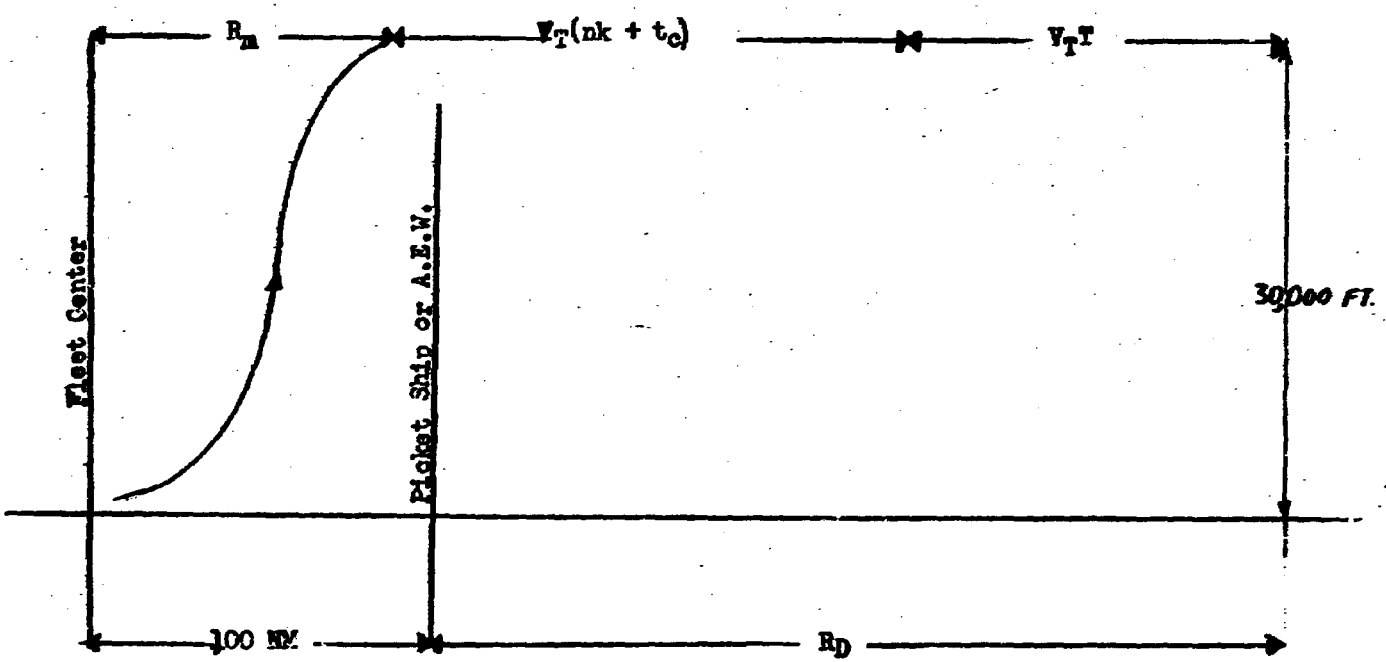

Required Detection Range

Figure 1

NOTE: Not drawn to scale

CONFIDENTIAL

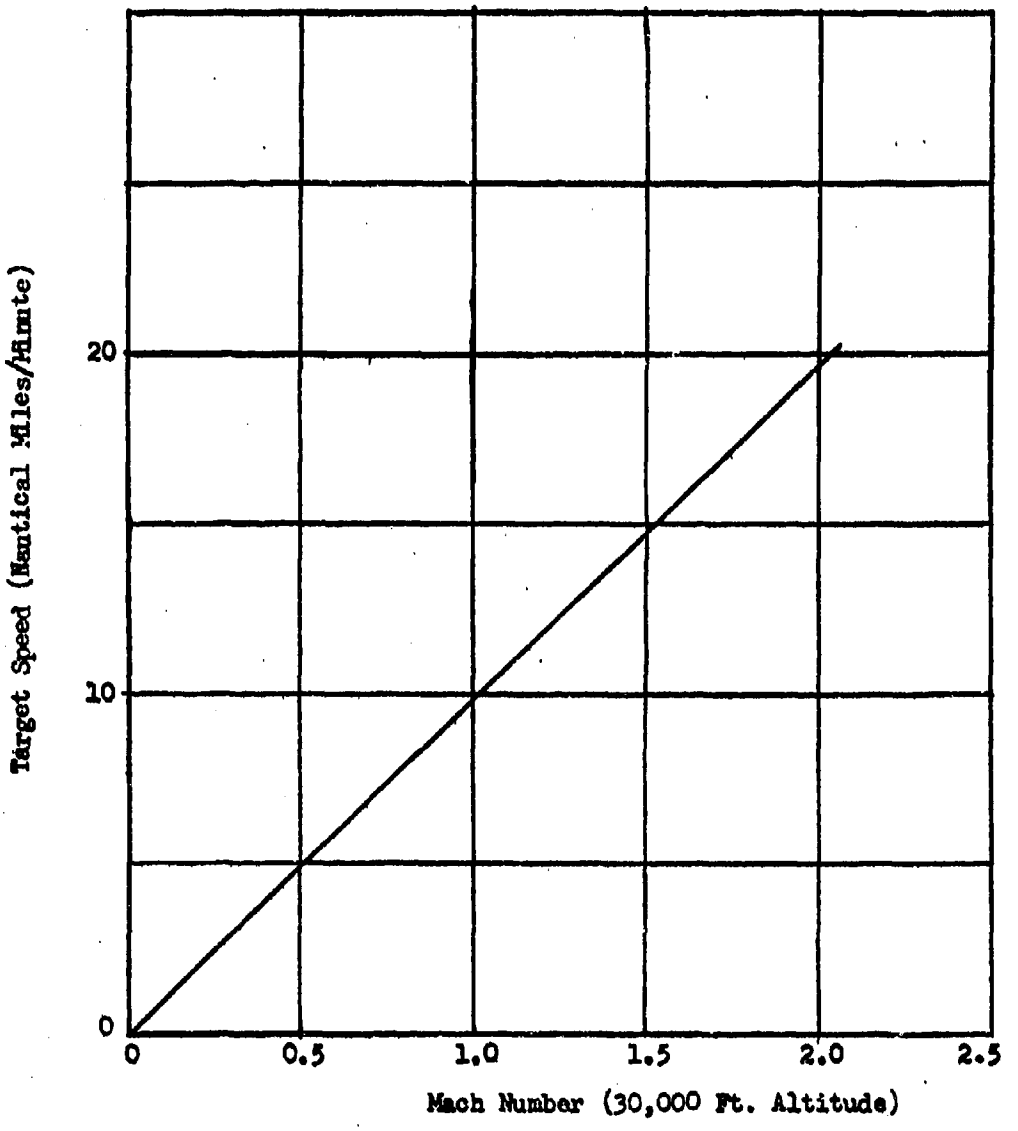

Speed Vs Mach Number

Figure 2

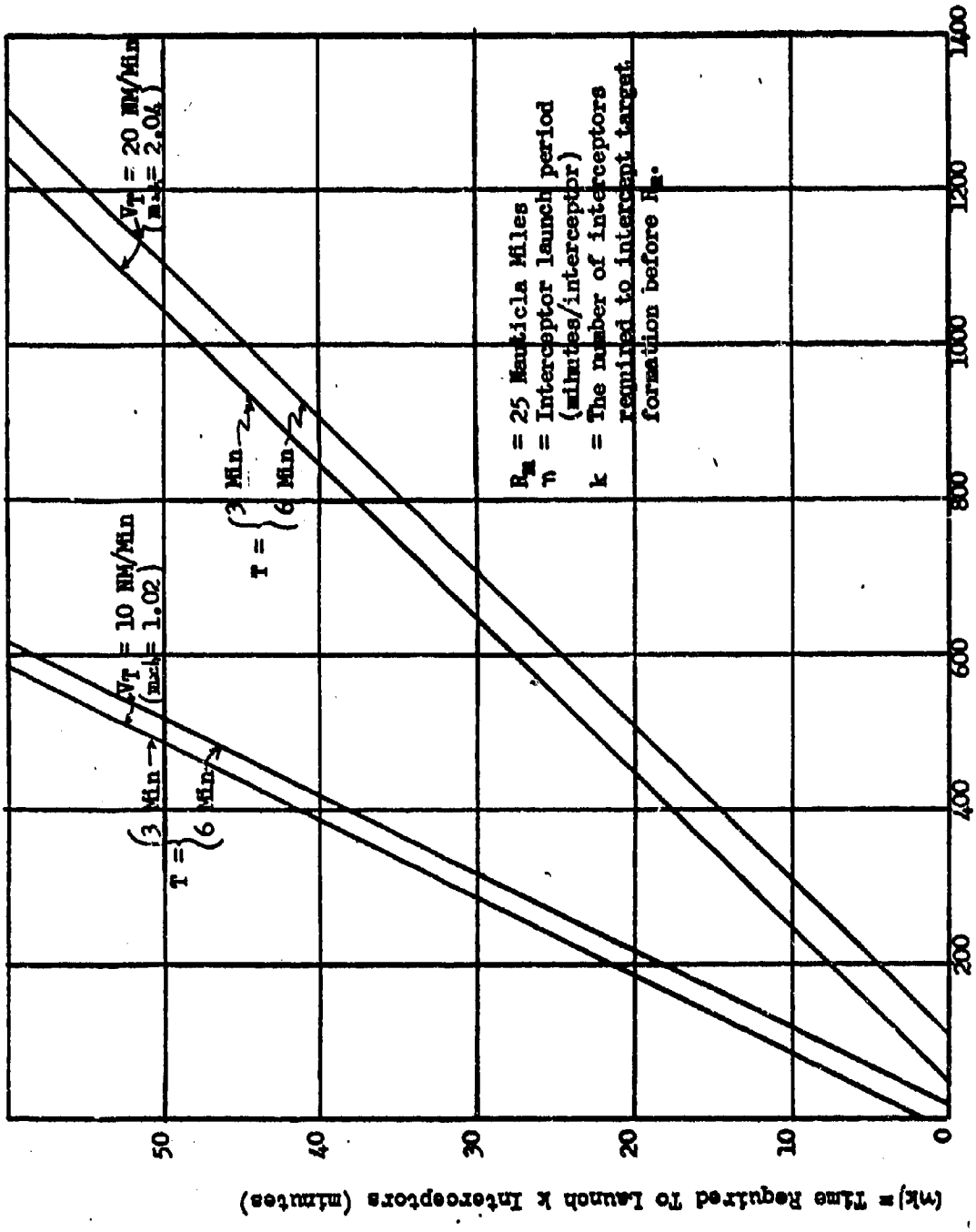
R_m = 25 Nautical Miles
n = Interceptor launch period (minutes/interceptor)
k = The number of interceptors required to intercept target formation before R_m.
V_T = 20 NM/Min ($_{max}$ = 2.04)
V_T = 10 NM/Min ($_{max}$ = 1.02)
T = 3 Min
T = 6 Min
T = 3 Min
T = 6 Min
(mk) = Time Required To Launch k Interceptors (Minutes)
0
10
20
30
40
50
200
400
600
800
1000
1200
1400
Required Detection Range, R_D (Nautical Miles)

Figure 3

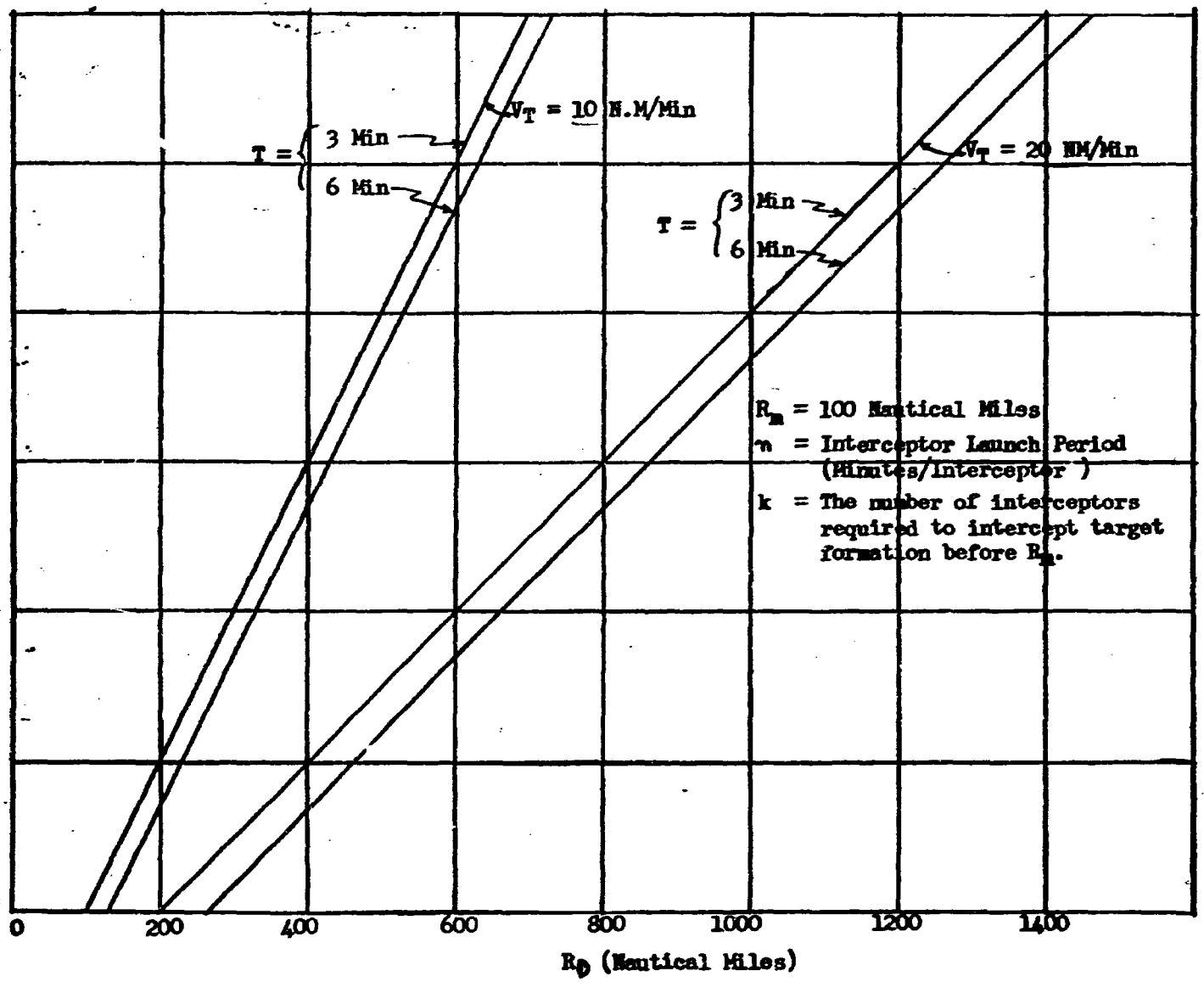
(nk) = Time Required To Launch k Interceptors (Minutes)
0
10
20
30
40
50
0
200
400
600
800
1000
1200
1400
R_p (Nautical Miles)
T = 3 Min
6 Min
V_T = 10 N.M/Min
T = 3 Min
6 Min
V_T = 20 NM/Min
R_m = 100 Nautical Miles
n = Interceptor Launch Period (Minutes/Interceptor)
k = The number of interceptors required to intercept target formation before R_m.

Figure 4

(a) The target is detected by AEW or picket ships at a range 300 nautical miles from fleet center. It should be emphasized that detection at 300 nautical miles from fleet center with current and projected 1960 equipment appears considerably optimistic.

(b) Minimum allowable target distance from fleet center is 100 nautical miles, a range contingent with the launching of glide bombs.

(c) There is a total system dead time of 3 minutes from initial target detection until initial interceptor vectoring.

(d) The interceptor is on CAP 100 nautical miles from fleet center at 30,000 ft. altitude at cruise condition. A deck launched interceptor against 30,000 ft. targets is also presented.

The effect of initial target detection range and total system dead time upon target penetration time will also be developed to generalize the results. Target altitudes of 30,000 and 50,000 feet are investigated.

3.1 Summary of Results

30,000 ft. cruise out to target

Target Speed (ft/sec)	Interceptor Speed (ft/sec)	Available Combat Time (minutes)
854	894	10.7
1518	894	3.82
1897	894	2.5

30,000 ft. accelerated out to target

Target Speed (ft/sec)	Interceptor Speed (ft/sec)	Available Combat Time (minutes)
854	1897	13.93
1518	1897	5.42
1897	1897	3.53

50,000 ft. immediate subsonic climb. Then cruise out to target

Target Speed (ft/sec)	Interceptor Speed (ft/sec)	Available Combat Time (minutes)
1940	873	2.3
1552	873	3.6
873	873	10.1

50,000 ft. run to supersonic speed at 30,000. Then supersonic climb

Target Speed (ft/sec)	Interceptor Speed (ft/sec)	Available Combat Time (minutes)
1940	1830	3.1
1552	1900	5
873	1940	13.18

3.2 Results

Figure 5 shows the acceleration characteristics of the F4H-1 interceptor from a cruise speed of 894 ft/sec to the maximum speed of 1897 ft/sec at 30,000 ft. altitude. This figure gives the interceptor's speed versus time whereas Figure 6 gives the distance traveled versus time. The time required to accelerate to maximum speed is approximately 3.45 minutes. Figure 7 represents an interception at 30,000 ft. altitude against a target whose speed is 1897 ft/sec. This figure gives the interceptor's distance which is identical with that given in Figure 6 but the distance traveled in Figure 7 is measured from fleet center. The interceptor's zero time position is 100 nautical miles from fleet center since the interceptor is assumed to be on CAP at this range. Therefore, the time shown on this figure corresponds to initial interceptor vectoring. Preceeding this time there is a system dead time. This dead time of 3 minutes is shown as a distance traversed by the target from the 300 nautical mile detection range. Thereafter, the target's distance is given as a linear function of time. The intersection of the target's distance with that of the interceptor gives the time of interception after initial interceptor vectoring and the distance from fleet center. The time allotted for target destruction is the time remaining from interception until the target's distance from fleet center is 100 nautical miles. The time for this condition is 3.5 minutes.

Figure 8 presents the accelerated condition at 30,000 ft. altitude with the three target speeds being investigated, 854, 1518, and 1897 ft/sec. The cruise condition is presented in Figure 9 .

The vectoring model assumed does not account for any distance traversed by the interceptor perpendicular to the target's track. This effect is somewhat taken into account by the fact that interception occurs at zero range.

Certain observations should be noted from Figure 8 .

(a) Target distances versus time is, of course, a straight line whose slope is target speed.

(b) Target detection range and total system dead time affect only the target distance from fleet center at zero time for a given target speed.

(c) The time allotted for target penetration is the difference between the time when the target reachs 100 nautical miles and the time of interception; and is a funtion of the zero time distance of the target, target speed, and interceptor's distance versus time curve.

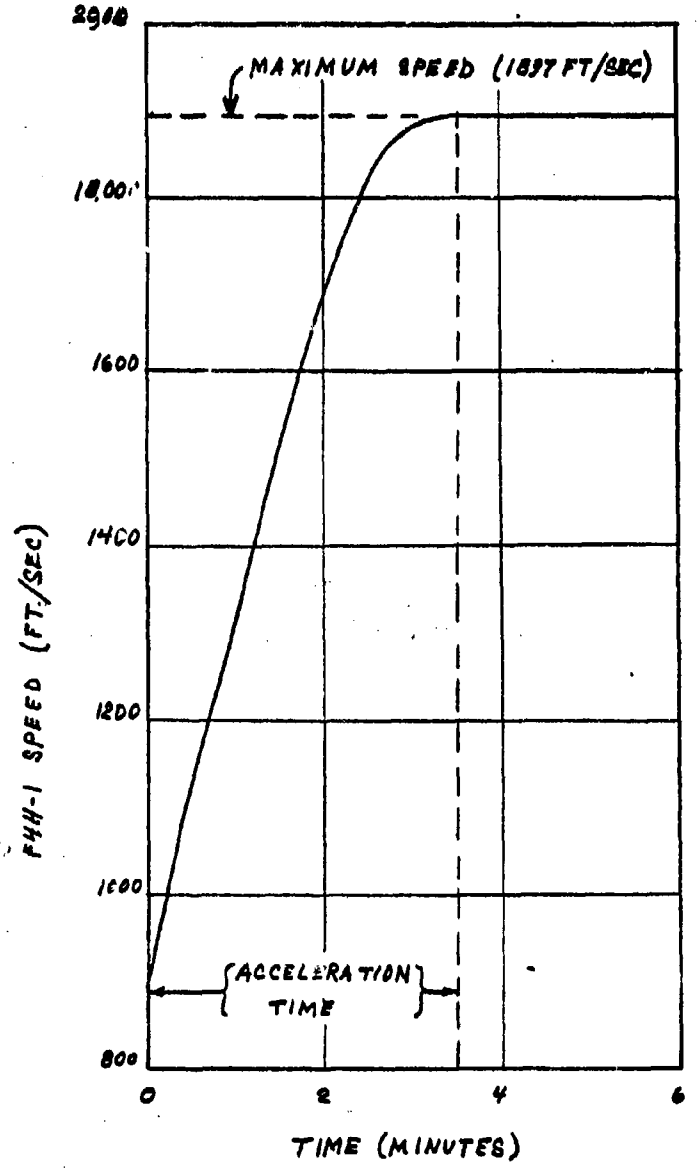

FHH-1 ACCELERATION CHARACTERISTICS AT 30,000 FT. ALTITUDE (SPEED)

FIGURE 5

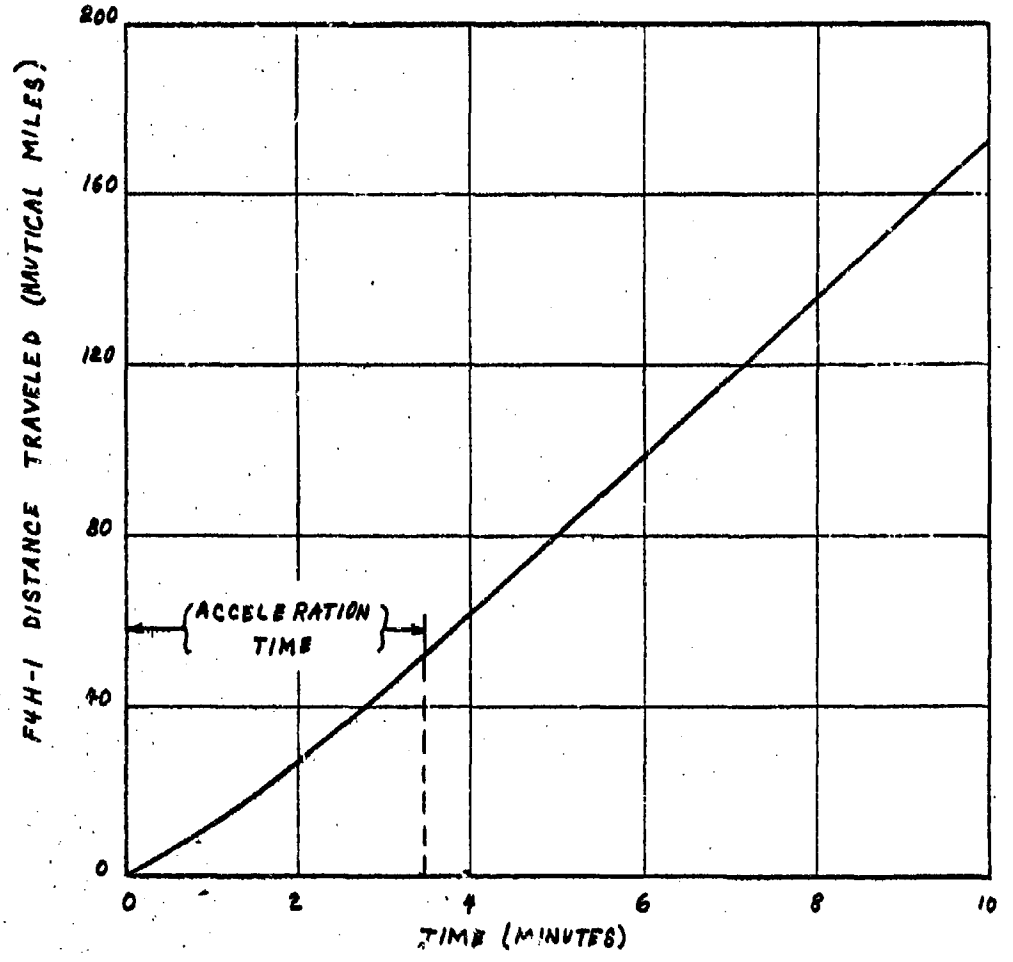

F4H-1 ACCELERATION CHARACTERISTICS
AT 30,000 FT ALTITUDE (DISTANCE)

FIGURE 6

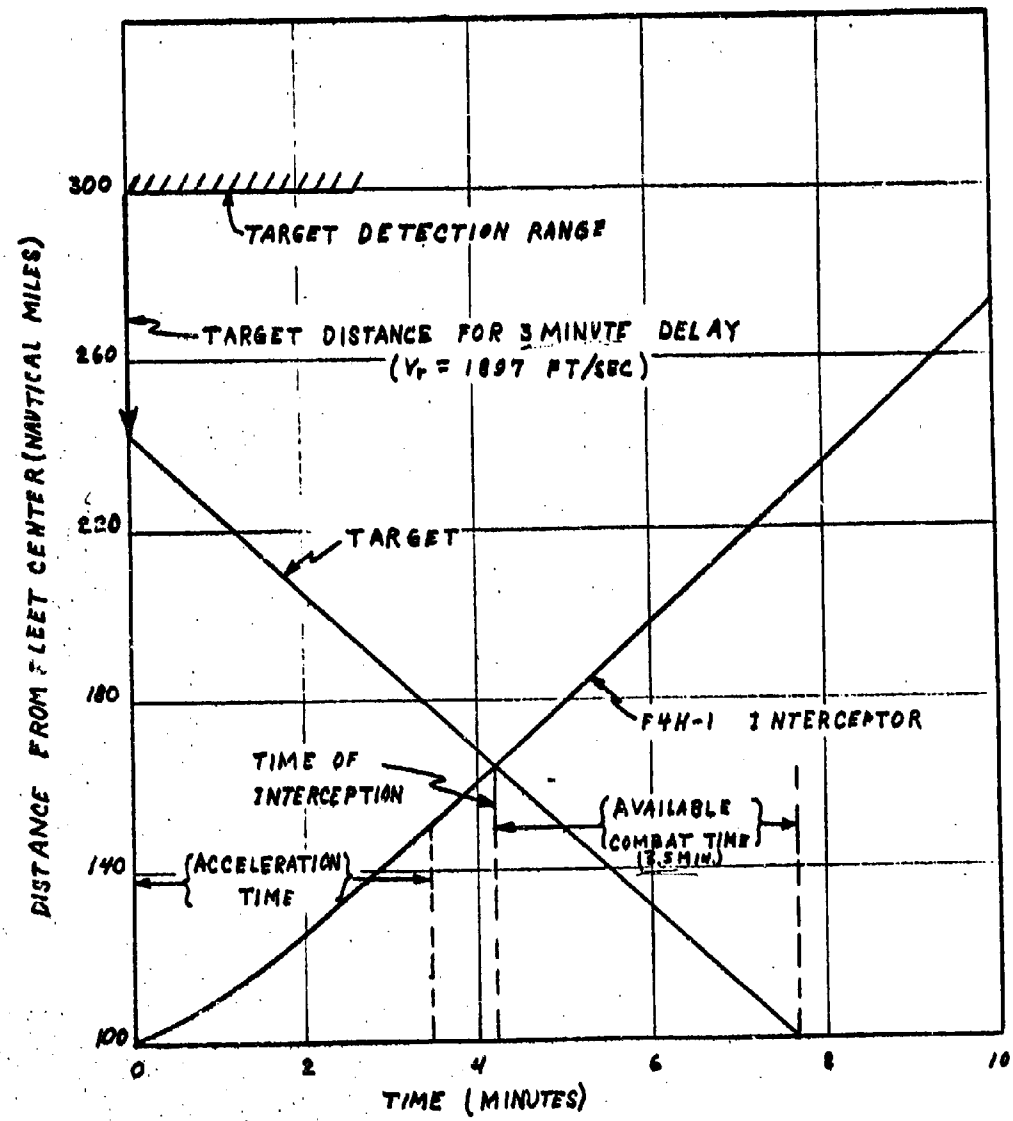

F4H-1 INTERCEPTION AT 36,000 FT. ALTITUDE (V_T = 1897 FT/SEC.)

FIGURE 7

F4H-1 AT 30,000 Ft. Altitude

Accelerated Condition

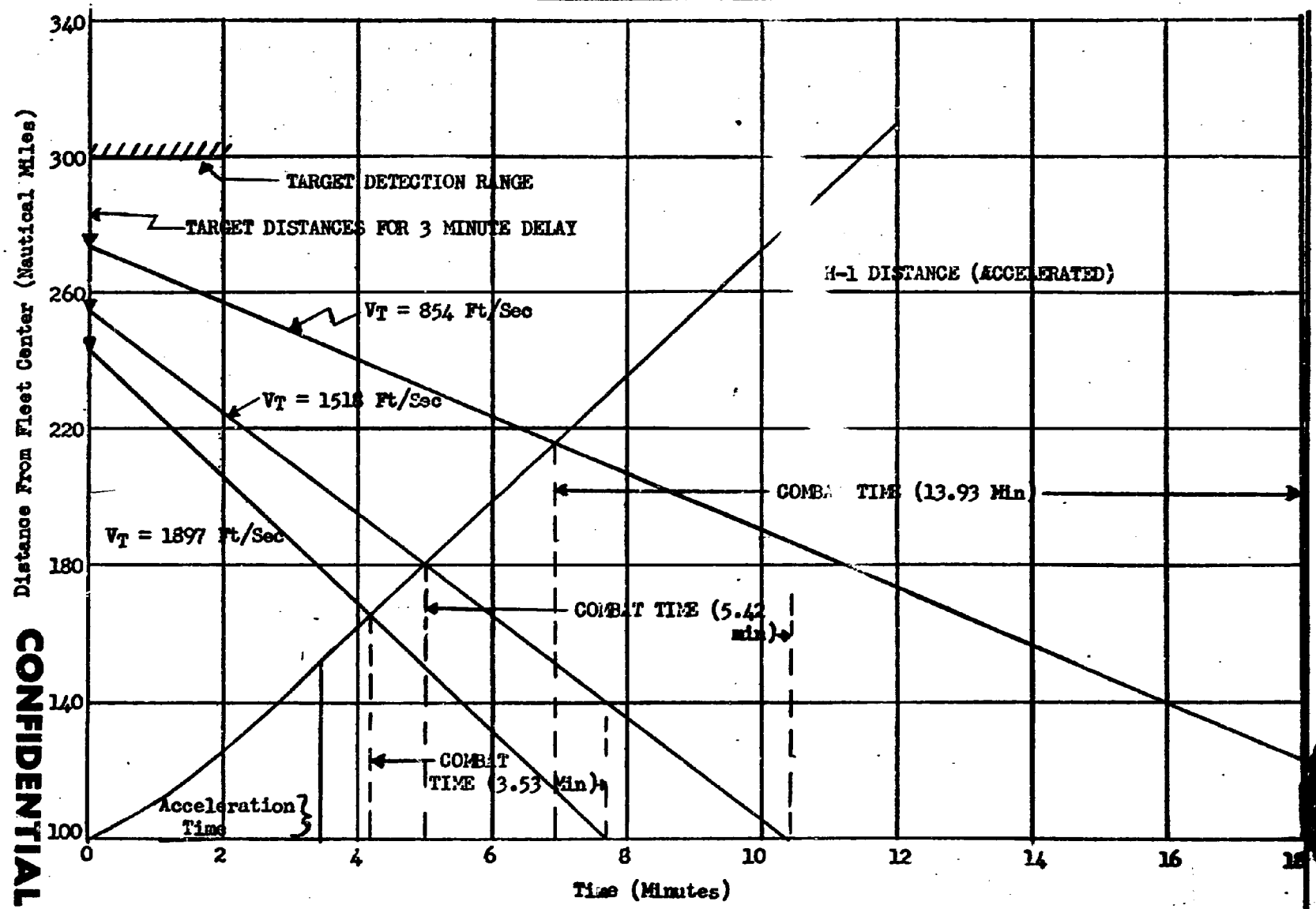

Figure 8

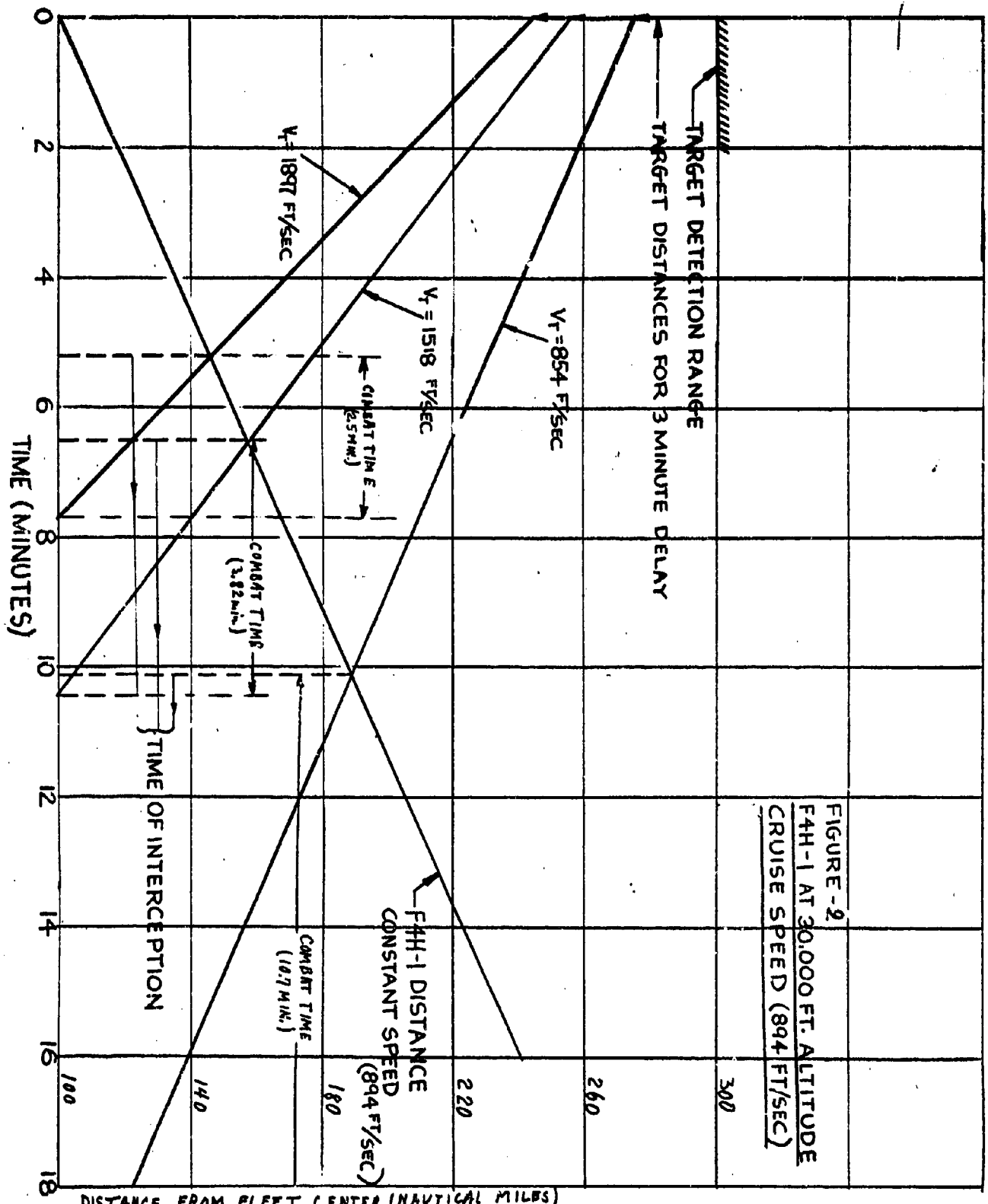

FIGURE -2
F4H-1 AT 30,000 FT. ALTITUDE
CRUISE SPEED (894 FT/SEC)

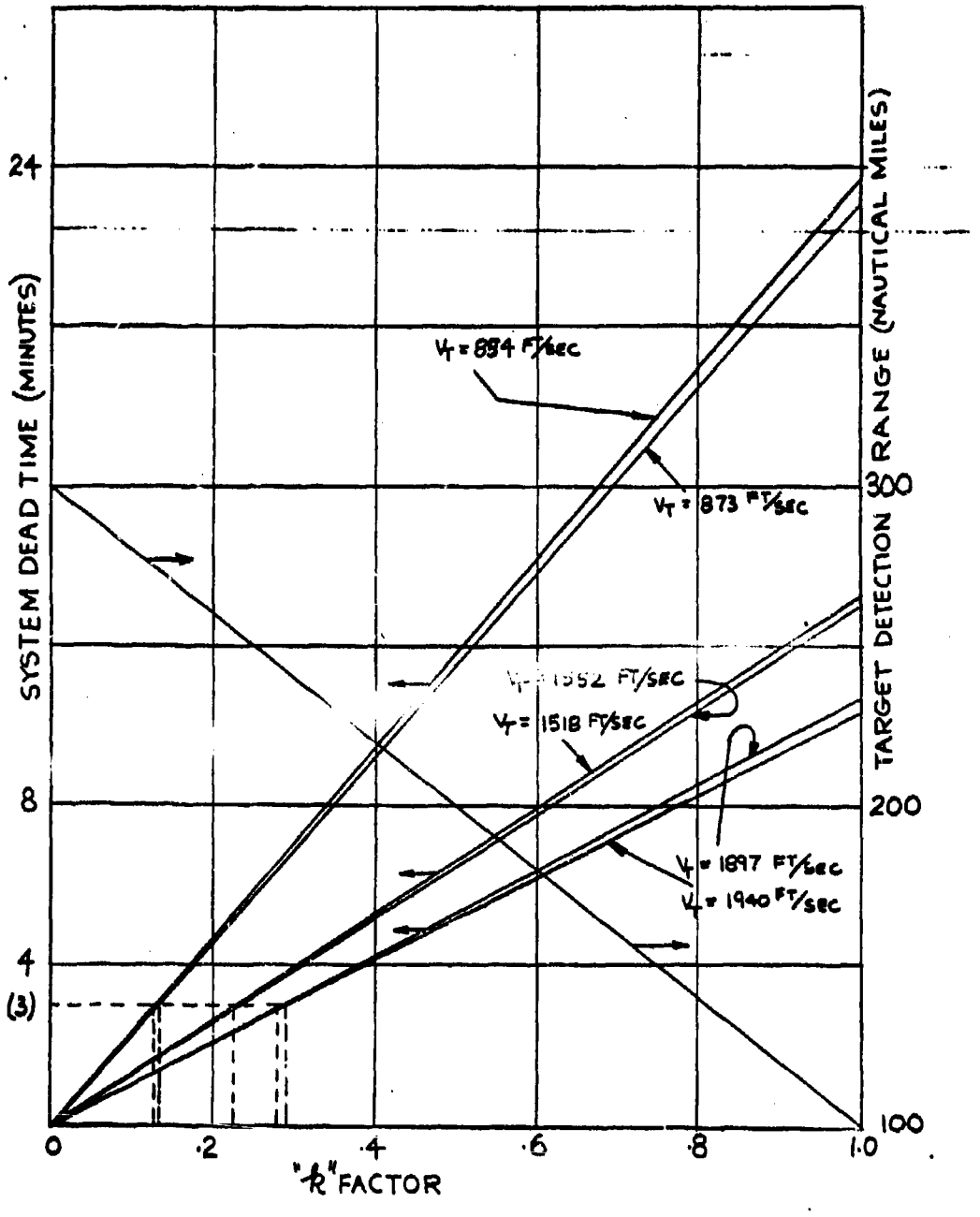
SYSTEM DEAD TIME (MINUTES)
TARGET DETECTION RANGE (NAUTICAL MILES)
24
8
4
(3)
300
200
100
0
.2
.4
.6
.8
1.0
"k" FACTOR
V_T = 884 FT/sec
V_T = 873 FT/sec
V_T = 1552 FT/sec
V_T = 1518 FT/sec
V_T = 1897 FT/sec
V_T = 1940 FT/sec

FIGURE - 10

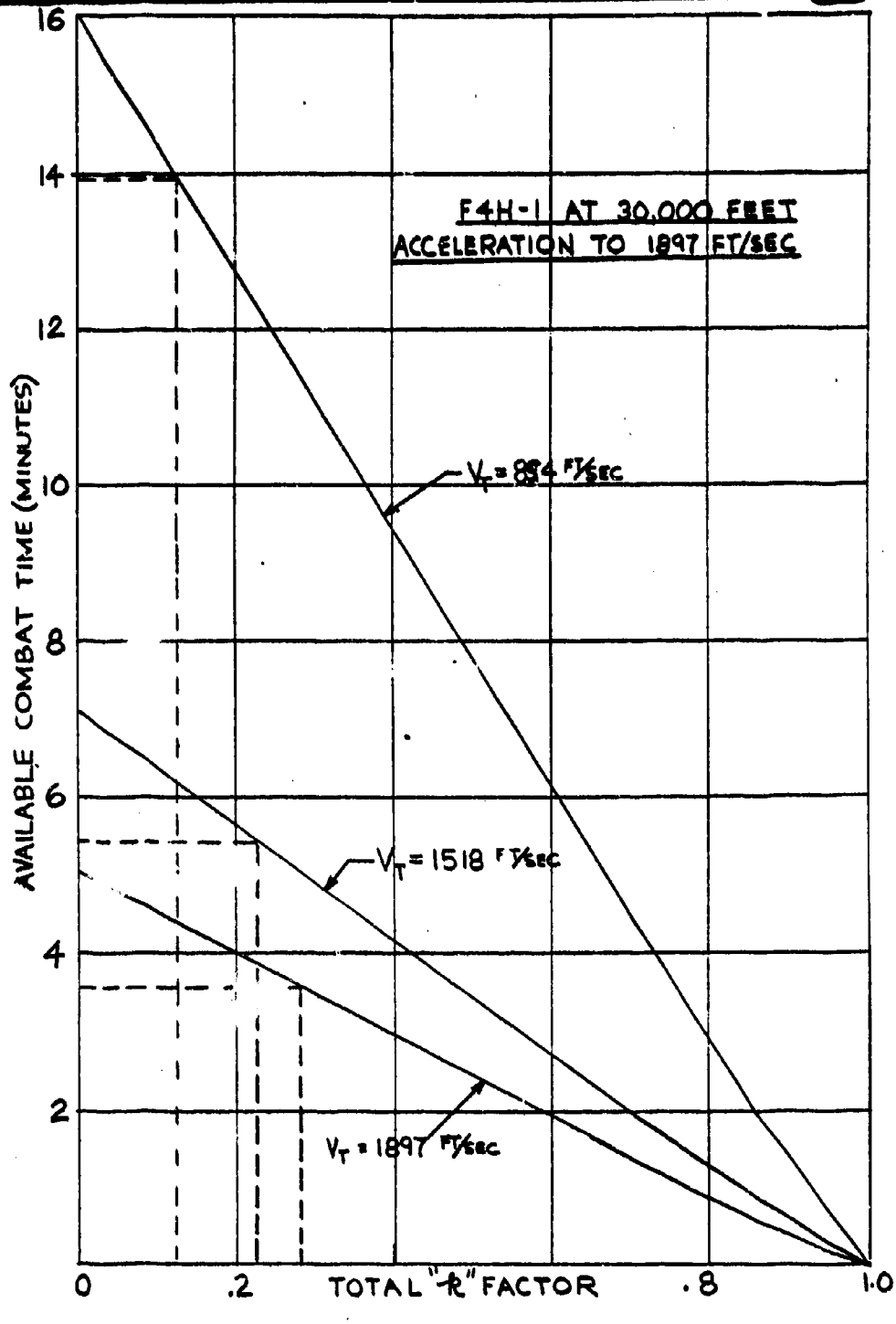
F4H-1 AT 30,000 FEET
ACCELERATION TO 1897 FT/SEC
V_T = 884 FT/SEC
V_T = 1518 FT/SEC
V_T = 1897 FT/SEC
AVAILABLE COMBAT TIME (MINUTES)
TOTAL "R" FACTOR
16
14
12
10
8
6
4
2
0
.2
.8
1.0

FIGURE-11

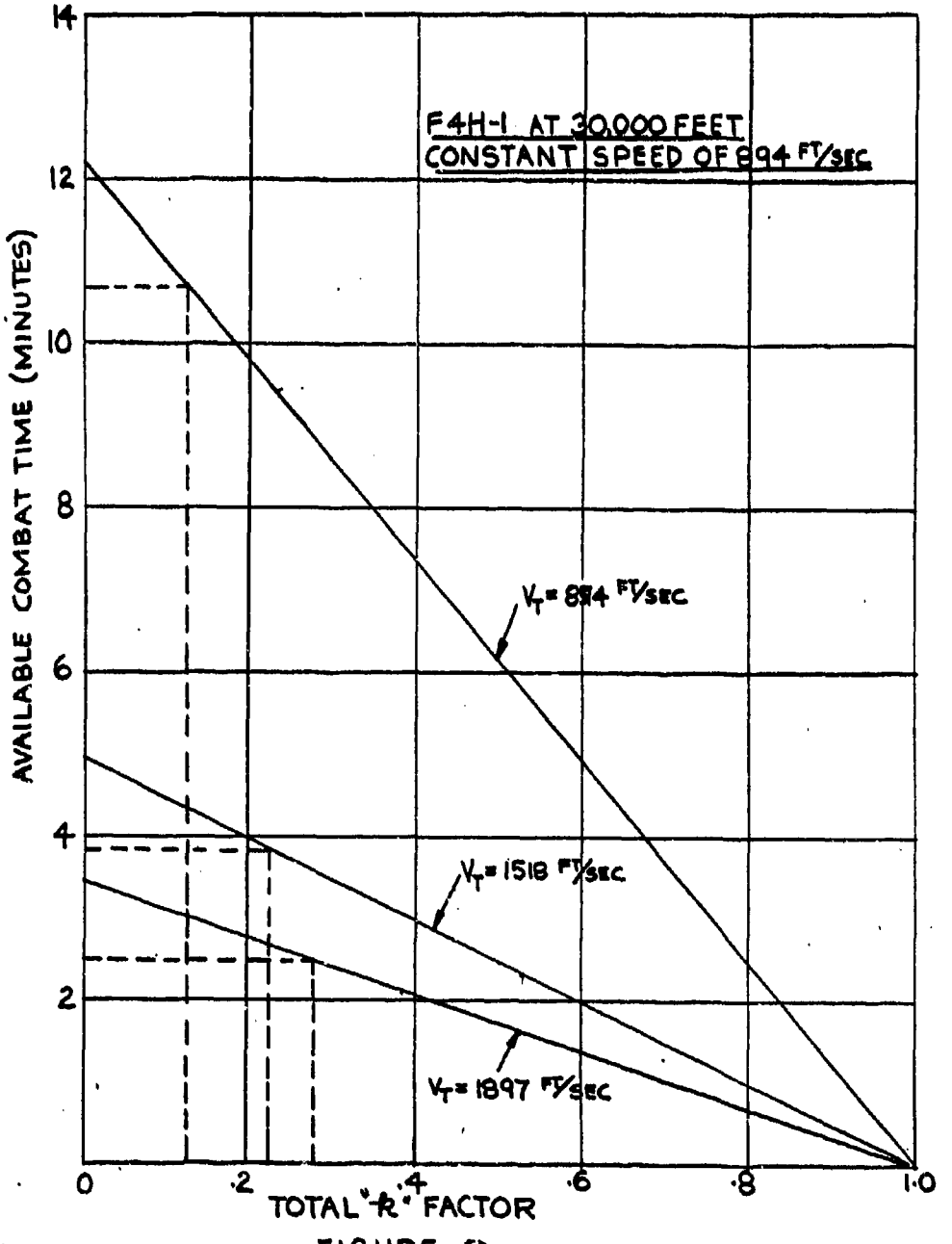
F4H-1 AT 30,000 FEET
CONSTANT SPEED OF 894 FT/SEC.
V_T = 894 FT/SEC.
V_T = 1518 FT/SEC.
V_T = 1897 FT/SEC.
AVAILABLE COMBAT TIME (MINUTES)
TOTAL "R" FACTOR
14
12
10
8
6
4
2
0
.2
.4
.6
.8
1.0

FIGURE - 12

F4H-1 Interception At 50,000 Ft. - Supersonic Climb from 30,000 Ft.

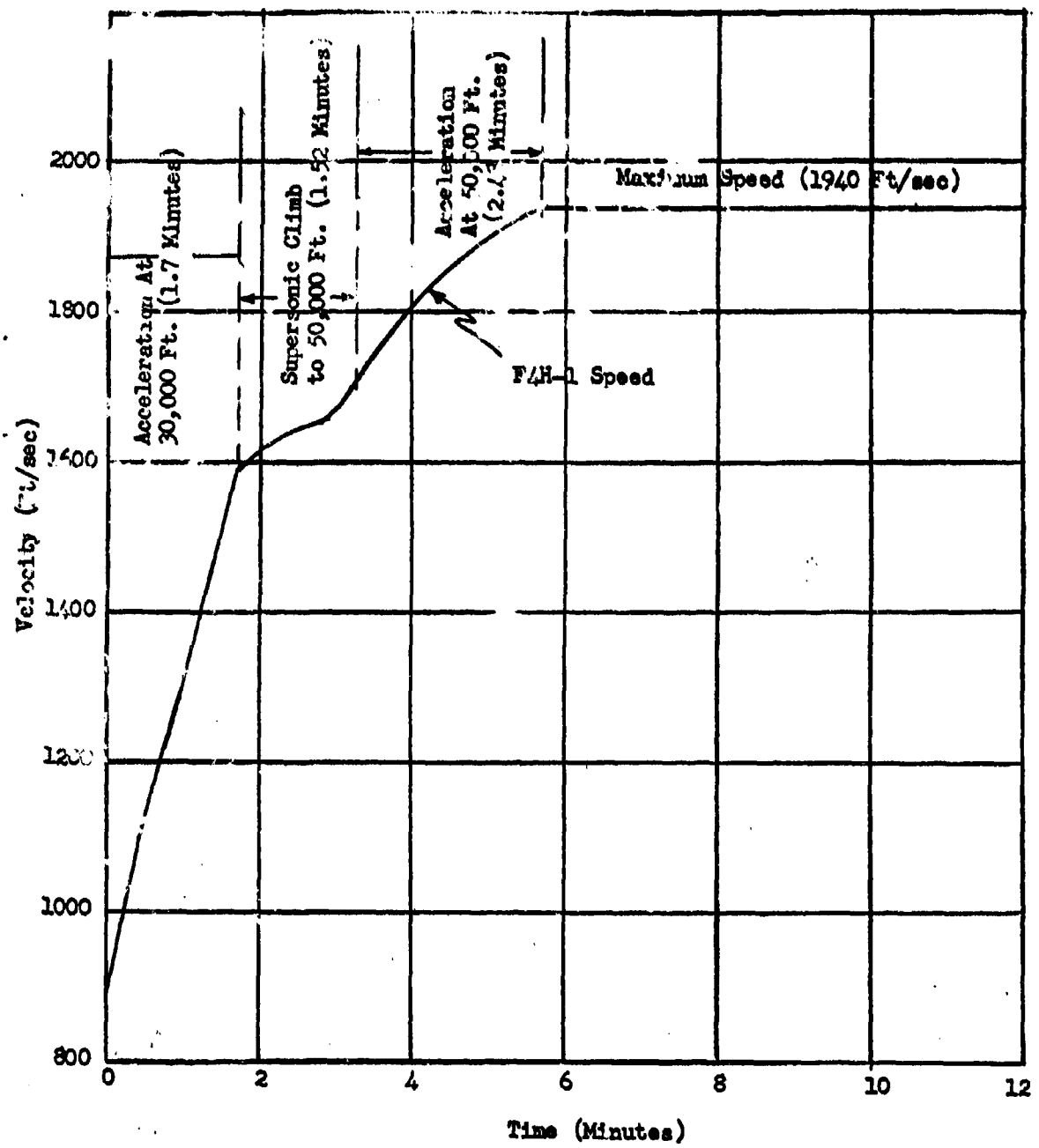

Figure 13

F4H-1 Interception At 50,000 Ft.
Supersonic Climb From 30,000 Ft.

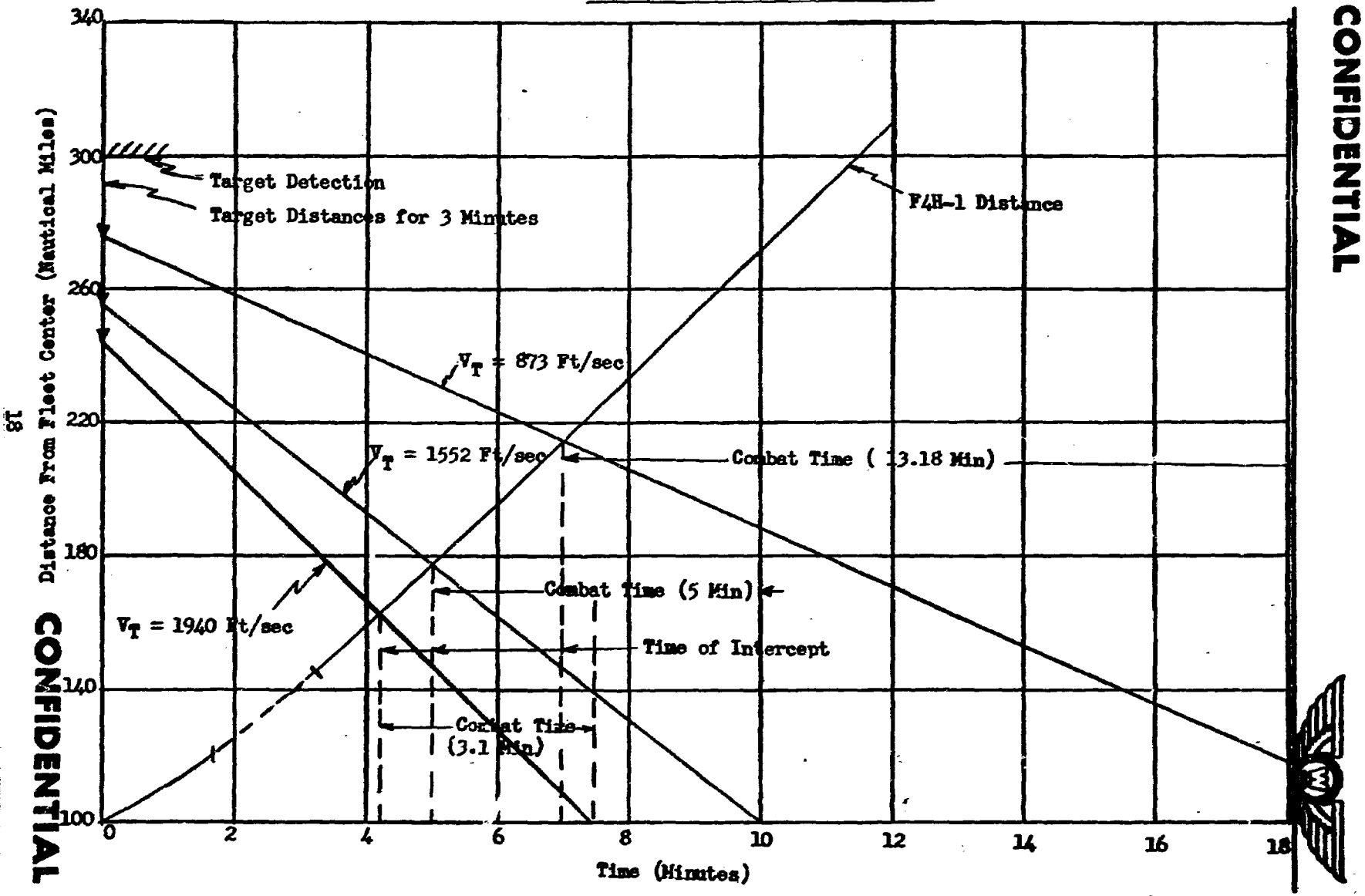

Figure 14

CONFIDENTIAL

CONFIDENTIAL

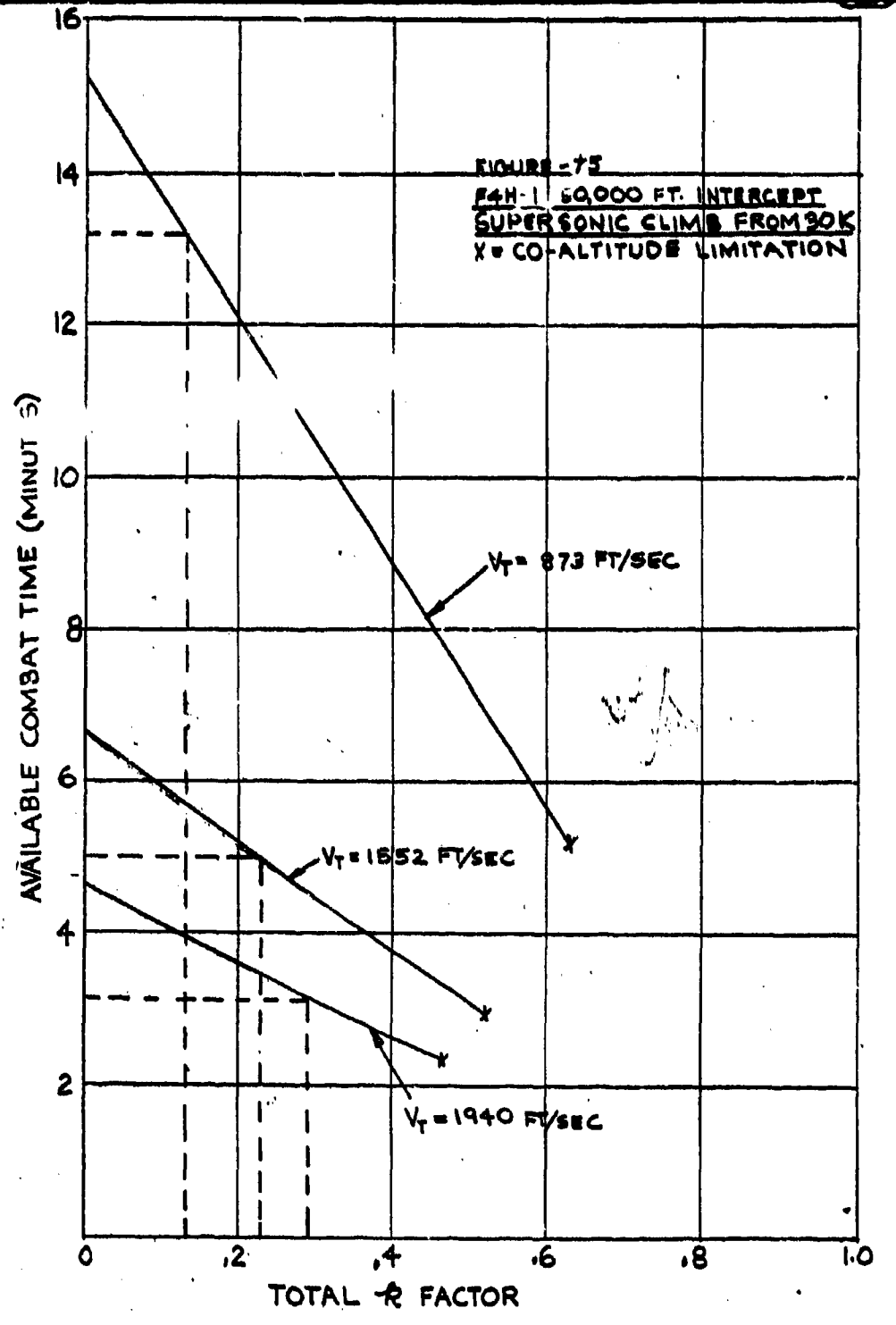
FIGURE - 75
F4H-1 50,000 FT. INTERCEPT
SUPERSONIC CLIMB FROM 30K
X = CO-ALTITUDE LIMITATION
V_T = 873 FT/SEC
V_T = 1552 FT/SEC
V_T = 1940 FT/SEC
AVAILABLE COMBAT TIME (MINUTES)
TOTAL $\frac{W}{\delta}$ FACTOR
16
14
12
10
8
6
4
2
0
.2
.4
.6
.8
1.0

From the above considerations a "k" factor is defined where 200 k is the change in the target's distance from fleet center at zero time. This "k" factor is related to the initial target detection range and total system dead time. Figure 10 illustrates this factor. The total "k" factor is that "k" due to a particular detection range plus that due to a particular dead time and target velocity.

Available combat time is shown in Figures 11 and 12 as a function of the total "k" factor and target speed for the accelerated and cruise speed conditions respectively.

The important facts from Figures 10-12 are tabulated below.

Total "k" factor	Target Speed (ft/sec)	Interceptor Speed (ft/sec)	Available Combat Time (minutes)
.126	854	1897	13.93
.227	1518	1897	5.42
.28	1897	1897	3.53
.126	854	894	10.7
.227	1518	894	3.82
.28	1897	894	2.5

The 50,000 ft. altitude target will be investigated in two ways: (1) to use best subsonic climb to 50,000 ft. from CAP at 30,000 ft. and (2) to use best supersonic climb to 50,000 ft. Climb data on the F4H-1 is given in Navy Missile Study Technical Report #2 - F4H-1 Basic Performance Data - 5/9/57 by R. B. Tucker - Confidential.

The speed and distance curves for the supersonic climb case are presented in Figures 13 and 14 respectively. The following facts are noted from Figure 13.

(a) Acceleration at 30,000 ft. to the best supersonic climb speed requires 1.7 minutes.

(b) Supersonic climb from 30,000 ft. to 50,000 ft. requires 1.52 minutes.

(c) Acceleration at 50,000 ft. to Mach 2 (1940 ft/sec) requires 2.48 minutes.

The available combat time for the supersonic climb case is presented in Figure 15 as a function of the total "k" factor. Co-altitude limitations are shown on this figure which represents the interceptor's termination of climb.

Figures 13, 14 and 15 give the following information.

Total "k" factor	Target Speed (ft/sec)	Interceptor Speed (ft/sec)	Available Combat Time (minutes)
.29	1940	1830	3.1
.23	1552	1900	5.0
.123	873	1940	13.18

Figures 16 , 17 , and 18 present the subsonic climb for an acceleration and constant speed after reaching 50,000 ft. Figure 16 shows the large acceleration time required at 50,000 ft. altitude to reach M 2.0 (1940 ft/sec). For this reason the available combat time is not given for acceleration - Figures 13 and 14 are more applicable. Figure 19 gives the available combat time for the cruise condition (obtained from Figure 18) and the following information.

Total "k" factor	Target Speed (ft/sec)	Interceptor Speed (ft/sec)	Available Combat Time (minutes)
.29	1940	873	2.3
.23	1552	873	3.6
.132	873	873	10.1

Figures 20 , 21 , and 22 presents a deck launched interceptor against targets at 30,000 ft. altitude. Here, the interceptor accelerates at sea level to climb speed, climbs to 30,000 ft., and accelerates to maximum speed. Assuming zero catapult time the following information is obtained from these figures.

Total "k" factor	Target Speed (ft/sec)	Interceptor Speed (ft/sec)	Available Combat Time (minutes)
.126	894	1897	0.37
.227	1518	1897	1.9
.28	1897	1897	9.4

F4H-1 50,000 Ft. Intercept - Subsonic Climb From 30,000 Ft.

Accelerated Condition

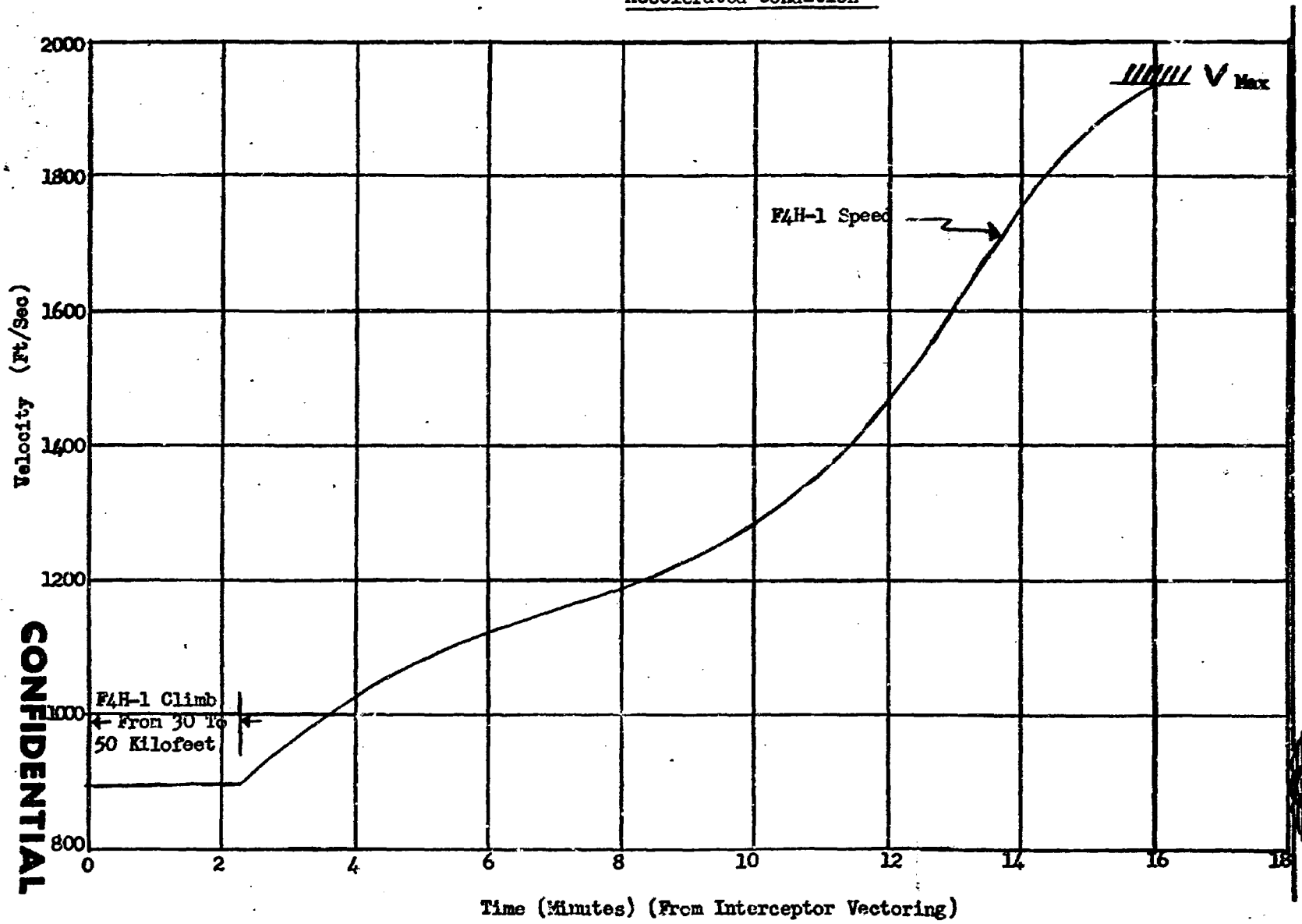

CONFIDENTIAL

CONFIDENTIAL

Figure

F4H-1 50,000 Ft. Intercept - Subsonic Climb From 30,000 Ft.

Accelerated Condition

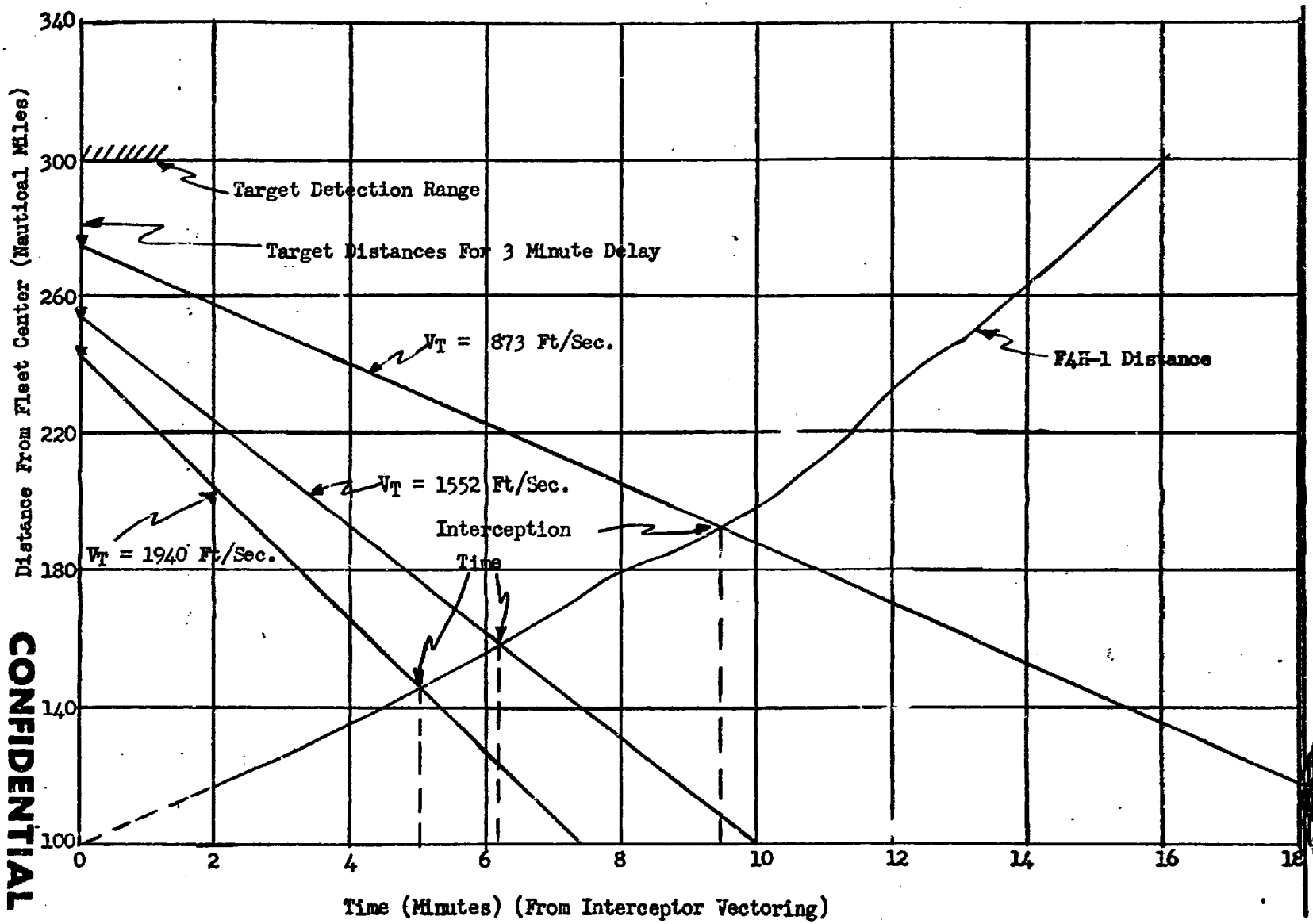

Figure /7

CONFIDENTIAL

FIGURE-18
F4H-1 50,000 FT. INTERCEPT
SUBSONIC CLIMB FROM 30,000 FT.
CONSTANT SPEED CONDITION
DISTANCE FROM TLEET CENTER
(NAUTICAL MILES)
300
260
220
180
140
100
TARGET DETECTION RANGE
TARGET DISTANCES FOR 3 MINUTE DELAY
V_T = 873 FT/SEC
V_T = 1552 FT/SEC
V_T = 1940 FT/SEC
F4H-1 DISTANCE
CONSTANT SPEED (873 FT/SEC)
INTERCEPT TIME
SUBSONIC CLIMB FROM 30,000 FT. (2.26 MIN.)
0
2
4
6
8
10
12
14
16
18
TIME (MINUTES)

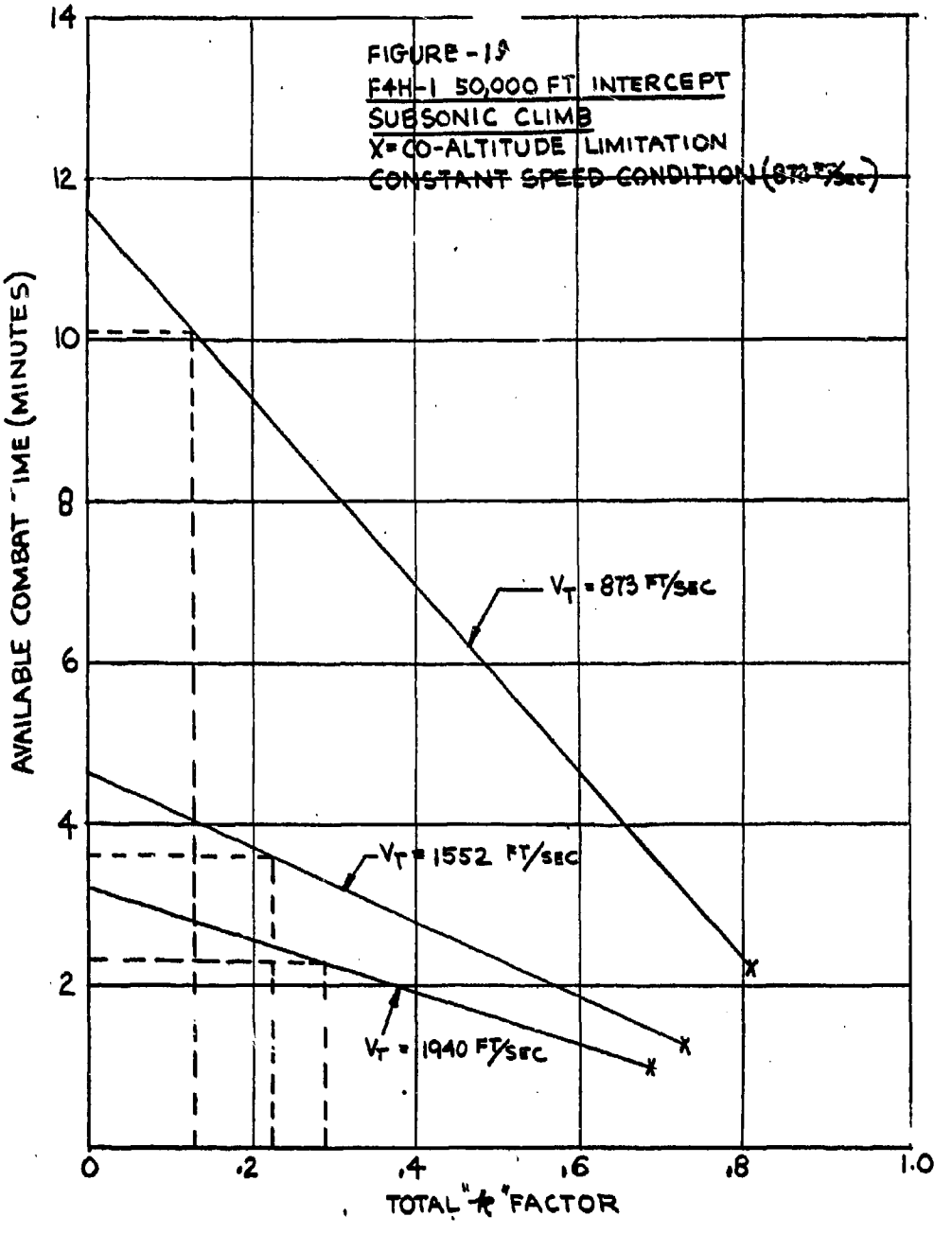
FIGURE - 19
F4H-1 50,000 FT INTERCEPT
SUBSONIC CLIMB
X = CO-ALTITUDE LIMITATION
CONSTANT SPEED CONDITION (873 FT/SEC)
AVAILABLE COMBAT TIME (MINUTES)
14
12
10
8
6
4
2
0
.2
.4
.6
.8
1.0
TOTAL "K" FACTOR
V_T = 873 FT/SEC
V_T = 1552 FT/SEC
V_T = 1940 FT/SEC

F4H-1 Climb to 30,000 Ft. Accelerated

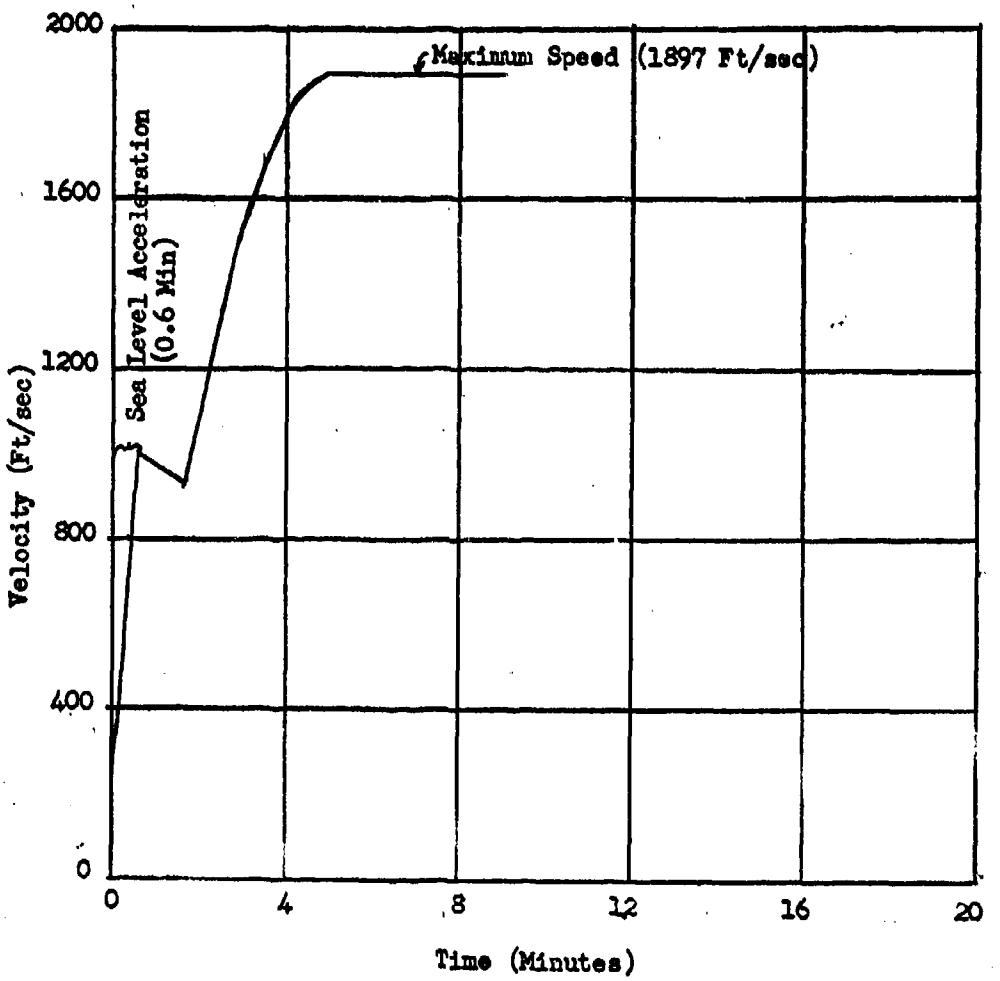

Figure 20

F4H-1 Climb To 30,000 Ft. Accelerated

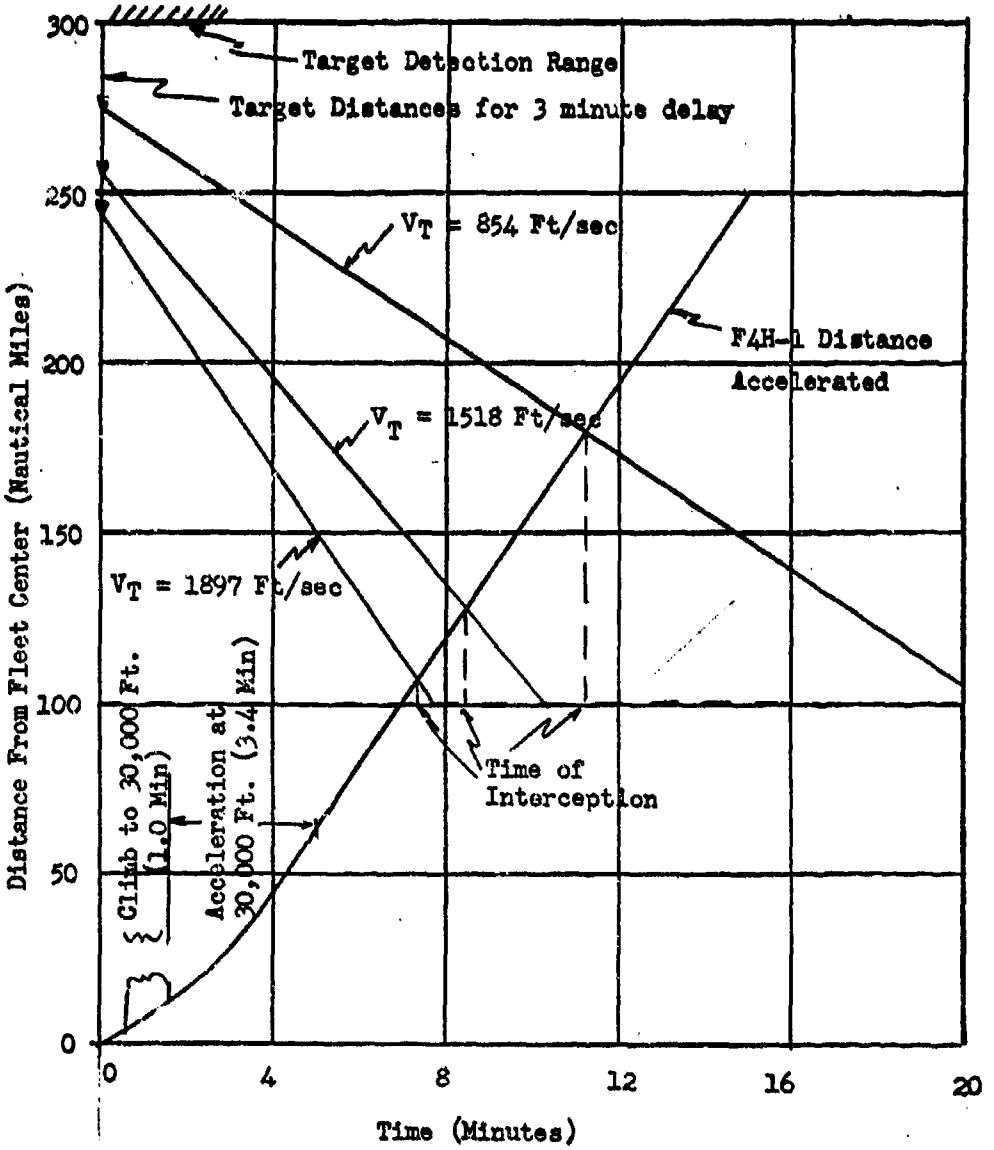

Figure 2/

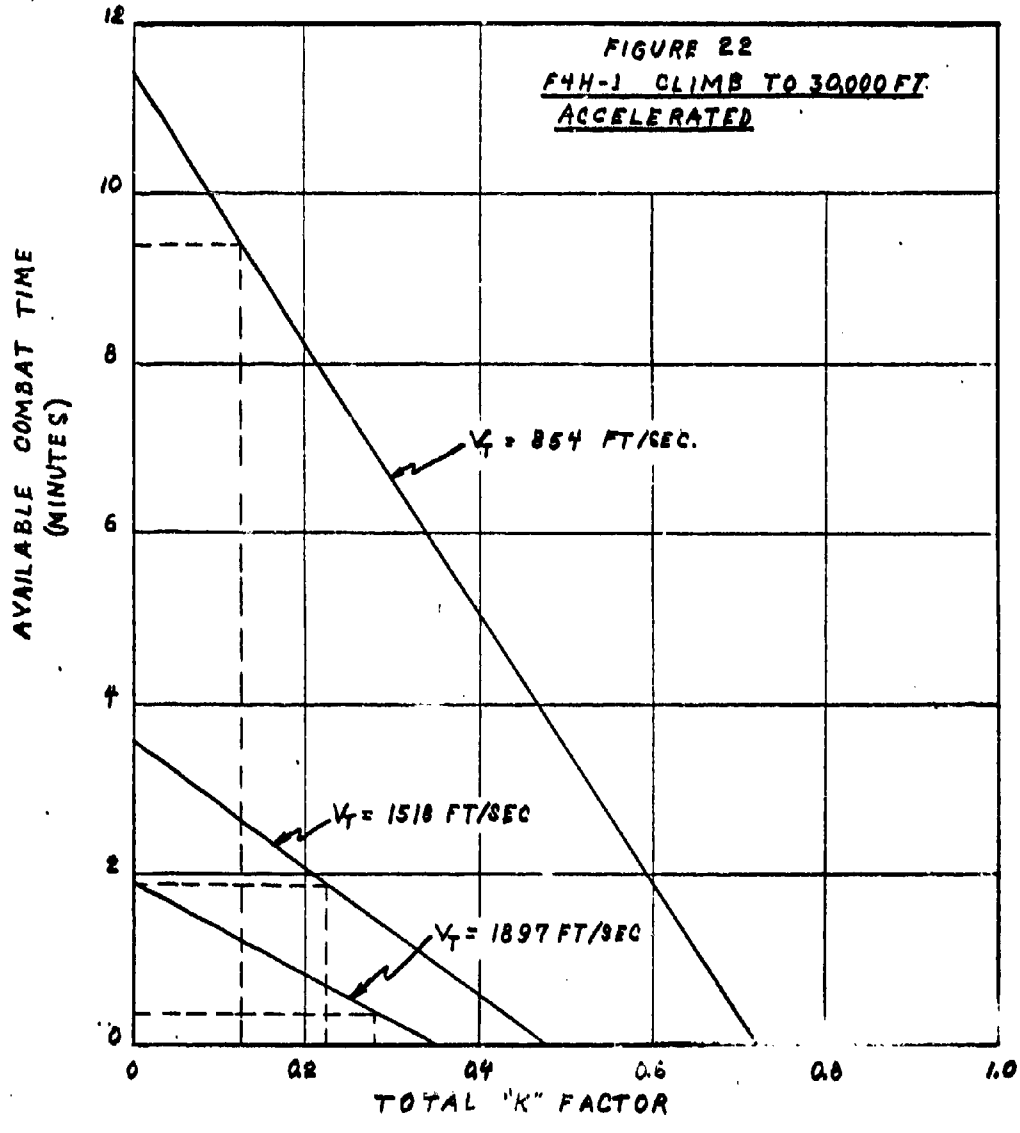
FIGURE 22
F4H-1 CLIMB TO 30,000 FT
ACCELERATED
AVAILABLE COMBAT TIME (MINUTES)
TOTAL "K" FACTOR
V_T = 854 FT/SEC.
V_T = 1518 FT/SEC
V_T = 1897 FT/SEC
12
10
8
6
4
2
0
0
0.2
0.4
0.6
0.8
1.0

Analytical Section Technical Memorandum No. 276

APPENDIX VIII

Sidewinder Operation With The F4H-1

R. G. Clanton

Assisted By
D. Nadolski

12/30/57

Distribution

Restricted - Proprietory
100, D. J. Povejsil, Mgr.
(30)103, R. G. Clanton, Supvr. Engr.

Uniterms

Sidewinder Missile
XLA Armament Control

90114
1/15/58:lm

28 pages

ABSTRACT

The Sidewinder 1A missile applied as part of the armament for the F4H-1 and AMCS-1A System is investigated. Missile launch zones, limiting attack courses which enter these zones, and vectoring considerations to get the interceptor into these attack zones are presented. The problem associated with interceptor slow down at high altitude is also presented. Finally the possible improvements arising from the Sidewinder 1C are discussed.

TABLE OF CONTENTS

TABLE OF FIGURES

1. Introduction

This report presents an analysis of some of the pertinent factors which enter into the determination of the tactical effectiveness of the Sidewinder air-to-air missile as employed in the F-4H1 weapon system. The Sidewinder model that will be used in this weapon system ultimately will be the model 1C. However, at the present time data defining the 1C capabilities has not been developed. In anticipation of the fact that the model 1A will be used initially in the weapon system this report deals essentially with the capabilities of the 1A. This report presents a development which leads from the presentation of Sidewinder 1A launch zones[1], to the limiting attack courses, and then to the effect upon vectoring tactics. This report deals only with the co-altitude attack capabilities. The factors which are not treated in this study but which are none the less of extreme importance are:

1. Missile storage problems on launching aircraft.
2. Missile lock on problems.
3. Missile launching transients.

For a description of Sidewinder 1A physical characteristics refer to reference 1.

The speed - altitude cases studied and presented in this report are listed in Table I.

STUDY SPEED - ALTITUDE CONDITIONS

Fighter Speed (Ft/sec)	Target Speed (Ft/sec)	Attack Altitude (Ft)
1940	1940 High	50,000
1940	1552 Medium	50,000
1940	873 Low	50,000
1897	1897 High	30,000
1897	1518 Medium	30,000
1897	854 Low	30,000
1189	1189 High	1,000
1189	951 Medium	1,000
1189	533 Low	1,000

Table 1

2. Summary of Results

2.1. A high degree of C.I.C. control is required if the Sidewinder 1A missile is to be successfully launched from the F4H-1 aircraft. This control is necessary to place the interceptor on an attack course from which the missile launch zone can be entered.

5

2.2. Collision vectoring is completely unsuited to the requirements imposed by this particular system.

2.3. Antiparallel vectoring with a commanded turn is suited to the F4H-1 – Sidewinder system. The use of a single commanded turn point results in an unhappy compromise. The commanded turn point should be adjusted as a function of interceptor-target closing rate.

2.4. Co-altitude targets at 50,000 feet altitude traveling at 1552 ft/sec can be attacked with questionable success by the F4H-1 employing the Sidewinder 1A due to interceptor slow down. At 30,000 feet altitude, this speed target can be successfully attacked.

2.5. Target penetration time and distance is a severe problem for all cases studied except the low speed target cases.

2.6. Although not studied in this report incremental altitude attacks on target operating at 50,000 feet will very seriously limit the target speeds which can successfully be attacked.

2.7. The effect of a target turn towards the attacking interceptor after AI radar lock on is to move the limiting attack course significantly to the rear. In other words a target maneuver can seriously degrade system performance.

2.8. The cases which have an interceptor to target speed ratio of 2 appear to exhibit very satisfactory performance.

3. Launch Zone Development

Typical launch zones for the Sidewinder 1A are presented as Figure 1. The launching aircraft must get within these zones with such a heading orientation that the target appears within $\pm 2^{\circ}$ of the missile's optical axis. To do this requires that the interceptor aircraft be flown on a pure pursuit course in the launch zone. An additional factor which is of significance to the development of the launch zones is the loci of points on pure pursuit courses for which the interceptor must execute a 3g turn rate. The radius of the loci is given below for constant speed attacks

$$r = \frac{V_T V_F}{2g\sqrt{N^2-1}}$$

where: V_T = target velocity

V_F = fighter velocity

N = lateral acceleration

This radius is drawn in figure 1 for N = 3.

SIDEWINDER 1A ATTACK ZONES

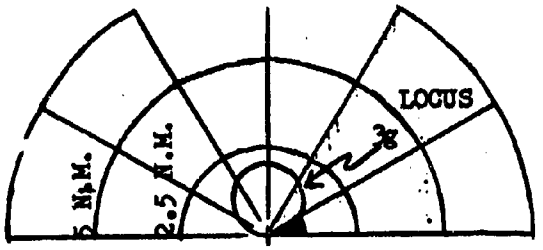

Altitude = 1000'
M Launch = 1.0
M Target = 1.0
Horizontal Attack

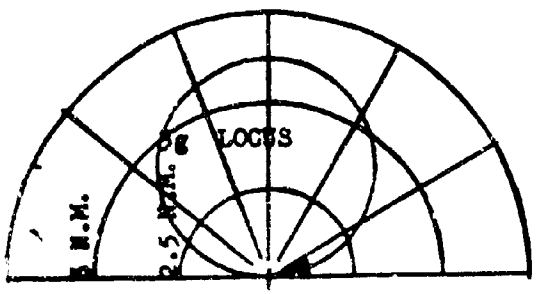

Altitude = 30,000'
Horizontal Attack
M Launch = 1.9
M Target = 1.9

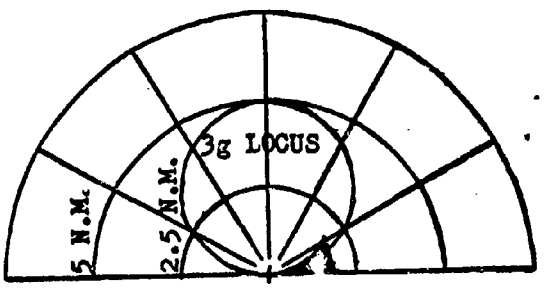

Altitude = 30,000'
Horizontal Attack
M Launch = 1.9
M Target = 1.5

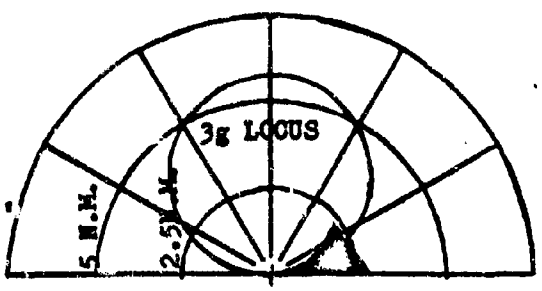

Altitude = 50,000'
Horizontal Attack
M Launch = 2.0
M Target = 2.0

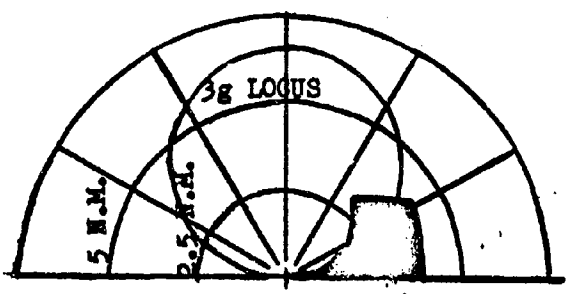

Altitude = 50,000'
Horizontal Attack
M Launch = 2.0
M Target = 1.6

Figure 1

4. Limiting Attack Courses

With the information developed in section 3 it is now possible to state the requirements of a limiting attack course. These are:

1. The interceptor must enter the attack zone on a pure pursuit course with the greatest angle off the tail possible.

2. The attack course must fall outside of the 3g loci.

Figures 2 thru 10 present the limiting pursuit courses which meet this criteria. It should be emphasized that these limit courses apply only to a non maneuvering target. A target which turns towards the interceptor results in a limit course considerably to the rear of those shown.

Particular attention is drawn to the 50,000 feet altitude case with an initial interceptor speed of 1940 ft/sec operating against a non-maneuvering target with a speed of 1552 ft/sec. This case is shown in Figure 3. Due to the loss of speed, the course which drew tangent to the loci of points on pure pursuit courses involving a 3g lateral turn can not close upon the target. Courses somewhat further to the rear do not require as high a rate of turn and consequently the interceptor does not slow down and the courses close upon the target. More will be shown about this case when vectoring is considered. Sufficient speed loss occurs for the F4H-1 at 50,000' to be a problem when employing sidewinder. There is no significant speed loss at the 30,000 or 1,000 feet altitude cases. Figures 11 and 12 present comparative slow down information for different altitudes.

5. Effects Upon Vectoring Tactics

A casual examination of the vectoring problem is sufficient to rule out collision vectoring as a means of approach tactis. The deficiencies of collision vectoring are:

extreme gimbal angle coverage requirements, if the interceptor is to be placed behind a limiting attack course.

extreme suseptibility to starting an attack course ahead of the limiting attack course.

It is also apparent that long range lock on in the forward hemisphere could place the interceptor on an attack course ahead of the limiting attack course.

In order to assess the problem imposed upon the vectoring agency comparative cases are presented for a situation in which the interceptor was vectored to a point with the following specifications:

Antiparallel
23 N.M. offset
27 N.M. range from target

At this point a 2 deg/sec turn is initiated to bring the interceptor to detection and a pursuit course. This particular vector point was choosen

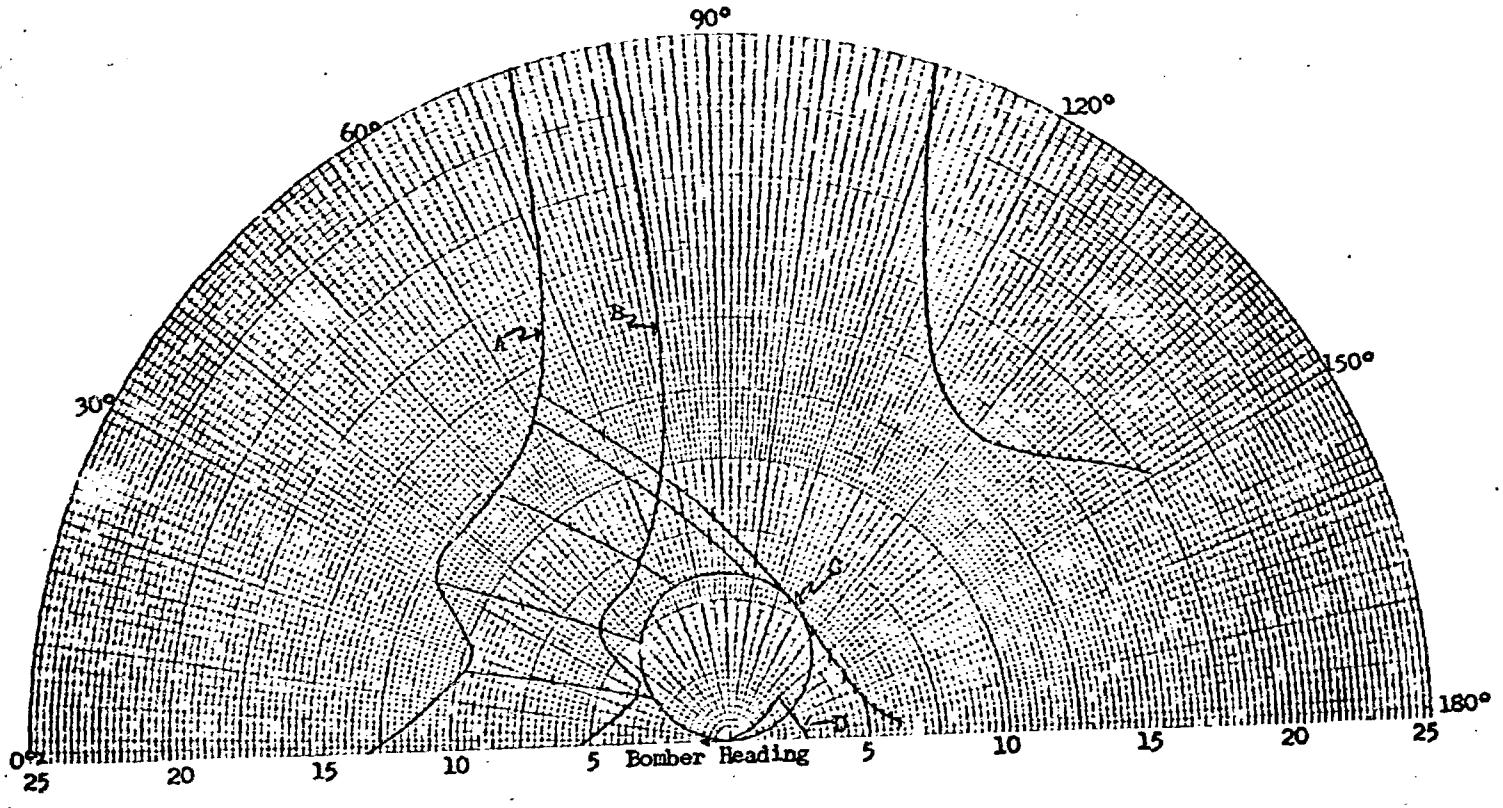

V_P = 1940 FPS (F4H-1)
V_T = 1940 FPS
Altitude = 50,000 Ft.
Range (n.m.)
Dash Marks at 5 sec intervals

Sidewinder 1A Attack Courses

A - 85% cumulative detection range (unimproved)
B - 10 sec lock-on time
C - 3 "g" Locus on pursuit courses
D - Firing zone - 1A

Figure 2

Sidewinder 1A Attack Courses

A - 85% cumulative detection range (unimproved)
B - 10 sec lock-on time
C - 3 "g" locus on pursuit courses
D - Firing zone - 1A

V_F = 1940 FPS (F4H)
V_T = 1552 FPS
Altitude = 50,000 Ft.
Range (n.m.)
Dash marks at 5 sec intervals

Figure 3

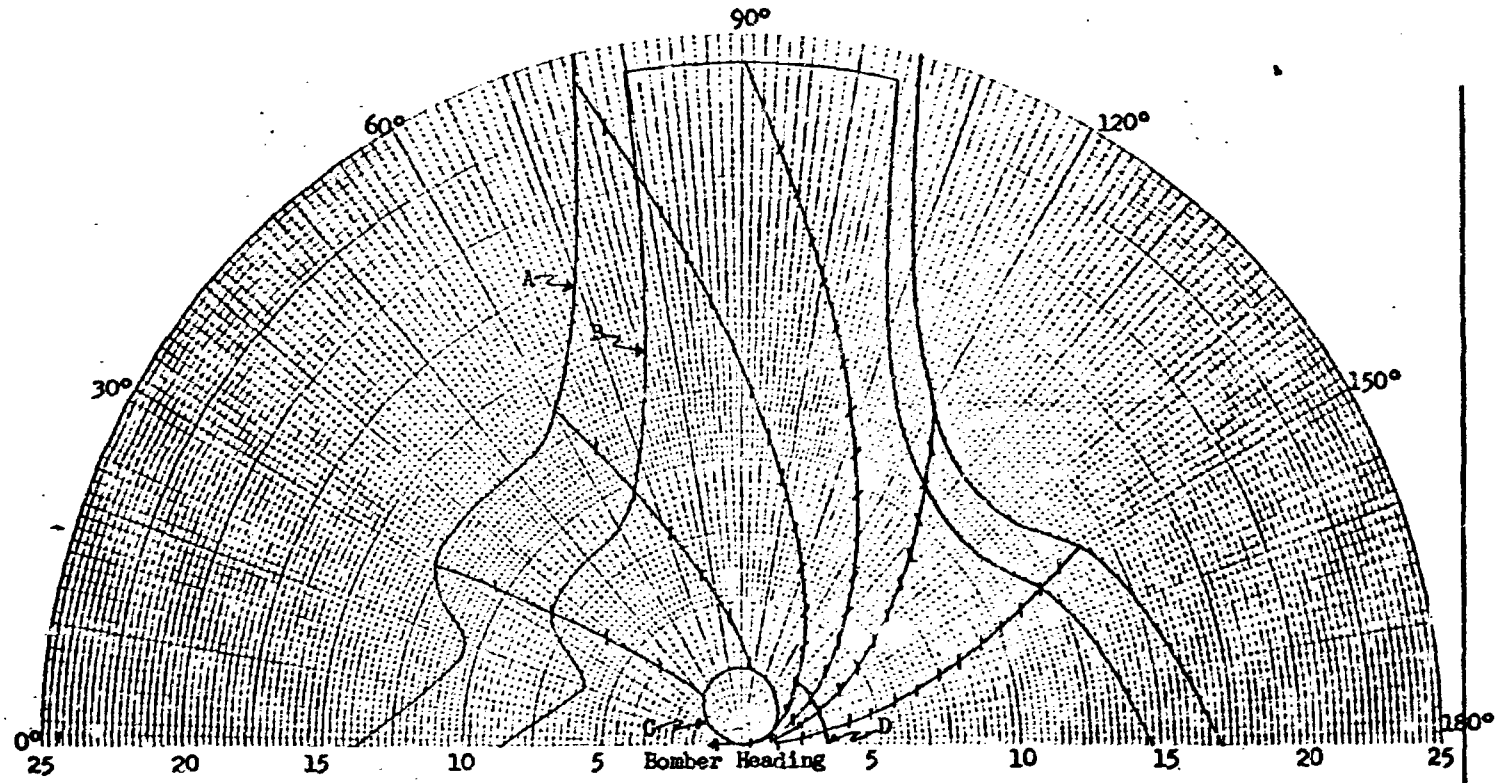

V_P = 1940 FPS (F4H-1)
V_T = 873 FPS
Altitude = 50,000 Ft.
Range (N.M.)
Dash marks at 5 sec intervals

Sidewinder 1A Attack Courses

A - 85% cumulative detection range
B - 10 sec lock-on time
C- 3"g" locus on pursuit courses
D - firing zone - 1A

Figure 4

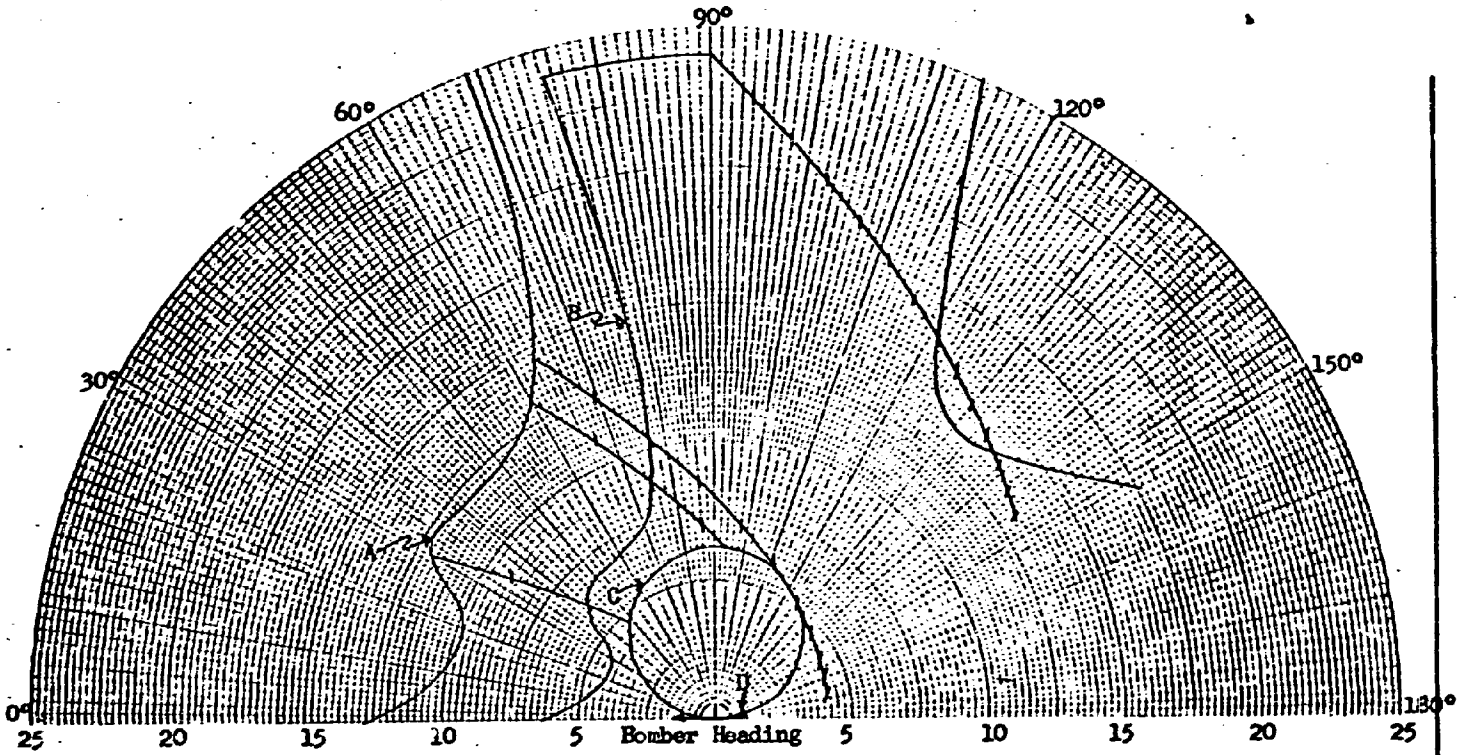

V_P = 1897 FPS (F4B-1)
V_T = 1897 FPS
Altitude = 30,000 Ft.
Range (N.M.)
Dash marks at 5 sec intervals

Sidewinder 1A Attack Courses

A - 85% cumulative detection range-(unimproved)
B - 10% lock-on time
C - 3 "g" locus on pursuit courses
D - Firing zone

Figure 5

12

Sidewinder IA Attack Courses

A - 85% cumulative detection range (unimproved)
B - 10 sec lock-on time - 1A
C - 3 "g" locus on pursuit courses
D - firing zone

V_F = 1897 FPS (F4H-1)
V_T = 1518 FPS
Altitude = 30,000 Ft.
Range (N.M.)
Dash marks at 5 sec intervals

Figure 6

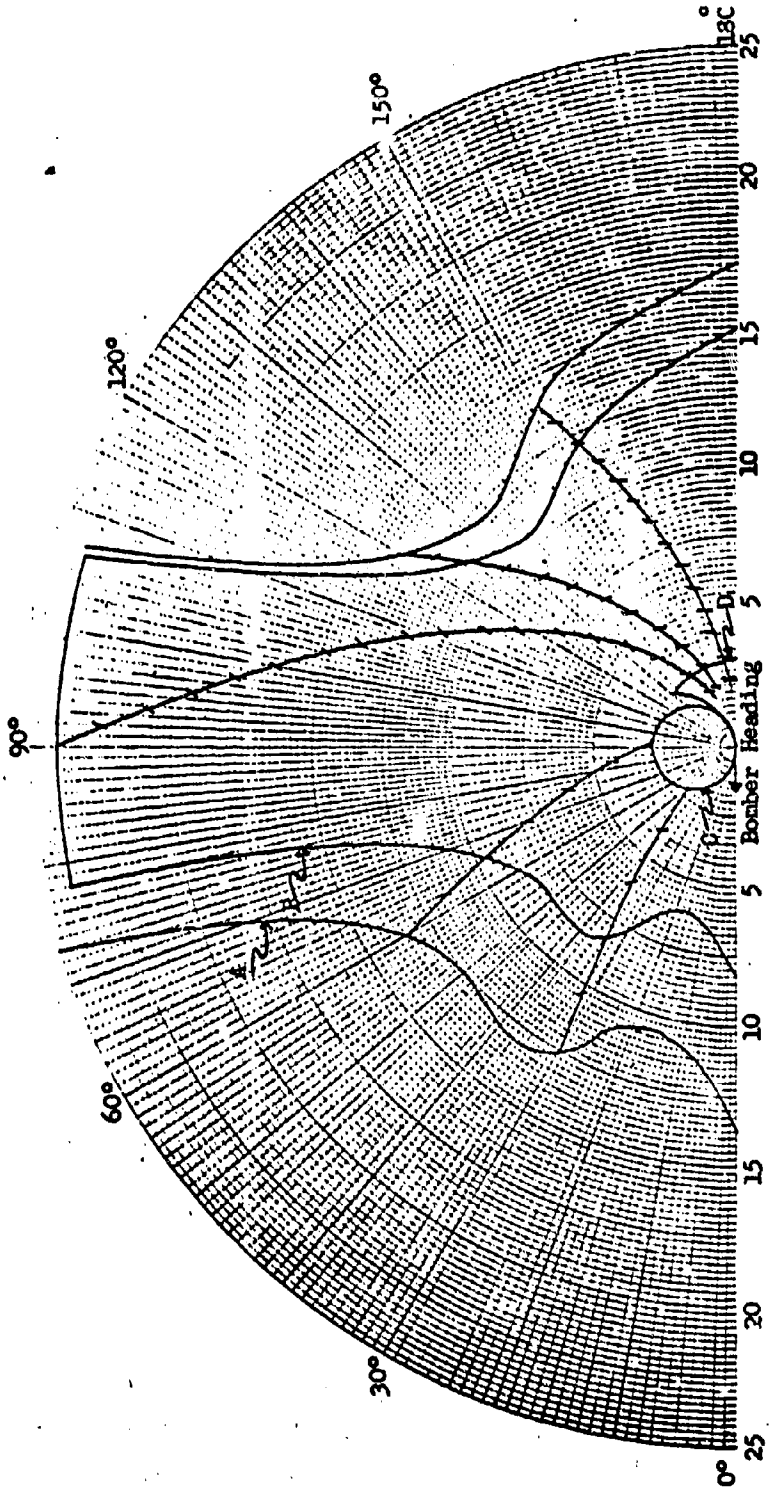

Sidewinder 1A Attack Courses

A - 85% cumulative detection range (unimproved)
B - 10 sec lock - on time 1A
C - 3 "g" locus on pursuit courses
D - Firing zone

V_P = 1897 FPS (P4H-1)
V_T = 854 FPS
Altitude =30,000 Ft.
Range (N.M.)
Dash marks at 5 sec intervals

Figure 7

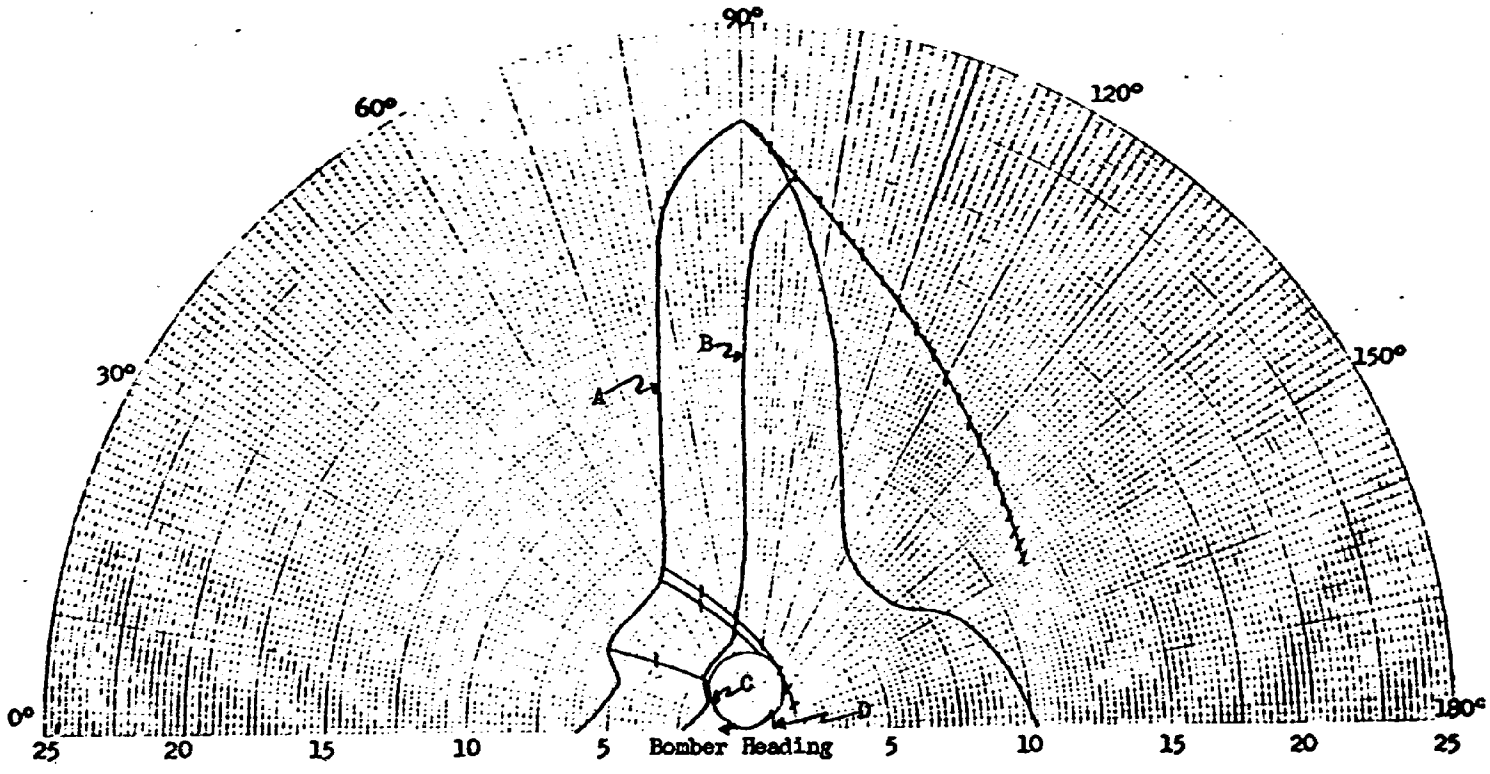

V_F = 1189 FPS (F4H)
V_T = 1189 FPS
Altitude = 1,000 Ft.
Range (N.M.)
Dash marks at 5 sec intervals

Sidewinder 1A Attack Courses

A - 85% cumulative detection range (unimproved)
B - 10 sec lock-on time
C - 3 "g" locus on pursuit courses
D - firing zone - 1A

Figure 8

Sidewinder 1A Attack Courses

A - 85% cumulative detection range (unimproved)
B - 10 sec lock - on time
C - 3 "g" locus on pursuit courses
D - firing zone - 1A

Vp = 1189 FEET/SEC
Vf = 951 FPS
Altitude = 1,000 Ft.
Range (N.M.)
Dash marks at 5 sec intervals

Figure 9

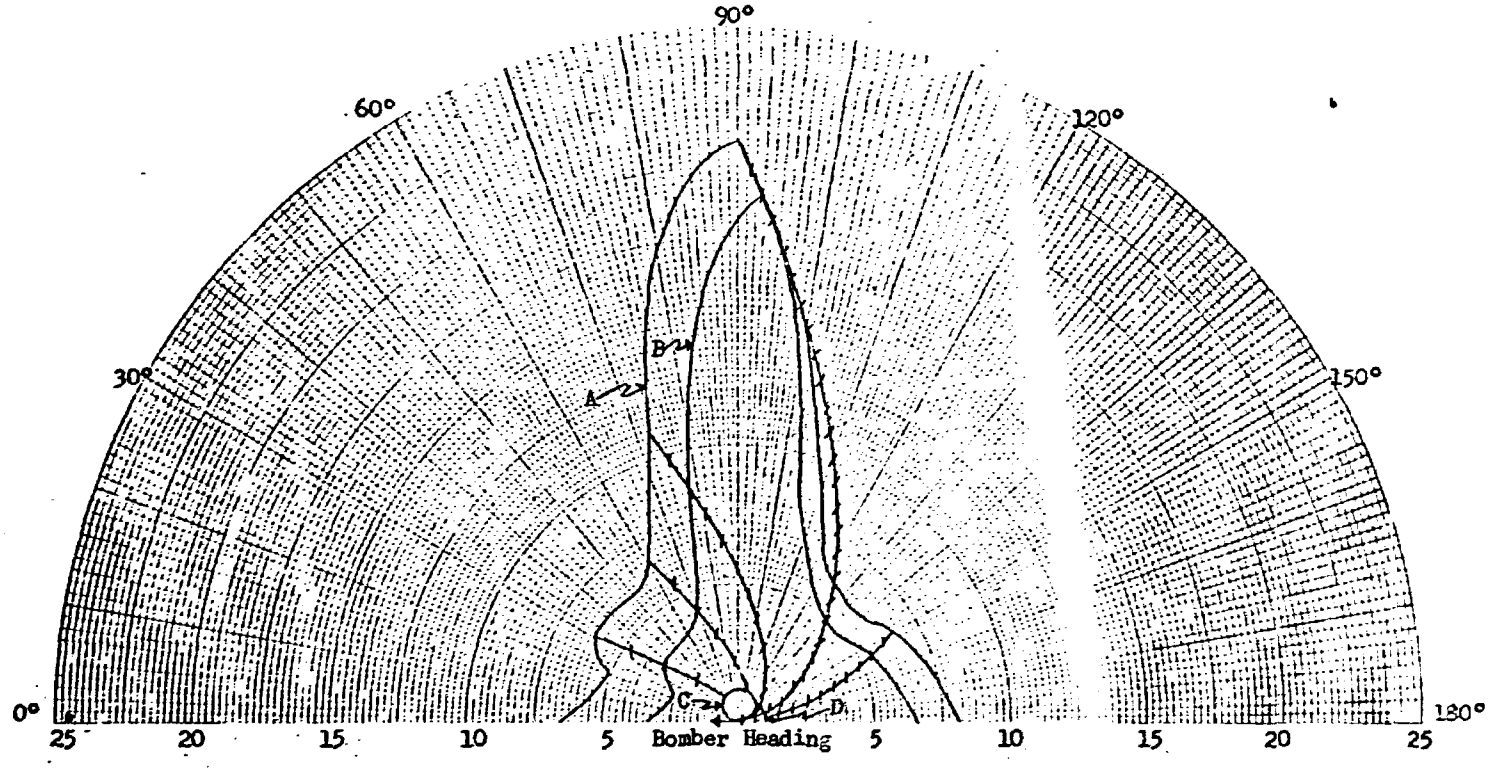

V_P = 1189 FPS (F4H)
V_T = 533 KPS
Altitude = 1,000 Ft.
Range (N.M.)
Dash marks at 5 sec intervals

Sidewinder 1A Attack Courses

A - 85% cumulative detection range (unimproved)
B - 10 sec lock - on time
C - 3 "g" locus on pursuit courses
D - firing zone - 1A

Figure 10

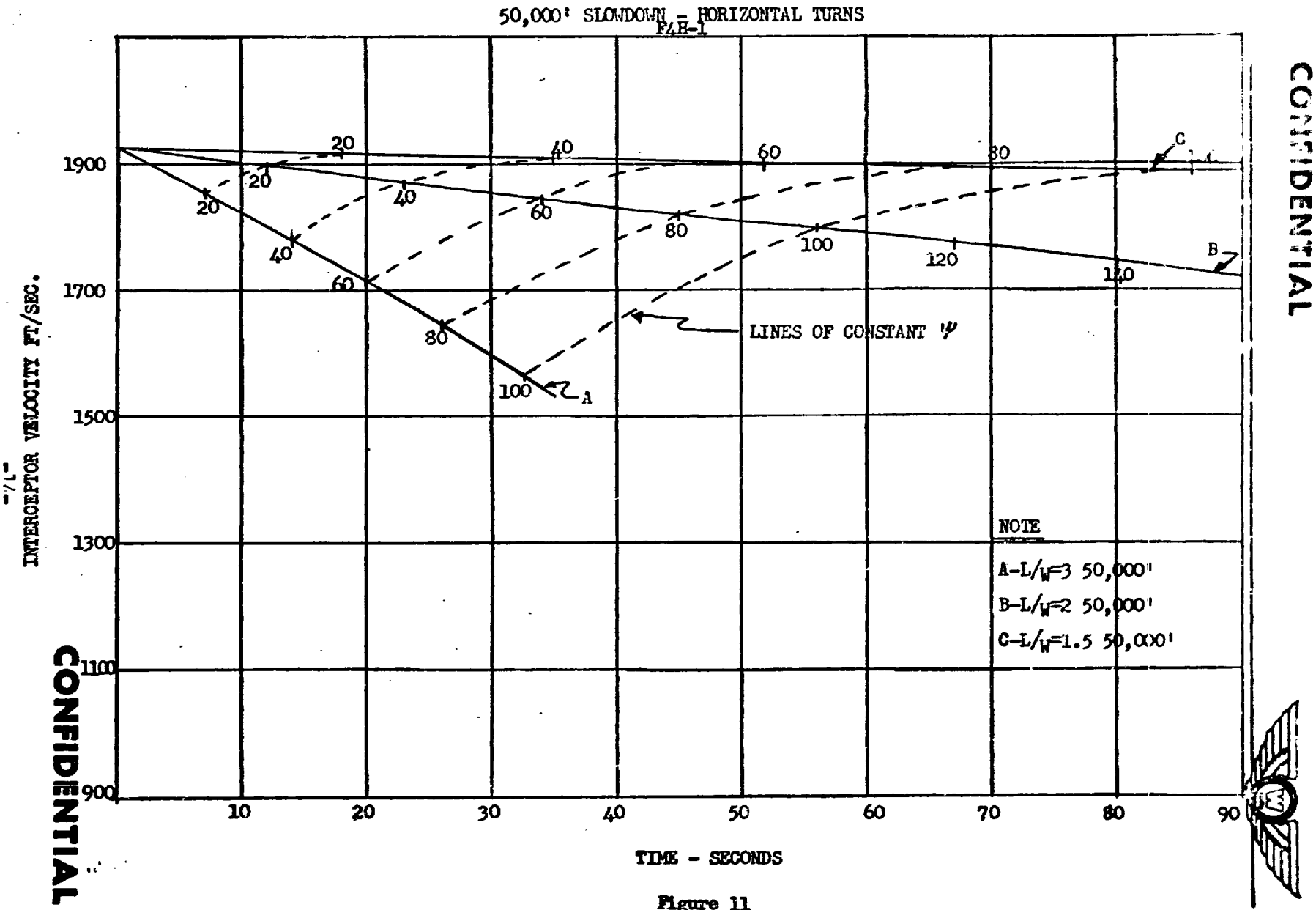
50,000' SLOWDOWN - HORIZONTAL TURNS
F4H-1
INTERCEPTOR VELOCITY FT/SEC.
1900
1700
1500
1300
1100
900
10
20
30
40
50
60
70
80
90
TIME - SECONDS
LINES OF CONSTANT Ψ
A
B
C
NOTE
A-L/W=3 50,000'
B-L/W=2 50,000'
C-L/W=1.5 50,000'

Figure 11

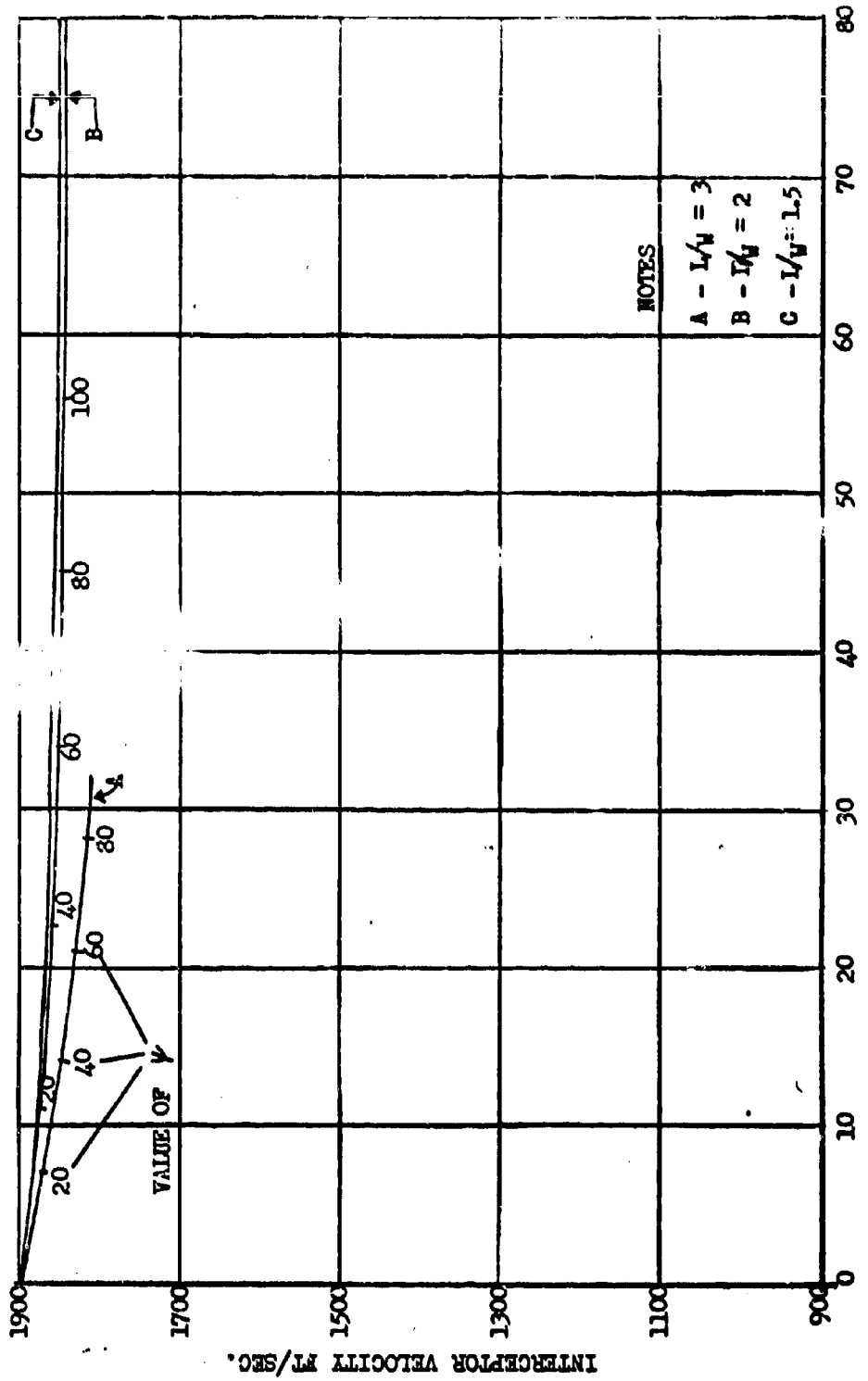
30,000' SLOPE - HORIZONTAL TURNS
F-H-1
INTERCEPTOR VELOCITY FT/SEC.
1900
1700
1500
1300
1100
900
0
10
20
30
40
50
60
70
80
VALUE OF ψ
20
40
60
80
100
C
B
NOTES
A - L/W = 3
B - L/W = 2
C - L/W = 1.5

Figure 12

to minimize the possibility of the interceptor's radar detecting the target too soon and the interceptor getting on a pursuit course ahead of the limit attack course.

This tactic generally brings the interceptor to a pure pursuit course about 90° off the target's nose between 10 and 15 N.M. range.

From an examination of Figures 13, 14, 15, 16, 17, and 18 which present the results of investigating the attack operation from the point of the CCI commanded turn, it is possible to draw certain general conclusions.

1. There is considerable mismatch between courses involving the low speed targets and the medium speed target. Compare the cases of V_T = 1552 ft/sec + 854 1/S in figures 13 and 14. This indicates that the CIC operation should adjust the commanded turn point as a function of range rate. The point used in this study is an unhappy compromise.

2. The medium speed target when operating at 50,000 feet can be attacked with questionable success due to the interceptor slow down.

3. A turn by the target towards the interceptor would result in failure for the attack courses for the low speed target shown in Figures 14, 16, and 18. By trading penetration time it is possible to make the system less sensitive to target maneuver. This is done by bringing the interceptor closer to a direct tail on attack.

Table 2 presents a summary of the average time spent from the commanded turn point to the firing zone. Note no time is given for the 50,000 feet HM case due to the questionable nature of this case.

Altitude (feet)	Case	Time (Seconds)
50,000	HM	?
	HL	100
30,000	HM	195
	HL	95
1,000	HM	274
	HL	145

Average Time Spent From Commanded Turn To Attack Zone

Table 2

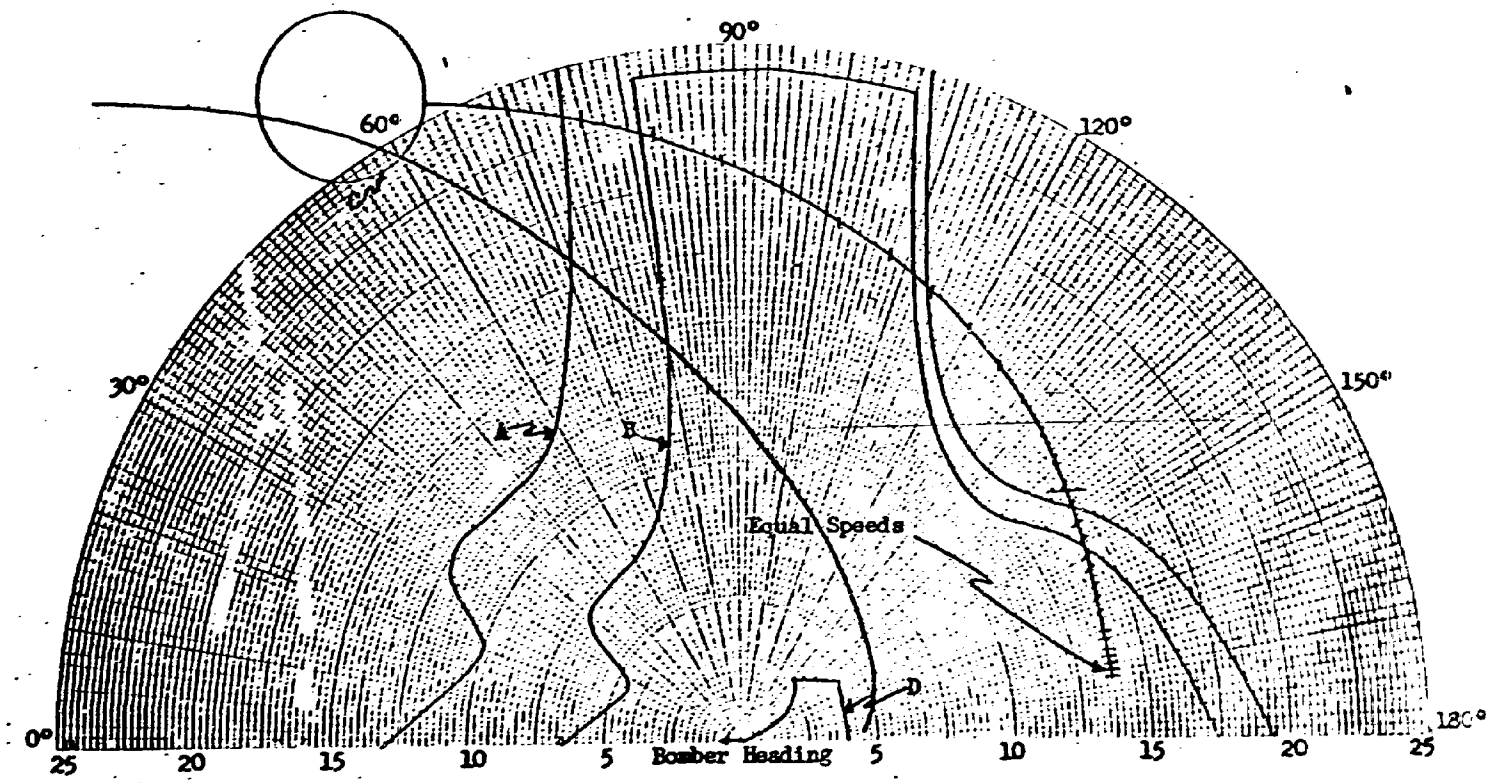

V_F = 1940 FPS (F4H-1)
V_T = 1552 FPS
$\dot{\psi}$ = 2 °/sec
Altitude = 50,000 Ft.
Range (N.M.)
Dash marks at 5 sec intervals

Sidewinder 1A Attack Course From Anti-Parallel Course

A - 85% cumulative detection range (unimproved)
B - 10 sec lock - on time
C - 1 σ vectoring distribution
D - firing zone - 1A

Figure 13

Sidewinder 1A Attack Course From Anti-Parallel Course

A - 85% cumulative detection range (unimproved)
B - 10 sec lock - on time
C - 1 σ vectoring distribution
D - firing zone - 1A

V_F = 1940 FPS (F4H-1)
V_T = 873 FPS
$\dot{\psi}$ = 2 °/sec
Altitude = 50,000 Ft.
Range (N.M.)
Dash marks at 5 sec intervals

Figure 14

22

Sidewinder 1A Attack Course From Anti-Parallel Course

A - 85% cumulative detection range (unimproved)
B - 10 sec lock-on time
C - 1 σ vectoring distribution
D - firing zone - 1A

V_F = 1897 FPS (F4H-1)
V_T = 1518 FPS
$\dot{\gamma}$ = 2 °/sec
Altitude = 30,000 Ft.
Range (n.m.)
Dash marks at 5 sec intervals

Figure 15

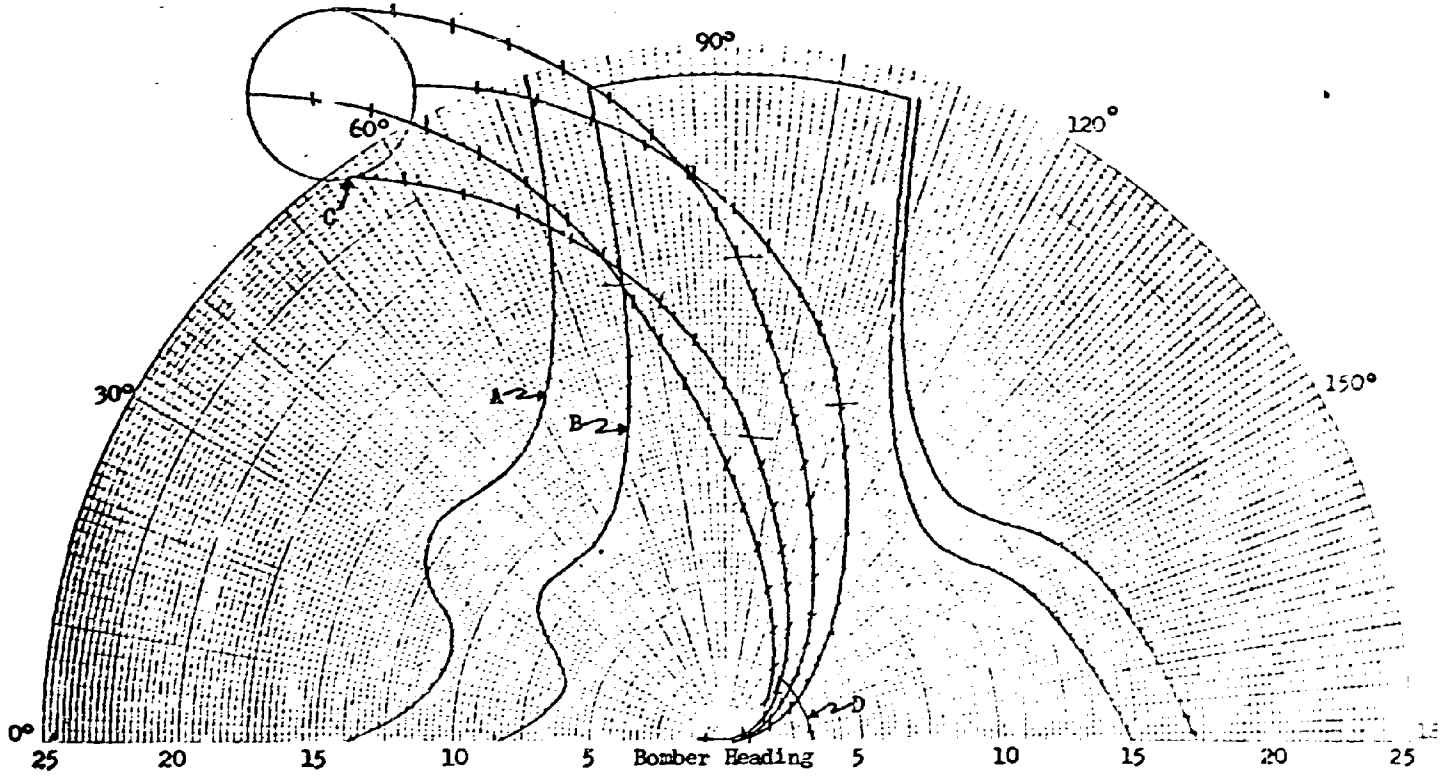

V_F = 1897 FPS (F4H-1)
V_T = 854 FPS
$\dot{\psi}$ = 2 °/sec
Altitude = 30,000 Ft.
Range (n.m.)
Dash marks at 5 sec intervals

Sidewinder 1A Attack Course From Anti-Parallel Course

A - 85% cumulative detection range (unimproved)
B - 10 sec lock - on time
C - 1 σ vectoring distribution
D - firing zone - 1A

Figure 16

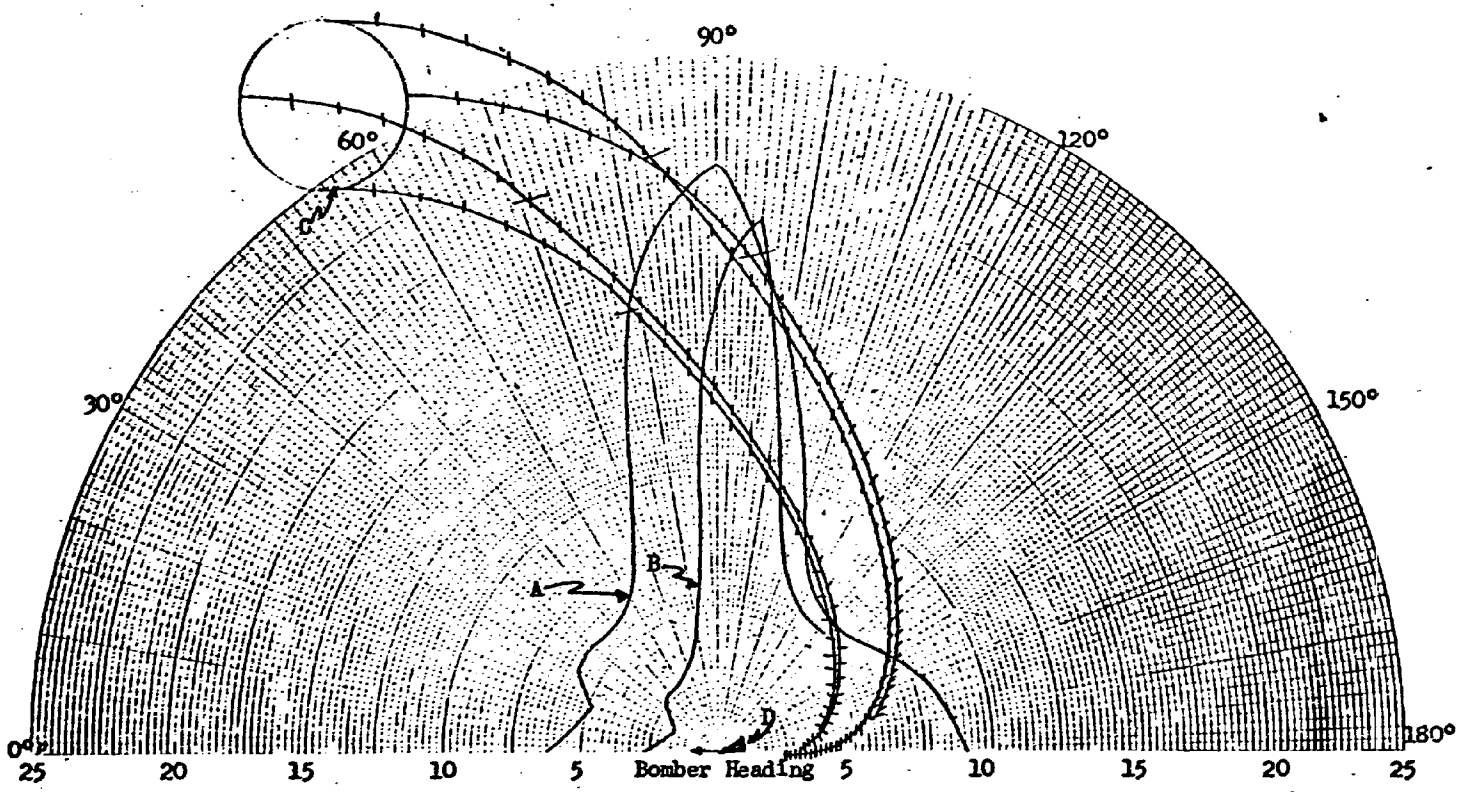

V_F = 1189 FPS (F4H-1)
V_T = 951 FPS
$\dot{\psi}$ = 2 °/sec
Altitude = 1,000 Ft.
Range (N.M.)
Dash marks at 5 sec intervals

Sidewinder 1A Course From Anti-Parallel Course

A - 85% cumulative detection range (unimproved)
B - 10 sec lock-on time
C - 1 σ vectoring distribution
D - firing zone - 1A

Figure 17

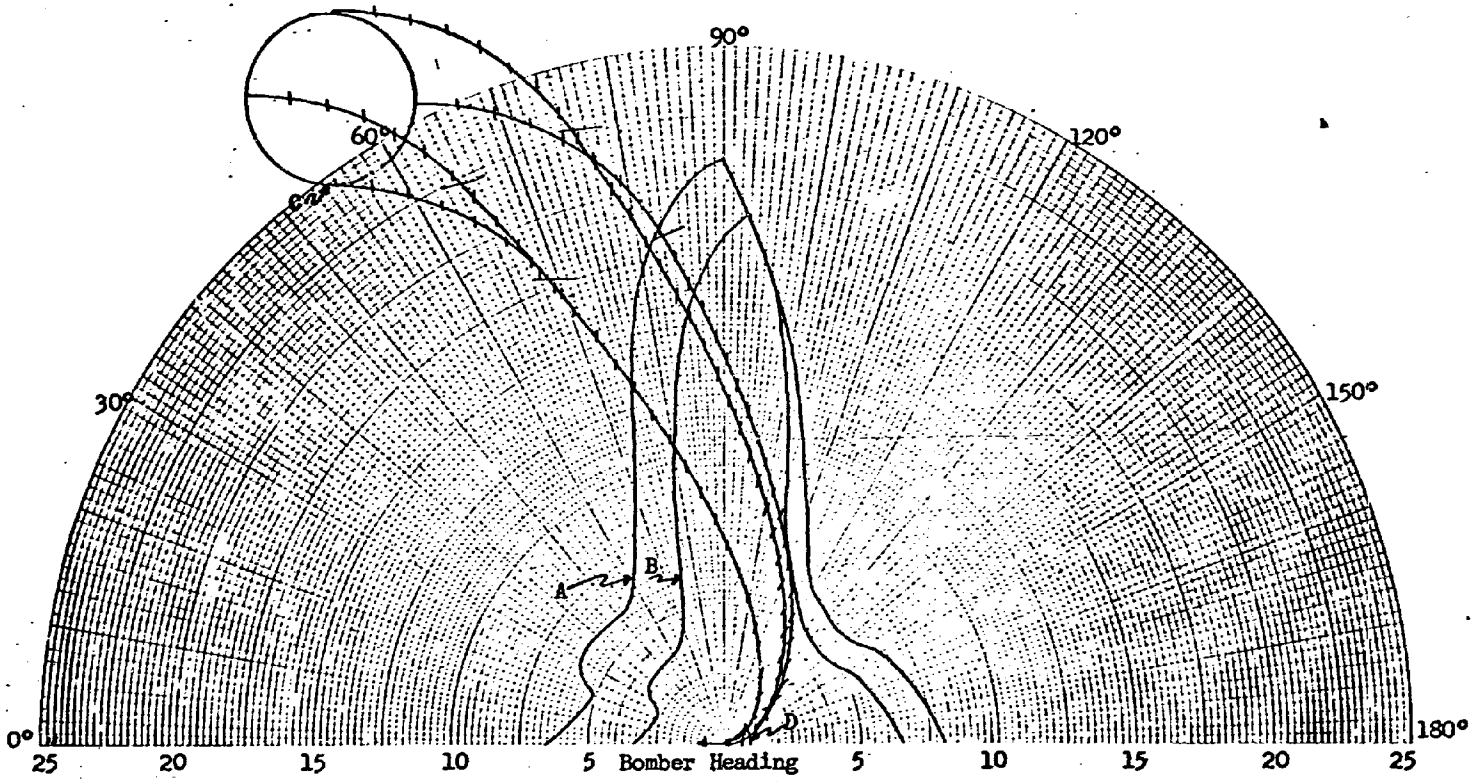

V_F = 1189 FPS (F4H-1)
V_T = 533 FPS
$\dot{\psi}$ = 2 °/sec
Altitude = 1,000 Ft.
Range (N.M.)
Dash Marks At 5 Sec Intervals

Sidewinder 1A Attack Course From Anti-Parallel Course
A - 85% cumulative detection range (unimproved)
B - 10 sec lock-on time
C - 1 σ vectoring distribution
D - Firing Zone - 1A

Figure 18

6. Summary

It is clearly evident that as the speed ratio of the interceptor and target approaches unity the capabilities of the Sidewinder 1A armament system operating with the F4H-1 steadily diminish. With a speed ratio $V_F/V_T = 2$ the system is possessed with considerable capability but at a speed ratio of V_F/V_T 1.5 the system suffers severly from penetration time and difficulty in entering the launch zone at high altitude due to interceptor slow down.

The Sidewinder 1C can be means of achieving larger laun[illegible]es improve the situation considerably. The magnitude of the improv[illegible]ts in the launch zones for the 1C is not known so no statement can be m[illegible]de at this time to the extent penetration time is reduced.

References

1. ANTM 220, Sidewinder 1 and 1A Description, M. Mazina, 8/29/57, Confidential.

Naval Research Laboratory
Technical Library
Research Reports Section

DATE: February 26, 2001

FROM: Mary Templeman, Code 5227

TO: **Code 5300 Paul Hughes**

CC: Tina Smallwood, Code 1221.1 ts 3/8/01

SUBJ: Review of NRL Reports

Dear Sir/Madam:

1. Please review NRL Report MR-754 Volumes I, II, III, IV, VII, VIII, IX, X, XI, XII, XIII, XIV, XV, MR-1372 and MR-1289 for:

   ☑ Possible Distribution Statement
   ☐ Possible Change in Classification

Thank you,

Mary Templeman

Mary Templeman
(202)767-3425
maryt@library.nrl.navy.mil

The subject report can be:

☒ Changed to Distribution A (Unlimited)
☐ Changed to Classification _____
☐ Other:

Ben H Cantrell 3-8-01

Signature Date

AN (1) AD- 368 356/XAG
FG (2) 010100
010303
150600
160401
CI (3) (U)
CA (5) NAVAL RESEARCH LAB WASHINGTON D C
TI (6) SUMMARY OF NAVY STUDY PROGRAM FOR F4H-1 AND F8U-3 WEAPON SYSTEMS. VOLUME IV. APPENDICES 1-8.
DN (9) Memo. rept.
RD (11) 1958
PG (12) 179 Pages
RS (14) NRL-MR-754-Vol-4-App
RC (20) Unclassified report
NO (21) See also Volume 3, AD-368 048L.
AL (22) Distribution: DoD only: others to Director, Naval Research Lab., Washington, D. C. 20390.
DE (23) (*JET FIGHTERS, AERIAL WARFARE)
MODELS(SIMULATIONS), NAVAL AIRCRAFT, PERFORMANCE(ENGINEERING), AERODYNAMIC CHARACTERISTICS (U) STABILITY, LOW ALTITUDE, HIGH ALTITUDE, AIR TO AIR MISSILES, AIRCRAFT INTERCEPTION, AERIAL TARGETS, TACTICAL WARFARE, RECOVERY, MANEUVERABILITY, LOADS(FORCES), AIRCRAFT FIRE CONTROL SYSTEMS, SEARCH RADAR, TARGET ACQUISITION, RANGE(DISTANCE), PURSUIT COURSES, INTERCEPT TRAJECTORIES, INTERCEPTION PROBABILITIES, RADAR HOMING, ERRORS, LAUNCHING, EARLY WARNING SYSTEMS, HEAT HOMING, EXTERIOR BALLISTICS
DC (24) (U)
ID (25) F-4 AIRCRAFT, F-8 AIRCRAFT, SIDEWINDER, SPARROW, TARGETING
IC (25) (U)
DL (33) 04
CC (35) 251950